

Biold2- and APEX2-based lipid droplet proteome analysis reveals new host factors for hepatitis C virus replication

Dissertation

Submitted to the
Department of Chemistry
Faculty of Mathematics, Informatics and Natural Science
University of Hamburg

In fulfillment of the requirements
for the degree of
Doctor of Natural Sciences (Dr. rer. nat)

by
Hanna Bley
Hamburg, 2021

Reviewer of the dissertation:

Prof. Dr. Eva Herker

Prof. Dr. Wolfram Brune

Oral defense:

January 21, 2022

The dissertation was conducted at the Leibniz Institute for Experimental Virology (HPI) between March 2017 and February 2019 and at the Institute of Virology of the Philipps University Marburg between February 2019 and November 2021, under the supervision of Prof. Dr. rer. nat. Eva Herker and PD Dr. rer. nat. habil. Markus Perbandt.

Publications, awards and presentations

Publications

Parts of the dissertation are in preparation of the following publications:

Bley H, Heidenfels E, Krisp C, Schöbel A, Schlüter H, Herker E. **New Insights into the Role of LARP1 in Hepatitis C Virus-infected Cells.** *Manuscript in preparation*

Bley H, Krisp C, Schlüter H, Herker E. **Lipid Droplet Proteome Analysis in Hepatitis C Virus-infected Cells using the Proximity Labeling Methods BioID2 and APEX2.** *Manuscript in preparation*

During the dissertation, the author participated in the following publication:

Bley H, Schöbel A, Herker E. (2020) **Whole Lotta Lipids – from HCV RNA Replication to the Mature Viral Particle.** *Int J Mol Sci.* 21 (8)

Awards

2021 HCV 2021 Young Investigator Grant
 27th International Symposium on Hepatitis C Virus and Related Viruses

Presentations

The author presented parts of the dissertation at the following conferences

- 07/2021 Hanna Bley, Elisa Heidenfels, Christoph Krisp, Hartmut Schlüter, and Eva Herker
 New Insights into the Role of LARP1 in Hepatitis C Virus-infected Cells
 27th International Symposium on Hepatitis C Virus and Related Viruses,
 digital (oral presentation)
- 03/2021 Hanna Bley, Elisa Heidenfels, Christoph Krisp, Hartmut Schlüter, and Eva Herker
 New Insights into the Role of LARP1 in Hepatitis C Virus-infected Cells
 30th Annual Meeting of the Society for Virology, *digital (poster presentation)*
- 11/2019 Hanna Bley, Christoph Krisp, Hartmut Schlüter, and Eva Herker

Identification of PLIN2 Proximal Proteins in Hepatitis C Virus-infected Hepatoma Cells

2nd Lipid Droplet Workshop, Marburg, Germany (oral presentation)

10/2019 Hanna Bley, Christoph Krisp, Hartmut Schlüter, and Eva Herker

Investigation of Annexin A3- and Perilipin 2-interacting Proteins in Hepatitis C Virus-infected Cells

18th Workshop “Cell Biology of Viral Infections”, German Society for Virology, Schöntal, Germany (oral presentation)

09/2019 Hanna Bley, Kathrin Rösch, Christoph Krisp, Hartmut Schlüter, and Eva Herker

Annexin A3: An Important Host Factor for HCV Infection

Annexins 2019-10th International Conference on Annexin Biology, Münster, Germany (oral presentation)

03/2019 Hanna Bley, Christoph Krisp, Hartmut Schlüter, and Eva Herker

Identification of Annexin A3 and Perilipin 2-interacting Proteins in Hepatitis C Virus-infected Cells using the Proximity Labeling Methods BioID2 and APEX2

29th Annual Meeting of the Society for Virology, Düsseldorf, Germany (poster)

10/2018 Hanna Bley, Christoph Krisp, Hartmut Schlüter, and Eva Herker

Identification of Annexin A3 and Perilipin 2-interacting Proteins in Hepatitis C Virus-infected Cells using BioID2 and APEX2

Joint Scientific Retreat, Leibniz Institute for Experimental Virology (HPI), Hamburg, Germany (oral presentation)

10/2018 Hanna Bley and Eva Herker

Identification of Annexin A3 and Perilipin 2-interacting Proteins in Hepatitis C Virus-infected Cells using the Proximity Labeling Methods BioID2 and APEX2

17th Workshop “Cell Biology of Viral Infections”, German Society for Virology, Schöntal, Germany (poster)

10/2017 Hanna Bley and Eva Herker

Identification of Annexin A3-interacting Proteins in Hepatitis C Virus-infected Cells using the Proximity Labeling Methods BioID2 and APEX2

Joint Scientific Retreat, Leibniz Institute for Experimental Virology (HPI), Hamburg, Germany (poster)

Contents

PUBLICATIONS, AWARDS AND PRESENTATIONS	I
ABBREVIATIONS	1
ZUSAMMENFASSUNG	7
ABSTRACT	9
1 INTRODUCTION	11
1.1 HEPATITIS C VIRUS.....	11
1.2 HCV INFECTION, DISEASE, AND TREATMENT	11
1.3 HCV EPIDEMIOLOGY AND CLASSIFICATION	12
1.4 HCV PARTICLES	13
1.5 HCV REPLICATION CYCLE	14
1.5.1 <i>HCV entry and viral transmission.....</i>	<i>15</i>
1.5.2 <i>HCV genome organization and translation</i>	<i>17</i>
1.5.3 <i>HCV RNA replication</i>	<i>21</i>
1.5.4 <i>HCV assembly and release of HCV particles</i>	<i>22</i>
1.6 LIPID DROPLETS	24
1.7 THE LD PROTEOME IN HCV-INFECTED CELLS	25
1.8 ANNEXIN A3 (ANXA3)	26
1.9 PERILIPIN (PLIN) 2	27
1.10 PROXIMITY LABELING	28
1.11 THE LA-RELATED PROTEIN (LARP) 1.....	29
2 AIM OF THE THESIS.....	31
3 RESULTS	32
3.1 LD PROTEOME ANALYSIS IN HEPATOMA CELLS	32
3.1.1 <i>Labeling of LD-proximate proteins in hepatoma cells</i>	<i>32</i>
3.1.2 <i>Generation and validation of BioID2 and APEX2 fusion proteins</i>	<i>32</i>
3.1.3 <i>SILAC and proximity labeling of ANXA3 and PLIN2-expressing hepatoma cells</i>	<i>40</i>
3.1.4 <i>SILAC and proximity labeling of ANXA3 and PLIN2 in HCV-infected hepatoma cells.....</i>	<i>43</i>
3.1.5 <i>Proximity labeling of HCV proteins using PLIN2-BioID2 and PLIN2-APEX2</i>	<i>49</i>
3.2 LD-LOCALIZATION AND INTERACTION WITH VIRAL PROTEINS OF IDENTIFIED HITS	53
3.3 FABP5 DOES NOT INFLUENCE THE HCV VIRAL LIFE CYCLE.....	57
3.4 ARL8B IS REQUIRED FOR HCV SPREADING.....	60
3.5 SART3 INTERACTS WITH CORE AND SUPPORTS VIRAL SPREADING AND VIRION PRODUCTION.....	63

3.6	NOB1 IS REDISTRIBUTED TO CORE-CONTAINING LDs, INTERACTS WITH CORE AND IS REQUIRED FOR VIRAL SPREADING	68
3.7	LARP1 IS INVOLVED IN THE HCV LIFE CYCLE.....	72
3.7.1	<i>LARP1 localizes to core-containing LDs.....</i>	72
3.7.2	<i>LARP1 interacts with core in an RNA-dependent manner</i>	73
3.7.3	<i>LARP1 deficiency impairs recruitment of HCV proteins and dsRNA to LDs</i>	74
3.7.4	<i>LARP1 is required for efficient HCV spreading infection</i>	80
3.7.5	<i>LARP1-knockdown does not affect HCV RNA replication and virion production</i>	81
3.7.6	<i>Cell-to-cell transmission is reduced in LARP1-depleted cells</i>	84
4	DISCUSSION.....	86
4.1	STRENGTH AND LIMITATIONS OF PROXIMITY LABELING USING BIOID2 AND APEX2	86
4.1.1	<i>Identification of the LD proteome using PLIN2-associated proximity labeling</i>	87
4.1.2	<i>Proximity labeling in HCV-infected cells.....</i>	88
4.2	INVESTIGATION OF IDENTIFIED HITS IN HCV-INFECTED CELLS.....	90
4.2.1	<i>FABP5 is not involved in the HCV viral life cycle</i>	90
4.2.2	<i>ARL8B is an HCV host factor</i>	91
4.2.3	<i>SART3 interacts with core and is recruited to LDs in HCV-infected cells.....</i>	93
4.2.4	<i>NOB1 is a new potential HCV host factor</i>	95
4.3	LARP1 IS A HOST FACTOR FOR HCV REPLICATION	96
4.3.1	<i>HCV core recruits LARP1 to LDs</i>	96
4.3.2	<i>LARP1 deficiency impairs recruitment of viral proteins and dsRNA to LDs.....</i>	97
4.3.3	<i>LARP1 is required for efficient HCV cell-to-cell transmission</i>	99
4.4	CONCLUDING REMARKS.....	101
5	MATERIAL.....	103
5.1	BACTERIA	103
5.2	EUKARYOTIC CELL LINES	103
5.3	SOLVENTS AND BUFFERS.....	105
5.3.1	<i>Lysis buffer.....</i>	105
5.3.2	<i>SDS PAGE and western blotting.....</i>	105
5.3.3	<i>Agarose gel electrophoresis.....</i>	106
5.3.4	<i>DNA and protein ladder.....</i>	106
5.3.5	<i>LD isolation buffer.....</i>	106
5.3.6	<i>Buffers for proximity labeling</i>	106
5.3.7	<i>Solutions for immunofluorescence staining.....</i>	107
5.3.8	<i>Buffer for annealing of primers</i>	107
5.4	INHIBITORS	107
5.5	ENZYMES.....	108

5.6	KITS	108
5.7	PLASMIDS.....	109
5.8	OLIGONUCLEOTIDES	114
5.9	ANTIBODIES AND DYES	117
5.10	CONSUMABLES.....	119
5.11	CHEMICALS.....	120
5.12	DEVICES.....	123
5.13	SOFTWARE	124
6	METHODS.....	125
6.1	MOLECULAR BIOLOGICAL METHODS.....	125
6.1.1	<i>Cultivation of bacteria</i>	<i>125</i>
6.1.2	<i>Plasmid isolation.....</i>	<i>125</i>
6.1.3	<i>Glycerol stocks</i>	<i>125</i>
6.1.4	<i>Cloning.....</i>	<i>125</i>
6.1.4.1	Polymerase chain reaction (PCR)	125
6.1.4.2	Overlap extension PCR	126
6.1.4.3	Restriction endonuclease digestion	127
6.1.4.4	Ligation.....	127
6.1.4.5	Ligation independent cloning.....	128
6.1.4.6	Bacterial transformation	128
6.1.4.7	Cloning of BiolD2 and APEX2 fusion constructs	129
6.1.4.8	Cloning of lentiviral expression plasmids for overexpression of identified hits	131
6.1.4.9	Phosphorylation and annealing of oligonucleotides	132
6.1.4.10	DNA Sequencing.....	132
6.1.5	<i>HCV RNA in vitro transcription.....</i>	<i>133</i>
6.1.6	<i>Phenol-chloroform extraction.....</i>	<i>133</i>
6.2	CELL CULTURE TECHNIQUES.....	133
6.2.1	<i>Cell culture</i>	<i>133</i>
6.2.2	<i>Thawing and freezing of eukaryotic cells.....</i>	<i>134</i>
6.2.3	<i>Electroporation of cells with HCV RNA</i>	<i>134</i>
6.2.4	<i>Generation of HCV stocks</i>	<i>134</i>
6.2.5	<i>Determination of viral titers (TCID₅₀).....</i>	<i>135</i>
6.2.6	<i>HCV infection and viral spreading.....</i>	<i>135</i>
6.2.7	<i>Luciferase assays to analyze viral replication</i>	<i>135</i>
6.2.7.1	HCV viral spreading and virion production.....	135
6.2.7.2	HCV RNA replication.....	136
6.2.8	<i>Flow cytometry</i>	<i>136</i>
6.2.9	<i>MTT viability assay</i>	<i>136</i>
6.2.10	<i>Production of lentiviral pseudoparticles and lentiviral transduction.....</i>	<i>136</i>

6.2.11	<i>Transfection of HEK293T cells using calcium phosphate precipitation</i>	137
6.2.12	<i>Transfection of Huh7 cells using FuGENE</i>	137
6.2.13	<i>Immunofluorescence and LD staining for confocal microscopy</i>	137
6.2.14	<i>LD isolation</i>	138
6.2.15	<i>Determination of infected foci for cell-to-cell transmission analysis</i>	138
6.2.16	<i>Co-culturing for cell-to-cell transmission analysis</i>	138
6.2.17	<i>SILAC and proximity labeling</i>	139
6.3	BIOCHEMICAL METHODS	139
6.3.1	<i>Cell lysates</i>	139
6.3.2	<i>SDS-PAGE and western blotting</i>	140
6.3.3	<i>Co-immunoprecipitation</i>	140
6.3.4	<i>RNA isolation</i>	141
6.3.5	<i>cDNA synthesis</i>	141
6.3.6	<i>Quantitative reverse transcriptase PCR (qRT-PCR)</i>	142
6.3.6.1	<i>HCV standards for qRT-PCR</i>	143
6.3.7	<i>Mass spectrometry (MS)</i>	143
6.3.7.1	<i>Protein digestion in the SDS-PAGE matrix</i>	143
6.3.7.2	<i>LC-MS/MS in Data Dependent and Data Independent mode</i>	143
6.3.7.3	<i>Data analysis and processing</i>	144
6.3.8	<i>Data analysis and statistical analysis</i>	144
7	REFERENCES	146
8	APPENDIX	168
8.1	<i>SUPPLEMENTARY DATA</i>	168
8.2	<i>LIST OF FIGURES</i>	172
8.3	<i>LIST OF TABLES</i>	173
8.4	<i>TOXICITY OF CHEMICALS</i>	176
8.5	<i>ACKNOWLEDGEMENT</i>	189
8.6	<i>EIDESSTATTLICHE VERSICHERUNG</i>	190

Abbreviations

°C	degree celsius
∞	infinite
aa	amino acid
ACN	acetonitrile
ACSL	acyl-CoA synthetase long-chain
ANXA	annexin
APEX	engineered ascorbate peroxidase
APO	apolipoprotein
ARL	ADP ribosylation factor-like protein
as	antisense
ATGL	adipose triglyceride lipase
ATP	adenosine triphosphate
BioID	biotin identification
BP	biotin phenol
BSA	bovine serum albumin
BSD	blasticidin S deaminase
BSL	biosafety level
C1QBP	complement component 1Q subcomponent-binding protein
CD81	cluster of differentiation 81
cDNA	complementary DNA
CK	casein kinase
CLDN1	claudin-1
CLSM	confocal laser scanning microscope
Con1 SGR	Con1 subgenomic replicon
cPLA2	cytosolic phospholipase A2
CTCF	corrected total cell fluorescence
CTD	C-terminal domain
d	day
D	domain
DAA	direct acting antivirals
DDA	data dependent acquisition
DDX	DEAD box RNA helicase
DENV	dengue virus

DGAT	diacylglycerol O-acyltransferase
DHCR	dehydrocholesterol reductase
DMSO	dimethyl sulfoxide
DMV	double membrane vesicle
DNA	deoxyribonucleic acid
dpe	days post electroporation
dpi	days post infection
DTT	1,4-dithiothreitol
ECMV	encephalomyocarditis virus
EF1a	eukaryotic translation elongation factor 1 alpha 1
EGFP	enhanced green fluorescent protein
EGFR	epidermal growth factor receptor
EM	electron microscopy
Env	envelope
ER	endoplasmic reticulum
ESCRT	endosomal sorting complex required for transport
FA	formic acid
FABP	fatty acid-binding protein
FCS	fetal calf serum
FLuc	firefly luciferase
fw	forward
Gag	group specific antigen
GLuc	<i>gaussia</i> luciferase
GO	gene ontology
gp	guinea pig
gt	goat
gt	genotype
h	hours
H	heavy
HA	hemagglutinin
HAT	half-a-tetratricopeptide repeat
HBS	hepes buffered saline
HCC	hepatocellular carcinoma
HCV	hepatitis C virus
HEK	human embryonic kidney
HIV-1	human immunodeficiency virus 1
HRP	horseradish peroxidase

HSPG	heparansulfat proteoglycan
Huh	human hepatoma
IF	immunofluorescence
IGF2BP1	insulin-like growth factor-II mRNA-binding protein 1
IKK	I κ B kinase
IP	immunoprecipitation
IRES	internal ribosomal entry site
JFH1	japanese fulminant hepatitis 1
kb	kilo basepair
kDa	kilo dalton
KEGG	Kyoto Encyclopedia of Genes and Genomes
L	liter
L	light
L1ORF1p	LINE1 open reading frame 1 protein
LARP	La-related protein
LC-MS/MS	liquid chromatography-tandem mass spectrometry
LD	lipid droplet
LDL	low-density lipoprotein
LDLR	low-density lipoprotein receptor
LIC	ligation independent cloning
LV	lentivirus
LVP	lipoviroparticle
M	mol/L
M	marker
m/z	mass to charge
MAPK	mitogen-activated protein kinase
MAVS	mitochondrial antiviral signaling protein
mg	milligram
min	minutes
miR	micro RNA
mL	milliliter
mM	millimolar
mm	millimeter
MMV	multi membrane vesicle
MOI	multiplicity of infection
mRNA	messenger RNA
ms	mouse

MS	mass spectrometry
mTORC	mechanistic target of rapamycin complex
MTP	microsomal triglyceride transport protein
MVBs	multivesicular bodies
MW	membranous web
NAFLD	non-alcoholic fatty liver disease
Neo ^R	neomycin resistance
NLS	nuclear localization sequence
nm	nanometer
no	number
NOB	NIN1-binding protein
NPC1L1	Niemann-Pick C1 like1
NS	non-structural
nt	nucleotide
NT	non-targeting
o/n	over night
OCLN	occludin
ORF	open reading frame
OSBP	oxysterol-binding protein
PABPC1	polyA binding protein cytoplasmic 1
PBS	phosphate buffered saline
PCBP	poly(rC)-binding protein
PCR	polymerase chain reaction
PEG	polyethylene glycol
PEG-IFN α	pegylated interferon alpha
PFA	paraformaldehyde
PI4P	phosphatidylinositol-4-phosphate
PI5P	phosphatidylinositol 5-phosphate
PLIN	Perilipin
PMSF	phenylmethylsulfonyl fluoride
PNS	post-nuclear supernatant
Pol	polymerase
polyA	polyadenylation
polyU	polyuridine
qRT	quantitative reverse transcriptase
r	pearson correlation coefficient
Rab	Ras-related in brain

rb	rabbit
RdRp	RNA-dependent RNA polymerase
rev	reverse
RFP	red fluorescent protein
RIG-I	retinoic acid inducible gene 1
RLU	relative light units
RNA	ribonucleic acid
RNA Pol II	RNA polymerase II promotor
RNP	ribonucleoprotein
ROI	region of interest
rpm	revolutions per minute
RRM	RNA recognition motif
rRNA	ribosomal ribonucleic acid
RT	reverse transcriptase
rt	room temperature
s	seconds
SARS-CoV2	severe acute respiratory syndrome coronavirus type 2
SART	squamous cell carcinoma antigen recognized by T-cells
SDS	sodium dodecyl sulfate
SDS-PAGE	sodium dodecyl sulfate polyacrylamide gel electrophoresis
SE	sterol ester
SEM	standard error of the mean
SG	stress granula
sh	short hairpin
SILAC	stable isotope labeling by amino acids in cell culture
SPP	signal peptide peptidase
SRBI	scavenger receptor B1
SV40 polyA	simian virus 40 polyA signal
SVR	sustained virological response
t	transduction/transfection
TAG	triglycerides
TCID ₅₀	50% tissue culture infective dose
TLR	toll-like receptor
T _m	melting temperature
ToMV	tomato mosaic virus
TOP	terminal oligopyrimidine
Trolox	6-hydroxy-2,5,7,8-tetramethylchroman-2-carboxylic acid

USP	ubiquitin-specific protease
UTR	untranslated region
UV	ultraviolet
V	volt
v/v	volume per volume
VAP	vesicle-associated membrane protein-associated protein
VLDL	very low-density lipoprotein
VLP	virus-like particles
w/v	weight per volume
WB	western blot
wt	wild type
x <i>g</i>	times gravity
YB-1	Y-box binding protein 1
ZAP	Zinc finger antiviral protein
μF	microfarrad
μg	microgram
μl	microliter
μM	micromolar

Zusammenfassung

Steigende Hepatitis-C-Virus (HCV)-Infektionsraten und die wachsende Opioidkrise in den USA zeigen eine demografische Verschiebung der Infektionslast hin zu jüngeren Menschen. Aufgrund der leichten Symptomatik bleiben viele Infektionen unerkannt, bis eine chronische Infektion Jahre später schwere Leberschäden verursacht. Die Einführung direkt wirkender antiviraler Medikamente (*direct-acting antivirals*, DAA) ermöglicht eine wirksame Behandlungsmöglichkeit für HCV Infektionen. Da kein Impfstoff zur Verfügung steht, bleibt HCV jedoch ein ernstzunehmendes Problem.

Der Lebenszyklus des HCV ist eng mit dem Lipidstoffwechsel des Wirts verbunden, wobei *lipid droplets* (LDs) als virale Assemblierungsplattformen dienen. Perilipin (PLIN) 2, das Hauptprotein an der LD-Oberfläche in Hepatozyten, spielt eine wichtige Rolle bei der HCV-Morphogenese, da es für die Bildung infektiöser Partikel benötigt wird. Eine frühere LD-Proteomanalyse ergab, dass eine HCV-Infektion die Proteinzusammensetzung an LDs in Huh7.5-Zellen erheblich verändert. In dieser Studie wurde Annexin A3 (ANXA3) als wichtiger Wirtsfaktor für HCV identifiziert, der in infizierten Zellen an die LDs rekrutiert wird und für die Reifung und den Austritt von HCV-Partikeln erforderlich ist.

In dieser Dissertation wurde ein *proximity labeling* der oben genannten Proteine durchgeführt, um die molekularen Details der späteren Schritte des HCV-Lebenszyklus weiter zu charakterisieren. Die Biotinligase BioID2 sowie die gentechnisch veränderte Ascorbatperoxidase APEX2 wurden an PLIN2 oder ANXA3 fusioniert, um Proteine in räumlicher Nähe von LDs in HCV-infizierten Zellen durch Massenspektrometrie zu identifizieren. Dafür wurden HCV-infizierte und nicht-infizierte Huh7.5-Zellen, die die jeweiligen Fusionsproteine stabil exprimierten, mittels SILAC analysiert, um die durch eine Infektion hervorgerufenen Unterschiede in ANXA3- und PLIN2-proximalen Proteinen zu ermitteln. Durch Massenspektrometrie identifizierte biotinylierte Proteine wurden auf ihre mutmaßliche Rolle im HCV-Lebenszyklus untersucht. Hierbei wurden die Proteine FABP5 (*fatty acid-binding protein 5*), ARL8B (*ADP ribosylation factor-like protein 8B*), SART3 (*RNA-binding protein squamous cell carcinoma antigen recognized by T-cells 3*; auch bekannt als TIP110), NOB1 (*NIN1-binding binding protein 1*) und LARP1 (*La-related protein 1*) charakterisiert und ARL8B, SART3, NOB1 und LARP1 als HCV-Wirtsfaktoren identifiziert. Mit besonderem Fokus auf LARP1 wurde eine Core-abhängige Rekrutierung zu LDs durch Westernblot und Immunfluoreszenzanalysen beobachtet. Darüber hinaus interagierte LARP1 RNA-abhängig mit Core, auch in Zellen, die nicht infiziert waren. Der *Knockdown* von LARP1 verringerte die HCV-Vermehrung,

ohne die HCV-RNA-Replikation oder die Virustiter zu verändern. Isolierte LD-Fractionen von HCV-infizierten Zellen sowie mikroskopische Analysen zeigten eine verminderte Rekrutierung der viralen Proteine Core und NS5A zu LDs in LARP1-Knockdownzellen. Immunfluoreszenzfärbung von HCV doppelsträngiger RNA (dsRNA) zeigte eine verringerte Signalintensität von dsRNA-Foci sowie eine verringerte Kolo-kalisierung von dsRNA mit LDs in infizierten LARP1-Knockdownzellen. Zudem reduzierte die Depletion von LARP1 die direkte Zell-zu-Zell-Übertragung (*cell-to-cell transmission*) von HCV signifikant.

Zusammenfassend erweitert diese Dissertation das Verständnis von LARP1 als HCV-Wirtsfaktor, der höchstwahrscheinlich an den späteren Schritten des viralen Lebenszyklus beteiligt ist und zur direkten Virusübertragung von Zelle zu Zelle beiträgt.

Abstract

With the growing opioid crisis in the USA, hepatitis C virus (HCV) infection rates increase and lead to a demographic shift towards young individuals. However, due to mild symptoms many infections remain unrecognized until chronic infection and inflammation cause severe liver damage years later. The introduction of direct-acting antivirals (DAA) has offered potent treatment options for HCV infections, but HCV remains a serious health concern, since a vaccine is not available. The HCV viral life cycle is tightly connected to the host lipid metabolism with lipid droplets (LDs) serving as viral assembly sites. Perilipin (PLIN) 2, the major LD-decorating protein in hepatocytes, has been shown to play an important role in HCV morphogenesis, as it is required for the formation of infectious HCV particles. A previous LD proteome analysis revealed that an HCV infection considerably changes the protein composition at LDs in Huh7.5 cells. In that study, annexin A3 (ANXA3) has been identified as an important host factor for HCV that redistributes to LD fractions and is required for HCV particle maturation and egress.

In this study, proximity labeling of the above-mentioned proteins was performed to further characterize the molecular details of the later steps of the HCV viral life cycle. The biotin ligase BiLD2 as well as the engineered ascorbate peroxidase APEX2 were genetically fused to PLIN2 or ANXA3 to identify proteins in spatial vicinity of LDs in HCV-infected cells by mass spectrometry. Therefore, HCV-infected and uninfected Huh7.5 cells stably expressing the respective fusion proteins were prepared for SILAC labeling to identify differences in ANXA3 and PLIN2-proximal proteins. Biotinylated proteins identified by mass spectrometry were investigated for their putative roles in the HCV life cycle. Here, the proteins FABP5 (fatty acid-binding protein 5), ARL8B (ADP ribosylation factor-like protein 8B), SART3 (RNA-binding protein squamous cell carcinoma antigen recognized by T-cells 3; also known as TIP110), NOB1 (NIN1-binding binding protein 1), and LARP1 (La-related protein 1) were investigated. The data revealed ARL8B, SART3, NOB1, and LARP1 as host factors for HCV replication. Focusing on LARP1 in greater detail, a core-dependent recruitment to LDs was observed by western blotting and immunofluorescence analysis. Additionally, LARP1 interacted with core in an RNA-dependent manner, even in the absence of infection. Knockdown of LARP1 decreased HCV spreading without altering HCV RNA replication or viral titers. Isolated LD fractions of HCV-infected cells as well as microscopic analyses showed an impaired recruitment of the viral proteins core and NS5A to LDs in LARP1-knockdown cells. Immunofluorescence staining of HCV double-stranded RNA (dsRNA) indicated a reduced signal intensity of dsRNA foci, as well as decreased colocalization of dsRNA

with LDs in infected LARP1-knockdown cells. In addition, LARP1 depletion caused a significant decrease in cell-to-cell transmission.

Taken together, this study expands the role of LARP1 as an HCV host factor that is most likely involved in the later steps of the viral life cycle, contributing to cell-to-cell transmission.

1 Introduction

1.1 Hepatitis C Virus

Hepatitis C virus (HCV) infection is a major cause of liver cirrhosis and hepatocellular carcinoma (HCC). HCV often causes mild symptoms and ~30% of infected individuals clear the virus within 6 months of infection, even without treatment (Micallef *et al.*, 2006). However, 70% develop a chronic infection with a 15–30% risk of establishing liver cirrhosis within 20 years (World Health Organization, 2021).

Globally, estimated 58 million people are chronically infected and 1.5 million new infections are reported on average per year. Of the 58 million chronically infected, only 21% were aware of their diagnosis in 2019 (World Health Organization, 2021). Annually, 0.3 million people die due to HCV-induced liver cirrhosis and HCC (World Health Organization, 2021). Recent studies have shown that the growing opioid epidemic in the US, which mostly affects millennials (born 1980–1995), is associated with rising numbers of acute HCV infections (Zibbell *et al.*, 2018) as well as a demographic shift towards younger individuals (Rose *et al.*, 2019).

1.2 HCV infection, disease, and treatment

HCV is a bloodborne virus causing inflammation of the liver leading to acute and chronic hepatitis. The main transmission routes are contaminated medical equipment, transfusion of unscreened blood products, and needle sharing for intravenous drug use (Thursz and Fontanet, 2014).

After initial infection, most individuals do not experience any symptoms. If symptomatic, patients may suffer from fatigue, nausea, fever, loss of appetite, abdominal pain, and yellowing of skin and eyes. For diagnosis, serological testing for anti-HCV antibodies identifies infection, followed by HCV RNA testing to diagnose chronic infection. However, due to the low rate of symptomatic infections, few people are diagnosed in the early stages of infection and are only diagnosed years later after liver damage has already occurred (World Health Organization, 2021).

For treatment, pan-genotypic direct-acting antivirals (DAA) are recommended, as this regimen can achieve sustained virological response (SVR) rates over 95% (Kohli *et al.*, 2015; Webster *et al.*, 2015; World Health Organization, 2021; Zhang, 2016). DAAs replaced the treatment with PEGylated interferon α (PEG-IFN α) in combination with the guanosine analogue ribavirin. Compared to DAA treatment, IFN therapy had a lower SVR rate especially in cases of advanced liver damage as well as severe side effects (Manns *et al.*, 2006; Webster *et al.*, 2015). DAAs aim to inhibit three targets of HCV: the

NS3/4A protease, NS5A, and the NS5B polymerase. These therapies interfere with HCV polyprotein processing or HCV RNA replication. Recent studies suggest including viral entry inhibitors in the treatment to limit re-infection of patients with liver transplants, which most likely occurs due to cell-to-cell transmission (Qian *et al.*, 2016). Despite the success of developing therapies, antiviral treatment remains expensive in many countries (Bidell *et al.*, 2016) and there is no vaccine available.

1.3 HCV epidemiology and classification

HCV belongs to the *Flaviviridae* family, which includes the genera *Flavivirus*, *Pegivirus*, and *Pestivirus* next to *Hepacivirus*. The genus *flavivirus* includes the human pathogenic yellow fever, west nile, dengue, zika, tick-borne encephalitis, and japanese encephalitis virus. HCV is the predominant member of the *hepacivirus* genus amongst non-primate hepaciviruses (Simmonds *et al.*, 2017). HCV was first identified in 1989 (Choo *et al.*, 1989) and today, seven genotypes (1–7) with several subtypes are described (Smith *et al.*, 2014). With 12 million chronically infected persons, the Eastern Mediterranean Region and Europe pose the highest disease burden worldwide.

Globally, genotype 1 is the most prevalent (46.2%) and accounts for most infections in Europe, North and South America as well as East Asia (Figure 1). The genotypes 2, 3, 4 and 6 cause 9.1%, 30.1%, 8.3% and 5.4% of HCV infections, respectively. Genotype 5 accounts for less than 1% of infections (Messina *et al.*, 2015) and only one infection has been reported with genotype 7 (Murphy *et al.*, 2007; Scheel and Rice, 2013). Sequence variance between the genotypes can be up to approximately 30–35% and up to 15% within the genotypes.

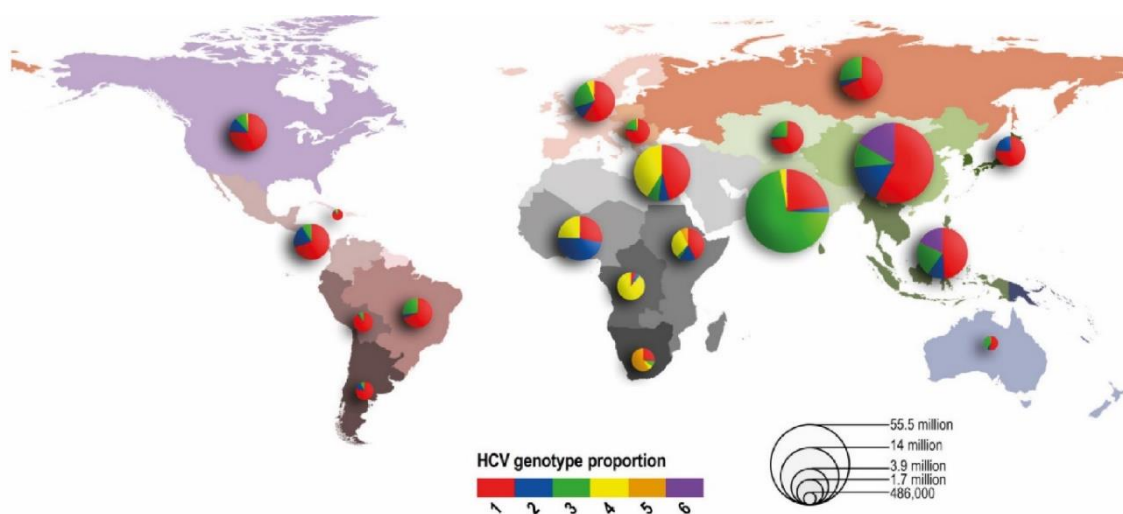


Figure 1: **Worldwide prevalence of HCV.**

Relative prevalence of genotypes is indicated by the color code, the size of pie charts represents with the number of cases (modified from Messina *et al.*, 2015).

1.4 HCV particles

HCV is an enveloped virus of 40–100 nm containing a positive-sense single-stranded RNA genome encapsidated by the core protein. Particles are pleiomorphic and surrounded by a membrane bilayer that embeds the glycoproteins E1 and E2 (Catanese *et al.*, 2013b; Gastaminza *et al.*, 2010) (Figure 2A). HCV particles associate with low density- and very-low density lipoproteins (LDL and VLDL) and neutral lipids as a lipoviriparticle (LVP) (Lavie and Dubuisson, 2017; Vieyres and Pietschmann, 2019). The lipid composition and protein/lipid ratio (buoyant density) of HCV particles are similar to those of LDL and VLDL (Bartenschlager *et al.*, 2011; Catanese *et al.*, 2013b; Lindenbach, 2013; Merz *et al.*, 2011). Cholesterol makes up half of the lipids associated with HCV. Depletion of cholesterol or hydrolysis of triglycerides leads to an altered density and reduced infectivity (Aizaki *et al.*, 2008; Shimizu *et al.*, 2010; Yamamoto *et al.*, 2011). HCV particles display a low buoyant density of 1.03–1.20 g/cm³ (Andre *et al.*, 2002). In cell culture, lower density fractions are the most infectious (Bradley *et al.*, 1991; Lindenbach *et al.*, 2006). High amounts of triglycerides and the apolipoproteins E (APOE) and B (APOB) are found in low-density fractions of density gradient isolates (<1.08 g/cm³), together with the majority of HCV RNA (Nielsen *et al.*, 2006; Nielsen *et al.*, 2008). Interestingly, APOA-I and APOC are additional components of LVPs (Lindenbach, 2013). For efficient particle production, the incorporation of APOE *via* interaction with the non-structural protein NS5A as well as E2 with is crucial (Benga *et al.*, 2010; Lee *et al.*, 2014). The involvement of APOE in particle production is strain and cell type specific, however, APOE incorporation is preferred over APOA1, APOA2, APOC1 or APOC3 (Weller *et al.*, 2017). Currently, two models are suggested to understand the interaction between viral particles and lipoproteins: (1) a transient or stable interaction between the HCV particle and lipoproteins (two-particle model) (Figure 2B) or (2) a hybrid lipoviriparticle, where lipoproteins and the particle share common membranes (single-particle model), which is supported by electron microscopy (EM) data (Figure 2C) (Catanese *et al.*, 2013b; Lindenbach and Rice, 2013). Apart from apolipoproteins, various other host proteins are associated with purified HCV particles, supporting the hypothesis of a complex virus-host interaction during particle production (Lussignol *et al.*, 2016).

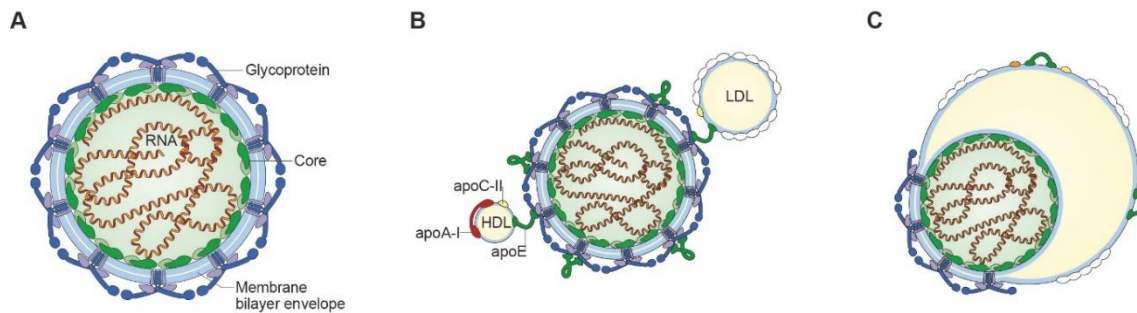


Figure 2: **Model of the HCV particle.**

(A) Morphology of the HCV virion showing the viral RNA encapsidated by the core protein, and the membrane bilayer with the E1/E2 glycoprotein dimers. (B) Two-particle model of the HCV LVP. (C) Single-particle model of the HCV LVP. (Modified from Lindenbach and Rice, 2013).

1.5 HCV replication cycle

Successful replication of HCV essentially depends on liver-specific factors, such as APOE and microRNA 122 (miR-122) (Chang *et al.*, 2007; Da Costa *et al.*, 2012; Jopling *et al.*, 2005). Thus, HCV specifically infects hepatocytes. Altogether, HCV replication is a multistep process strongly dependent on the host cell machinery. A model of the HCV life cycle is illustrated in Figure 3.

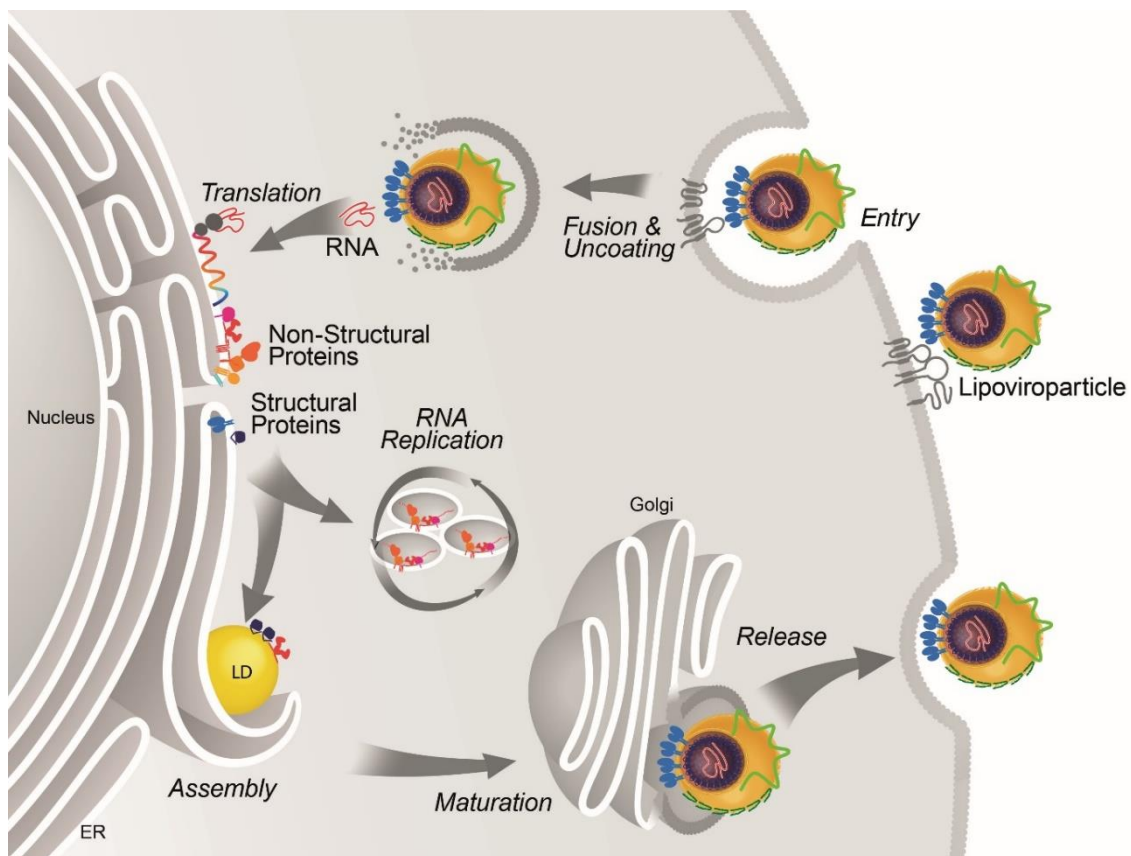


Figure 3: **The HCV replication cycle.**

Following attachment to hepatocyte surface receptors and clathrin-mediated endocytosis, the viral genome is uncoated and translated into one single polypeptide, which is subsequently

processed by cellular and viral proteases into the three structural proteins (the capsid protein core and the envelope glycoproteins E1 and E2) and the seven non-structural proteins (p7, NS2, NS3, NS4A, NS4B, NS5A and NS5B). HCV RNA replication is localized at characteristic vesicular membrane structures, mainly double membrane vesicles (DMVs). The replication vesicles containing the viral proteins NS3–NS5B are located in close proximity to cytosolic LDs. LDs act as assembly platform for HCV progeny particles. For maturation, the virion associates with lipoproteins and most likely egresses *via* the secretory pathway. (Figure kindly provided by Eva Herker (modified from Herker and Ott, 2012)).

1.5.1 HCV entry and viral transmission

HCV entry into hepatocytes is dependent on the interaction of viral envelope proteins and host lipoproteins on viral particles and the host factors expressed at the surface of the cell. The four major factors initiating HCV entry are the cluster of differentiation 81 (CD81), scavenger receptor class B type I (SRBI), claudin-1 (CLDN1), and occludin (OCLN) (Colpitts *et al.*, 2020; Lindenbach and Rice, 2013). Though none of these factors accounts for the specific tissue tropism of HCV, OCLN and CD81 confer to the narrow species tropism (Ding *et al.*, 2017; Dorner *et al.*, 2013; Ploss *et al.*, 2009). HCV can enter hepatocytes *via* two distinct paths: (1) cell-free virus entry and (2) through cell-to-cell transmission. HCV reaches the liver *via* the bloodstream as a LVP and enters the cell *via* clathrin-mediated endocytosis. Attachment to hepatocytes relies on lipoprotein components associated with the viral particle — APOE in particular (Andre *et al.*, 2002; Hishiki *et al.*, 2010; Jiang *et al.*, 2012; Maillard *et al.*, 2006; Merz *et al.*, 2011; Sir *et al.*, 2012) — as well as viral glycoproteins interacting with highly sulfated heparin sulfate proteoglycans (HSPGs) (Barth *et al.*, 2006b; Koutsoudakis *et al.*, 2006; Morikawa *et al.*, 2007), the LDL receptor (LDLR) (Agnello *et al.*, 1999; Molina *et al.*, 2007; Monazahian *et al.*, 1999; Wunschmann *et al.*, 2000), and SRBI (Barth *et al.*, 2005; Bartosch *et al.*, 2003; Catanese *et al.*, 2007; Dao Thi *et al.*, 2012; Dreux *et al.*, 2009a; Scarselli *et al.*, 2002) on the cell surface (Figure 4). Interestingly, the phosphatidylserine receptor TIM-1/human hepatitis A virus cellular receptor 1 (HAVCR1)/CD365, which serves as a host factor for multiple flaviviruses, has recently been identified as an entry factor for HCV (Kachko *et al.*, 2018; J. Wang *et al.*, 2017). After initial attachment *via* lipoproteins, the host cell receptors SRBI, CD81, and CLDN interact with the viral envelope proteins allowing internalization of the virus. Binding of HCV E2 to SRBI activates lipid transfer of SRBI, exposing binding sites of E2, thus allowing the interaction of E2 with CD81 (Dreux *et al.*, 2009a). Intriguingly, after depletion of SRBI, small amounts of virions are still able to enter the cell (Kalemera *et al.*, 2019). However, binding of E2 to CD81 is crucial to promote virion internalization by activating receptor tyrosine kinases such as epidermal growth factor receptor (EGFR) and Rho and Ras GTPases (Brazzoli *et al.*, 2008; Lupberger *et al.*, 2011; Pileri *et al.*, 1998). EGFR is involved in recruiting clathrin-coated

vesicles for internalization (Baktash *et al.*, 2018). Downstream activation leads to actin rearrangements, enabling CD81 to interact with the tight junction protein CLDN1, a process that drives HCV entry (Harris *et al.*, 2010; Harris *et al.*, 2008). Another tight junction protein, OCLN, has been proposed as an essential entry factor for later post-binding steps (Benedicto *et al.*, 2009; Sourisseau *et al.*, 2013). Most likely, OCLN is involved in endocytosis by interaction with the GTPase dynamin II (Liu *et al.*, 2010). Recently, the Abl tyrosine kinase was identified as a host factor promoting clathrin-mediated endocytosis (Min *et al.*, 2017), as well as the transferrin receptor 1 (TfR1) for particle uptake (Martin and Uprichard, 2013), however, the exact mechanism is still poorly understood. The Niemann-Pick C1-like 1 (NPC1L1) cholesterol absorption receptor facilitates HCV entry as a cholesterol receptor (Sainz *et al.*, 2012). Subsequently, interaction of the entry factors leads to clathrin-mediated or dynamin-dependent endocytosis (Blanchard *et al.*, 2006; Farquhar *et al.*, 2012). Acidic endosomes drive the low pH-dependent HCV fusion in order to release the viral genome into the cytoplasm (Bartosch *et al.*, 2003; Meertens *et al.*, 2006; Tscherne *et al.*, 2006).

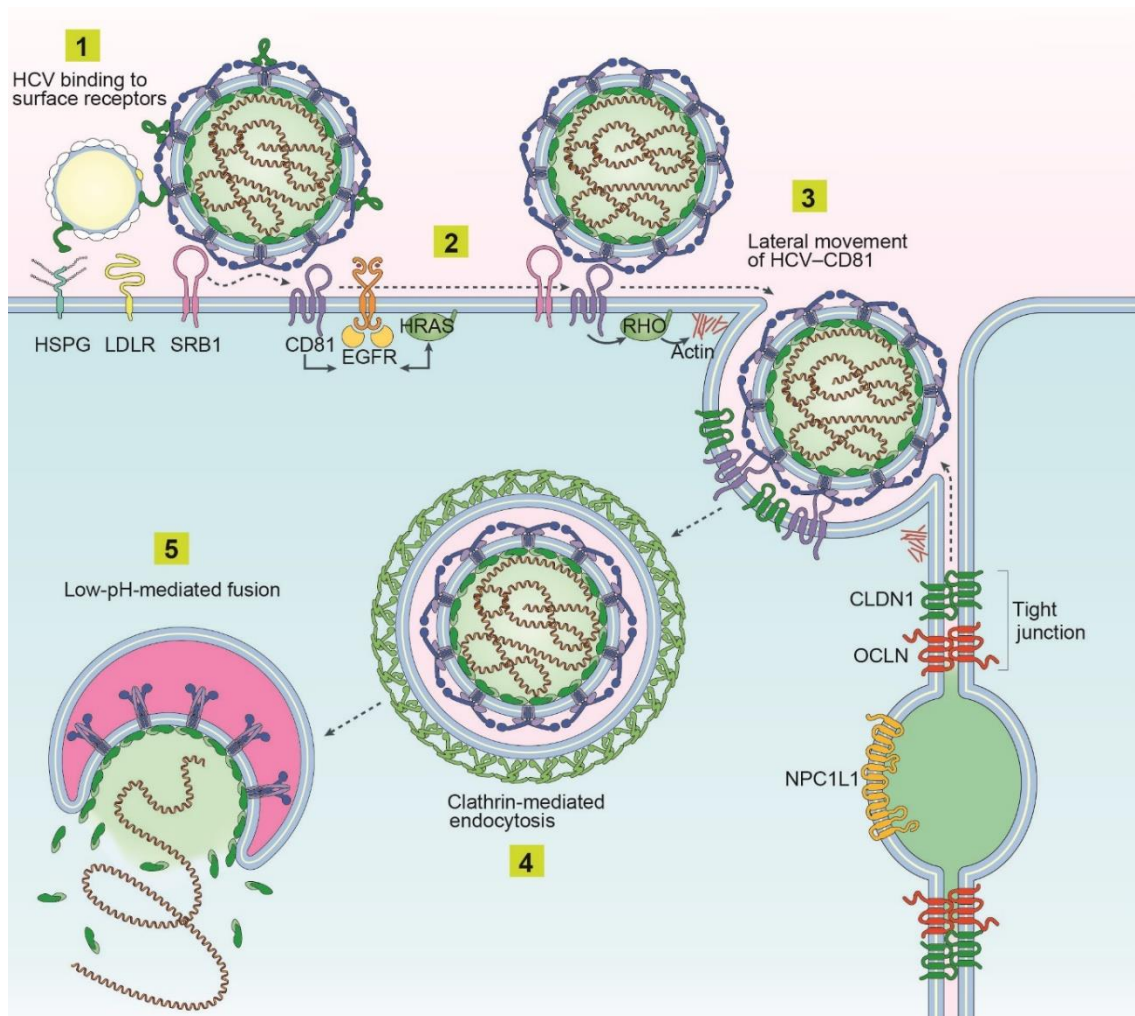


Figure 4: **Model of HCV entry.**

HCV LVPs attach to the hepatocyte surface *via* heparin sulphate proteoglycans (HSPG), low-density-lipoprotein receptor (LDLR) and scavenger receptor class B member 1 (SRBI). E2 binding to SRBI leads to a lipid transfer and exposes the E2 binding site for CD81 (1). Interaction of E2 with CD81 activates a signaling cascade through the epidermal growth factor receptor (EGFR)/HRAS and Rho GTPases (2). This induces lateral movement of HCV-CD81 (3) and interaction of CD81 with CLDN1, initiating internalization of HCV *via* clathrin-mediated endocytosis (4). A low pH of endosomes enables virion fusion (5). NPC1L1 (Niemann-pick C1 like 1); OCLN (occludin). (Modified from Lindenbach and Rice, 2013).

While the previously described mechanisms apply to cell-free infection, HCV can spread to neighboring cells after initial infection *via* cell-to-cell transmission. A recent study showed that glycometabolism regulates HCV release *via* cell-free transmission, whereas cell-to-cell transmission was not affected, supporting the theory of two distinct pathways (Yu *et al.*, 2021). Likely, cell-to-cell transmission largely contributes to viral persistence and resistance to neutralizing antibodies (Brimacombe *et al.*, 2011; Timpe *et al.*, 2008). Thus, cell-to-cell transmission potentially promotes chronic infection (Barretto *et al.*, 2014). Interestingly, a study reported that DAA-resistant HCV strains use cell-to-cell transmission as the main route of viral spreading, therefore promoting viral persistence (Xiao *et al.*, 2014). The process has not been investigated as intensely as cell-free entry, however, various factors involved in cell-free entry appear to promote cell-to-cell transmission as well (Colpitts *et al.*, 2020; Miao *et al.*, 2017; Xiao *et al.*, 2014). Studies have suggested that CD81, SRBI, CLDN1, OCLN, EGFR, NPC1L1, and LDLR contribute to cell-to-cell transmission (Brimacombe *et al.*, 2011; Catanese *et al.*, 2013a; Timpe *et al.*, 2008). Seemingly, spreading between adjacent hepatocytes requires mature particles, as one recent study showed that HCV structural proteins and p7 are needed for efficient cell-to-cell transmission (Zhao *et al.*, 2017). In line, APOE expression in donor cells is essential for cell-to-cell transmission (Gondar *et al.*, 2015; Hueging *et al.*, 2014; Zhao *et al.*, 2017), while APOE expression in recipient cells does not affect transmission (Gondar *et al.*, 2015; Zhao *et al.*, 2017). CD81-independent cell-to-cell transmission has been reported (Jones *et al.*, 2010; Witteveldt *et al.*, 2009). Additionally, HCV RNA containing exosomes have been isolated, however, if transfer of replication competent HCV genomes or virions is functional *via* this route is still under debate (Longatti *et al.*, 2015; Medvedev *et al.*, 2017; Zhao *et al.*, 2017). In summary, these results indicate that cell-free entry and cell-to-cell transmission require the same players, but the regulation and interplay of viral and host factor differs and the exact mechanism of cell-to-cell transmission remains poorly understood.

1.5.2 HCV genome organization and translation

The HCV genome is a 9.6 kb positive single-stranded RNA. It contains a 5'- and a 3'-untranslated region (UTR), flanking a single open reading frame (ORF) (Figure 5). The

5'-UTR includes the internal ribosome entry site (IRES) and binding sites for the miR-122 (Jopling *et al.*, 2008). Binding of miR-122 to the 5'-UTR plays a pivotal role for HCV replication by protecting the RNA from degradation (Jopling *et al.*, 2005; Sedano and Sarnow, 2014). At the ER, translation is initiated by the IRES, resulting in one single polyprotein (Moradpour *et al.*, 2007). Co- and post-translational processing by cellular and viral proteases give rise to the three structural proteins (core, E1 and E2) as well as the seven non-structural proteins (p7, NS2, NS3, NS4A, NS4B, NS5A and NS5B). Structural proteins and p7 are cleaved by the ER signal peptidases. The non-structural proteins on the other hand are processed by the NS2 cysteine autoprotease dividing NS2/NS3, whereas the NS3/4A serine protease cleaves the remaining non-structural proteins (Figure 5) (Scheel and Rice, 2013).

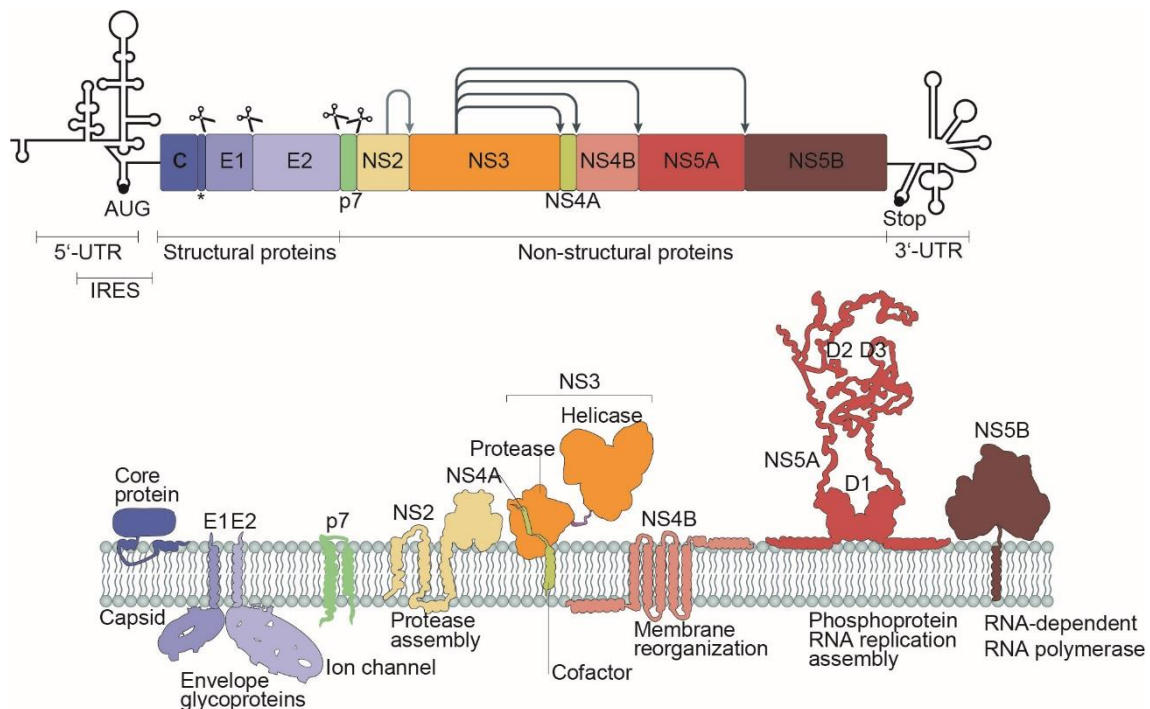


Figure 5: HCV genome organization and viral protein membrane topology.

The ~9.6 kb long HCV RNA genome is flanked by 5'- and 3'-UTRs. The 5'-UTR contains the internal ribosome entry site (IRES) that initiates cap-independent translation of the viral RNA into a precursor polyprotein. Processing of the polyprotein by viral proteases is indicated by arrows, cleavage by cellular signal peptidases is indicated by scissors. Processing of the core protein C-terminal domain by cellular signal peptide peptidase is indicated by an asterisk. (Modified from Neufeldt *et al.*, 2018).

Core

The main function of the core protein is the formation of the viral nucleocapsid surrounding the RNA genome (Gawlik and Gallay, 2014). After cleavage by the signal peptidase, the immature form of core is a 191-amino-acid protein (23 kDa). After further

C-terminal processing, the mature core protein yields 177 amino acids (21 kDa) and is an α -helical dimer (Boulant *et al.*, 2005; Lussignol *et al.*, 2016; McLauchlan *et al.*, 2002). The immature core consists of three domains (D1, D2, and D3). The hydrophilic domain at the N-terminus (D1) (~117 aa) is rich in basic residues. It is mainly involved in RNA binding (Ivanyi-Nagy *et al.*, 2006; Santolini *et al.*, 1994; Yu *et al.*, 2009) and required for homo-oligomerization ensuring efficient particle formation (Klein *et al.*, 2005; Kunkel and Watowich, 2002; Matsumoto *et al.*, 1996; Nakai *et al.*, 2006; Nolandt *et al.*, 1997). The hydrophobic D2 domain of ~50 aa consists of a helix-turn-helix motif facilitating the association of core with membranes of the ER, including the membranous web, and LDs as well as proper folding (Boulant *et al.*, 2006; Boulant *et al.*, 2005). The D2-dependent association with LDs is essential for particle production (Boulant *et al.*, 2006; Miyanari *et al.*, 2007; Shavinskaya *et al.*, 2007), as core mutants that are unable to associate with LDs are degraded by the proteasome. The highly hydrophobic D3 domain at the C-terminus functions as signal peptide for E1 at the ER (Santolini *et al.*, 1994). Cleavage of D3 by the signal peptide peptidase removes the signal peptide for ER localization and is therefore crucial for the production of infectious particles (McLauchlan *et al.*, 2002; Targett-Adams *et al.*, 2008). Core plays a central role in recruiting the replication complexes and non-structural proteins to the assembly sites at LDs (Miyanari *et al.*, 2007). Expression of core and interaction with numerous host proteins results in altered cellular functions such as the lipid metabolism, apoptosis, and cell signaling (Khaliq *et al.*, 2011; McLauchlan *et al.*, 2002). Thus, core expression has been linked to development of steatosis (Moriya *et al.*, 1997; Perlemuter *et al.*, 2002) and cancerogenesis (Moriya *et al.*, 1998; Tanaka *et al.*, 2008), indicating a key role in HCV-induced liver diseases.

E1 and E2

The envelope proteins E1 (35 kDa) and E2 (72 kDa) are post-translationally N-glycosylated and build the viral envelope by forming heterodimers (Deleersnyder *et al.*, 1997; Dubuisson *et al.*, 2002). The C-terminally located transmembrane domains have ER retention properties (Op De Beeck *et al.*, 2000). The N-terminus harbors a large ectodomain facing the ER lumen (Voisset and Dubuisson, 2004). Both envelope proteins are essential for viral entry by interacting with various HCV receptors (Barth *et al.*, 2006a; Barth *et al.*, 2006b), as well as for lipoviriparticle formation by incorporating APOE *via* the interaction between APOE and E2 (Lee *et al.*, 2014).

p7

p7 is a small (7 kDa) hydrophobic transmembrane protein. It harbors two transmembrane segments forming a cytosolic loop and both, the N- and C-terminus are facing the ER lumen (Carrere-Kremer *et al.*, 2002). As a viroporin, p7 forms ion channels by oligomerizing to hexamers (Griffin *et al.*, 2003; Pavlovic *et al.*, 2003). By directly interacting with NS2, p7 is important for viral assembly (Popescu *et al.*, 2011; Steinmann *et al.*, 2007). Wozniak *et al.* suggested an ion channel activity would protect progeny virions from acidification during maturation and egress (Wozniak *et al.*, 2010).

NS2

NS2 is 23 kDa with three transmembrane domains at the N-terminus. The NS2 cysteine protease is responsible for cleaving the NS2/NS3 junction. The catalytic activity is located at the C-terminus of NS2 and N-terminally at NS3 (Grakoui *et al.*, 1993; Hijikata *et al.*, 1993). Similar to p7, HCV RNA replication is independent on NS2. However, NS2 is required for HCV assembly by promoting binding of E1/E2, p7 and NS3/4A and it directly interacts with p7 (Jones *et al.*, 2007; Popescu *et al.*, 2011).

NS3/4A

NS3 (70 kDa) is a multifunctional protein containing a serine protease at the N-terminus and an RNA helicase/NTPase at the C-terminus (Moradpour *et al.*, 2007). NS4A (6 kDa) serves as a cofactor for the serine protease activity and its N-terminal α -helix ensures membrane association of the NS3/4A complex (Brass *et al.*, 2008; Wolk *et al.*, 2000). The NS3/4A complex is responsible for cleavage of non-structural proteins of the HCV precursor polyprotein (Failla *et al.*, 1994). Interestingly, the NS3/4A protease targets host factors such as the 24-dehydrocholesterol reductase (DHCR24), thus directly regulating the host lipid metabolism (Tallorin *et al.*, 2020). Additionally, by cleaving the mitochondrial antiviral signaling protein (MAVS) and TLR3 adaptor TRIF, NS3/4A severely interferes with cellular immune cascades supporting HCV immune evasion (Cao *et al.*, 2015; K. Li *et al.*, 2005; X. D. Li *et al.*, 2005; Meylan *et al.*, 2005).

NS4B

The 27 kDa integral membrane protein NS4B has four transmembrane domains and two N-terminally located α -helices. NS4B is palmitoylated at its C-terminus to form oligomers (Yu *et al.*, 2006). Importantly, NS4B plays a crucial role in inducing membrane alterations forming the membranous web (Egger *et al.*, 2002). Small portions of NS4B are located close to the LD surface, however, NS4B likely remains attached to the ER, suggesting NS4B tethers ER and LDs (Tanaka *et al.*, 2013).

NS5A

The phosphoprotein NS5A can be found in the basally phosphorylated (56 kDa) and hyperphosphorylated (58 kDa) form. Besides core, NS5A is the second viral protein that localizes to LDs. The protein consists of three distinct domains. The D1 domain contains an N-terminally located amphipathic helix anchoring the protein to the ER membrane (Brass *et al.*, 2002; Penin *et al.*, 2004). D1 shows RNA-binding properties (Huang *et al.*, 2005; Tellinghuisen *et al.*, 2005), facilitates binding to LDs, and is crucial for the formation of double membrane vesicles (DMVs). Both D1 and D2 are involved in HCV RNA replication (Romero-Brey *et al.*, 2012), but deletion mutations in the D2 domain had no effect on RNA replication (Appel *et al.*, 2005; Blight *et al.*, 2000). D3 plays an essential role in HCV assembly by interacting with core (Masaki *et al.*, 2008; Miyanari *et al.*, 2007).

NS5B

The RNA-dependent RNA polymerase (RdRp) NS5B is a tail anchored 68 kDa protein (Schmidt-Mende *et al.*, 2001). ER membrane association is mediated by the C-terminus, which is required for RNA replication, but dispensable for the polymerase activity itself (You *et al.*, 2004). Facing the cytosol is the catalytic domain acting as RNA polymerase using the genome as a template to synthesize complementary negative-strand RNA intermediate and subsequently positive-strand RNA (Moradpour *et al.*, 2007). NS5B has three RdRp characteristic subdomains called finger, palm, and thumb domains. The interaction between finger and thumb forms an enclosed active site (Bressanelli *et al.*, 1999; Lesburg *et al.*, 1999).

1.5.3 HCV RNA replication

NS5B facilitates viral replication by synthesizing *de novo* positive-strand RNA *via* a negative-strand RNA intermediate. HCV RNA replication occurs in close association with cellular membrane rearrangements forming the replication organelles. HCV replication organelles are membrane protrusions forming clusters of single-membrane vesicles (SMVs), multi-membrane vesicles (MMVs), and — more dominantly — DMVs, known as the membranous web. Functionally, they shield the viral RNA from cellular immune sensors. Synthesis of NS3–NS5B induces membranous web formation independent of viral RNA replication (Neufeldt *et al.*, 2018). Likely, DMVs originate from the ER, since their outer membranes are often attached to the ER (Romero-Brey *et al.*, 2012). Membrane rearrangements are largely driven by NS4B and NS5A. Expression of NS4B induces membrane alterations (Egger *et al.*, 2002; Gosert *et al.*, 2003) and expression of NS5A leads to DMV formation (Ivashkina *et al.*, 2002; Romero-Brey *et al.*, 2012; Wolk

et al., 2008). Efficient viral replication requires a specific lipid composition of membranes. Membranes of replication complexes are rich in cholesterol and sphingolipids (Popescu *et al.*, 2014). To establish this particular lipid environment, several host factors are required. NS5A binds and activates the phosphatidylinositol-4 kinase-IIIa (PI4KA), increasing PI4P levels in the membranes (Ahn *et al.*, 2004; Berger *et al.*, 2011; Reiss *et al.*, 2011). Depletion of PI4KA leads to accumulation of NS5A at membranes and smaller DMVs (Bley *et al.*, 2020). PI4P also recruits the lipid transfer proteins oxysterol-binding protein (OSBP) and the phosphatidylinositol 4-phosphate adaptor protein 2 (FAPP2) to PI4P-rich domains, enabling lipid trafficking (Khan *et al.*, 2014; Wang *et al.*, 2014). HCV replication is severely affected by inhibiting these proteins, due to changes in membranous web morphology and lipid compositions (Neufeldt *et al.*, 2018; Wang and Tai, 2017). Another lipid transfer protein, the Niemann-Pick-type C1 (NPC1) protein is located at late endosomes and lysosomal membranes and is responsible for the required cholesterol transport to the membranous web (Stoeck *et al.*, 2018).

1.5.4 HCV assembly and release of HCV particles

Following viral RNA replication, core, E1, E2 and the viral genome assemble to a particle and bud into the ER before exiting the cell (Figure 6). The exact processes of the late stages of the HCV life cycle, however, are still not completely understood. The recruitment of core to cytosolic LDs is essential for particle production as mutations that prevent core from trafficking to LDs severely inhibit assembly (Boulant *et al.*, 2006; Boulant *et al.*, 2007; Miyanari *et al.*, 2007; Shavinskaya *et al.*, 2007). The mitogen-activated protein kinase (MAPK)-regulating protein cytosolic phospholipase A2 (cPLA2) (Menzel *et al.*, 2012) as well as the diacylglycerol-O-acyltransferase 1 (DGAT1) (Herker *et al.*, 2010) are responsible for core trafficking to LDs. Furthermore, core recruits NS5A to LDs *via* direct interaction, which is enhanced by DGAT1 (Appel *et al.*, 2008; Camus *et al.*, 2013; Masaki *et al.*, 2008). Likely, NS5A is important for the association of core with viral RNA, thus enhancing nucleocapsid formation (Masaki *et al.*, 2008). Interestingly, specific phosphorylation of C-terminal residues within NS5A by casein kinase II α (CKII α) is needed for assembly (Tellinghuisen *et al.*, 2008a). The interaction of p7 with NS2 associates the E1/E2 heterodimer and NS3/4A. This plays an organizing role in recruiting the non-structural proteins and core-containing LDs to the viral assembly sites (Counihan *et al.*, 2011; Jirasko *et al.*, 2010; Popescu *et al.*, 2011). Viral particles obtain their membranes by budding through the ER lumen, requiring the endosomal sorting complex required for transport (ESCRT) pathway (Ariumi *et al.*, 2011b; Corless *et al.*, 2010; Welsch *et al.*, 2007). On purified HCVcc particles E1 and E2 contain high-mannose complex N-linked glycans, suggesting trafficking through the Golgi (Vieyres *et al.*, 2010).

As HCV particles transit through the secretory pathway, they associate with APOE-containing VLDLs (Gastaminza *et al.*, 2008). Intriguingly, HCV particle production is blocked by inhibiting the microsomal triglyceride transfer protein (MTP), which is required for lipidation of APOB in the ER lumen (Gastaminza *et al.*, 2008; Huang *et al.*, 2007; Jiang and Luo, 2009). Even though this step is important for APOB trafficking during VLDL assembly (Olofsson *et al.*, 2000), HCV assembly is dependent on APOE rather than APOB at least in cultured hepatoma cells (Jiang and Luo, 2009). While the envelopment of viral particles is independent of APOE, APOE is essential for maturation of infectious particles (Hueging *et al.*, 2014; Lee *et al.*, 2014). Additionally, secreted particles have a lower buoyant density compared to intracellular particles, supporting the crucial step of lipoprotein association during viral egress (Gastaminza *et al.*, 2006). In conclusion, the data suggest that HCV shares at least part of the canonical secretory pathway with nascent VLDL. In contrast, recent studies report viral exiting *via* the endosomal pathway (Bayer *et al.*, 2016). Hence, deciphering the detailed processes of HCV maturation and egress is of great interest.

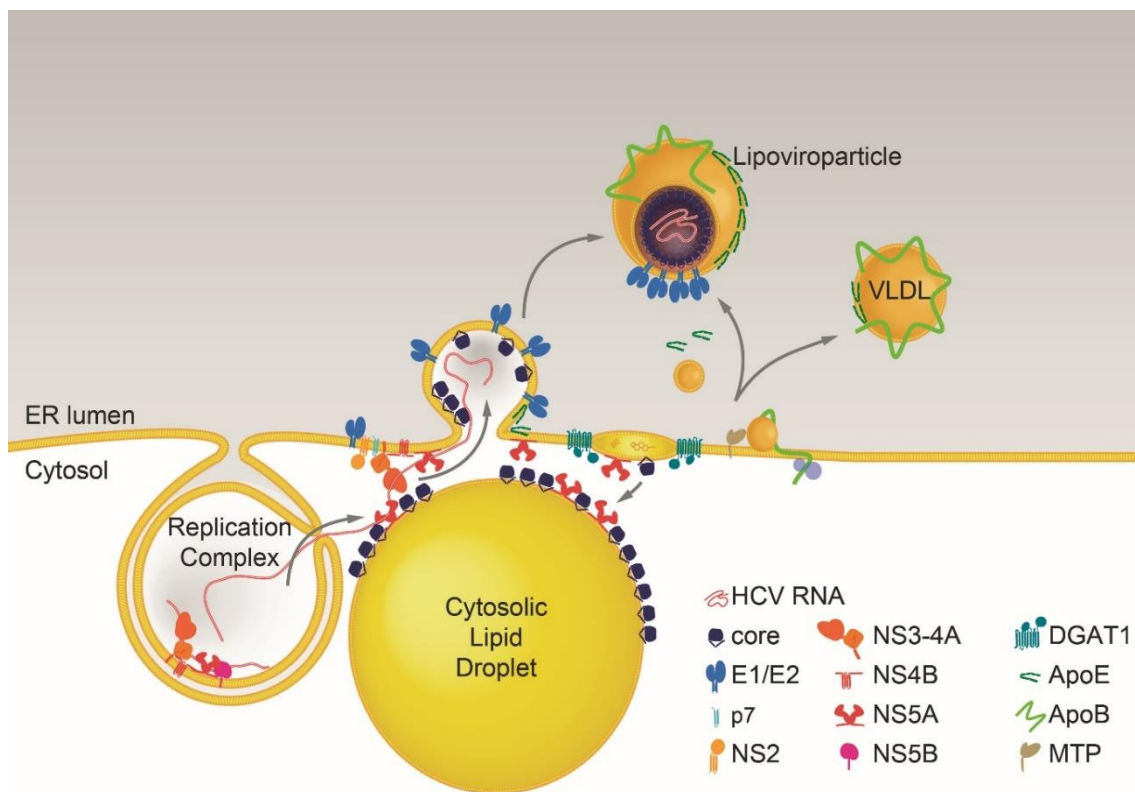


Figure 6: **Model of HCV assembly and maturation.**

The core protein localizes to LDs and recruits the HCV replication complex in close proximity to LDs at the ER. The direct interaction between core and NS5A likely facilitates the interaction of core with viral RNA during encapsidation. The interaction of p7 with NS2 and NS3/4A relocates core from LDs to the assembly sites. Further, the p7/NS2 complex recruits the E1/E2 heterodimer.

Nascent virions mature by associating with lipoproteins, forming LVPs and egress *via* the secretory pathway. (Illustration kindly provided by Eva Herker).

1.6 Lipid droplets

Lipid droplets (LDs) are storage organelles found in most eukaryotic cell types and play a central role for lipid homeostasis in the cell. LDs consist of a hydrophobic core of neutral lipids, mainly triacylglycerol (TAG) and sterol esters (SE), surrounded by a phospholipid monolayer (Thiam *et al.*, 2013). They are decorated by a distinct set of proteins (Figure 7). Mainly, LD-associated proteins are involved in the lipid metabolism including proteins of the perilipin family, but proteins acting in membrane trafficking and protein degradation are also part of the LD proteome, emphasizing the versatile role of LDs in the cell. As the cellular lipid metabolism is dependent on LDs, they constantly alternate between states of growth and breakdown. This occurs either through lipolysis *via* enzymatic hydrolysis mediated by lipases or through lipophagy, a selective form of autophagy (Olzmann and Carvalho, 2019). Imbalance of the lipid metabolism is associated not only with metabolic disorders, such as non-alcoholic fatty liver disease (NAFLD) (Ipsen *et al.*, 2018; Pei *et al.*, 2020) but also with neurodegenerative disorders such as Huntington's disease and Parkinson (Cole *et al.*, 2002; Martinez-Vicente *et al.*, 2010). Interestingly, various diseases like obesity, atherosclerosis and liver steatosis are connected to an aberrant accumulation of LDs (Greenberg *et al.*, 2011).

LDs originate from the ER by accumulation of neutral lipids in between the ER membrane leaflets forming a lens and eventually budding or staying attached to the ER (Thiam *et al.*, 2013 2013). The last step of TAG synthesis is catalyzed by the enzymes diacylglycerol acyltransferase 1 and 2 (DGAT1 and DGAT2). Notably, DGAT1 plays a relevant role for HCV particle formation by recruiting the viral proteins core and NS5A to LDs (Camus *et al.*, 2013; Herker *et al.*, 2010). Originating from the ER, LDs associate with other organelles *via* membrane contact sites as a form of direct communication (Olzmann and Carvalho, 2019). Research over the last years has shown that the organization of LD contact sites is heavily influenced by metabolic diseases, such as steatosis, but also by infections with pathogens (Herker *et al.*, 2021). Strikingly, LDs are hijacked by various viruses, bacteria, and parasites such as HCV, dengue virus (DENV), Rotaviruses, *Chlamydia trachomatis*, *Mycobacterium tuberculosis* (Mtb), *Plasmodium falciparum*, *Leishmania*, and *Toxoplasma gondii* (Bosch *et al.*, 2021; Herker and Ott, 2012; Roingeard and Melo, 2017).

During HCV infection, LDs are essential for assembly and maturation, however, viral RNA replication can be observed in LD fractions (Miyanari *et al.*, 2007). Intriguingly, recent studies suggest that LDs provide a lipid source for RNA replication complexes as

well as virion morphogenesis. Breakdown of LDs by adipose triglyceride lipase (ATGL)-driven lipolysis is required for infectious lipovirion production (Vieyres *et al.*, 2020). Additionally, correlative light and electron microscopy and electron tomography showed that DMVs, representing HCV replication organelles, are wrapped around LDs (Lee *et al.*, 2019).

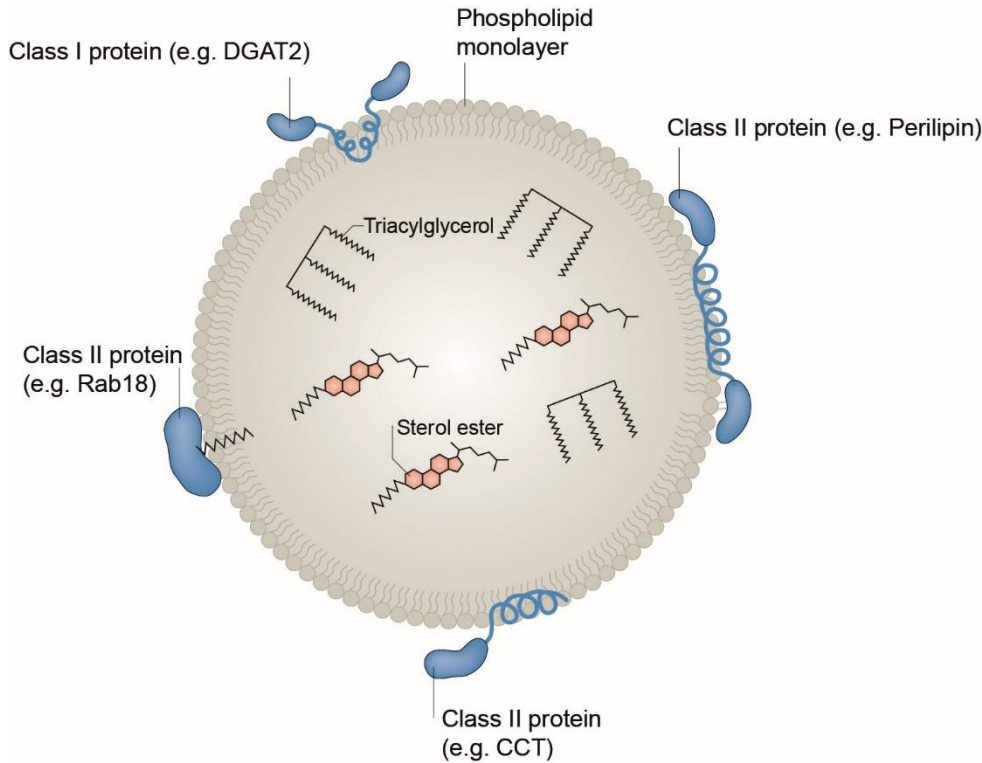


Figure 7: **Schematic model of LDs.**

LDs contain neutral lipids (sterol esters and triacylglycerol) surrounded by a phospholipid monolayer, in which LD-associated proteins are embedded. (Modified from Olzmann and Carvalho, 2019).

1.7 The LD proteome in HCV-infected cells

Proteome-based approaches have revealed a range of LD-associated proteins (Bersuker *et al.*; Brasaemle *et al.*, 2004; Liu *et al.*, 2004). Concerning HCV replication, numerous host proteins located at the LD surface like perilipin (PLIN)-2, PLIN3 and the small GTPase Rab18 are crucial for particle production (Lassen *et al.*, 2019; Ploen *et al.*, 2013a; Vogt *et al.*, 2013). Depletion of PLIN2 induces ER membrane wrapping around LDs and inhibits the transfer of core to LDs (Lassen *et al.*, 2019). Rab18 initiates trafficking of core to LDs *via* direct LD membrane contact sites (Dansako *et al.*, 2014). Both, Rab18 and PLIN3 interact with NS5A to enhance RNA replication, likely by initiating close contact of replication complexes and LD membranes (Salloum *et al.*, 2013; Vogt *et al.*, 2013).

A recent quantitative proteome analysis unveiled that the LD proteome changes considerably upon HCV infection (Rösch *et al.*, 2016). Evaluating enriched proteins at LDs during HCV infection, this approach identified numerous proteins that were previously published as HCV host factors, such as the DEAD box proteins 1 and 3 (DDX1 and DDX3) and the Insulin-like growth factor-II mRNA-binding protein 1 (IGFBP1). DDX1 binds the HCV 5'- and 3'-UTR. Depletion of DDX1 impairs HCV RNA replication (Tingting *et al.*, 2006). DDX3 binds core and increases viral replication (Ariumi *et al.*, 2007) and downregulation of DDX3 reduces MTP expression that is required for viral particle production and APOB lipidation (Gastaminza *et al.*, 2008; Tsai *et al.*, 2017). IGFBP1 is involved in HCV RNA translation (Weinlich *et al.*, 2009). In conclusion, a distinct LD proteome is directly connected to efficient HCV replication.

1.8 Annexin A3 (ANXA3)

The above mentioned quantitative LD proteome analysis revealed annexin (ANXA) A3 as a host co-factor for HCV particle production (Rösch *et al.*, 2016). ANXA3 belongs to the family of annexins that are Ca^{2+} - and phospholipid-binding proteins. All annexins have a conserved core domain, which harbors the Ca^{2+} - and lipid-binding sites. They bind to negatively charged phospholipids in a Ca^{2+} -dependent manner that allows binding to cellular membranes. Annexins are usually localized in the cytosol. Various annexins act as viral host factors: ANXA1 and ANXA5 have been described as proviral factors for Influenza A Virus (IAV) (Arora *et al.*, 2016; Berri *et al.*, 2014). Further, it has been suggested that HCV replication is impaired by ANXA1 expression (Hiramoto *et al.*, 2015). ANXA2 is required for the recruitment of non-structural proteins to induce membranous web formation to ensure functional HCV RNA replication (Saxena *et al.*, 2012). Others have reported that ANXA2 plays a role in HCV assembly rather than RNA replication (Backes *et al.*, 2010).

During HCV-infection, relocalization of ANXA3 to LDs is facilitated by the viral proteins core and NS5A. Knockdown of ANXA3 decreases HCV replication without affecting early stages of the HCV life cycle. ANXA3 depletion reduces secretion of APOE and virion infectivity (Figure 8). The secretion of APOE and viral particles is dependent on an HCV-induced Golgi fragmentation to which ANXA3 contributes (Rösch *et al.*, 2016). This shows that ANXA3 functions as a host factor promoting HCV replication by affecting the incorporation on APOE into viral particles and the interaction of APOE with E2. However, even though ANXA3 is recruited to LDs by core and NS5A, ANXA3 does not directly interact with viral proteins, leading to the hypothesis that other proteins might be bridging this interaction.

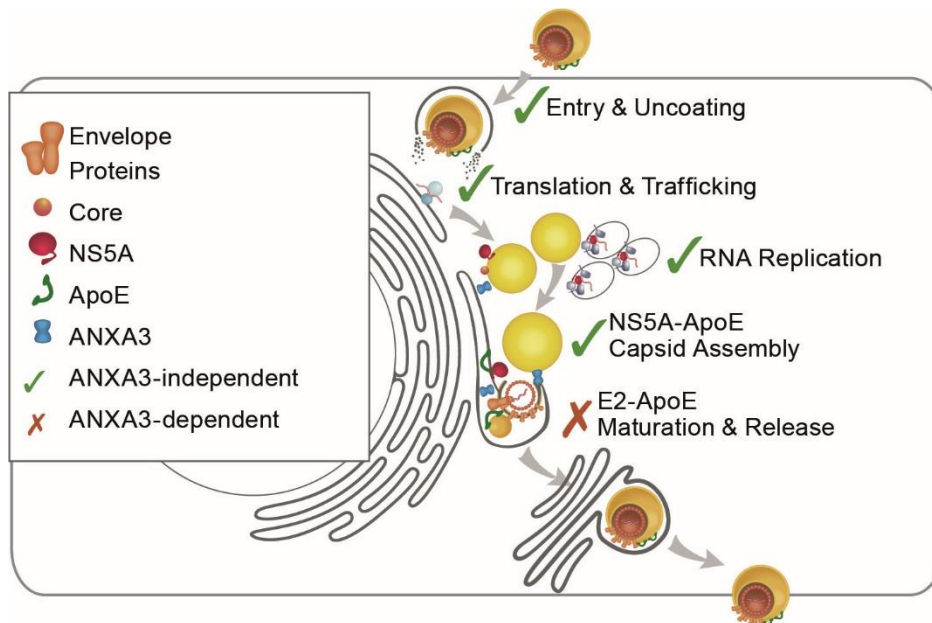


Figure 8: **ANXA3-dependent steps of the HCV replication cycle.**

In HCV-infected cells, ANXA3 localizes to LDs and facilitates the interaction of E2 and APOE, thus promoting the incorporation of APOE into infectious viral particles. (Modified from Rösch *et al.*, 2016).

1.9 Perilipin (PLIN) 2

Perilipins are the most abundant lipid droplet proteins. PLIN2 and PLIN3 are ubiquitously expressed while PLIN1, 4, and 5 are rather tissue specific (Sztalryd and Brasaemle, 2017). PLIN2 is the major LD-coating protein and is used as a LD marker protein (Conte *et al.*, 2016; Fujimoto *et al.*, 2004; Mak *et al.*, 2008). It is degraded in the cytoplasm if not bound to the LD surface (Takahashi *et al.*, 2016; Xu *et al.*, 2005). Interestingly, PLIN3 is recruited to LDs in PLIN2^{-/-} mice, but it cannot completely compensate PLIN2 functions (Libby *et al.*, 2016). Generally, PLIN2 is highly responsible for LD stability and lipid accumulation by regulating lipolysis and autophagy (Kaushik and Cuervo, 2015; Listenberger *et al.*, 2007). Overexpression of PLIN2 constricts lipolysis by decreasing the ATGL access to LDs, thus leading to elevated TAG levels (Bell *et al.*, 2008; Listenberger *et al.*, 2007).

Interestingly, Lassen *et al.* showed that PLIN2 depletion severely affects HCV particle assembly and the production of infectious viral particles, whereas HCV RNA replication and lipid homeostasis are largely unaffected (Lassen *et al.*, 2019). The recruitment of core and NS5A to LDs is impaired due to ER membrane alterations surrounding LDs in infected PLIN2 knockdown cells. Silencing of PLIN2 decreases cellular APOE levels and secretion through lysosomal degradation, but does not affect the density of APOE-containing lipoproteins. Hence, PLIN2 expression is likely required for functional HCV virion assembly.

Considering PLIN2 the major LD-associated protein, other groups have used PLIN2 as a bait protein to study the LD proteome (Bersuker *et al.*, 2018). To be able to evaluate a complex LD proteome, the ATGL complex as well as PLIN2 were used in combination with proximity labeling in Huh7 and U2O2 cells. The number of identified proteins was considerably reduced compared to previous LD proteome studies using isolated LDs. The authors did not observe ER luminal proteins, but several enzymes involved in TAG and SE synthesis as well as lipolysis. Thus, using a PLIN2 associated proximity labeling method provides a more distinct insight into the LD proteome.

1.10 Proximity labeling

Proximity labeling is a recently described method to identify protein-protein interactions in living cells. Two prominent options are the proximity-dependent biotin identification (BioID2) (Kim *et al.*, 2016) and the engineered ascorbate peroxidase APEX2 (Lam *et al.*, 2015). Both, BioID2 and APEX2 act as promiscuous biotin labeling methods and can be fused to a protein of interest. As the biotinylation of proximal proteins occurs in living cells, weak or transient interactions as well as interactions with membrane proteins can be identified using mass spectrometry (MS).

BioID2 is based on the bacterial biotin ligase BirA from *Aquifex aeolicus* that normally binds bio-AMP and specifically regulates the biotinylation of the acetyl-CoA carboxylase (Choi-Rhee *et al.*, 2004; Cronan, 2005). The mutation in the conserved catalytic domain reduces the affinity to the reactive bio-AMP and allows a premature release of the reactive biotin to covalently interact with amines on proximate proteins within an estimated range of 10 nm (Figure 9). Biotinylated proteins can be captured by affinity purification for identification by MS to detect protein associations (Roux *et al.*, 2012). BioID2 was developed as a smaller version (~27 kDa) of the precursor BioID (~30 kDa) (Kim *et al.*, 2016). Recently, the even smaller TurboID was developed, which allows a shorter labeling time (Branon *et al.*, 2018).

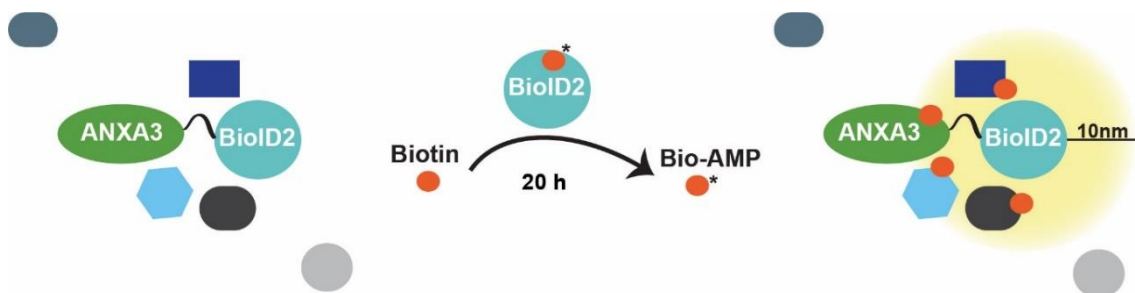


Figure 9: **Model of BioID2-mediated labeling.**

Cellular expression of a protein of interest fused to the promiscuous biotin ligase (BioID2) enables biotinylation of proximate proteins. The reactive bio-AMP covalently interacts with amines on proximate proteins within an estimated range of 10 nm. Biotinylated proteins can be captured by affinity purification for identification by MS to detect protein associations.

The engineered soybean mutant ascorbate peroxidase (APEX2) uses hydrogen peroxide as an oxidant to catalyze the one-electron oxidation of biotin-phenol (Hung *et al.*, 2014; Lam *et al.*, 2015; Martell *et al.*, 2012; Rhee *et al.*, 2013). The short-lived biotin-phenoxyl radical is highly reactive and covalently biotinylates electron-rich amino acids, such as tyrosine, tryptophan, cysteine and histidine of proteins proximal to the APEX2 fusion protein (Figure 10). APEX2 maintains membrane- and protein complex integrity and can therefore be active in subcellular compartments. APEX2 is similar in size to BioID2 with ~28 kDa to allow a comparable effect on fusion to a protein of interest. The spatial resolution using this method is estimated to be 10-20 nm, which is a considerably larger radius than for BioID2 (Hung *et al.*, 2016; Hung *et al.*, 2014). Notably, another crucial difference between both methods is the longer labeling time with BioID2 (~20h) compared to the very short snapshot of one minute labeling using APEX2.

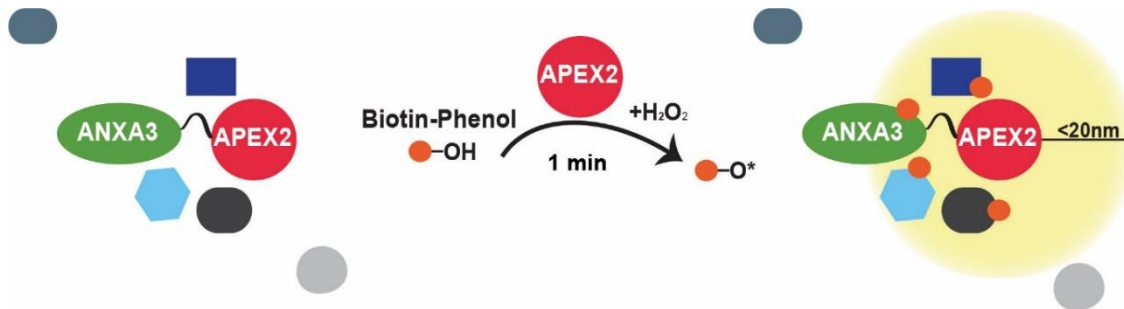


Figure 10: **Model of APEX2-mediated labeling.**

The engineered soybean mutant ascorbate peroxidase (APEX2) uses hydrogen peroxide as an oxidant to catalyze the one-electron oxidation of biotin-phenol. The reactive biotin-phenoxyl radical covalently biotinylates electron-rich amino acids like tyrosine, tryptophan, histidine and cysteine of proteins proximal to the APEX2 fusion protein. Biotinylated proteins can be analyzed by MS.

1.11 The La-related protein (LARP) 1

The La-related protein (LARP) 1 has a conserved La domain and a RNA-binding region (Bayfield *et al.*, 2010; Bousquet-Antonelli and Deragon, 2009). It is a major target downstream of the mechanistic (also known as mammalian) target of rapamycin complex (mTORC1) (Fonseca *et al.*, 2015; Hong *et al.*, 2017; Tcherkezian *et al.*, 2014). By binding to the 5' motif of terminal oligopyrimidine (TOP) mRNA, LARP1 stabilizes and regulates their translation (Aoki *et al.*, 2013; Fonseca *et al.*, 2015; Gentilella *et al.*, 2017; Lahr *et al.*, 2017; Philippe *et al.*, 2020; Philippe *et al.*, 2018). LARP1 was identified as a biomarker in ovarian, lung, and hepatocellular cancer (Hopkins *et al.*, 2016; Xie *et al.*, 2013). Interestingly, proximity-based mapping of stress granules (SGs) and processing bodies (P-bodies) revealed LARP1 in close proximity to the stress granule-associated

protein polyadenylate-binding protein 1 (PABPC1) (Youn *et al.*, 2018). LARP1 and PABPC1 are found in ribonucleoprotein (RNP) complexes (Burrows *et al.*, 2010; Suzuki *et al.*, 2016) and previous studies have reported that RNP complexes such as SGs and P-bodies are located proximal to LDs in HCV-infected cells (Ariumi *et al.*, 2011a; Chatel-Chaix *et al.*, 2011; Pene *et al.*, 2015; Schöbel *et al.*, 2021). In context of HCV infection, LARP1 relocates to core-containing LDs in infected cells, most likely as part of a RNP complex (Chatel-Chaix *et al.*, 2013) and associates with particles (Plissonnier *et al.*, 2019). The exact role of LARP1 in HCV replication has been contradictory. Chatel-Chaix *et al.* showed that LARP1 knockdown decreased HCV replication using a Con1 subgenomic replicon as well as in context of full infection (Chatel-Chaix *et al.*, 2013). Additionally, enhanced HCV particle production and elevated core levels were detected in the supernatant of LARP1-depleted cells with an increased extracellular infectivity, postulating that LARP1 is part of a host protein complex that regulates the NS3-dependent steps during later stages in the HCV life cycle.

In contrast to that, a different study suggested that extracellular infectivity was decreased in LARP1-knockdown cells, while intracellular infectivity was increased (Plissonnier *et al.*, 2019).

Intriguingly, in DENV and SARS-CoV2-infected cells LARP1 knockdown reduces viral titers (Schmidt *et al.*, 2021; Suzuki *et al.*, 2016).

2 Aim of the thesis

A cell culture-based system has allowed to study the HCV viral life cycle *in vitro*. Nevertheless, especially viral assembly, maturation, and egress remain poorly understood. LDs play an essential role for viral assembly, acting as central hubs. Previous studies have shown that LD-associated proteins, such as PLIN2 and PLIN3 are involved in efficient HCV replication. A recent LD proteome analysis highlighted that the LD proteome severely changes during HCV infection and identified ANXA3 as a critical host factor that relocates to LDs during HCV infection and is involved in maturation of HCV lipovirions.

The aim of this study was to further investigate the LD proteome in HCV-infected cells using the two proximity labeling methods BioID2 and APEX2. As baits for labeling, the LD-associated protein PLIN2, as well as the above-mentioned HCV host factor ANXA3 were used. An advantage of proximity labeling is the possibility to identify not only new potential interaction partners, but also proteins in spatial proximity, thus enabling a broader insight into alterations of the protein composition at LDs in HCV-infected cells. Selected hits were evaluated for their functional role during HCV replication in more detail by assessing viral spreading, HCV RNA replication, and cellular localization as well as the interaction with viral proteins.

3 Results

3.1 LD proteome analysis in hepatoma cells

3.1.1 Labeling of LD-proximate proteins in hepatoma cells

Previous studies have reported that the LD proteome is severely altered during HCV infection (Rösch *et al.*, 2016; Schöbel *et al.*, 2021). Rösch *et al.* showed the recruitment of numerous host proteins to LDs in HCV-infected cells and found that annexin A3 (ANXA3) relocates to LDs in HCV-infected cells. ANXA3 was identified as a host factor for HCV particle production as it is required for incorporation of apolipoprotein E (APOE) into lipoviroparticles (LVP) (Rösch *et al.*, 2016).

In order to further investigate changes in the LD proteome during HCV infection, proximity labeling was performed. The previously described biotin ligase BioID2 (Kim *et al.*, 2016; Roux *et al.*, 2012) and engineered ascorbate peroxidase APEX2 (Hung *et al.*, 2014; Lam *et al.*, 2015; Martell *et al.*, 2012; Rhee *et al.*, 2013) enable the identification of proteins in close proximity to a protein of interest. To study and compare the LD proteome of HCV-infected and uninfected hepatoma cells, ANXA3 or the LD-associated protein perilipin 2 (PLIN2) were used as bait proteins. Combining proximity labeling with stable isotope labeling by amino acids in cell culture (SILAC) allows a direct comparison between two cell populations. One population is labelled with “heavy” amino acids and the other with “light” (normal) amino acids. Due to the incorporation of heavy amino acids, a mass shift of the peptides can be detected compared to the control. The two proteomes can be quantified by mass spectrometry (MS) based on their molecular weight (Mann, 2006).

3.1.2 Generation and validation of BioID2 and APEX2 fusion proteins

To construct the bait proteins, ANXA3 or PLIN2 were N-terminally fused to either an HA-tagged BioID2 or a FLAG-tagged APEX2 protein. At the C-terminus, a 2A skipping site followed by an mCherry reporter was added to identify successfully transfected cells. To enable stable expression, the fusion protein expression cassettes were then cloned into the lentiviral expression vector pSicoR-MS1ΔU6. As a control, BioID2^{2A-mCherry} or APEX2^{2A-mCherry} without the respective bait proteins were cloned into pSicoR-MS1ΔU6.

Next, functional biotinylation of the generated constructs was validated by western blot and immunofluorescence analysis. Huh7.5 cells were transduced with lentiviral particles to stably express ANXA3-BioID2^{HA-2A-mCherry} (ANXA3-BioID2) or the BioID2^{HA-2A-mCherry} (BioID2) control (Figure 11A). Cells were treated with 10 μM biotin for ~20 hours or left untreated. Cells were lysed and biotinylated proteins were captured by pull down with

streptavidin agarose beads and subjected to western blotting (Figure 11B). As expected, bands were detected at ~70 kDa for lysates of ANXA3-BioID2-expressing cells and at 35 kDa in the BioID2 expressing samples, confirming the expression of the ANXA3-BioID2 fusion protein as well as of the BioID2 control. However, in both samples a band with an additional molecular weight of ~35 kDa was detected. This indicates that the 2A ribosomal skipping site does not efficiently skip prior to mCherry translation, leading to the expression of the respective mCherry-fused proteins. Biotinylated proteins were visualized using Streptavidin-HRP, which resulted in multiple bands in the biotin-treated samples, confirming successful biotinylation and showing the range of biotinylated proteins.

Interestingly, overexpressed ANXA3-BioID2 was pulled down upon biotin labeling *via* streptavidin, but not the endogenous ANXA3. The BioID2 control was detected in the streptavidin pull down of both, biotin-treated and untreated samples.

Proper localization of the biotinylated proteins was visualized by immunofluorescence (Figure 11C). LDs were stained with BODIPY 665. Alexa Fluor 405-coupled streptavidin showed cytosolic biotinylation of biotin-treated ANXA3-BioID2-expressing cells, which was not detected in untreated cells. The control cells expressing BioID2 showed a mostly nuclear located biotinylation. It is important to mention that the BODIPY signal was detected in the mCherry channel to some extent. Nevertheless, the mCherry signal was still distinguishable from the LD staining (Figures 11–14).

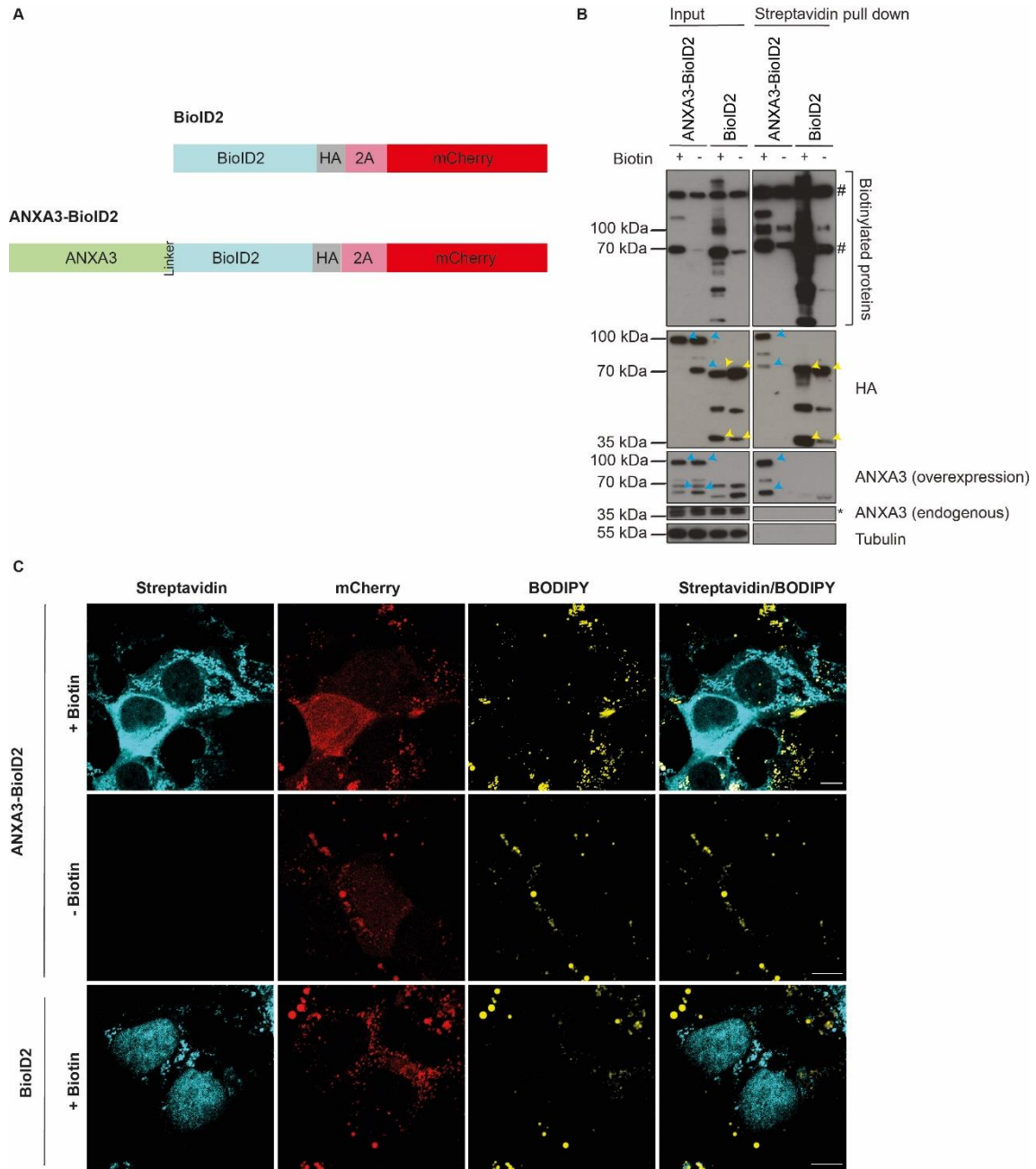


Figure 11: Proximity labeling with ANXA3-BioID2.

Cells were transduced with lentiviral particles for the stable expression of the ANXA3-BioID2^{HA-2A-mCherry} (ANXA3-BioID2) fusion protein or BioID2^{HA-2A-mCherry} (BioID2) (A). For proximity labeling, cells were incubated with 10 μ M biotin for 20 hours at 37 $^{\circ}$ C. Cells were either lysed and biotinylated proteins were collected on streptavidin-conjugated agarose beads, or fixed for immunofluorescence analysis. (B) Western blot analysis of streptavidin pull down showed biotinylated proteins in Huh7.5 cells stably expressing the ANXA3-BioID2 or BioID2. Cells were treated as described above and lysed under stringent conditions to collect biotinylated proteins by incubation with streptavidin-conjugated agarose beads. Biotinylated proteins were detected with streptavidin-HRP. Expression of ANXA3-BioID2 and BioID2 was analyzed using an ANXA3 and/or HA-specific antibody. Tubulin served as loading control. Blue arrows indicate ANXA3-BioID2 and yellow arrows indicate BioID2 detection bands. Asterisks indicate unspecific bands. # indicates endogenous biotinylated proteins (n = 2). (C) Immunofluorescence staining of biotinylated proteins in Huh7 cells stably expressing ANXA3-BioID2 or BioID2. Cells were infected with a Jc1^{NS5AB-EGFP} reporter (MOI 0.01) for 10 days. Labeling was performed as described above and cells were fixed. LDs were stained with BODIPY 665 and biotinylated proteins were detected

using a streptavidin-conjugated Alexa-Fluor 405 antibody. Scale bars = 10 μ m. Shown are representative experiments (n = 2).

Analogous to the validation of the ANXA3-BioID2 and the BioID2 constructs, the functionality of the PLIN2-BioID2^{HA-2A-mCherry} (PLIN2-BioID2) construct (Figure 12A) was analyzed as described above. Expression was validated by western blot using HA and PLIN2-specific antibodies (Figure 12B). Similar to data shown for ANXA3-BioID2 in Figure 11, the 2A site does not efficiently skip prior to mCherry translation. Upon biotin treatment, multiple bands were detectable in the BioID2 control. For PLIN2-BioID2 samples, the tubulin signal was less intense, indicating that a lower amount of protein was loaded. Consequently, only a weak expression of PLIN2-BioID2 and low biotinylation were detectable. Immunofluorescence staining with streptavidin depicted a punctual localization in the cytosol, partially localizing to LDs in biotin-treated cells, but not in untreated cells (Figure 12C).

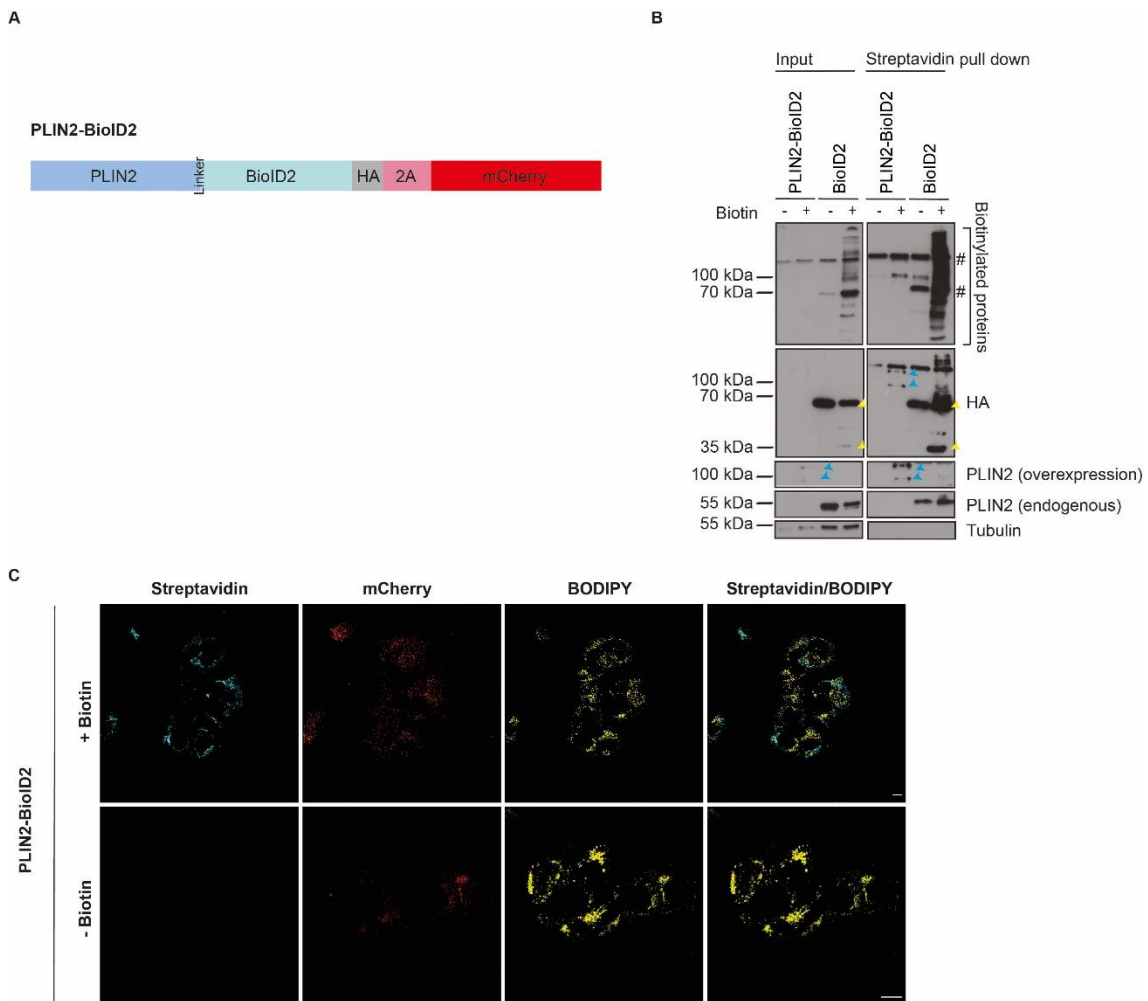


Figure 12: Proximity labeling with PLIN2-BioID2.

Huh7.5 cells were transduced with lentivirus to establish a stable expression of the PLIN2-BioID2^{HA-2A-mCherry} (PLIN2-BioID2) (A). The cells were supplemented with oleic acid 20 hours prior labeling with 10 μ M biotin for 20 hours at 37 $^{\circ}$ C. Cells were either lysed and biotinylated proteins

were collected on streptavidin-conjugated agarose beads or fixed for immunofluorescence analysis. (B) Western blot analysis of streptavidin pull down showed biotinylated proteins in Huh7.5 cells stably expressing PLIN2-BioID2 or BioID2. Cells were treated as described above and lysed under stringent conditions to collect biotinylated proteins by incubation with streptavidin-conjugated agarose beads. Biotinylated proteins were detected with streptavidin-HRP. Expression of PLIN2-BioID2 and BioID2 was analyzed using a PLIN2 and/or HA-specific antibody. Tubulin served as loading control. Blue arrows indicate PLIN2-BioID2 and yellow arrows indicate BioID2 detection bands. Asterisks indicate unspecific bands. # indicates endogenous biotinylated proteins (n = 1). (C) Immunofluorescence staining of biotinylated proteins in Huh7.5 cells stably expressing PLIN2-BioID2. Cells were treated as described above, and LDs were stained with BODIPY 665. Biotinylated proteins were detected using a streptavidin-conjugated Alexa-Fluor 405 antibody. Scale bars = 10 μ m (n = 1).

For APEX2 labeling, Huh7.5 cells were transduced with lentiviral particles for stable expression of ANXA3-^{FLAG}APEX2^{2A-mCherry} (ANXA3-APEX2) or the ^{FLAG}APEX2^{2A-mCherry} (APEX2) control (Figure 13A). Cells were treated with 500 μ M biotin-phenol (BP) for 30 minutes at 37 °C and hydrogen peroxide (H₂O₂) for 1 minute at room temperature. Prior to lysis, cells were washed in quencher solution. For western blot analysis, a streptavidin pull down was performed to capture biotinylated proteins. Development after streptavidin-HRP incubation showed multiple bands of biotinylated proteins in the samples that were treated with BP and H₂O₂, but not in samples that were only treated with either BP or H₂O₂ (Figure 13B). Similar to the results of the BioID2 constructs, the unskipped as well as the skipped fusion protein was detected in cell lysates using a FLAG-specific antibody. Interestingly, APEX2-mediated proximity labeling was not sufficient to pull down ANXA3-APEX2 or APEX2 with streptavidin using a FLAG-specific or ANXA3-specific antibody. Immunofluorescence staining of fully labelled ANXA3-APEX2 cells using an Alexa Fluor 405-coupled streptavidin visualized biotinylation of proteins located in the cytoplasm (Figure 13C), which was not detected in cells only treated with either BP or H₂O₂. Streptavidin staining of labelled APEX2 cells led to staining of the whole cell.

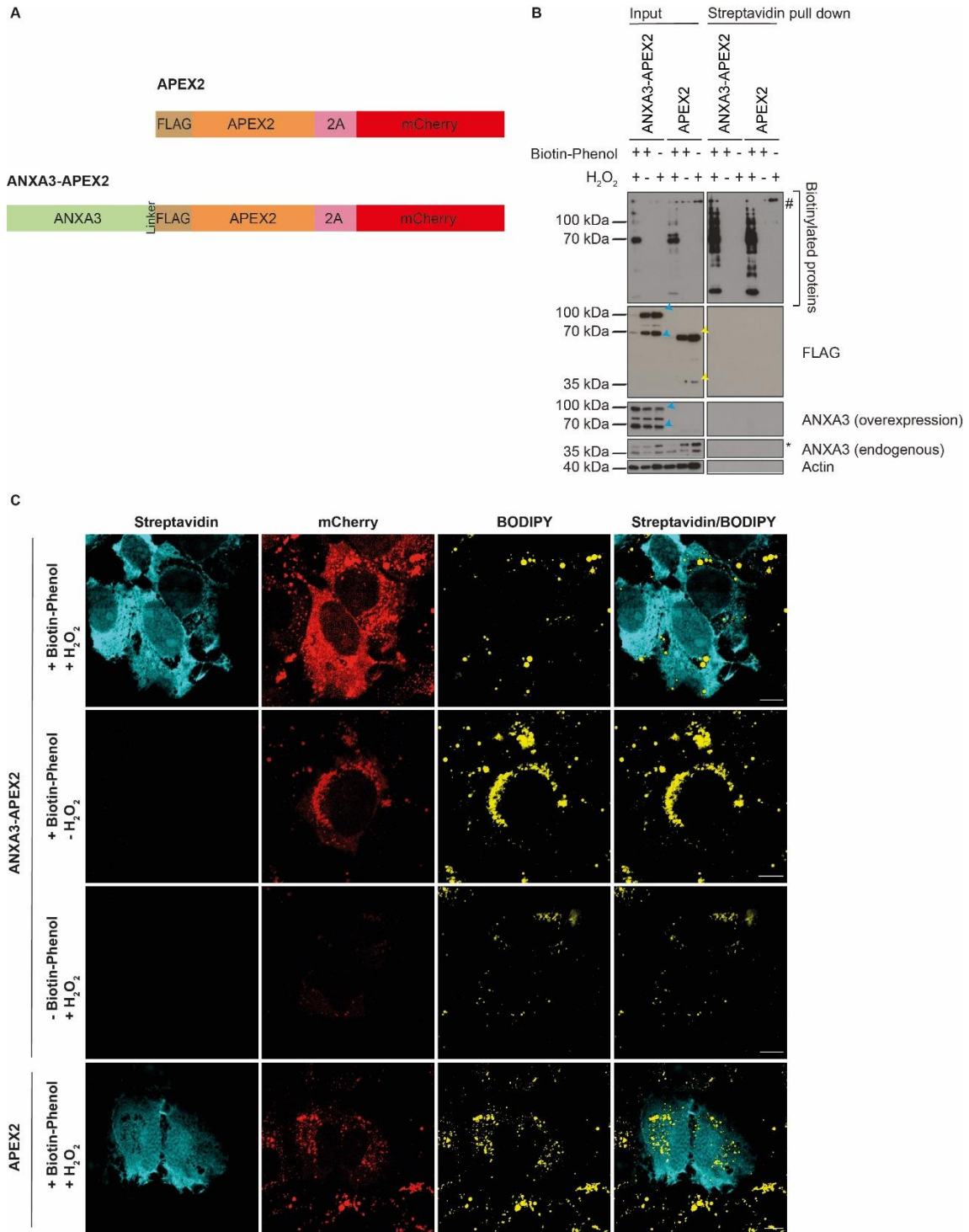


Figure 13: Proximity labeling with ANXA3-APEX2.

Cells were transduced with lentivirus for the expression of ANXA3-^{FLAG}APEX2^{2A-mCherry} (ANXA3-APEX2) fusion protein or ^{FLAG}APEX2^{2A-mCherry} (APEX2) (A). The cells were incubated with 500 μ M BP for 30 minutes at 37 °C, followed by another incubation with H₂O₂ for 1 minute. The reaction was stopped using quencher solution. Cells were either lysed and biotinylated proteins were collected on streptavidin-conjugated agarose beads or fixed for immunofluorescence analysis. (B) Western blot analysis of streptavidin pull down showed biotinylated proteins in Huh7.5 cells stably expressing ANXA3-APEX2. Cells were treated as described above and lysed under stringent conditions to collect biotinylated proteins by incubation with streptavidin-conjugated agarose beads. Biotinylated proteins were detected with streptavidin-HRP. Expression of ANXA3-APEX2 and APEX2 was analyzed using an ANXA3 and/or FLAG-specific antibody. Actin served

as loading control. Blue arrows indicate ANXA3-APEX2 and yellow arrows indicate APEX2 detection bands. Asterisks indicate unspecific bands. # indicates endogenous biotinylated proteins (n = 2). (C) Immunofluorescence staining of biotinylated proteins in Huh7 cells stably expressing ANXA3-APEX2 and were infected with a Jc1^{NS5AB-EGFP} reporter (MOI 0.01) for 10 days. Cells were treated as described above, and LDs were stained with BODIPY 665. Biotinylated proteins were detected using a streptavidin-conjugated Alexa-Fluor 405 antibody. Scale bars = 10 μ m. Shown are representative experiments (n = 2).

Huh7.5 cells were transduced with lentivirus to stably express PLIN2-^{FLAG}APEX2^{2A-mCherry} (PLIN2-APEX2) (Figure 14A) or the ^{FLAG}APEX2^{2A-mCherry} (APEX2) control (Figure 13A) and the streptavidin pull down was performed as described above. Western blot analysis using a FLAG-specific and a PLIN2-specific antibody showed, similar to ANXA3-APEX2, the expression of the unskipped PLIN2-APEX2 and APEX2 fusion protein as well as the skipped version (Figure 14B). However, PLIN2-APEX2 and APEX2 were not detected by streptavidin pull down, similar to the data observed with ANXA3-APEX2 shown in Figure 13B. Using streptavidin-HRP, biotinylated proteins were detected in samples that were labelled with BP and H₂O₂. The typical ladder that can be detected upon proximity labelling was more pronounced using the APEX2 control than in the PLIN2-APEX2 samples.

Streptavidin staining and microscopic analysis showed a specific ring-like pattern of biotinylated proteins surrounding LDs, similar to the known PLIN2 localization (Figure 14C). Biotinylation was only detectable with an Alexa Fluor 405-conjugated streptavidin in cells that were treated with both, BP and H₂O₂.

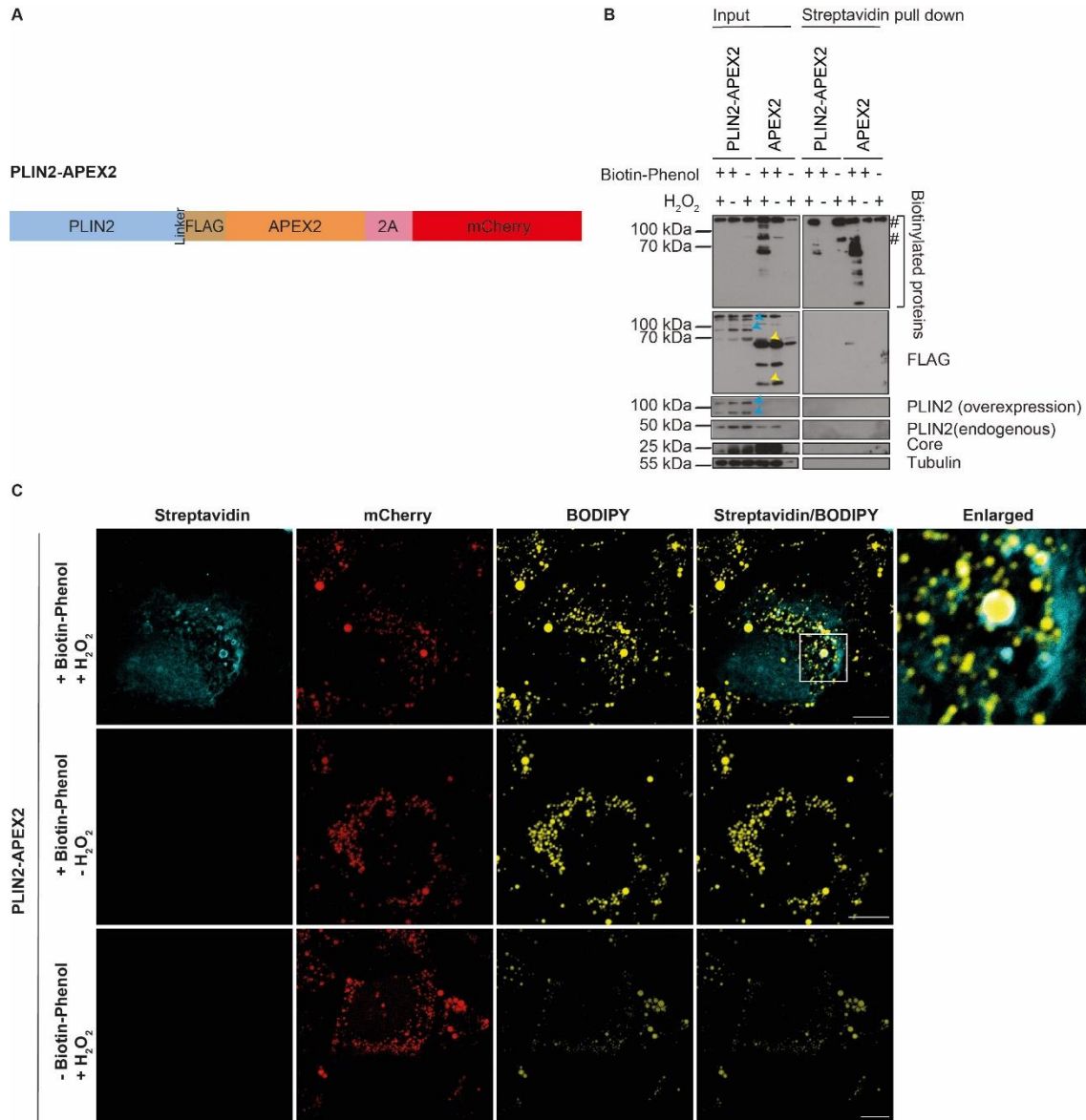


Figure 14: Proximity labeling with PLIN2-APEX2.

Cells stably expressing PLIN2-^{FLAG}APEX2^{2A}-mCherry (PLIN2-APEX2) (A) were infected with a Jc1^{NS5AB-EGFP} reporter for 10 days (MOI 0.01) and supplemented with oleic acid 20 hours prior to labeling. The cells were incubated with 500 μ M BP for 30 minutes at 37 °C, followed by another incubation with H₂O₂ for 1 minute. The reaction was stopped using quencher solution. Cells were either lysed and biotinylated proteins were collected on streptavidin-conjugated agarose beads or fixed for immunofluorescence analysis. (B) Western blot analysis of streptavidin pull down showed biotinylated proteins in Huh7.5 cells stably expressing PLIN2-APEX2 or APEX2. Cells were treated as described above and lysed under stringent conditions to collect biotinylated proteins by incubation with streptavidin-conjugated agarose beads. Biotinylated proteins were detected with streptavidin-HRP. Expression of PLIN2-APEX2 and APEX2 was analyzed using a PLIN2 and/or FLAG-specific antibody. HCV infection was confirmed using a core-specific antibody. Tubulin served as loading control. Blue arrows indicate PLIN2-APEX2 and yellow arrows indicate APEX2 detection bands. Asterisks indicate unspecific bands. # indicates endogenous biotinylated proteins (n = 2). (C) Immunofluorescence staining of biotinylated proteins in Huh7 cells stably expressing the PLIN2-APEX2 fusion protein. Huh7 cells were treated as described above, and LDs were stained with BODIPY 665. Biotinylated proteins were detected using a streptavidin-conjugated Alexa-Fluor 405 antibody. Scale bars = 10 μ m. Shown are representative (n = 2).

As others have reported before, endogenous biotinylated proteins were detectable at ~130 kDa in western blot analyses using HRP-coupled streptavidin (Hung *et al.*, 2016). These bands were evident in all experimental set ups with BioID2 as well as APEX2 and appeared in samples from untreated cells (Figures 11–14B).

These data indicate that the generated BioID2 and APEX2 fusion constructs are functional for proximity labelling. Biotinylated proteins localized similar to the described endogenous ANXA3 or PLIN2 localization. Interestingly, western blot analysis was not sufficient to detect the fusion proteins *via* streptavidin pull down for APEX2 samples, but for BioID2 samples.

3.1.3 SILAC and proximity labeling of ANXA3 and PLIN2-expressing hepatoma cells

Huh7.5 cells were cultured in media containing heavy R10K8 or light R0K0 amino acids. Incorporation was confirmed by MS. In order to investigate the LD proteome *via* ANXA3 and PLIN2 proximity labeling, heavy or light amino acid cultured Huh7.5 cells were transduced with lentiviral expression constructs for ANXA3-BioID2, ANXA3-APEX2, PLIN2-BioID2 or PLIN2-APEX2 or the respective control BioID2 or APEX2. As a control, the labeling conditions were switched, so that cells expressing the fusion protein were cultured in heavy amino acid media for two experiments and in light amino acid media for the other two experiments. Cells expressing ANXA3-BioID2, PLIN2-BioID2 or BioID2 were labeled with Biotin for 20 hours, lysed and biotinylated proteins were pulled down using streptavidin-conjugated agarose resins. ANXA3-APEX2, PLIN2-APEX2 and APEX2-expressing cells were labeled using BP for 30 minutes and H₂O₂ for 1 minute. Biotinylated proteins were captured by streptavidin pull down and separated *via* SDS-PAGE, followed by Coomassie-Blue staining (Roti-blue). Gel digestion and MS as described in 6.3.7.1 – 6.3.7.3 was performed by C. Krisp and H. Schlüter at the Core Facility Mass Spectrometric Proteomics of the University Medical Center Hamburg-Eppendorf. For all constructs, multiple peptides of the respective fusion proteins were detected by MS (Figure 15).

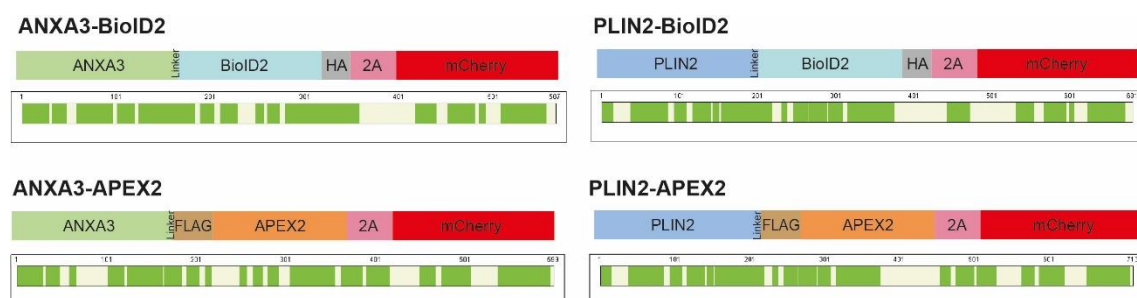


Figure 15: **Peptide coverage of BioID2 and APEX2 fusion proteins.**

Schematic illustration of fusion proteins with the respective detected peptide coverage using MS.

Pull down samples of cells expressing the ANXA3 or PLIN2 fusion proteins were compared to their respective control in four independent experiments. Detection ratios were centered by light over heavy peptides or heavy over light peptides for the label-switch by dividing through the median. The hits were ranked by mean enrichment of all four replicates with a set cutoff above 1.5-fold enrichment. In total, 736 proteins that were enriched or depleted with multiple peptides using ANXA3-BioID2 (Figure 16A), 774 using ANXA3-APEX2 (Figure 17A), 727 using PLIN2-BioID2 (Figure 18A) and 849 using PLIN2-APEX2 (Figure 19A) were identified. Next, proteins that were significantly enriched in pull down samples of cells expressing the ANXA3 or PLIN2 fusion proteins were selected ($p \leq 0.05$), leading to the identification of 17 proteins using ANXA3-BioID2, 3 using ANXA3-APEX2, 24 using PLIN2-BioID2 and 3 using PLIN2-APEX2 (Figures 16–19B). Overlap of all identified hits (enriched and depleted) from both PLIN2 screens with the previously published LD proteome by Bersuker *et al.* using PLIN2-APEX2 and ATGL-APEX2 in hepatoma cells (Bersuker *et al.*, 2018) revealed a total correlation of 93 proteins (Figure 20).

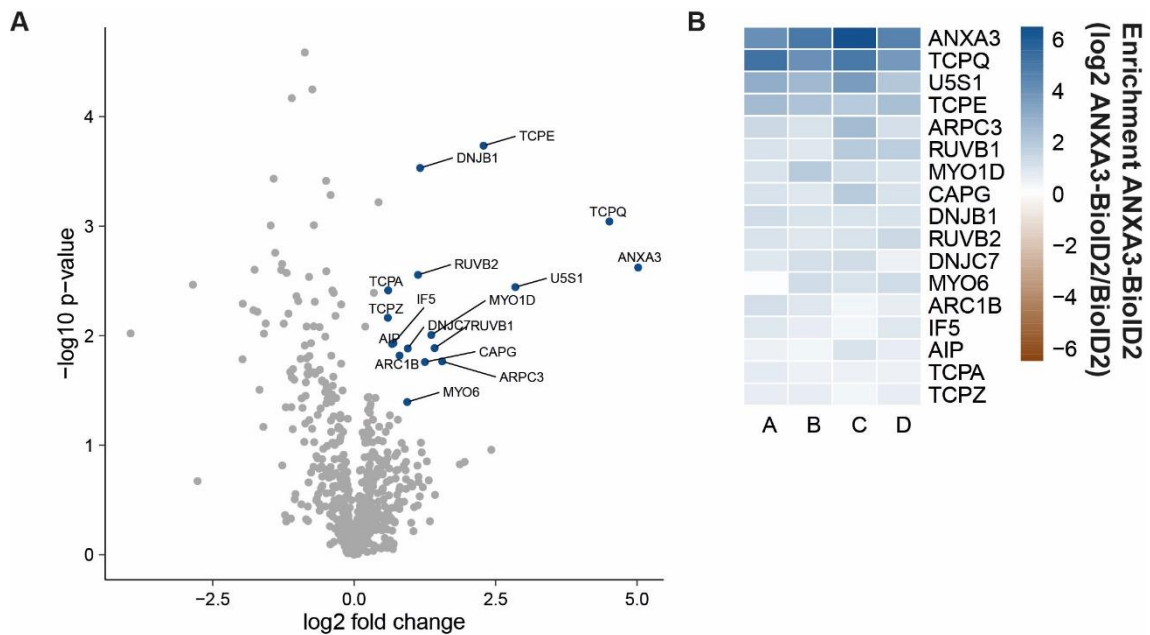


Figure 16: Quantitative analysis of ANXA3-BioID2 proximity labeled cells.

(A) Volcano plot showing identified proteins using ANXA3-BioID2 expressing Huh7.5 cells (1.5-fold cutoff). Highlighted are significantly enriched hits ($p \leq 0.05$). (B) Heatmap illustrating the significantly enriched proteins (1.5-fold cutoff, $p \leq 0.05$). (n = 4).

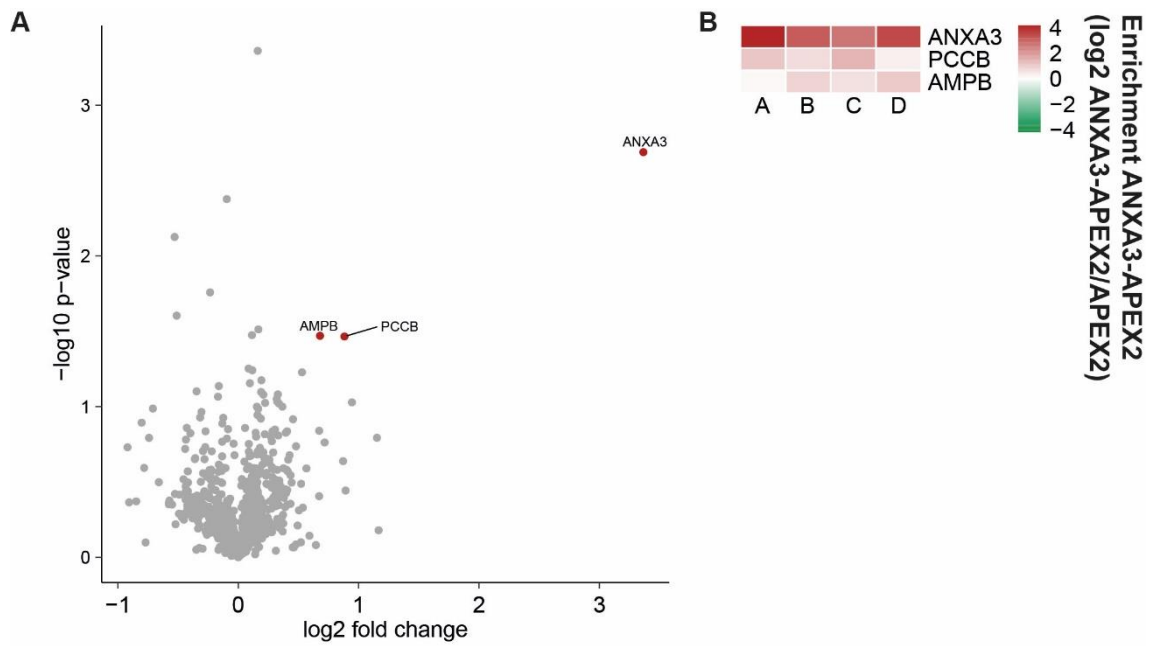


Figure 17: **Quantitative analysis of ANXA3-APEX2 proximity labeled cells.**

(A) Volcano plot showing identified proteins using ANXA3-APEX2 expressing Huh7.5 cells (1.5-fold cutoff). Highlighted are significantly enriched hits ($p \leq 0.05$). (B) Heatmap illustrating the significantly enriched proteins (1.5-fold cutoff, $p \leq 0.05$). ($n = 4$).

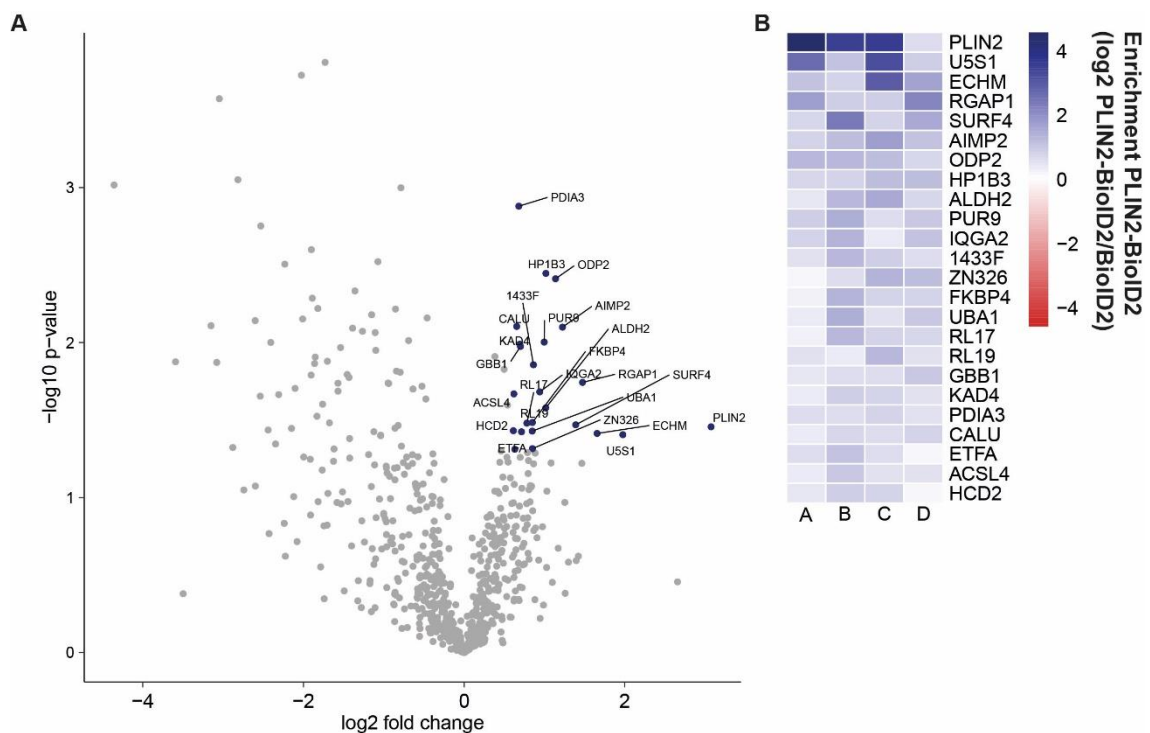


Figure 18: **Quantitative analysis of PLIN2-BioID2 proximity labeled cells.**

(A) Volcano plot showing identified proteins using PLIN2-BioID2 expressing Huh7.5 cells (1.5-fold cutoff). Highlighted are significantly enriched hits ($p \leq 0.05$). (B) Heatmap illustrating the significantly enriched proteins (1.5-fold cutoff, $p \leq 0.05$). ($n = 4$).

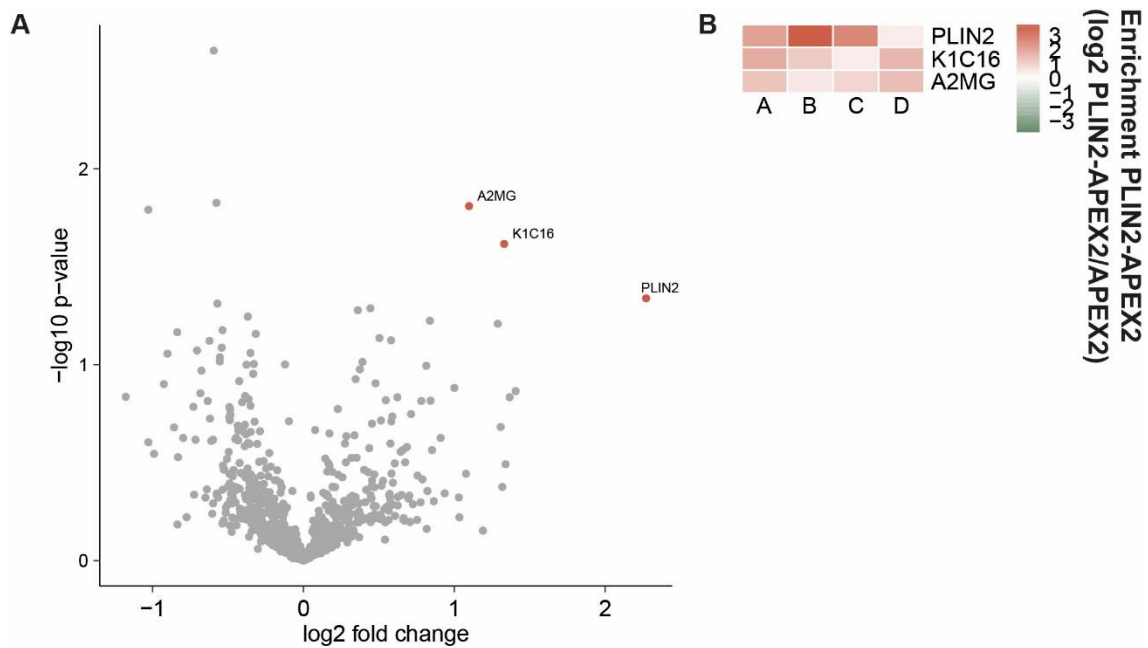


Figure 19: **Quantitative analysis of PLIN2-APEX2 proximity labeled cells.**

(A) Volcano plot showing identified proteins using PLIN2-APEX2 expressing Huh7.5 cells (1.5-fold cutoff). Highlighted are significantly enriched hits ($p \leq 0.05$). (B) Heatmap illustrating the significantly enriched proteins (1.5-fold cutoff, $p \leq 0.05$). ($n = 4$).

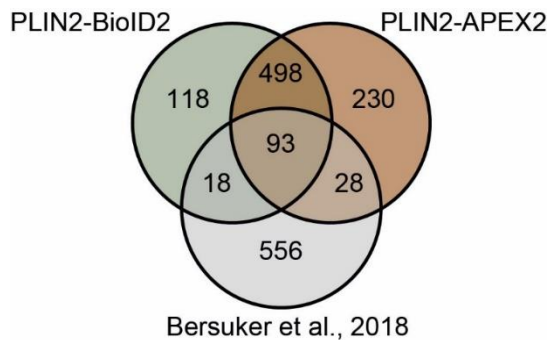


Figure 20: **Comparison of LD proteomes.**

Overlap of proteins identified by PLIN2-BioID2 and PLIN2-APEX2 labeled cells with the LD proteome described by Bersuker *et al.*, 2018.

3.1.4 SILAC and proximity labeling of ANXA3 and PLIN2 in HCV-infected hepatoma cells

To study changes in the LD proteome during HCV infection, heavy or light amino acid supplemented cells were transduced with lentiviral expression constructs for ANXA3-BioID2, ANXA3-APEX2, PLIN2-BioID2 or PLIN2-APEX2 and infected with an HCV Jc1^{NS5AB-EGFP} (Webster *et al.*, 2013) reporter strain or left uninfected. Two to 3 weeks post infection, cells were labeled as described above using biotin or BP/H₂O₂ (Figure 21). As an additional control, MS analysis was performed as described above comparing HCV-infected and uninfected control cells only expressing BioID2 or APEX2 (Figure S 1, S 2).

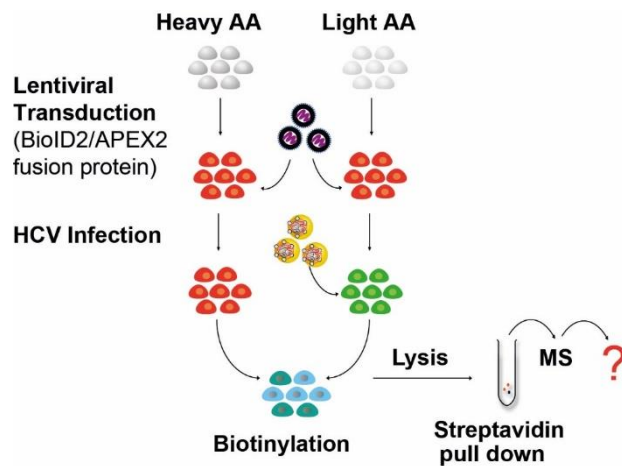


Figure 21: **Mass spectrometry of SILAC labeled cells.**

Huh7.5 cells cultured in media containing heavy or light amino acids were transduced with lentivirus expressing either ANXA3-BioID2, ANXA3-APEX2, PLIN2-BioID2 or PLIN2-APEX2 and infected with a Jc1^{NS5AB-EGFP} reporter strain (MOI 0.01). Cells were labeled *via* the BioID2 or APEX2 method, biotinylated were proteins pulled down using streptavidin-conjugated agarose beads and subjected to MS. HCV-infected cells were compared to uninfected cells.

Analysis was performed as described above. 543 proteins with multiple peptides that were enriched or depleted in infected cells using ANXA3-BioID2 compared to non-infected cells (Figure 22A), 709 using ANXA3-APEX2 (Figure 23A), 659 using PLIN2-BioID2 (Figure 24A) and 641 using PLIN2-APEX2 (Figure 25A) were identified. 19 proteins that were significantly enriched or depleted ($p \leq 0.05$) in infected cells were identified with ANXA3-BioID2 (Figure 22B), 5 using ANXA3-APEX2 (Figure 23B), 47 using PLIN2-BioID2 (Figure 24B) and 16 using PLIN2-APEX2 (Figure 25B).

Notably, ANXA3 was identified in the PLIN2-BioID2 and PLIN2-APEX2 screens along with other LD-associated proteins like PLIN3, ACSL3 and the DEAD-box proteins (DDX) (Rösch *et al.*, 2016; Vogt *et al.*, 2013).

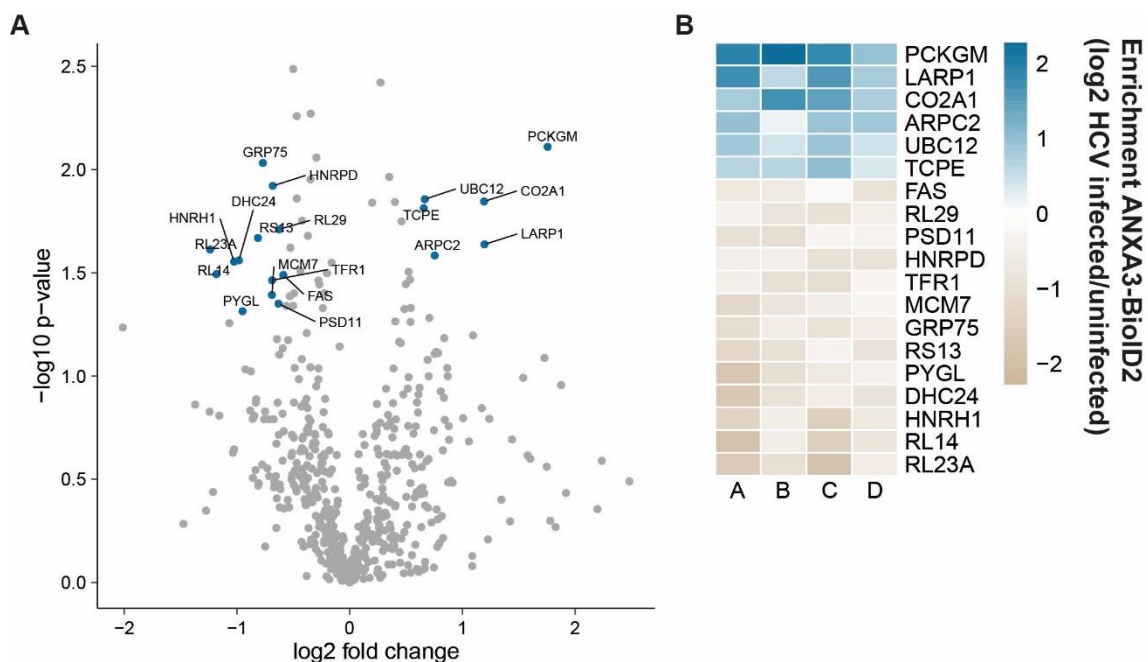


Figure 22: **Quantitative analysis of HCV-infected ANXA3-BioID2 proximity labeled cells.**

(A) Volcano plot showing identified proteins in infected ANXA3-BioID2 expressing Huh7.5 cells (1.5-fold cutoff). Highlighted are significantly enriched or depleted hits ($p \leq 0.05$). (B) Heatmap illustrating the significantly enriched or depleted proteins (1.5-fold cutoff, $p \leq 0.05$). (n = 4).

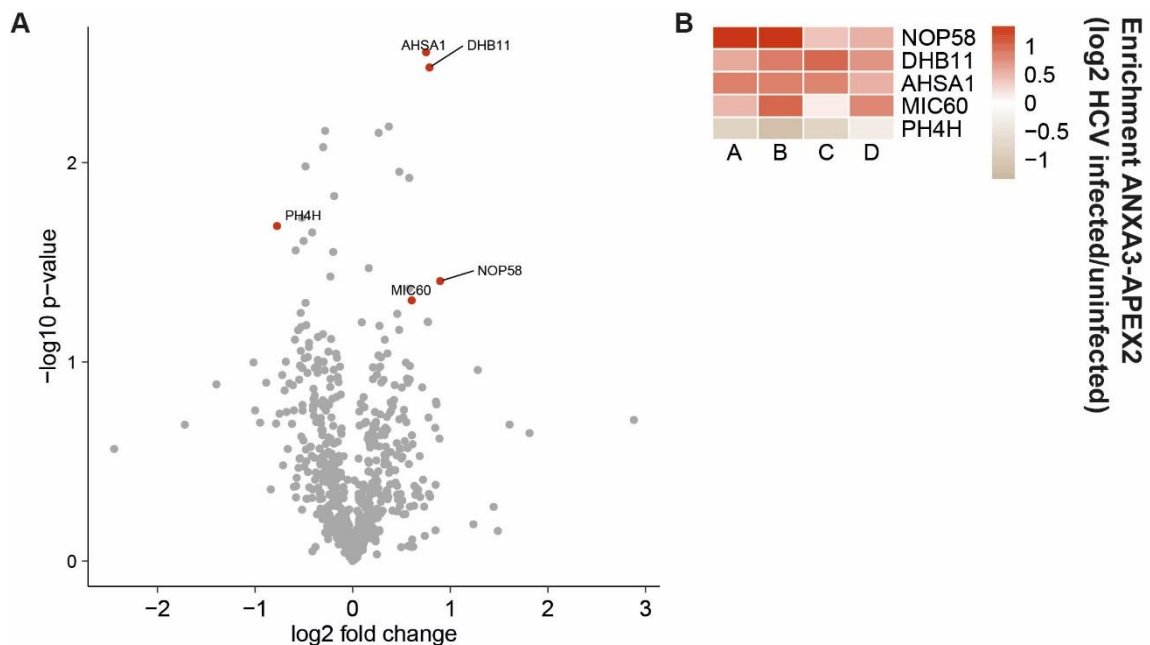


Figure 23: **Quantitative analysis of HCV-infected ANXA3-APEX2 proximity labeled cells.**

(A) Volcano plot showing identified proteins in infected ANXA3-APEX2 expressing Huh7.5 cells (1.5-fold cutoff). Highlighted are significantly enriched or depleted hits ($p \leq 0.05$). (B) Heatmap illustrating the significantly enriched or depleted proteins (1.5-fold cutoff, $p \leq 0.05$). (n = 4).

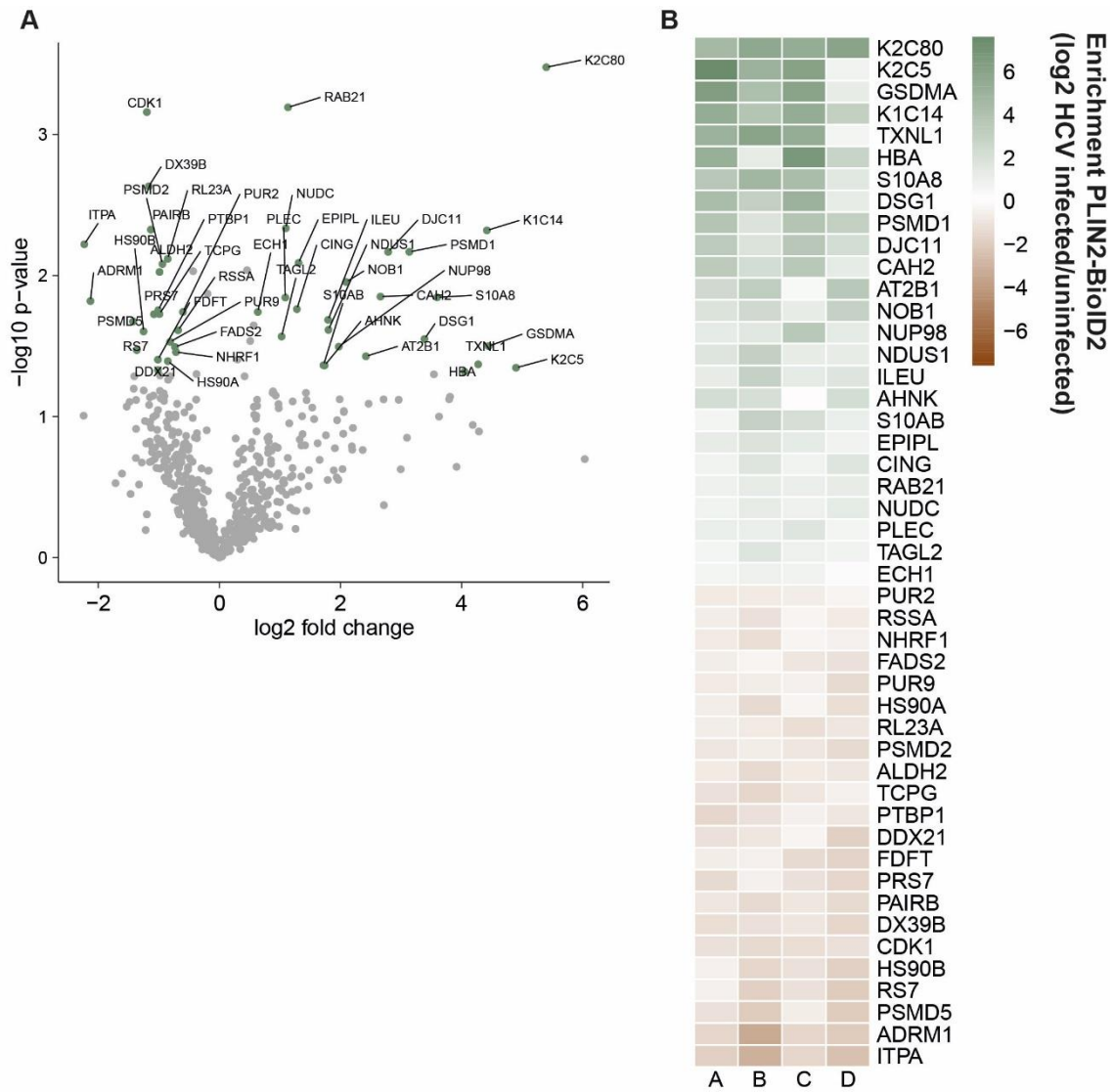


Figure 24: **Quantitative analysis of HCV-infected PLIN2-BioID2 proximity labeled cells.** (A) Volcano plot showing identified proteins in infected PLIN2-BioID2 expressing Huh7.5 cells (1.5-fold cutoff). Highlighted are significantly enriched or depleted hits ($p \leq 0.05$). (B) Heatmap illustrating the significantly enriched and depleted proteins (1.5-fold cutoff, $p \leq 0.05$). ($n = 4$).

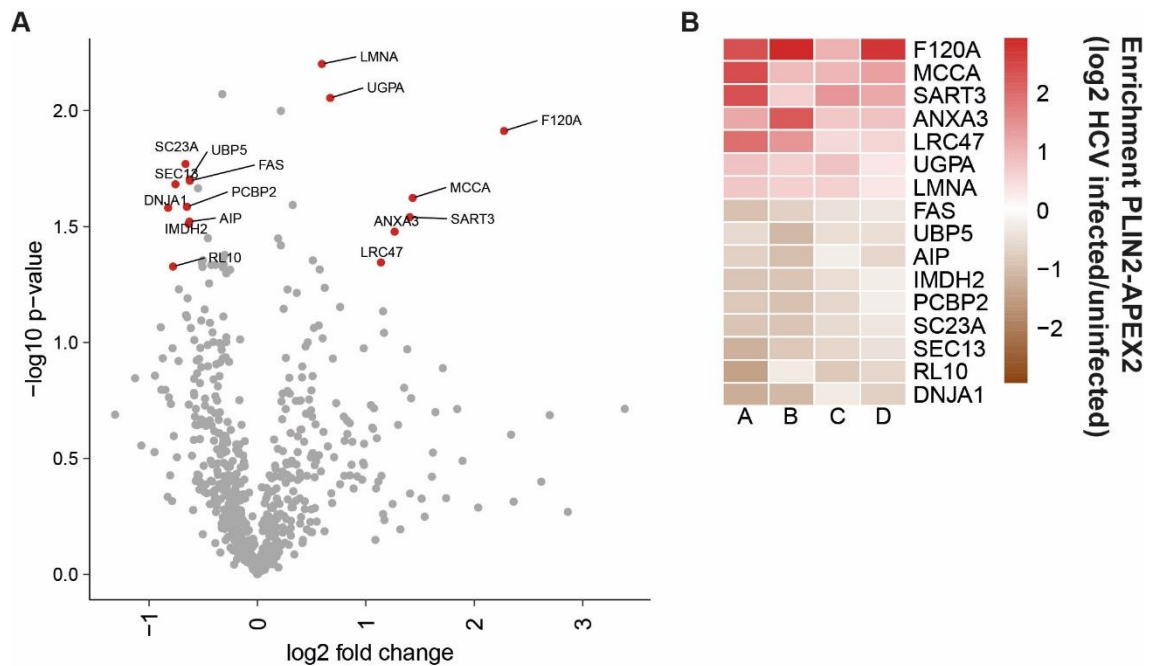


Figure 25: **Quantitative analysis of HCV-infected PLIN2-APEX2 proximity labeled cells.**

(A) Volcano plot showing identified proteins in infected PLIN2-APEX2 expressing Huh7.5 cells (1.5-fold cutoff). Highlighted are significantly enriched or depleted hits ($p \leq 0.05$). (B) Heatmap illustrating the significantly enriched and depleted proteins (1.5-fold cutoff, $p \leq 0.05$). ($n = 4$).

Comparison of all identified hits from ANXA3-BioID2 samples with ANXA3-APEX2 samples revealed an overlap of 441 proteins (Figure 26A). Thus, most hits identified with BioID2 were also detected with APEX2. Overlapping both ANXA3 screens with the previously published LD proteome in infected cells (Rösch *et al.*, 2016) resulted in 77 commonly identified proteins, mainly including described LD-associated proteins like PLIN2, PLIN3, ACSL3 and DDX (Figure 26B). Similarly, the hits identified by using PLIN2-BioID2 and PLIN2-APEX2 mostly overlapped in a total of 492 proteins (Figure 27A). Comparison with the LD proteome of HCV-infected cells revealed 90 proteins overlapping (Figure 27B).

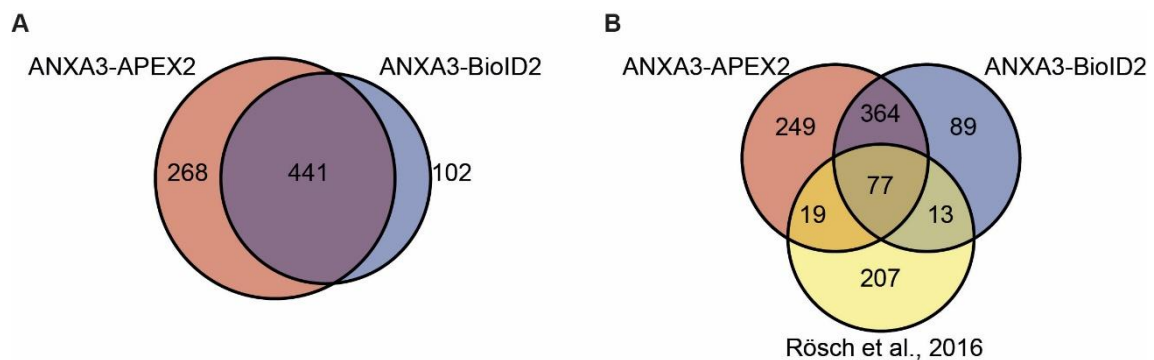


Figure 26: **Comparison of LD proteomes of HCV-infected cells.**

(A) Venn diagram depicting the number of overlapping proteins detected by ANXA3-BioID2 and ANXA3-APEX2 labeling in HCV-infected cells. (B) Overlap of proteins identified by proximity

labeling in HCV-infected ANXA3-BioID2 and ANXA3-APEX2-expressing cells with the identified LD proteome in HCV-infected cells by Rösch *et al.*, 2016.

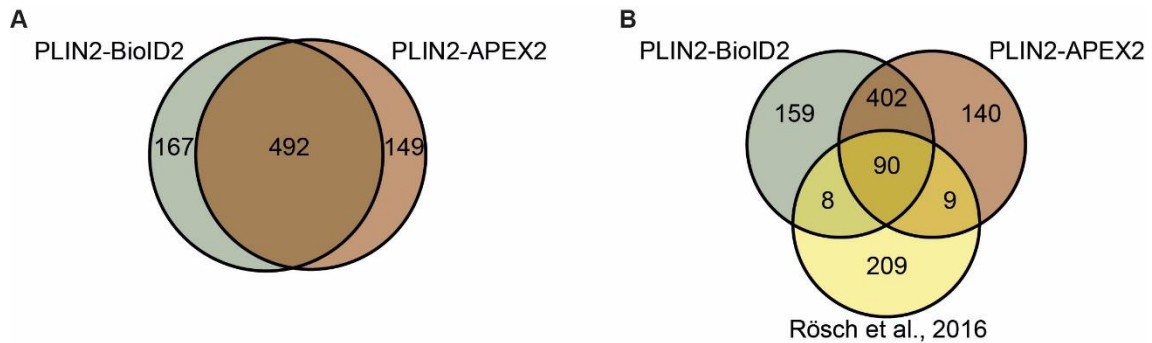


Figure 27: **Comparison of LD proteomes of HCV-infected cells.**

(A) Venn diagram depicting the number of overlapping proteins detected by PLIN2-BioID2 and PLIN2-APEX2 labeling in HCV-infected cells. (B) Overlap of proteins identified by proximity labeling in HCV-infected PLIN2-BioID2 and PLIN2-APEX2-expressing cells with the identified LD proteome in HCV-infected cells by Rösch *et al.*, 2016.

Gene ontology (GO) analyses were performed to associate the altered proteome in HCV-infected cells with molecular functions. Interestingly, most identified proteins with ANXA3 as well as PLIN2 screens are connected to viral processes and RNA metabolism (Figure 28).

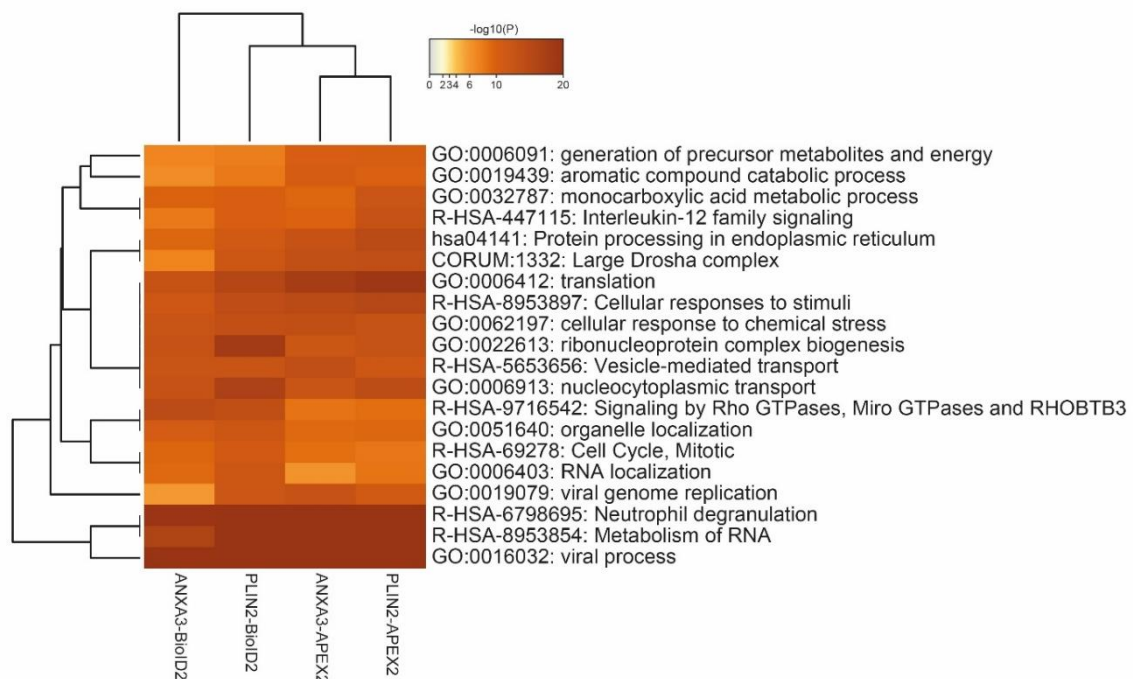


Figure 28: **Gene ontology.**

Heatmap representing top 20 enriched terms of identified hits in HCV-infected cells using ANXA3-BioID2, ANXA3-APEX2, PLIN2-BioID2 and PLIN2-APEX2 proximity labeling in all four experiments. Via Metascape the following resources were used: GO Biological Processes, GO Molecular Function, KEGG Pathways, Canonical Pathways, Reactome Gene Set and CORUM biological processes. Shown is the statistical significance ($-\log_{10}(P)$ value).

3.1.5 Proximity labeling of HCV proteins using PLIN2-BioID2 and PLIN2-APEX2

During HCV virion assembly the capsid protein core and NS5A are recruited to LDs (Camus *et al.*, 2013; Miyanari *et al.*, 2007). A recent study proposed that other proteins recruited to LDs upon HCV infection are not directly located at the surface of LDs, but rather at the surrounding ER-derived membranes (Lee *et al.*, 2019). Due to their spatial vicinity, proximity labeling of the LD-associated PLIN2 in HCV-infected cells was expected to cause labeling of the different HCV proteins. However, HCV proteins were absent in MS analysis.

In order to further investigate proximity labeling of HCV proteins at LDs, Huh7.5 cells stably expressing PLIN2-BioID2, PLIN2-APEX2 or the respective controls were electroporated with Jc1ΔE1/E2^{NS5AB-EGFP-BSD} reporter RNA that enables steady RNA replication and encapsidation, but not virion maturation due to the partial deletion in the envelope glycoproteins. Labeling, lysis and the streptavidin pull down were performed as described before and samples were analyzed by western blotting (Figure 29A). Using PLIN2-APEX2 as bait, core was specifically pulled down as a biotinylated protein, whereas PLIN2-BioID2 led to biotinylation of NS5A (Figure 29B). Additionally, NS5A was detected in the pull down samples of both, PLIN2-APEX2 and the APEX2 control. NS3 was biotinylated and captured with streptavidin in all samples, including the BioID2 and APEX2 controls. Of note, as shown above, the BioID2 and APEX2 controls led to biotinylation in the whole cell, which could include unspecific labeling of HCV proteins. Arguably, detection of HCV proteins by using only BioID2 or APEX2 not necessarily serves as a negative control.

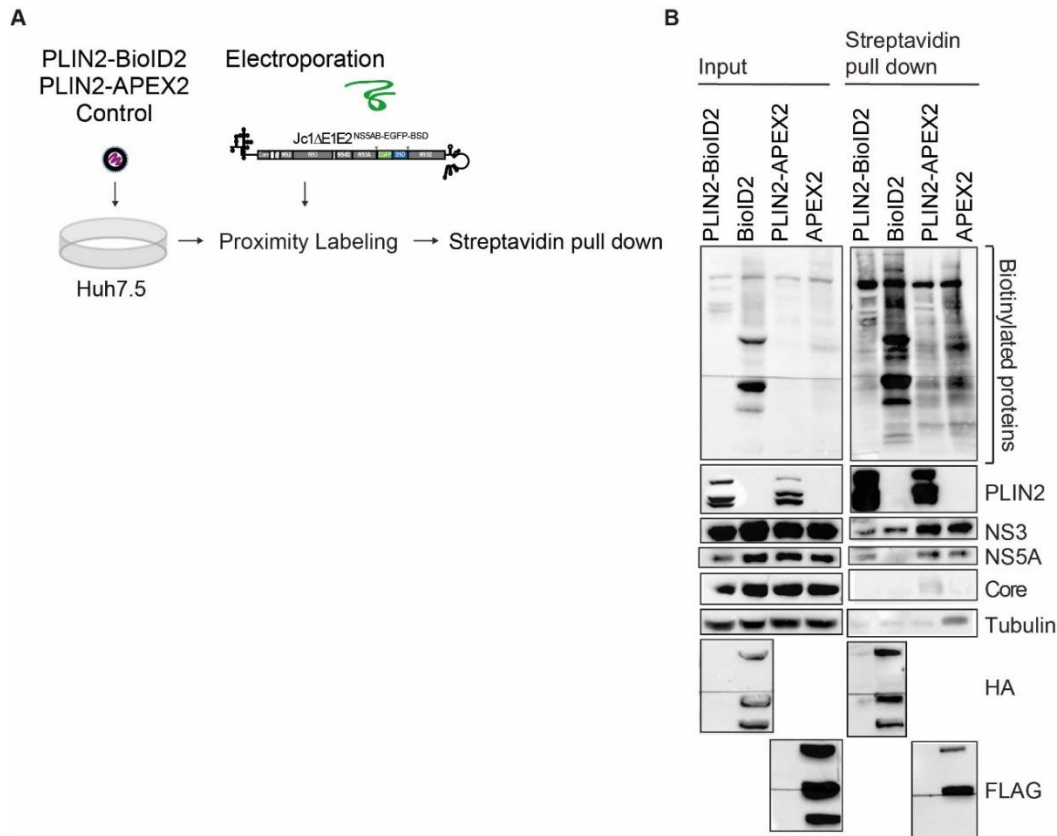


Figure 29: Selected HCV proteins are detected by PLIN2 proximity labeling during HCV replication.

(A) Huh7.5 cells were transduced with lentiviral constructs for PLIN2-BioID2, PLIN2-APEX2 or the respective controls and electroporated with Jc1ΔE1/E2^{NS5AB-EGFP-BSD} RNA. Cells were proximity labeled and biotinylated proteins were pulled down using streptavidin-coupled agarose beads followed by western blot analysis. (B) Western blot analysis of streptavidin pull down. To detect biotinylated proteins streptavidin-HRP was used. A PLIN2-specific antibody was used to verify PLIN2 fusion protein expression and HA or FLAG-specific antibodies were used to detect expression of BioID2 or APEX2. Membranes were probed with specific antibodies against the indicated viral proteins. Tubulin served as a loading control (n = 1).

To elevate the expression rates, HEK293T were transiently co-transfected cells with either PLIN2-BioID2 or PLIN2-APEX2 and plasmids for the expression of the single HCV proteins core, E1, E2, NS2, NS3, NS4A, NS4B, or NS5A (Figure 30A), all possessing a 3xFLAG-Tag (Ramage *et al.*, 2015). Labeling and streptavidin pull down were performed as described before for western blot analysis. PLIN2 overexpression highly varied between the samples, and subsequently the detection of biotinylated proteins with streptavidin-HRP showed an unequal biotinylation rate (Figure 30B–C). For the PLIN2-APEX2 and core, NS4B and E2 co-transfected samples the typical band ladder of biotinylated proteins was not detectable (Figure 30C). Nevertheless, using a FLAG-specific antibody core, NS2, NS3, NS4B and NS5A were detected in the PLIN2-BioID2 streptavidin pull down samples (black arrows, Figure 30B). The streptavidin pull down of PLIN2-APEX2 samples co-captured NS3 and E2, in spite of the low biotinylation rate (Figure 30C, black arrows).

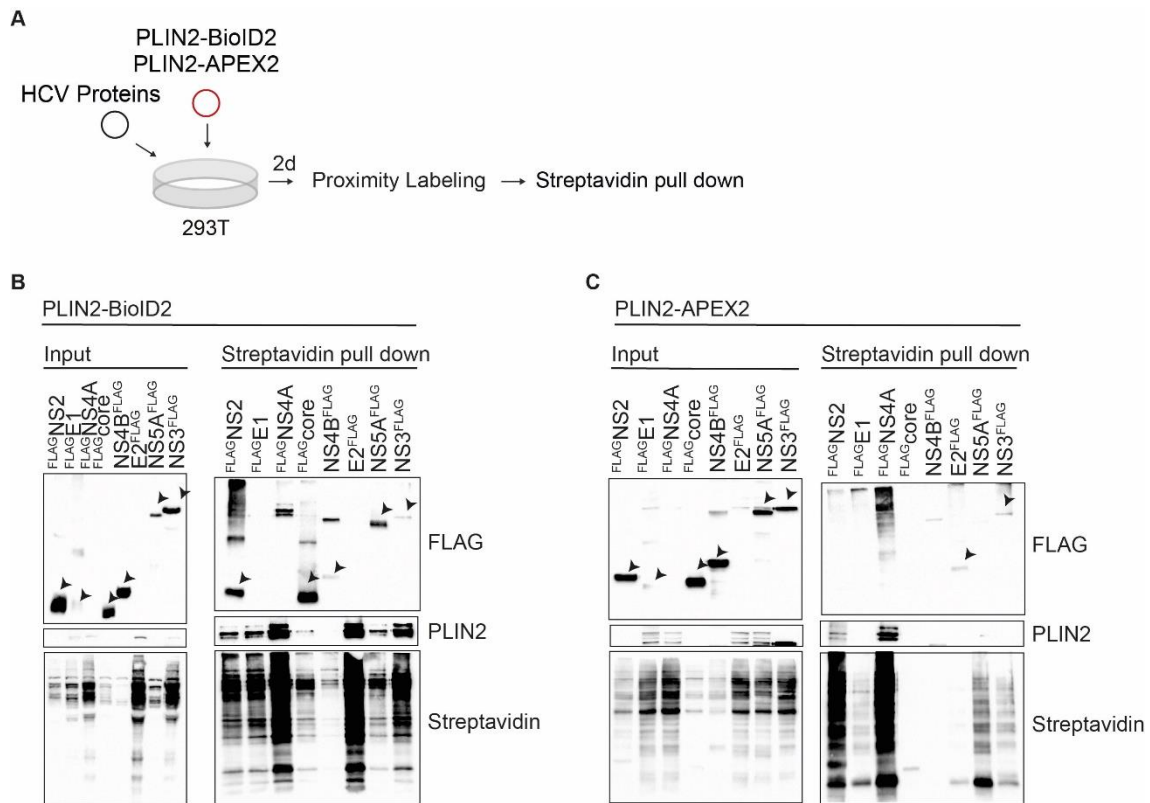


Figure 30: Transiently expressed HCV proteins are detected in close proximity to PLIN2 in HEK293T cells.

(A) HEK293T cells were co-transfected with PLIN2-BioID2, PLIN2-APEX2 and the indicated FLAG-tagged HCV protein expression plasmids and supplemented with oleic acid one day prior to lysis. Cells were proximity labeled and biotinylated proteins were pulled down by streptavidin-coupled agarose beads followed by western blot analysis. (B) Western blot analysis of streptavidin pull down of PLIN2-BioID2-expressing cells. (C) Western blot analysis of streptavidin pull down of PLIN2-APEX2-expressing cells. (B–C) To detect biotinylated proteins streptavidin-HRP was used and a FLAG specific antibody to detect the single FLAG-tagged HCV proteins. PLIN2 expression was detected using a PLIN2-specific antibody. Arrows mark correct bands for the indicated HCV proteins. (n = 1).

To attempt a stable expression of either PLIN2-BioID2 or PLIN2-APEX2, HEK293T cells were first transduced with lentiviral particles to express the PLIN2-BioID2 or PLIN2-APEX2 fusion protein, followed by transient transfection with plasmids expressing the FLAG-tagged HCV proteins core, E1, E2, p7, NS2, NS3, NS4A, NS4B, or NS5A (Figure 31A). Western blot analysis of input samples revealed that p7 was not sufficiently expressed (Figure 31B–C). The HCV proteins core, E2, NS2, NS3, NS4B and NS5A were captured by streptavidin pull down with PLIN2-BioID2 (Figure 31B). Interestingly, biotinylated proteins were detected in PLIN2-BioID2 samples of the streptavidin pull down, though, as visualized by probing membranes with streptavidin, biotinylation rates were low and varied. Using PLIN2-APEX2 a comparable biotinylation was observed in all samples prior to streptavidin pull down, but not after pull down (Figure 31C).

Interestingly, core, E2, NS3, and NS4B were still detectable in the streptavidin pull down samples. Repeating this experiment, the similar issues were observed (Figure S 3).

These data indicate that western blot analysis of biotinylated proteins upon PLIN2-BioID2 or PLIN2-APEX2 labeling can detect most transiently expressed HCV proteins. Seemingly, even lower biotinylation rates are sufficient to capture proximate proteins. Importantly, selected HCV proteins localize in spatial proximity to PLIN2 and therefore LDs.

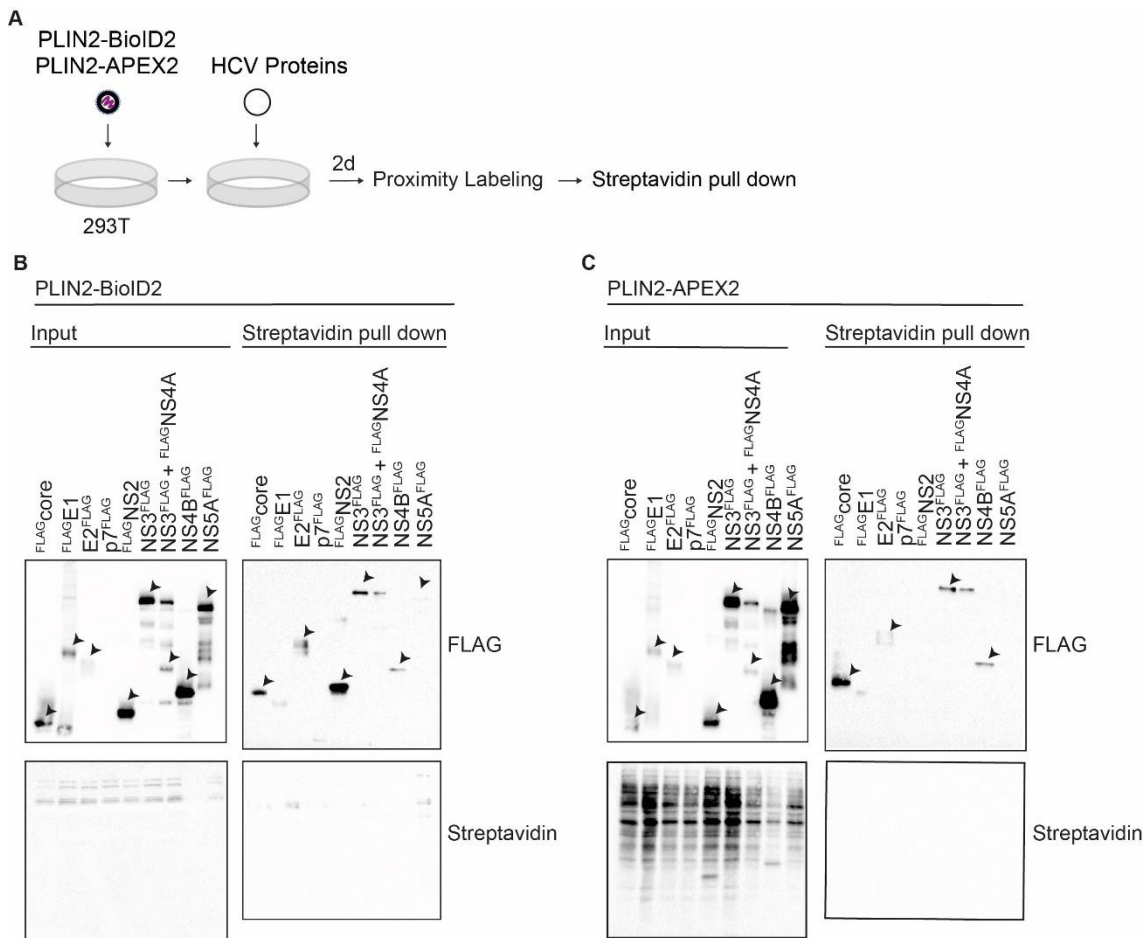


Figure 31: Transiently expressed HCV proteins are detected in close proximity of PLIN2 expressing HEK293T cells.

(A) HEK293T cells were transduced with lentivirus for stable PLIN2-BioID2 or PLIN2-APEX2 expression followed by transfection with the indicated FLAG-tagged HCV protein expression plasmids 2 days post transduction. One days later, cell were supplemented with oleic acid and after one more day, cells were proximity labeled and biotinylated proteins pulled down by streptavidin-coupled agarose beads followed by western blot analysis. (B) Western blot analysis of streptavidin pull down of PLIN2-BioID2-expressing cells. (C) Western blot analysis of streptavidin pull down of PLIN2-APEX2-expressing cells. To detect biotinylated proteins streptavidin-HRP was used and a FLAG-specific antibody to detect FLAG-tagged HCV proteins. (n = 2).

3.2 LD-localization and interaction with viral proteins of identified hits

To study the functional relevance of hits identified by proximity labeling in infected cells, enriched proteins of interest were selected for further investigation (Table 1). The fatty acid-binding protein 5 (FABP5) was enriched in infected ANXA3-BioID2 cells. The ADP-ribosylation factor-like protein 8B (ARL8B) was enriched in infected PLIN2-BioID2, PLIN2-APEX2 and ANXA3-BioID2 cells. The RNA-binding squamous cell carcinoma antigen recognized T cell protein (SART3, also known as HIV-1 Tat interacting protein if 110kDa (Tip110)) was enriched in the PLIN2-BioID2, the ANXA3-BioID2 screen and significantly enriched using PLIN2-APEX2. The RNA-binding protein NOB1 was identified *via* PLIN2-BioID2 as a significantly enriched protein. The RNA-binding La-related protein 1 (LARP1) was significantly enriched in infected ANXA3-BioID2 cells, but an enrichment was also detected with ANXA3-APEX2 and PLIN2-APEX2.

Table 1: Investigated hits identified as LD-proximate proteins in HCV-infected cells.

Protein	Identified Screen	Significantly enriched
FABP5	ANXA3-BioID2	
ARL8B	PLIN2-BioID2 PLIN2-APEX2 ANXA3-BioID2	
SART3	PLIN2-APEX2 PLIN2-BioID2 ANXA3-BioID2	yes
NOB1	PLIN2-BioID2	yes
LARP1	ANXA3-BioID2 ANXA3-APEX2 PLIN2-APEX2	yes

In order to validate that the identified hits are enriched in LD fractions, LDs were isolated from infected and uninfected Huh7.5 cells and analyzed by western blotting. For HCV infection, cells were infected with a Jc1^{NS5AB-EGFP} reporter strain for 2–3 weeks and uninfected cells of the same passage were used as uninfected control (mock). LDs were isolated by sucrose density centrifugation. Analysis of the LD marker PLIN2 confirmed enrichment of LDs (Brasaemle *et al.*, 1997; Fujimoto *et al.*, 2004). Detection of core served as control for HCV infection. LARP1 and SART3 were enriched in LD fractions of infected cells compared to non-infected cells, whereas NOB1 was detected in equal amounts at LDs of infected and uninfected cells (Figure 32A). ARL8B was not detected at LDs; however, an increased expression in the post-nuclear supernatant (PNS) of infected cells was observed, which is in agreement to what others have shown before (Jones-Jamtgaard *et al.*, 2019). Likewise, FABP5 was not enriched in LD fractions of infected or uninfected cells.

To investigate whether HCV RNA replication or the formation of replication organelles is causing the redistribution of the investigated host proteins to LDs, Huh7 cells were electroporated with Jc1ΔE1/E2^{NS5AB-EGFP-BSD} or Con1 subgenomic replicon (Con1-SGR) (Choi *et al.*, 2004) RNA. The Jc1ΔE1/E2^{NS5AB-EGFP-BSD} enables HCV replication and encapsidation, but no virion secretion due to a deletion in the envelope proteins, whereas the subgenomic replicon only contains the non-structural proteins NS3–NS5B to provide HCV RNA replication. Jc1ΔE1/E2^{NS5AB-EGFP-BSD} cells were cultivated under blasticidin selection and LDs were isolated 8 days post electroporation. Con1-SGR-electroporated Huh7 cells were grown under G418 selection and LDs were isolated 7 days post electroporation. Huh7 cells were used as the untransfected control. LARP1 was enriched at LDs of Jc1ΔE1/E2^{NS5AB-EGFP-BSD} harboring cells, but not control cells and to a lesser extent at LDs of Con1-SGR cells (Figure 32B). SART3 was enriched at LDs of Jc1ΔE1/E2^{NS5AB-EGFP-BSD} harboring cells as well as Con1-SGR cells. NOB1 was detected at LDs of all samples, but enriched at LDs of Jc1ΔE1/E2^{NS5AB-EGFP-BSD} and Con1-SGR-expressing cells. ARL8B was not found in LD fractions. Note, that the expression of ARL8B in the PNS of Huh7 cells is very low. FABP5 was detected in LD fractions of control and Con1-SGR cells in similar amounts and slightly reduced in Jc1ΔE1/E2^{NS5AB-EGFP-BSD} LD fractions.

The trafficking of the viral proteins core and NS5A is pivotal for HCV capsid formation and virion morphogenesis (Appel *et al.*, 2008; Boulant *et al.*, 2008; Camus *et al.*, 2013; Herker *et al.*, 2010; Miyanari *et al.*, 2007; Paul *et al.*, 2014; Shavinskaya *et al.*, 2007; Vogt *et al.*, 2013). In addition, it has been shown that some host factors are recruited following expression of at least one of those two LD-associated viral proteins (Rösch *et al.*, 2016; Schöbel *et al.*, 2021). Since the Jc1ΔE1/E2^{NS5AB-EGFP-BSD} construct contains core, but the Con1-SGR only expresses the proteins NS3–NS5B, it is possible that the expression and LD localization of core causes the differences in protein enrichment to LDs of Jc1ΔE1/E2^{NS5AB-EGFP-BSD} and Con1-SGR cells. Further, NS5A expression and LD localization could be involved in the redistribution of SART3 and ARL8B to LDs in Con1-SGR cells.

To further decipher the role of core of NS5A in the hit-protein recruitment to LDs, LDs were isolated from Huh7 cells that were transduced with lentivirus expressing either FLAG^{core} or NS5A^{FLAG}. As a control, Huh7 cells were transduced with lentivirus expressing an empty vector. LARP1 was only enriched at LDs of FLAG^{core}-expressing cells, but not NS5A^{FLAG}-expressing cells (Figure 32C). SART3 was not enriched at LDs compared to the control. NOB1 was detected at LDs of all samples, supporting the data shown in Figure 32A and 32B. ARL8B recruitment to LD fractions upon FLAG^{core} or NS5A^{FLAG} expression was not detected, however, in line with the data in Figure 32A, ARL8B is only

marginally expressed in Huh7 cells and was only detectable in the PNS of NS5A^{FLAG}-expressing cells (Figure 32C). FABP5 was detected in LD fractions of all samples. Still, a slight enrichment in LD fractions isolated from ^{FLAG}core-expressing cells compared to NS5A^{FLAG} and control cells was observed (Figure 32C).

These data indicate that LARP1 recruitment to LDs is dependent on core expression. SART3 was not enriched at LDs upon core or NS5A expression, suggesting a dependency on HCV RNA replication. NOB1 was detected in LD fractions even in the control cells, however, NOB1 was slightly enriched at LDs of HCV-replicating cells compared to the control. In contrast, ARL8B was not detected in LD fractions. Interestingly, FABP5 was not enriched in LD fractions of infected Huh7.5 cells, but at LDs of Huh7 cells expressing ^{FLAG}core.

To study a possible interaction of the identified hits with the viral proteins core and NS5A, Huh7.5 cells were transduced with lentivirus expressing either FLAG-tagged core or NS5A, lysed and subjected to immunoprecipitation followed by western blot analysis of the endogenous proteins. SART3, LARP1 and NOB1 co-precipitated with ^{FLAG}core but not with NS5A^{FLAG} (Figure 32D). FABP5 was co-precipitated in lysates from ^{FLAG}core-expressing cells, however, a smaller amount of FABP5 was also pulled down in control cells. ARL8B did not co-precipitate with ^{FLAG}core or NS5A^{FLAG}. As shown before (Rösch *et al.*, 2016), ANXA3 did not interact with core or NS5A.

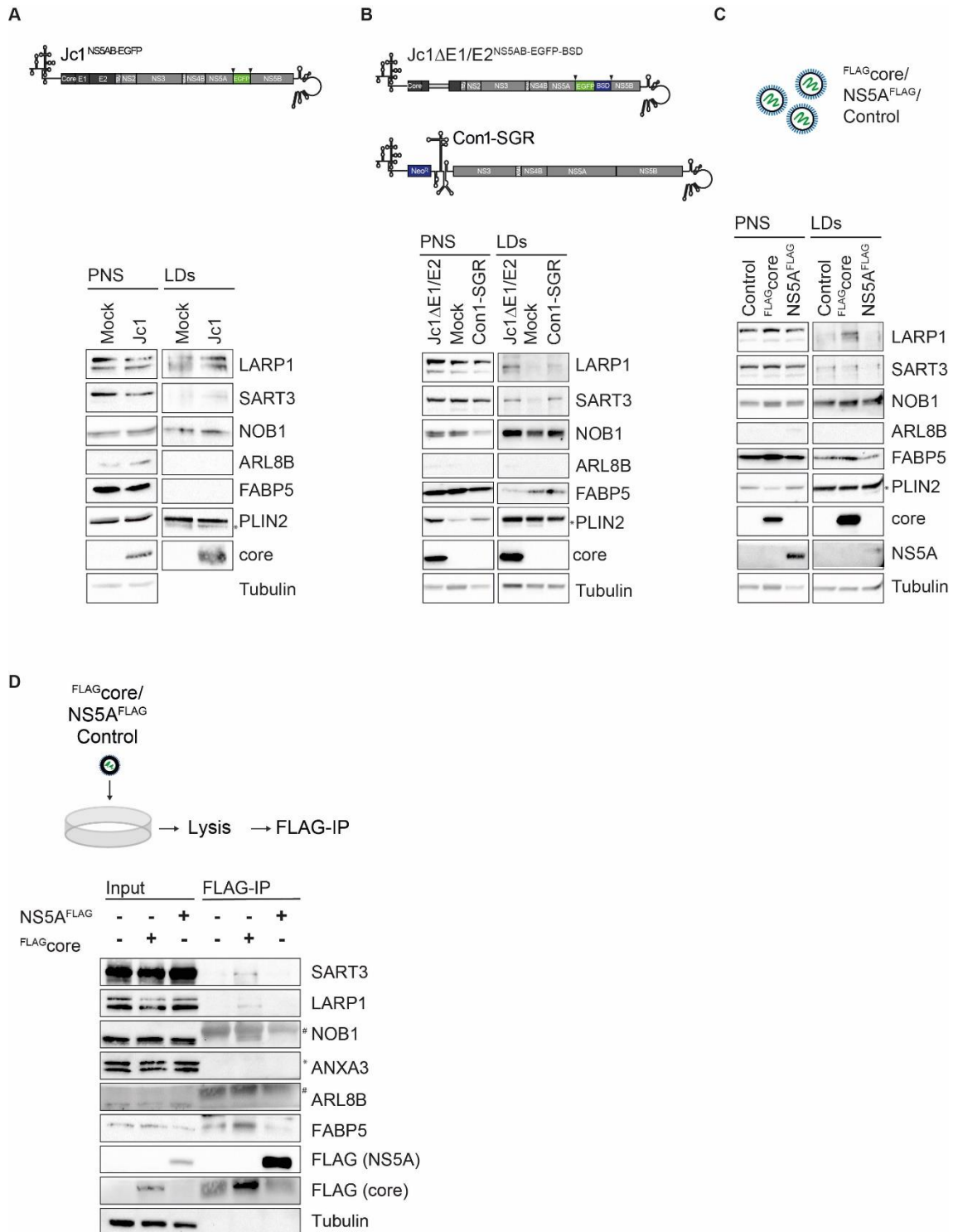


Figure 32: LD-localization and interaction with viral proteins of identified hits.

(A) Huh7.5 cells were infected with Jc1^{NS5AB-EGFP} (MOI 0.1) and LDs were isolated 14 dpi and analyzed by western blotting. (B) Huh7 cells were electroporated with either Jc1ΔE1/E2^{NS5AB-EGFP-BSD} or Con1-SGR RNA and selected for replication with blasticidin or G418, respectively. Isolated LDs were analyzed by western blotting. (C) LDs were isolated from Huh7 cells transduced with lentivirus expressing FLAG^{core}, NS5A^{FLAG} or a control and analyzed by western blotting. Membranes were probed using specific antibodies against the indicated proteins. Tubulin served as loading control for the post-nuclear supernatant (PNS) and PLIN2 was used as control for equally loaded LDs. (A–C) Shown are representative experiments (n = 3). (D) Huh7.5 cells were transduced with lentivirus expressing FLAG^{core} and NS5A^{FLAG} or the respective control. Three days post transduction cells were lysed and subjected to FLAG-specific immunoprecipitation (IP)

followed by western blot analysis using the indicated protein-specific antibodies and a FLAG-specific antibody. Tubulin was used as loading control ($n = 1$). Asterisks indicate unspecific bands. # indicate heavy and light antibody chains.

3.3 FABP5 does not influence the HCV viral life cycle

To further investigate the relocalization of FABP5 to LDs of core-expressing cells, Huh7 cells stably expressing a T7-tagged FABP5 construct and transiently expressing ^{FLAG}core were analyzed by immunofluorescence staining using a FABP5-specific antibody and confocal microscopy. The cytosolic localization of FABP5 was not altered by core expression in the cells (Figure 33A). These data were confirmed by using a T7-specific antibody (Figure 33B).

To further validate the interaction between FABP5 and core indicated by co-immunoprecipitation shown in Figure 32D, immunoprecipitation experiments were repeated using HEK293T cells and transient transfection. Cells were co-transfected with ^{T7}FABP5 and ^{FLAG}core expression plasmids, lysed and FLAG or T7-specific immunoprecipitations were performed for western blot analysis. Using a FLAG or T7-specific antibody, no co-precipitation between ^{T7}FABP5 and ^{FLAG}core was detected (Figure 33C).

To study the role of FABP5 in HCV infection, Huh7.5 were transduced with lentivirus expressing shFABP5 or a non-targeting control. Efficient knockdown rates were validated by qRT-PCR and western blotting (Figure 33D–E). Cell viability was monitored (Figure 33F). To analyze HCV spreading infection FABP5-knockdown cells were infected with a low multiplicity of infection (MOI) of Jc1^{NS5AB-EGFP}. Two, 4, and 6 days post infection (dpi) cells were analyzed by flow cytometry (Figure 33G). EGFP-positive cells were reduced by ~23% in FABP5-knockdown cells relative to the control at 4 dpi and by ~14% at 6 dpi. However, these values remained in the margin of error and were not significant. As an alternative method, FABP5-knockdown cells were infected with a Jc1^{p7-GLuc-2A-NS2} reporter strain. Supernatants were harvested 2, 4 and 6 dpi and infection rates were determined by performing a *gaussia* luciferase assay (Figure 33H). Infection rates in FABP5-knockdown cells were equal to the control. To assess if virion production is altered, naïve Huh7.5 cells were infected with the supernatant of infected FABP5-knockdown cells. Again, *gaussia* luciferase values were comparable between shFABP5 and shNT samples (Figure 33I). This suggests that depletion of FABP5 does not alter viral spreading or virion production.

To examine HCV RNA replication, FABP5-knockdown cells were electroporated with Jc1ΔE1/E2^{NS5AB-FLuc} RNA and the firefly luciferase activity was measured 4 hours, and 1, 2 and 3 days post electroporation (dpe). Values of 1, 2, and 3 dpe were normalized to protein concentrations and the 4 hour values (Figure 33J). FABP5-knockdown cells showed similar values to the non-targeting control. Taken together, these data suggest no specific role for FABP5 in HCV replication and spreading infection.

Results

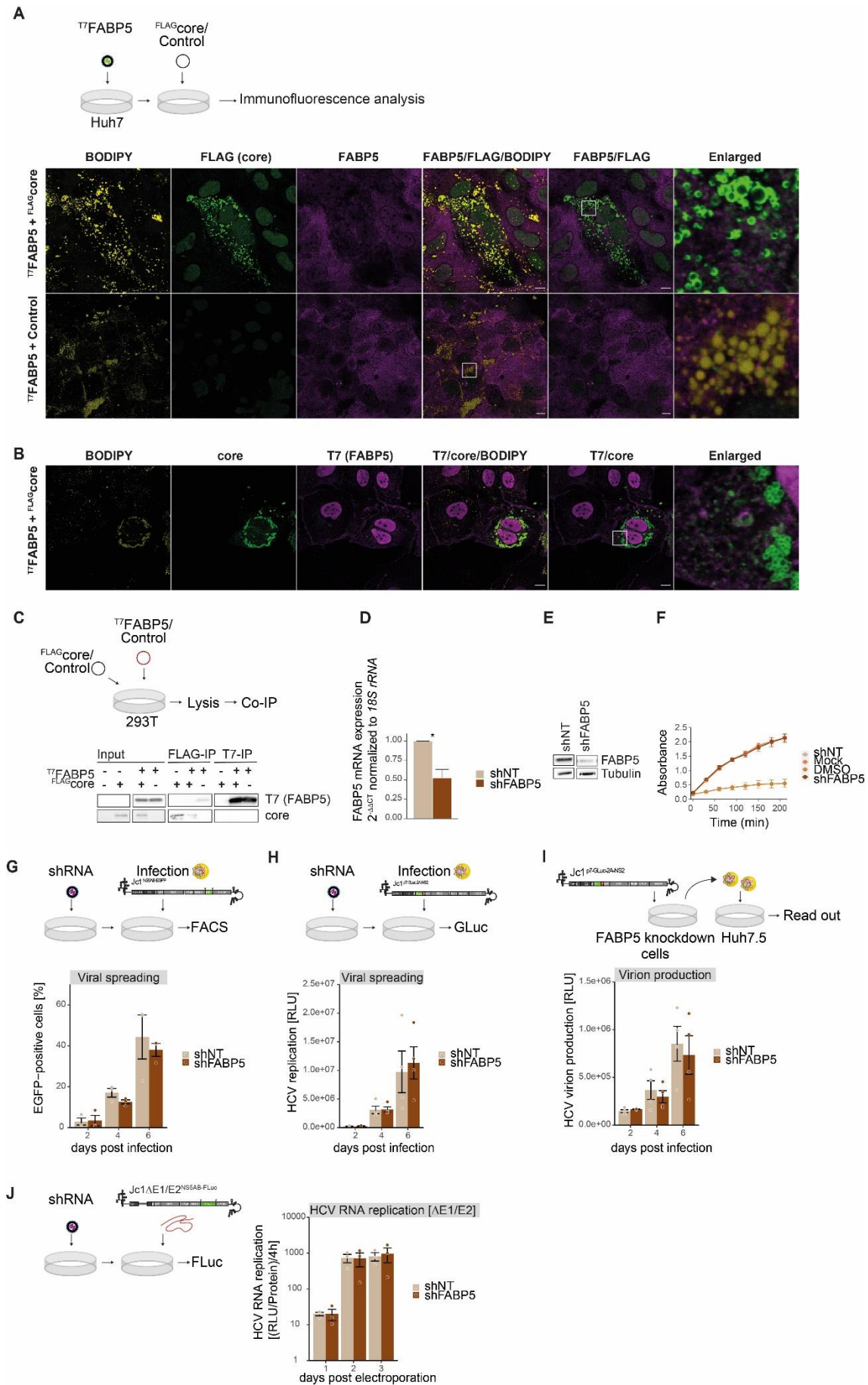


Figure 33: FABP5 is not involved in the HCV life cycle.

(A) Huh7 cells were transduced with a lentiviral particles for stable expression of ^{T7}FABP5 3 days prior to transfection with a ^{FLAG}core expression plasmid or a control vector. Three days later cells were fixed and stained for immunofluorescence with FABP5-specific and FLAG-specific antibodies (A) or T7- specific and core-specific antibodies (B). LDs were stained using BODIPY 493/503. White squares indicate enlarged areas. Scale bars = 10 μ m. (n = 1). (C) HEK293T cells were co-transfected with ^{FLAG}core and ^{T7}FABP5 expression plasmids or respective controls. Three days later cells were lysed and immunoprecipitation with FLAG-coupled beads or T7-coupled beads was performed. For western blot analysis of lysates (Input) and co-immunoprecipitated samples, membranes were probed with core and T7-specific antibodies. Shown is one representative experiment (n = 2). (D) Huh7.5 were transduced with lentivirus carrying either shRNA targeting FABP5 (shFABP5) or a non-targeting sequence (shNT). Knockdown efficacy was verified by qRT-PCR. Shown are $2^{-\Delta\Delta CT}$ values normalized to 18S rRNA and shNT (Mean \pm SEM, *p \leq 0.05, n = 3). (E) Protein levels of FABP5 in shFABP5 and shNT-transduced Huh7.5 cells were compared by western blot using a FABP5-specific antibody. Tubulin served as loading control (n = 3). (F) Viability assay for shRNA transduced cells. Cells treated with 10% DMSO (DMSO) served as non-viable control. (Mean \pm SEM, n = 4). (G) Huh7.5 cells were transduced with lentiviral particles for shFABP5 or shNT. Three days after transduction cells were infected with Jc1^{NS5AB-EGFP} (MOI 0.002) and cells were fixed 2, 4 and 6 dpi for FACS analysis. Shown are relative numbers of EGFP-positive cells (Mean \pm SEM, n = 3). (H) Huh7.5 were transduced with lentivirus carrying shFABP5 or shNT. Three days after transduction cells were infected with Jc1^{p7-GLuc-2A-NS2} (MOI 0.5), supernatants were harvested 2, 4 and 6 dpi and analyzed by luciferase assay (Mean \pm SEM, n = 4). (I) Naïve Huh7.5 cells were incubated with supernatant from (H) and analyzed by luciferase assay 2 days later. (Mean \pm SEM, n = 4). (J) Huh7.5 cells were transduced with lentivirus expressing shFABP5 or shNT electroporated with Jc1 Δ E1/E2^{NS5AB-FLuc} luciferase reporter RNA and analyzed by luciferase assay. HCV RNA replication was measured by luciferase activity. Shown is RLU per microgram (μ g) protein normalized to the 4 hour (h) time point (Mean \pm SEM, n = 3). (RLU, relative light units).

3.4 ARL8B is required for HCV spreading

A recent study reported that ARL8B is upregulated in HCV-infected cells and plays a role in an HCV-induced autophagic block that is crucial for virion secretion (Jones-Jamntgaard *et al.*, 2019). ARL8B expression was increased in HCV-infected cells by 3-fold and ARL8B localized at lysosomes. Overexpression of ARL8B led to redistribution of lysosomes to the cell periphery, which blocked autophagosome-lysosome fusion. Knockdown of ARL8B restored normal autophagosome-lysosome fusion in HCV-infected cells. Virion secretion was reduced in ARL8B-knockdown cells, whereas HCV RNA replication was not altered.

The data shown in Figure 32 did not indicate a relocalization of ARL8B to LDs. Combined with the data reported by Jones-Jamntgaard *et al.*, ARL8B most likely localizes to lysosomes in HCV-infected cells and might spatially be in close proximity to LDs or interact *via* membrane contact sites.

To visually investigate this hypothesis, Huh7 cells stably expressing ^{T7}ARL8B were transiently transfected with a ^{FLAG}core expression plasmid and the subcellular localization of ARL8B was analyzed by immunofluorescence staining and confocal microscopy. First, cells overexpressing ^{T7}ARL8B and stained with an ARL8B-specific antibody were

analyzed (Figure 34A). ^{T7}ARL8B appeared in cytosolic puncta as described by others (Jones-Jamtgaard *et al.*, 2019) and localized in close proximity to LDs, but did not colocalize with core at LDs. Next, a T7-specific antibody was used for staining of ^{T7}ARL8B (Figure 34B). Supporting the previous data, ARL8B did not colocalize with core.

In line with Jones-Jamtgaard *et al.*, an elevated expression of overexpressed ARL8B was observed in infected cells (Figure 34C). Additionally, Huh7.5 cells stably overexpressing ^{T7}ARL8B showed an increased core protein level after HCV infection (Figure 34C).

Likely, ARL8B is increased upon HCV infection, and in turn supports further HCV replication, thus leading to increased core expression in the cell. This effect is independent of a direct interaction with viral proteins.

In order to further investigate the functional role of ARL8B during HCV infection, ARL8B was downregulated in Huh7.5 cells using lentiviral shRNA. Knockdown efficiency was validated by qRT-PCR (Figure 34D) and western blot analysis (Figure 34E). Cell viability was compared to the non-targeting control (Figure 34F).

HCV spreading was studied by infecting ARL8B-knockdown cells with a low MOI of Jc1^{NS5AB-EGFP} and EGFP-positive cells were monitored at 2, 4 and 6 dpi by flow cytometry (Figure 34G). The ratio of infected cells in the shARL8B population was decreased by ~50% at 4 dpi and by ~70% at 6 dpi compared to the non-targeting control. To confirm these data, knockdown cells were infected with a Jc1^{p7-GLuc-2A-NS2} reporter strain and supernatants were measured for *gaussia* luciferase activity 2, 4 and 6 dpi. HCV spreading was decreased by 60% in ARL8B-knockdown cells at 4 and 6 dpi (Figure 34H). Incubating naïve Huh7.5 cells with the supernatant of infected shARL8B cells harvested at 6 dpi showed a marginal reduction in *gaussia* luciferase values (Figure 34I). The effect of ARL8B depletion on HCV RNA replication was studied by electroporating ARL8B-knockdown cells with Jc1ΔE1/E2^{NS5AB-FLuc} RNA. Firefly luciferase activity was determined 4 hours, 1, 2 and 3 dpe. ARL8B knockdown did not show any changes in HCV RNA replication (Figure 34J).

These data support previous studies that illustrate an ARL8B-dependent role for HCV infection in the later stages of the viral life cycle.

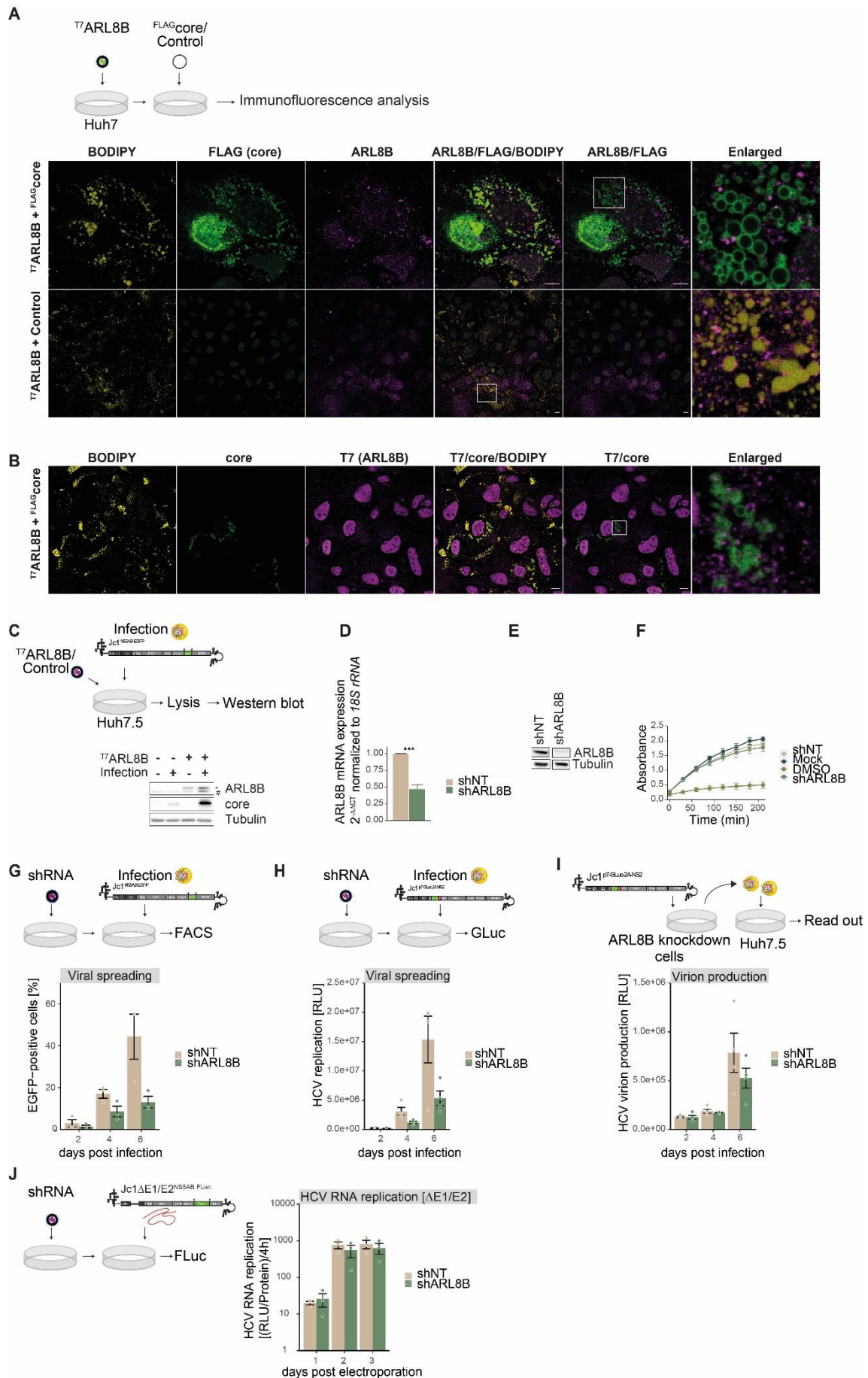


Figure 34: ARL8B is required for HCV spreading.

(A) Huh7 cells were transduced with lentiviral particles for stable ^{T7}ARL8B expression 3 days prior to transfection with a ^{FLAG}core or a control expression plasmid. Three days later cells were fixed and stained with ARL8B-specific and FLAG-specific antibodies (A) or T7- specific and core-specific antibodies (B). LDs were stained using BODIPY 493/503. White squares indicate enlarged areas. Scale bars = 10 μ m. (A) n = 2, (B) n = 1. (C) Huh7.5 cells were transduced with lentivirus expressing ^{T7}ARL8B and infected with Jc1^{NS5AB-EGFP} (MOI 0.2) for 6 days, lysed and analyzed by western blotting using an ARL8B-specific antibody. # indicates endogenous ARL8B and * marks T7-tagged ARL8B. Core served as marker for HCV infection and tubulin was used as loading control (n = 1). (D) Huh7.5 were transduced with lentivirus carrying either shARL8B or shNT. Knockdown efficacy was verified by qRT-PCR. Shown are 2^{- $\Delta\Delta$ CT} values normalized to 18S rRNA and shNT. Experiments were performed in technical duplicates. (Mean \pm SEM, ***p \leq 0.01, n = 3). (E) Protein levels of ARL8B in shARL8B and shNT-transduced Huh7.5 cells were compared by western blot using an ARL8B-specific antibody. Tubulin served as loading control (n = 3). (F) Viability assay for shRNA transduced cells. Cells treated with 10% DMSO (DMSO) served as non-viable control. (Mean \pm SEM, n = 4). (G) Huh7.5 cells were transduced with lentiviral particles to express shARL8B or shNT. Three days post transduction cells were infected with Jc1^{NS5AB-EGFP} (MOI 0.002) and cells were fixed 2, 4 and 6 dpi for FACS analysis. Viral spreading is shown in relative numbers of EGFP-positive cells (Mean \pm SEM, n = 3). (H) Huh7.5 were transduced with lentivirus carrying shARL8B or shNT. Three days after transduction cells were infected with Jc1^{p7-GLuc-2A-NS2} (MOI 0.5), supernatants were harvested 2, 4 and 6 dpi and analyzed by luciferase assay (Mean \pm SEM, n = 4). (I) Naïve Huh7.5 cells were incubated with supernatant from (H) and analyzed by luciferase assay 2 days later (Mean \pm SEM, n = 4). (J) shARL8B or shNT Huh7.5 cells were electroporated with Jc1 Δ E1/E2^{NS5AB-FLuc} RNA. HCV RNA replication was measured by luciferase activity. Shown is RLU per μ g protein normalized to the 4 h time point. (Mean \pm SEM, n = 3). (RLU, relative light units).

3.5 SART3 interacts with core and supports viral spreading and virion production

The RNA-binding protein SART3 is a substrate targeting factor for the ubiquitin-specific protease 15 (USP15). USP15 regulates HCV RNA replication and LD formation (Kusakabe *et al.*, 2019; Whitmill *et al.*, 2016). Interestingly, SART3 interacts with Y-box protein1 (YB1), another RNA-binding protein that is recruited to LDs during HCV infection as part of a ribonucleoprotein (RNP) complex and regulates virion assembly in an NS3 dependent manner (Chatel-Chaix *et al.*, 2013). The data shown in Figure 32 suggest that SART3 is recruited to LDs, not upon expression of viral proteins core and NS5A, but upon HCV replication. Of note, LD fractions of HCV-infected cells were analyzed by western blotting and probed with an USP15-specific antibody. Preliminary data indicate an enrichment of USP15 in LD fractions of HCV-infected cells, matching previously published results by Kusakabe *et al.* (Figure S 4).

In order to further investigate the cellular localization of SART3, immunofluorescence analyses of core-expressing cells were performed. To do so, Huh7 cells were transduced with lentivirus expressing ^{T7}SART3 and transfected with a ^{FLAG}core expression plasmid. Using an SART3-specific antibody, a strong nuclear localization of ^{T7}SART3 was

observed (Figure 35A), but ^{T7}SART3 was also detectable in the cytoplasm in low amounts. This phenotype was confirmed using a T7-specific antibody (Figure 35B). The cytosolic signal of SART3 showed a partial co-occurrence with core. However, this signal was very weak and punctual. Thus, SART3 is mainly expressed in the nucleus, but at least partially co-occurs with core.

To explore the observed connection between SART3 and core (Figure 32D) in more detail, HEK293T cells were co-transfected with ^{T7}SART3 and ^{FLAG}core expression plasmids, lysed and subjected to FLAG or T7-specific immunoprecipitation. Western blot analysis confirmed an interaction between SART3 and core (Figure 35C).

Thus, these data reveal an interaction between SART3 and core. However, microscopic analysis revealed that levels of SART3 at LDs remain low upon core expression compared to its nuclear localization. Possibly, SART3 is part of a RNP complex that is recruited to LDs during HCV infection.

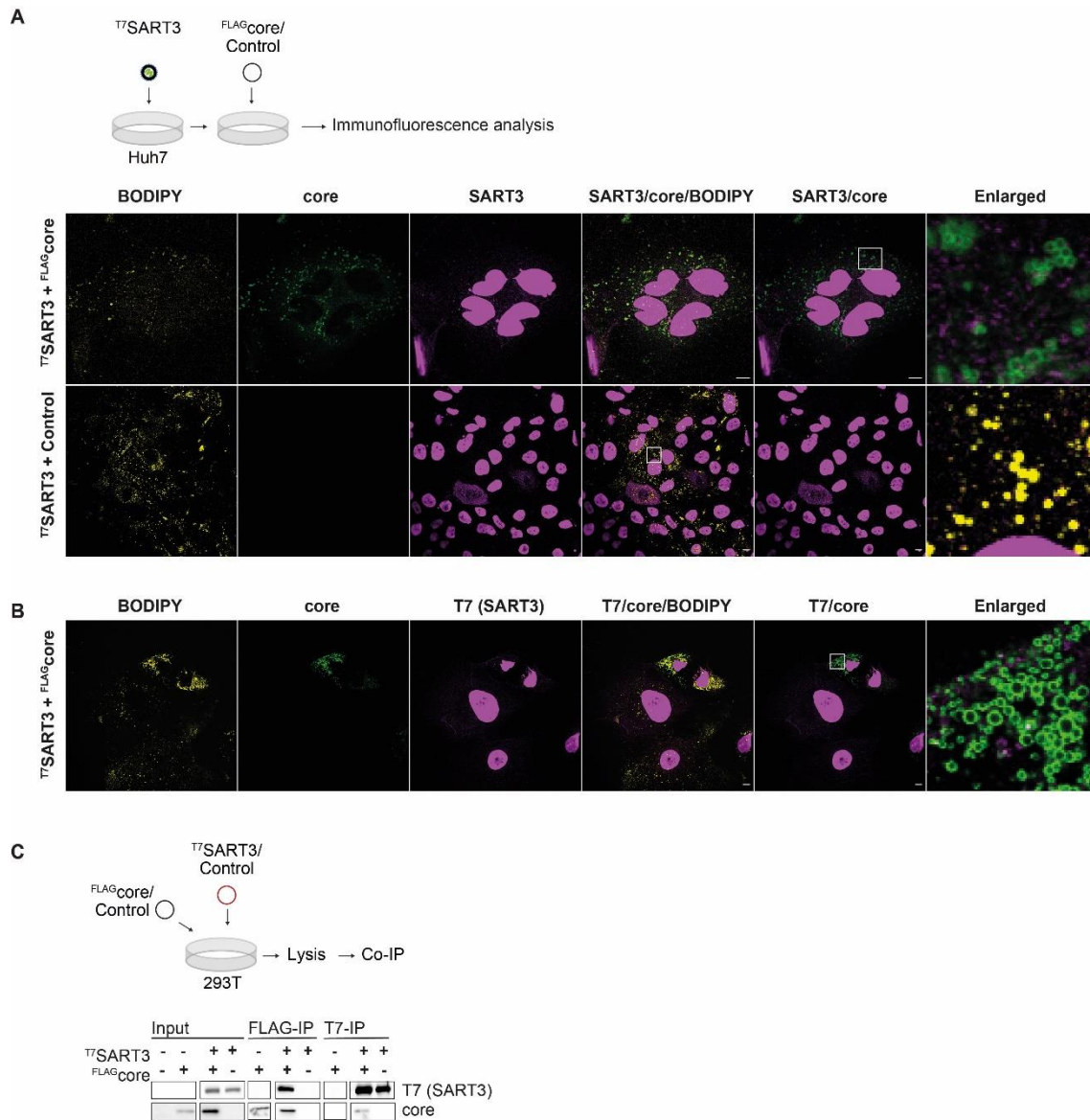


Figure 35: SART3 interacts with core.

(A) Huh7 cells were transduced with lentiviral particles for T7SART3 expression 3 days prior to transfection with expression plasmids for FLAGcore or an empty vector control. Three days later cells were fixed and stained with SART3-specific and core-specific antibodies (A) or T7-specific and core-specific antibodies (B). LDs were stained using BODIPY 493/503. White squares indicate enlarged areas. Scale bars = 10 μ m. (A) n = 2, (B) n = 1. (C) HEK293T cells were transfected with FLAGcore and T7SART3 expression plasmids or the respective controls. Three days later cells were lysed and immunoprecipitation was performed using FLAG-coupled beads or T7-coupled beads. Western blots were probed with core and T7-specific antibodies. Shown is one representative experiment (n = 2).

Since SART3 interacts with the viral capsid protein, it might serve as host factor in the HCV viral life cycle. To investigate the role of SART3, Huh7.5 cells were transduced with lentiviral particles expressing a SART3 targeting shRNA. The knockdown efficiency was validated by qRT-PCR (Figure 36A) as well as western blot analysis (Figure 36B) and cell viability was measured (Figure 36C). To study HCV spreading, shSART3 and shNT knockdown cells were infected with Jc1^{NS5AB-EGFP} and EGFP-positive cells were

quantified by flow cytometry 2, 4 and 6 dpi (Figure 36D). Compared to the non-targeting control, the infected cell ratio in shSART3 cells was reduced by 35% at 4 dpi and 20% at 6 dpi. However, the measured data varied and only two replicates were concluded. As an alternative method, knockdown cells were infected with a Jc1^{p7-GLuc-2A-NS2} reporter strain and supernatants were analyzed for *gaussia* luciferase activity at 2, 4 and 6 dpi. HCV spreading was not affected in SART3-knockdown cells 4 and 6 dpi (Figure 36E). To study virion production, naïve Huh7.5 cells were incubated with the supernatant of infected SART3-knockdown cells and *gaussia* luciferase activity was analyzed 2 days later. No difference in luciferase activity compared to the non-targeting control was observed (Figure 36F). Interestingly, in ^{T7}SART3-overexpressing cells HCV spreading and virion production was slightly increased (Figure 36G, H). ^{T7}SART3 overexpression was validated by western blotting (Figure 36I).

This suggests that depletion of SART3 does not alter viral spreading, but overexpression of SART3 leads to slightly higher virion production.

To study a potential role of SART3 in HCV RNA replication, shSART3 and shNT knockdown cells were electroporated with Jc1 Δ E1/E2^{NS5AB-FLuc} (Δ E1/E2) RNA and firefly luciferase activity was measured 4 hours, 1, 2 and 3 dpe. SART3 depletion did not show any alterations in HCV RNA replication (Figure 36J). By using the Jc1 Δ E1/E2^{NS5AB-FLuc} reporter, capsid formation is still enabled due to the presence of the core protein. To specifically investigate RNA replication, SART3 knockdown or ^{T7}SART3-overexpressing cells were electroporated with JFH1^{FLuc-P2A-NS3-NS5B} SGR RNA, lacking the structural proteins core, E1, and E2, as well as NS2 and p7. Firefly luciferase activity was measured 4 hours, 1, 2 and 3 dpe and analyzed as described before. RNA replication was marginally reduced in SART3-depleted cells (Figure 36K) and slightly increased in SART3-overexpressing cells (Figure 36L).

These data highlight SART3 as a core-interacting protein that is recruited to LDs mainly in HCV replicating cells. Increased virion production is observed in SART3-overexpressing cells, independent of HCV RNA replication. Most likely, SART3 acts as a regulator in the later steps of the HCV viral life cycle. However, due to the minor effects SART3 only relocates as part of a RNP complex to LDs.

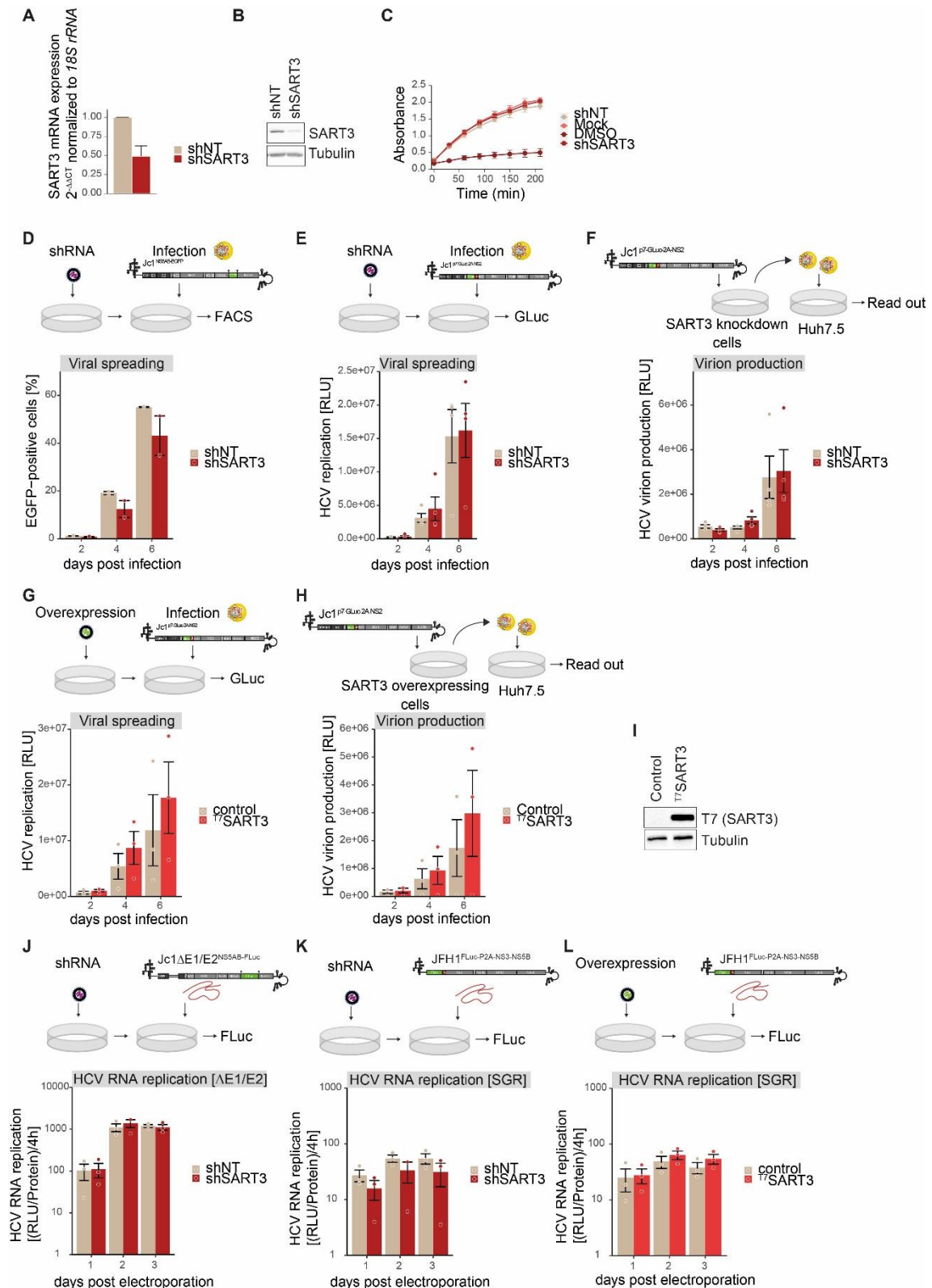


Figure 36: **SART3 overexpression supports HCV virion production.**

(A) Huh7.5 were transduced with lentivirus carrying either shSART3 shNT. Knockdown efficacy was verified by qRT-PCR. Shown are 2^{-ΔΔCT} values normalized to 18S rRNA and shNT. Experiments were performed in technical duplicates. (Mean ± SEM, n = 2). (B) Protein levels of SART3 in shSART3 and shNT-transduced Huh7.5 cells were compared by western blot using a SART3-specific antibody. Tubulin served as a loading control (n = 3). (C) Viability assay for shRNA transduced cells. Cells treated with 10% DMSO (DMSO) served as non-viable control. (Mean ± SEM, n = 4). (D) Huh7.5 cells were transduced with lentiviral particles for shSART3 or

shNT expression. Three days post transduction cells were infected with Jc1^{NS5AB-EGFP} (MOI 0.002) and fixed 2, 4 and 6 dpi for FACS analysis. Shown are relative numbers of EGFP-positive cells (Mean \pm SEM, n = 2). (E) Huh7.5 cells were transduced with lentivirus carrying either shSART3 or shNT. Three days post transduction cells were infected with Jc1^{p7-GLuc-2A-NS2} (MOI 0.5), supernatants were harvested 2, 4 and 6 dpi and analyzed by measuring luciferase activity (Mean \pm SEM, n = 4). (F) Huh7.5 cells were incubated with supernatants from (E) and supernatants harvested after 2 days and analyzed by luciferase assay (Mean \pm SEM, n = 4). (G) Viral replication in ^{T7}SART3-overexpressing cells and control cells treated as described in (E) (Mean \pm SEM, n = 3). (H) Huh7.5 cells were incubated with supernatants from (G), supernatants were harvested after 2 days and analyzed by luciferase assay (Mean \pm SEM, n = 3). (I) Overexpression of ^{T7}SART3 was confirmed by western blot analysis of cell lysates. Membranes were probed with T7-specific antibodies and tubulin served as a loading control (n = 3). (J) Huh7.5 cells were transduced with lentivirus expressing shSART3 or shNT, electroporated with Jc1 Δ E1/E2^{NS5AB-FLuc} RNA and HCV RNA replication was analyzed by luciferase activity. Huh7.5 cells expressing shSART3 or shNT (K) or ^{T7}SART3 and control cells (L) were electroporated with JFH1^{FLuc-P2A-NS3-NS5B} (SGR) RNA. HCV RNA replication was measured by luciferase activity. Shown is RLU per μ g protein normalized to the 4 h time point. (Mean \pm SEM, n = 3). (RLU, relative light units).

3.6 NOB1 is redistributed to core-containing LDs, interacts with core and is required for viral spreading

The previous LD isolation experiments revealed that NOB1 is located at LDs, independent of HCV replication or single expression of core and NS5A. Nevertheless, the data suggest that NOB1 is slightly enriched in LD fractions of HCV replicating cells (Figure 32). Thus, NOB1, like other RNA-binding proteins such as YB-1 (Chatel-Chaix *et al.*, 2013) might be involved in pro- or antiviral molecular mechanisms during HCV infection.

In order to visualize the results obtained from western blot analysis of LD fractions (Figure 32), Huh7 cells transduced with a lentiviral vector to stably express ^{T7}NOB1 and transfected with a ^{FLAG}core expression plasmid were analyzed by confocal microscopy. Staining with a NOB1-specific antibody showed a ring-like recruitment of NOB1 to core-containing LDs, overlapping with the core signal (Figure 37A).

FLAG-specific immunoprecipitation of lysates obtained from ^{FLAG}core-expressing Huh7.5 cells confirmed an interaction between core and NOB1 (Figure 32D). To verify the interaction between NOB1 and core, HEK293T cells were transiently co-transfected with ^{T7}NOB1 and ^{FLAG}core expression plasmid DNA. Lysates were subjected to either FLAG-specific immunoprecipitation as described before or NOB1-specific immunoprecipitation using a NOB1-specific antibody and protein G beads. Both approaches confirmed the interaction of NOB1 and core, as ^{T7}NOB1 was detected in the immunoprecipitated ^{FLAG}core sample and *vice versa* (Figure 37B). In the sample only expressing ^{FLAG}core, core was also detected in the NOB1-precipitated samples, possibly due to the interaction

with endogenous NOB1. Co-immunoprecipitation of core and $T7^{NOB1}$ was additionally validated by T7-specific immunoprecipitation using T7-beads (Figure S 6).

In conclusion, immunofluorescence staining demonstrated NOB1 recruitment to LDs in core-expressing cells and co-immunoprecipitation experiments affirmed an interaction between NOB1 and core.

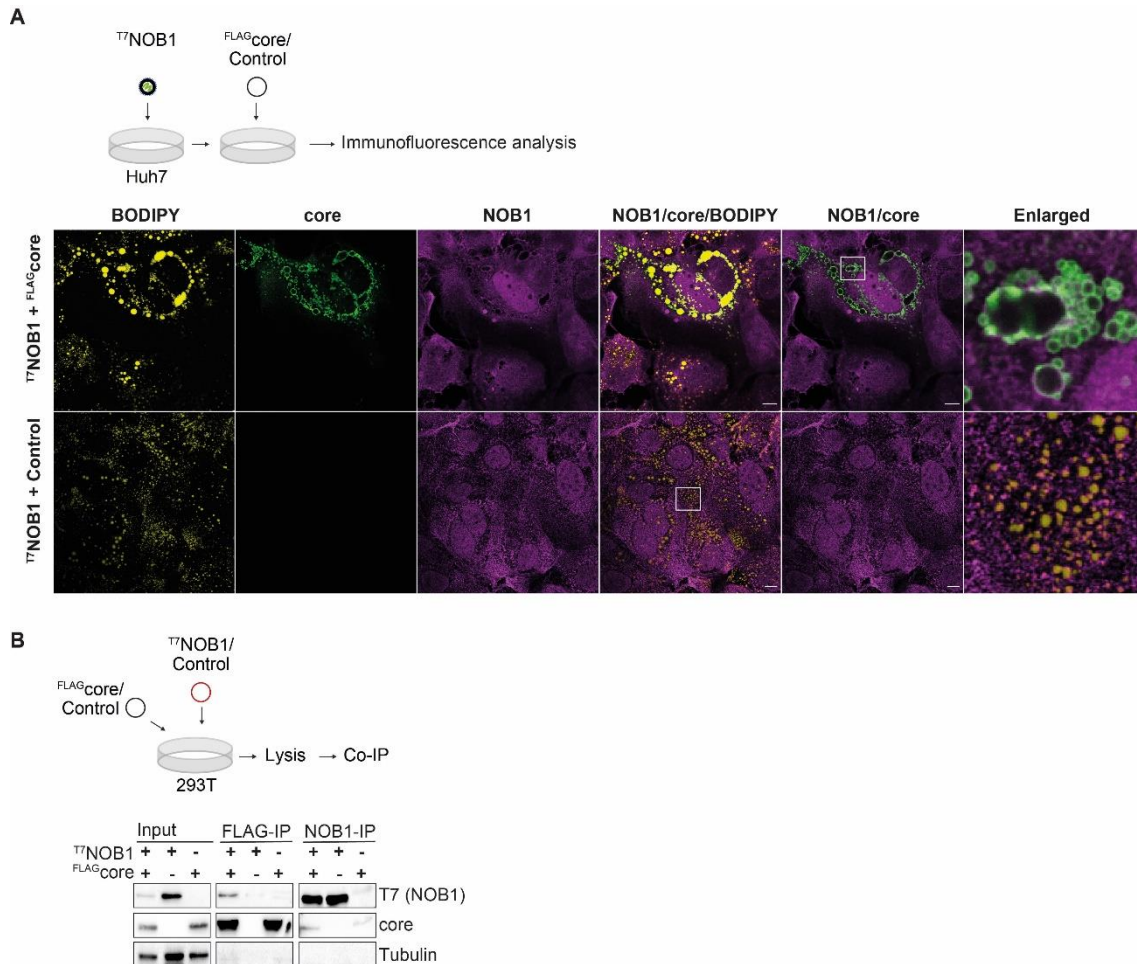


Figure 37: NOB1 localizes to core-containing LDs and interacts with core.

(A) Huh7 cells were transduced with lentiviral particles for expression of $T7^{NOB1}$ 3 days prior to transfection with a $FLAG^{core}$ expression plasmid or a control vector. Three days later cells were fixed and stained with NOB1-specific and core-specific antibodies. LDs were stained using BODIPY 493/503. White squares indicate enlarged areas ($n = 1$). Scale bars = 10 μm . (B) HEK293T cells were transfected with $FLAG^{core}$ and $T7^{NOB1}$ expressing plasmids or respective controls. Three days later cells were lysed and samples were immunoprecipitated using FLAG-coupled beads or using a NOB1-specific antibody and protein G beads. Western blots were probed with core and T7-specific antibodies. Tubulin was used as loading control. Shown is one representative experiment ($n = 3$).

To understand the role of NOB1 on HCV viral spreading, NOB1 was downregulated using lentiviral shRNA as described before and knockdown efficiency as well as cell vitality were validated (Figure 38A–C). Next, shNOB1 or shNT-transduced Huh7.5 cells were challenged with Jc1^{NS5AB-EGFP}. Cells were fixed at 2, 4, and 6 dpi and the percentage

of EGFP-positive cells was evaluated *via* flow cytometry. Viral spreading in NOB1-depleted cells led to a 60% decrease at 4 dpi and a ~50% decrease at 6 dpi compared to the control (Figure 38D). Using the Jc1^{p7-GLuc-2A-NS2} reporter strain, this effect was less pronounced (Figure 38E). Spreading after 4 and 6 dpi was only decreased by ~30% in NOB1-depleted cells. However, overexpression of ^{T7}NOB1 caused an increase in *gaussia* luciferase activity of ~20% (Figure 38G), supporting the results from the knockdown experiments. To decipher if the spreading effect is caused by impaired virion production, naïve Huh7.5 cells were incubated with supernatants of infected NOB1-knockdown cells. *Gaussia* luciferase activity was analyzed 2 days later. Replication was not altered in cells that were re-infected with viral supernatants of NOB1-knockdown cells (Figure 38F). Re-infection of Huh7.5 cells with virus produced by ^{T7}NOB overexpressing-cells led to an increase in virion production (Figure 38H). ^{T7}NOB overexpression was verified by western blot analysis (Figure 38I).

To question if HCV RNA replication is altered by NOB1, Huh7.5 cells were transduced with lentivirus carrying shNOB1 or ^{T7}NOB1 and the respective controls. Knockdown cells were then electroporated with Jc1ΔE1/E2^{NS5AB-FLuc} (ΔE1/E2) RNA (Figure 38J) and knockdown cells as well as ^{T7}NOB1-overexpressing cells were electroporated with JFH1^{FLuc-P2A-NS3-NS5B} SGR RNA (Figure 38K–L). Neither NOB1 depletion nor overexpression showed any changes in RNA replication of both reporters.

Taken together, HCV spreading and virion production is decreased in NOB1-depleted cells, without affecting HCV RNA replication. Though, the data for spreading assays and virion production demonstrate the mean of three to four independent replicates that show a high variation. Thus, the values were not significant.

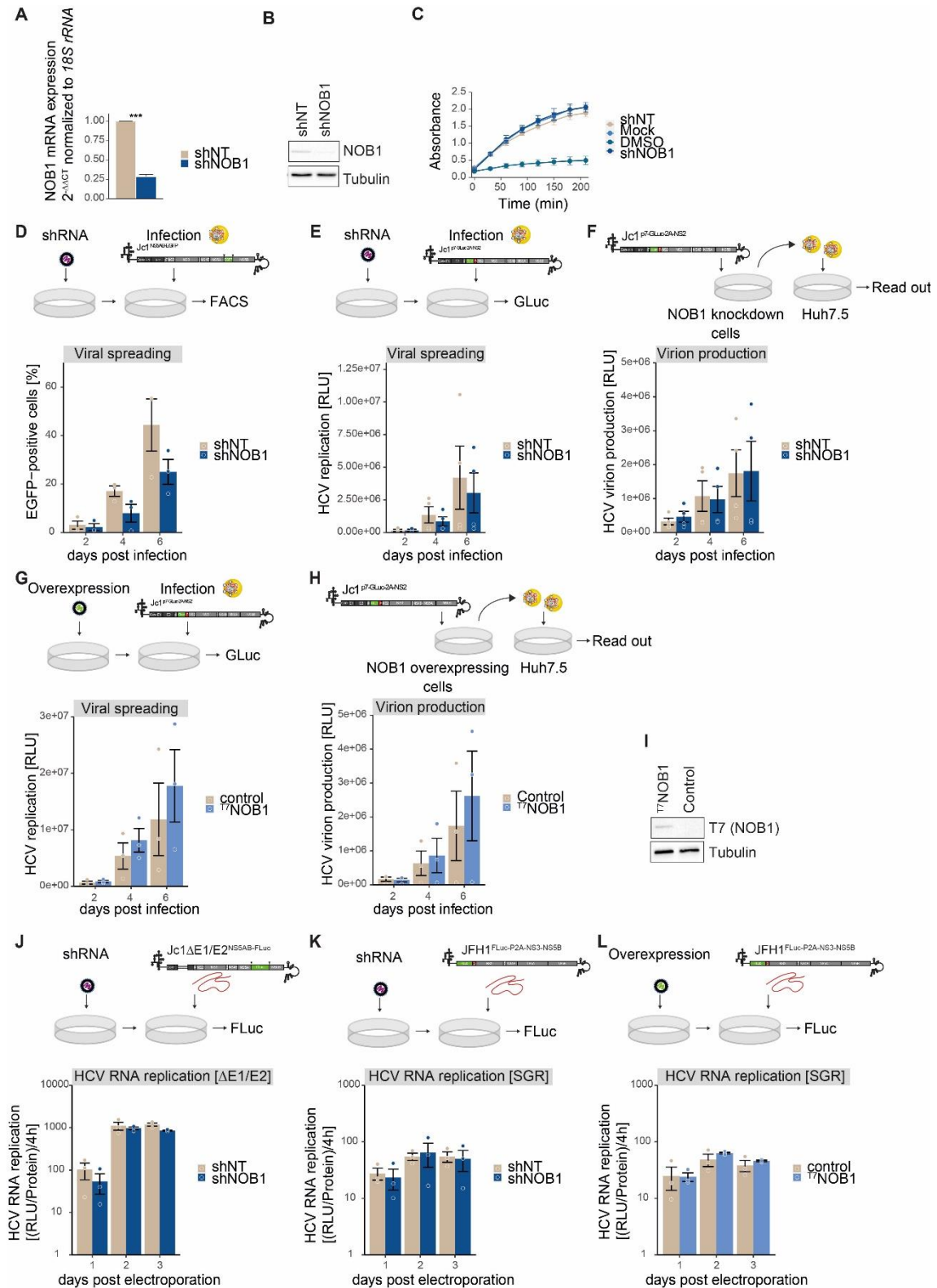


Figure 38: HCV viral spreading and virion production is delayed in NOB1-knockdown cells. (A) Huh7.5 were transduced with lentivirus carrying either shNOB1 or shNT. Knockdown efficacy was verified by qRT-PCR. Shown are 2^{-ΔΔCT} values normalized to 18S rRNA and shNT. Experiments were performed in technical duplicates (Mean ± SEM, ***p ≤ 0.01, n = 3). (B) Protein levels of NOB1 in shNOB1 and shNT-transduced Huh7.5 cells were compared by western blot using a NOB1-specific antibody. Tubulin served as loading control (n = 3). (C) Viability assay for shRNA transduced cells. Cells treated with 10% DMSO (DMSO) served as non-viable control (Mean ± SEM, n = 4). (D) Huh7.5 cells were transduced with lentiviral particles to express shNOB1

or shNT. Three days post transduction cells were infected with Jc1^{NS5AB-EGFP} (MOI 0.002) and cells were fixed 2, 4 and 6 dpi for FACS analysis. Shown are relative numbers of EGFP-positive cells (Mean \pm SEM, n = 3). (E) Huh7.5 were transduced with lentivirus carrying shNOB1 or shNT. Three days post transduction cells were infected with Jc1^{p7-GLuc-2A-NS2} (MOI 0.5) supernatants were harvested 2, 4 and 6 dpi and infection rates were measured by luciferase activity (Mean \pm SEM, n = 4). (F) Huh7.5 cells were incubated with supernatants from (E) and supernatants harvested after 2 days and analyzed by luciferase assay (Mean \pm SEM, n = 4). (G) Huh7.5 cells were transduced with lentivirus for the overexpression of ^{T7}NOB1 or the respective vector control. Three days after transduction cells were infected with Jc1^{p7-GLuc-2A-NS2} (MOI 0.5) and supernatants were harvested 2, 4 and 6 dpi and analyzed by luciferase assay (Mean \pm SEM, n = 3). (H) Huh7.5 cells were incubated with supernatants from (G) and supernatants harvested after 2 days and analyzed by luciferase assay (Mean \pm SEM, n = 3). (I) Overexpression of ^{T7}NOB1 was confirmed by western blot analysis of cell lysates. Membranes were incubated with T7-specific antibodies and tubulin served as a loading control (n = 3). (J) Huh7.5 cells were transduced with lentivirus expressing shNOB1 or shNT, electroporated with Jc1 Δ E1/E2^{NS5AB-FLuc} RNA and analyzed by luciferase assay at the indicated time points. Huh7.5 shNOB1 and shNT-expressing cells (K) or ^{T7}NOB1-overexpressing and control cells (L) were electroporated with JFH1^{FLuc-P2A-NS3-NS5B} SGR RNA and HCV RNA replication was analyzed by luciferase activity at the indicated time points. Shown is RLU per μ g protein normalized to the 4 h time point. (Mean \pm SEM, n = 3). (RLU, relative light units).

3.7 LARP1 is involved in the HCV life cycle

3.7.1 LARP1 localizes to core-containing LDs

LARP1 has previously been described as an HCV host factor (Chatel-Chaix *et al.*, 2013; Plissonnier *et al.*, 2019; Plissonnier *et al.*, 2016). The exact role of LARP1 in HCV-infected cells, however, remains unclear, since the results are conflicting. Others have shown that LARP1 is recruited to core-containing LDs during HCV infection (Chatel-Chaix *et al.*, 2013; Plissonnier *et al.*, 2019). The data in Figure 32 indicated a core-dependent relocalization to LD fractions. To confirm these data, Huh7 cells were transduced with lentiviral particles for the overexpression of ^{T7}LARP1, followed by transient transfection with ^{FLAG}core and prepared for immunofluorescence staining. Even in cells just expressing the core protein, LARP1 localized to core-containing cells in a ring-like pattern (Figure 39). These data suggest that the single expression of core is sufficient to recruit LARP1 to LDs, even in the absence of full infection.

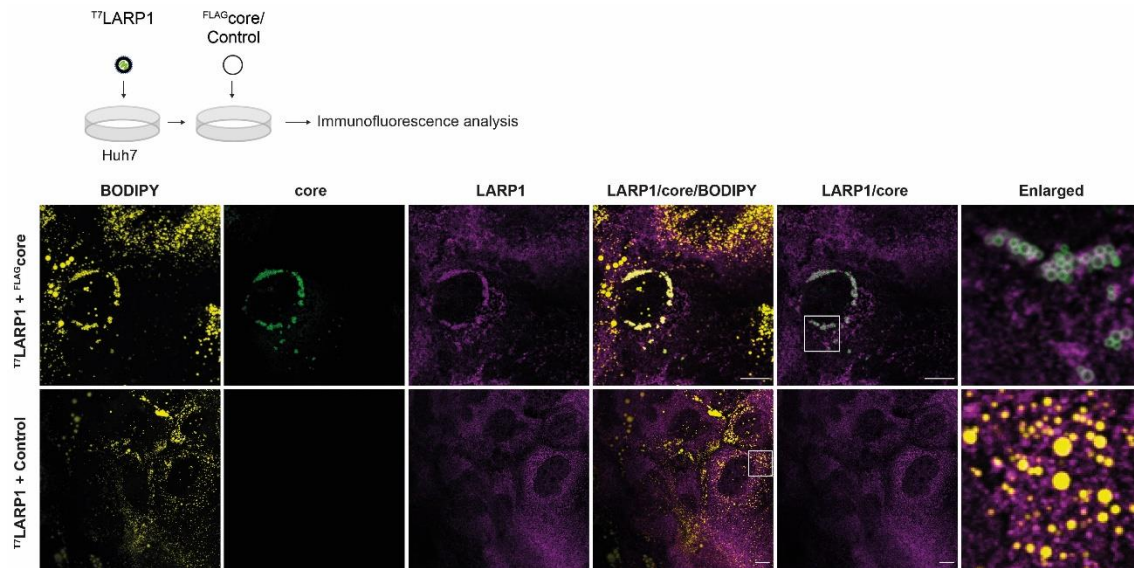


Figure 39: **LARP1 localizes to core-containing LDs.**

Huh7 cells were transduced with a lentivirus for $T7$ LARP1 expression 3 days prior to transfection with expression plasmids for $FLAG^{core}$ or a control. Three days later cells were fixed and stained with specific antibodies against LARP1 and core. LDs were stained using BODIPY 493/503. White squares indicate enlarged areas (n = 2). Scale bars = 10 μ m.

3.7.2 LARP1 interacts with core in an RNA-dependent manner

To confirm the possible interaction of LARP1 with core shown in Figure 32D, HEK293T cells were transfected with $FLAG^{core}$ and $T7$ LARP1 or respective controls for co-immunoprecipitation experiments using FLAG beads. Using a LARP1-specific antibody, LARP1 was detected in the $FLAG^{core}$ -precipitated samples (Figure 40A). Of note, an interaction between LARP1 and the proximity labeling bait protein ANXA3 was not detected (Figure S 5), and the interaction between LARP1 and core did not show a dependency on ANXA3 expression.

It has been proposed that LARP1 is part of a RNP complex that is located at core-containing LDs (Chatel-Chaix *et al.*, 2013). Since the core D1 domain is involved in RNA binding (Fan *et al.*, 1999; Santolini *et al.*, 1994; Shimoike *et al.*, 1999), and it has been shown that core is able to interact with host proteins in an RNA-dependent manner (Schöbel *et al.*, 2021), it was addressed if LARP1 interacts with core *via* RNA. Thus, lysates generated from $FLAG^{core}$ -expressing Huh7.5 were treated with RNase A prior to FLAG-specific immunoprecipitation followed by western blot analysis (Figure 40B). Successful RNase A treatment was confirmed by agarose gel electrophoresis and GelGreen staining. Whereas the LARP1-core interaction was recapitulated in untreated samples, no co-precipitation was observed in RNase A treated samples, illustrating that LARP1 and core interact in an RNA-dependent manner. A LARP1-specific

immunoprecipitation was performed as well, but core was not detectable *via* LARP1 immunoprecipitation (Figure S 7).

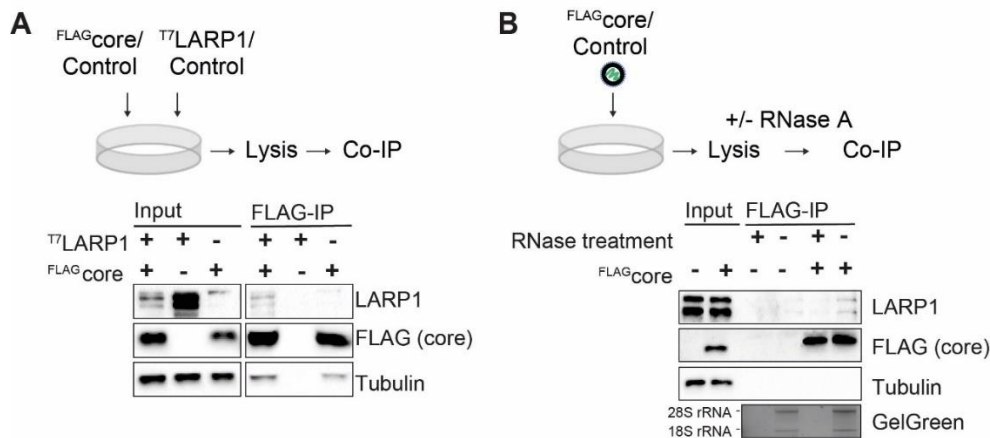


Figure 40: LARP1 interacts with core in an RNA-dependent manner.

(A) HEK293T cells were transfected with FLAG^{core} and T7LARP1 expression plasmids or respective controls. Co-immunoprecipitation (Co-IP) of cell lysates was performed by using FLAG-coupled beads. Lysates (Input) and Co-IP samples were analyzed by western blotting using FLAG and LARP1-specific antibodies. Tubulin served as loading control. (B) To analyze a potential RNA-mediated interaction, Huh7.5 cells were transduced with lentivirus for FLAG^{core} expression or a control. Lysates were pre-treated with RNase A or RNaseOut and subjected to FLAG-specific immunoprecipitation. Samples were analyzed by western blotting using FLAG and LARP1-specific antibodies. Tubulin served as a loading control. RNase A treatment was confirmed by agarose gel electrophoresis and GelGreen staining. Shown are representative experiments. (n = 3).

3.7.3 LARP1 deficiency impairs recruitment of HCV proteins and dsRNA to LDs

The trafficking of the HCV proteins core and NS5A to LDs is crucial for capsid formation and virion morphogenesis (Appel *et al.*, 2008; Miyanari *et al.*, 2007; Paul *et al.*, 2014). Additional studies have shown that assembly is at least partially dependent on various host factors that are present at LDs in HCV-infected cells (Lassen *et al.*, 2019; Rösch *et al.*, 2016). LARP1 localizes to LDs in a core-dependent manner, but the function of LARP1 at LDs remains unclear. To further understand the impact of LARP1 on the later steps of HCV infection, it was investigated if the absence of LARP1 would disrupt the recruitment of viral proteins to LDs.

Thus, lentiviral particles for the expression of shLARP1 were generated. Efficient knockdown rates of transduced Huh7.5 cells were validated by qRT-PCR and western blot analysis (Figure 41A–B) and the viability of cells was validated (Figure 41C).

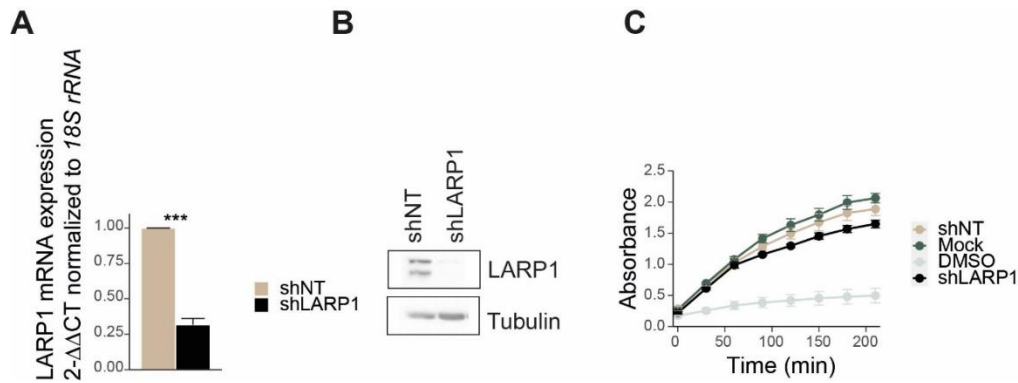


Figure 41: **Validation of LARP1-knockdown cells.**

Huh7.5 were transduced with lentivirus carrying either shLARP1 or shNT. (A) Knockdown efficacy was verified by qRT-PCR. Shown are 2^{-ΔΔCT} values normalized to 18S rRNA and shNT. Two biological replicates were performed in technical duplicates (Mean ± SEM, ***p ≤ 0.001). (B) Protein levels of LARP1 in shLARP1 and shNT-transduced Huh7.5 cells were compared by western blot using a LARP1-specific antibody. Tubulin served as loading control (n = 3). (C) Viability assay for shRNA transduced cells. Cells treated with 10% DMSO (DMSO) served as non-viable control (Mean ± SEM, n = 4).

shLARP1 and shNT-transduced cells were infected with a Jc1^{p7-GLuc-2A-NS2} reporter strain or left uninfected and LDs were isolated 2–3 weeks later (Figure 42A). Western blot analysis revealed that while core levels in cell lysates were only slightly reduced, and NS5A protein levels in the cell lysates were comparable in shLARP1 and shNT cells, the amount of core in LD fractions was reduced by ~56% in LARP1-deficient cells (Figure 42B). Likewise, NS5A levels were reduced by ~53% in LD fractions in LARP1-knockdown cells. Interestingly, relocalization of ANXA3 to LDs was not affected by the absence of LARP1, but ANXA3 levels in cell lysates were slightly reduced in LARP1-knockdown cells.

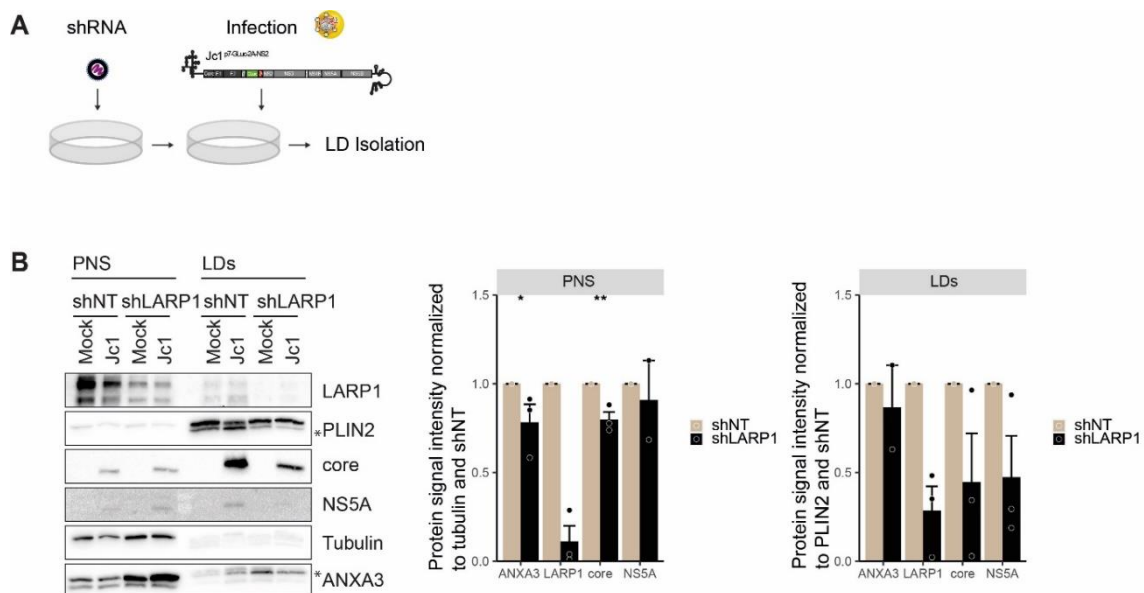


Figure 42: **LARP1 knockdown reduces core and NS5A localization to LDs.**

(A) Huh7 cells were transduced with lentivirus carrying shLARP1 or shNT and infected with Jc1^{p7-GLuc-2A-NS2} (MOI 0.2). Further analysis was performed 14 dpi. (B) LDs were isolated and protein levels of ANXA3, LARP1, core and NS5A in post-nuclear supernatants (PNS) and LD fractions were analyzed by western blotting and quantified. Tubulin served as loading control for PNS samples and PLIN2 for LDs, respectively. Shown is a representative experiment. Asterisks indicate unspecific bands. Quantifications illustrate volume intensity of ANXA3, LARP1, core and NS5A bands normalized to tubulin for PNS and to PLIN2 levels in LD fractions and the shNT control (Mean \pm SEM, * $p \leq 0.05$; ** $p \leq 0.01$, $n = 2-3$).

To further characterize the impaired recruitment of core and NS5A to LDs in the absence of LARP1, immunofluorescence staining of infected shLARP1 and shNT cells was conducted (Figure 43A). Core appeared in the described ring-like shape surrounding LDs in both, shLARP1 and shNT cells (Figure 43B). The NS5A signal on the other hand was spotted in the perinuclear region in close proximity to LDs. In LARP1-knockdown cells, a greater distance between the NS5A signal and LDs was observed (Figure 43D). Thus, colocalization of both viral proteins with LDs was analyzed by calculating the Manders' colocalization coefficient to quantify the overlapping signals of one channel with the other, as well as the Pearson's correlation coefficient to determine overall correlation of the two signals. The overlapping signal of core with LDs (M1) was significantly decreased in LARP1-knockdown cells related to the control, even though the reversed correlation (M2) and Pearson's correlation coefficient did not show any differences (Figure 43C). Colocalization analysis of NS5A with LDs depicted a significantly lower overlap of the LD signal with NS5A (M2) as well as a reduced Pearson's correlation of both signals (Figure 43E). Even though microscopy analysis confirmed the phenotype observed in LD fractions one way or the other, it did not reflect the strong effect. As it has been shown before, the resolution of confocal microscopy is limited in distinguishing between the localization at the LD surface and the localization at surrounding membranes (Lassen *et al.*, 2019; Lee *et al.*, 2019). Thus, these data implicate an impaired recruitment of the viral proteins core and NS5A to LDs in LARP1-deficient cells.

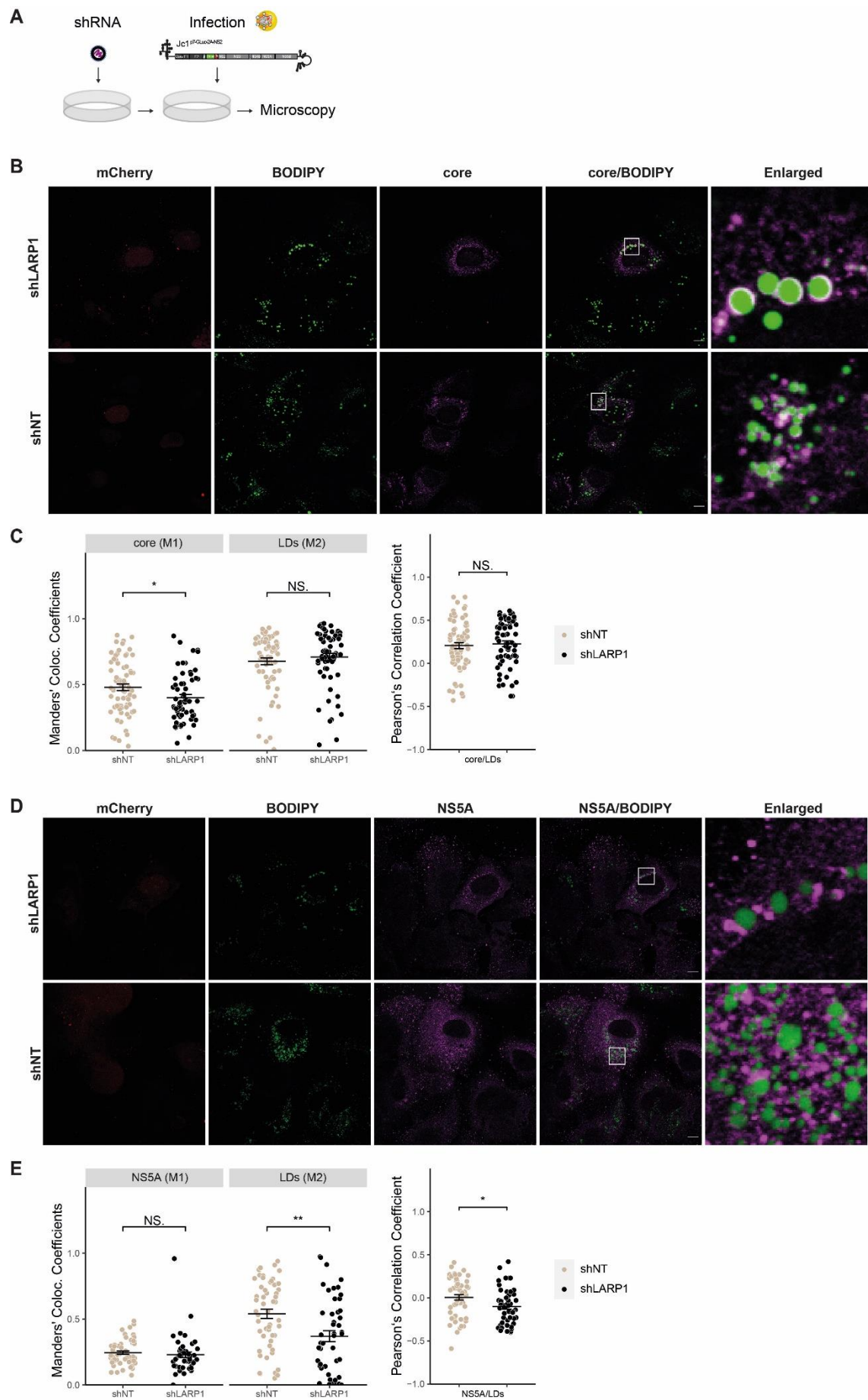


Figure 43: LARP1 knockdown impairs core and NS5A recruitment to LDs.

(A) Huh7 cells were transduced with lentivirus carrying shLARP1 or shNT infected with Jc1^{p7-GLuc-2A-NS2} (MOI 0.2) and analyzed by immunofluorescence microscopy 2–3 weeks post infection. (B) Immunofluorescence staining was performed using a core-specific antibody. LDs were visualized by BODIPY 493/503. (C) Colocalization of core and LDs was compared between shNT and shLARP1 cells from (B) by calculation of Manders' coloc coefficient and Pearson's correlation coefficient using the coloc2 function of Fiji (n = 69 (shNT), n = 63 (shLARP1)). (D) Immunofluorescence staining was performed using a NS5A-specific antibody and LDs were visualized by BODIPY 493/503. (E) Colocalization of NS5A and LDs was compared between shNT and shLARP1 cells from (D) by calculation of Manders' coloc coefficient and Pearson's correlation coefficient using the coloc2 function of Fiji (n = 54 (shNT), n = 48 (shLARP1)). Cells from 3 independent experiments were analyzed. (Mean \pm SEM, *p \leq 0.05; **p \leq 0.01; NS: not significant). Scale bars = 10 μ m.

Since the proximal recruitment of replication complexes to LDs is critically dependent on the localization of core to LDs (Miyanari *et al.*, 2007), the colocalization of double-stranded RNA (dsRNA) with LDs in LARP1-knockdown cells was further investigated. LARP1-depleted cells or Huh7 cells transduced with the non-targeting control were infected with a Jc1^{p7-GLuc-2A-NS2} reporter strain. Fixed cells were stained for dsRNA using a specific antibody (Targett-Adams *et al.*, 2008) 2–3 weeks post infection (Figure 44A). The Manders' colocalization coefficient and Pearson's correlation coefficient were determined as described above. Whereas the dsRNA and LD signals overlapped in shNT cells, LARP1-deficient cells displayed a significant decrease in colocalization of dsRNA with LDs (M1) (Figure 44B-C). The overall correlation, as indicated by the Pearson's correlation coefficient, did not differ. Next, the morphology of dsRNA foci was analyzed by evaluating the number per cell and size. Compared to control cells, quantity and size of dsRNA foci was not changed in LARP1-knockdown cells (Figure 44D-E). As mentioned above, the impaired core and NS5A recruitment to LDs in shLARP1 cells is likely preventing the proper localization of replication complexes to LDs, as displayed in the reduced colocalization of dsRNA and LDs. To determine the amount of dsRNA the corrected total cell fluorescence (CTCF) of the dsRNA signal was calculated. Indeed, CTCF values were significantly decreased in LARP1-knockdown cells compared to control cells (Figure 44F). Taken together, these results indicate that LARP1 deficiency impairs the relocalization of the viral proteins core and NS5A to LDs and consequently decreases the recruitment of replication complexes to LD proximity.

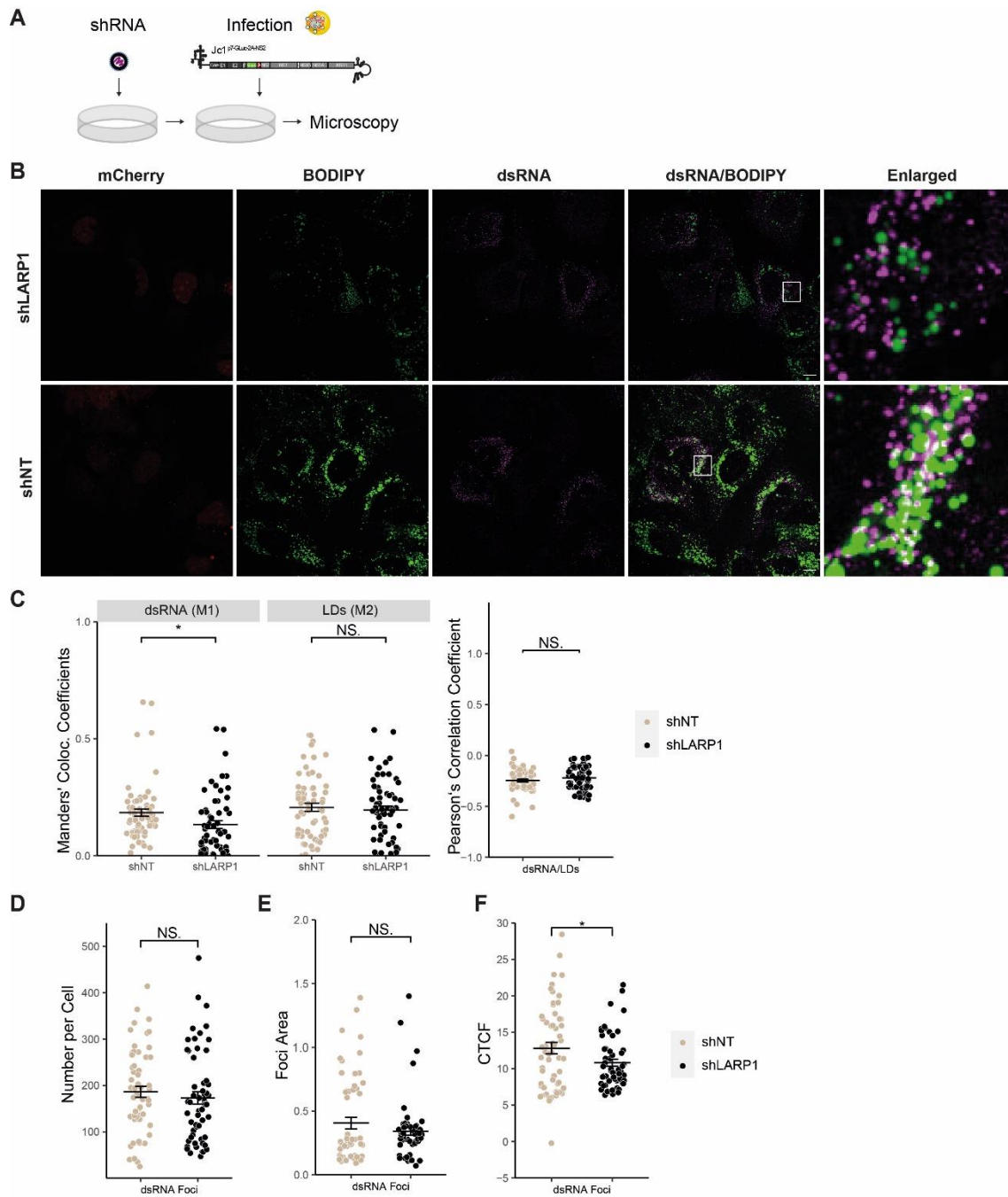


Figure 44: LARP1 knockdown reduces HCV dsRNA foci and colocalization with LDs.

(A) Huh7 cells were transduced with lentivirus carrying shLARP1 or shNT, infected with Jc1^{p7-GLuc-2A-NS2} (MOI 0.2) and fixed for immunofluorescence analysis 14 dpi. (B) Cells were stained with a dsRNA-specific antibody (J2) to visualize the HCV double-stranded RNA. LDs were visualized with BODIPY 493/503. (C) Colocalization of dsRNA and LDs was compared between shNT and shLARP1 cells from (B) by calculation of Manders' coloc coefficient and Pearson's correlation coefficient using the coloc2 function of Fiji (n = 65 (shNT), n = 61 (shLARP1)). To analyze the appearance of dsRNA foci in infected shLARP1 compared to shNT cells from (B) the number of foci per cell (D), the particle area (E) and the corrected total cell fluorescence (CTCF) (F) were determined using the Particle Analyzer function of Fiji. (D–F) n = 57 (shNT), n = 57 (shLARP1). Cells from 2 independent experiments were analyzed. (Mean ± SEM, *p ≤ 0.05; NS: not significant). Scale bars = 10 µm.

3.7.4 LARP1 is required for efficient HCV spreading infection

To decipher the functional role of LARP1 in HCV infection, LARP1-knockdown cells were infected with a Jc1^{NS5AB-EGFP} reporter strain and the percentage of EGFP-positive cells was measured at 2, 4 and 6 dpi by flow cytometry (Figure 45A). The percentage of infected cells was considerably reduced in LARP1-knockdown cells by ~82% at 4 dpi and by 85% at 6 dpi compared to the control cells. As before, HCV spreading was additionally analyzed by infecting LARP1-knockdown cells with the Jc1^{p7-GLuc-2A-NS2} reporter strain and *gaussia* luciferase activity was measured 2, 4, and 6 days dpi. HCV replication decreased by ~50% at 4 dpi and by ~40% at 6 dpi in shLARP1 cells compared to the shNT control (Figure 45B). Interestingly, the same assay using ¹⁷LARP1-overexpressing cells did not reveal an effect (Figure 45C). ¹⁷LARP1 expression was validated by western blot (Figure 45D). Additionally, intracellular RNA was isolated to determine HCV RNA copy numbers in shLARP1 and shNT cells 3 and 6 dpi. HCV RNA level were significantly reduced in LARP1-depleted cells (Figure 45E). As HCV replication and assembly are dependent on the phosphorylation (p56) and hyperphosphorylation (p58) of NS5A, respectively (Lemay *et al.*, 2013; Tellinghuisen *et al.*, 2008b), the phosphorylation of NS5A was investigated by western blotting. However, NS5A phosphorylation was not altered in shLARP1 cells compared to shNT cells (Figure S 8). Taking together the results of different methods, these data suggest that HCV spreading kinetics are slower in shLARP1 cells compared to the shNT control.

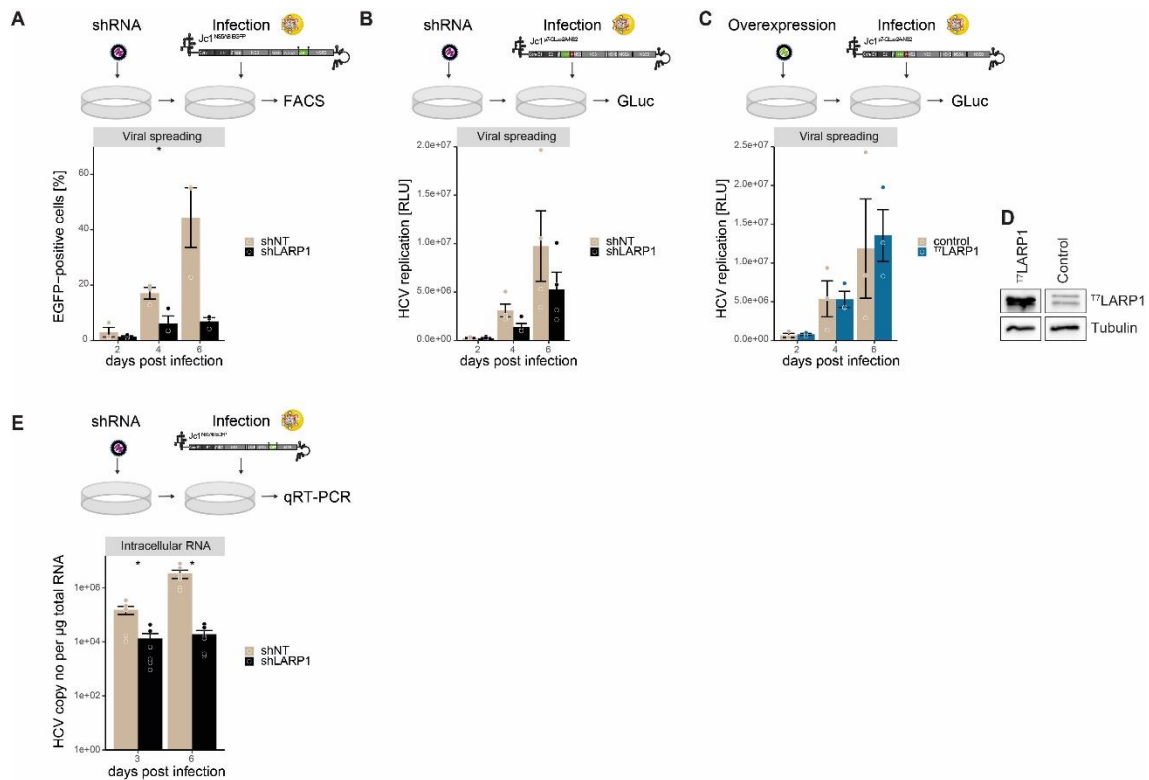


Figure 45: HCV viral spreading is delayed in LARP1-knockdown cells.

(A) Huh7.5 cells were transduced with lentivirus expressing shLARP1 or shNT. Three days after transduction cells were infected with Jc1^{NS5AB-EGFP} (MOI 0.002) and cells were fixed 2, 4 and 6 dpi for FACS analysis. Shown are relative numbers of EGFP-positive cells (Mean \pm SEM, $n = 3$, $*p \leq 0.05$). (B) Huh7.5 were transduced with lentivirus carrying shLARP1 or shNT. Three days after transduction cells were infected with Jc1^{p7-GLuc-2A-NS2} (MOI 0.5), supernatants were harvested 2, 4 and 6 dpi and infection rates were analyzed by luciferase activity (Mean \pm SEM, $n = 4$). (C) Huh7.5 were transduced with lentivirus to stably overexpress T⁷LARP1 or the empty vector control. Three days after transduction cells were infected with Jc1^{p7-GLuc-2A-NS2} (MOI 0.5), supernatants were harvested 2, 4 and 6 dpi and analyzed by luciferase assay (Mean \pm SEM, $n = 4$). (D) Overexpression of LARP1 was validated by western blotting using a LARP1-specific antibody ant tubulin as a loading control ($n = 3$). (E) Huh7.5 cells were transduced with lentivirus carrying shLARP1 or shNT and infected with Jc1^{NS5AB-EGFP} (MOI 0.002). Three and 6 dpi, total cellular RNA was isolated and HCV RNA copy numbers were determined by qRT-PCR. Depicted are HCV RNA copy numbers per μ g of total RNA (Mean \pm SEM, $n = 3$, $*p \leq 0.05$). (RLU, relative light units).

3.7.5 LARP1-knockdown does not affect HCV RNA replication and virion production

As others have previously reported a decreased HCV RNA replication upon LARP1 downregulation (Chatel-Chaix *et al.*, 2013), HCV RNA replication was investigated by using two different HCV luciferase reporter constructs under LARP1-knockdown as well as overexpression conditions. Huh7.5 cells were transduced with lentiviral particles for the expression of either shLARP1 or T⁷LARP1, or the respective controls. First, shLARP1 cells were electroporated with Jc1 Δ E1/E2^{NS5AB-FLuc} RNA and the firefly luciferase activity was measured at 4 hours and 1, 2 and 3 dpe. Values of 1, 2 and 3 dpe were normalized

to protein concentrations and the 4 hour values. Knockdown of LARP1 did not alter HCV RNA replication (Figure 46A). Considering that core can translocate LARP1 to LDs and subsequently might affect HCV replication levels, luciferase assays were additionally performed using the JFH1^{FLuc-P2A-NS3-NS5B} SGR. However, HCV RNA replication in LARP1-knockdown cells differed only slightly from control cells (Figure 46B). In line, ³⁵S-LARP1 overexpression did not affect HCV RNA replication (Figure 46C). This suggests that HCV RNA replication is mostly independent of LARP1 expression.

Since the effect on HCV spreading in LARP1-knockdown cells appears to be independent of HCV RNA replication, this poses the question if later steps in the HCV life cycle are affected. Published data concerning LARP1-dependent particle production is conflicting (Chatel-Chaix *et al.*, 2013; Plissonnier *et al.*, 2019). To study infectious virion production in LARP1-knockdown cells, shLARP1 and shNT cells were electroporated with Jc1^{NS5AB-EGFP}. Total cellular RNA as well as viral RNA from the supernatant were isolated at 3 and 6 dpe. HCV copy numbers were determined by qRT-PCR (Figure 47A). In agreement with the data previously shown, intracellular HCV RNA copy numbers were not altered by depletion of LARP1 (Figure 47B). Surprisingly, extracellular HCV RNA copy numbers did also not change in shLARP1 cells compared to shNT cells (Figure 47C). In order to examine alterations in the infectivity of secreted virions, viral titers were determined by the 50% tissue culture infective dose (TCID₅₀) (Lindenbach *et al.*, 2005). LARP1-knockdown and control cells were transfected with Jc1^{NS5AB-EGFP} RNA as described before, and lysates as well as supernatants from cell culture media were transferred to Huh7.5 RFP-NLS-IPS reporter cells (Jones *et al.*, 2010) at 3 and 6 dpe. After 3 days, the infectivity was analyzed by limiting dilution titration. Intracellular viral titers were slightly reduced in LARP1-knockdown cells 3 dpe compared to control cells, but remained unaffected at 6 dpe (Figure 47D). Extracellular viral titers were increased in LARP1-knockdown cells at 6 dpe (Figure 47E). However, these alterations were not significant. Thus, absence of LARP1 does not inhibit HCV particle production, but rather impairs spreading to neighboring cells.

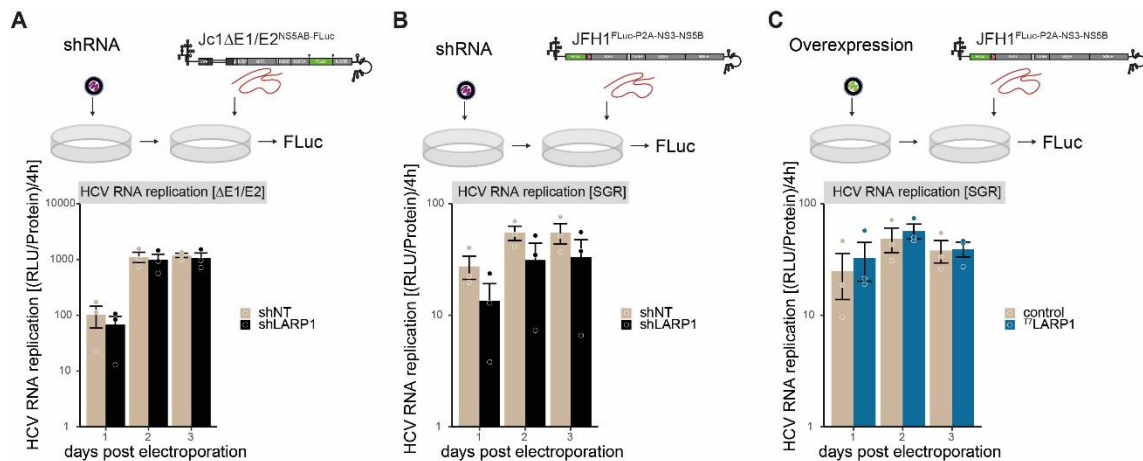


Figure 46: LARP1 knockdown or overexpression does not affect HCV RNA replication.

(A) Huh7.5 cells were transduced with lentivirus expressing shLARP1 or shNT and electroporated with $Jc1\Delta E1/E2^{NS5AB-FLuc}$ ($\Delta E1/E2$) RNA. HCV RNA replication was analyzed by luciferase at 1, 2 and 3 days post electroporation (dpe). Huh7.5 shLARP1 and shNT expressing cells (B) or $T7LARP1$ -overexpressing and control cells (C) were electroporated with $JFH1^{FLuc-P2A-NS3-NS5B}$ SGR RNA. HCV RNA replication was analyzed by measuring the luciferase activity at the indicated time points. Shown is RLU per μg protein normalized to the 4 h time point. (Mean \pm SEM, $n = 3$, RLU, relative light units).

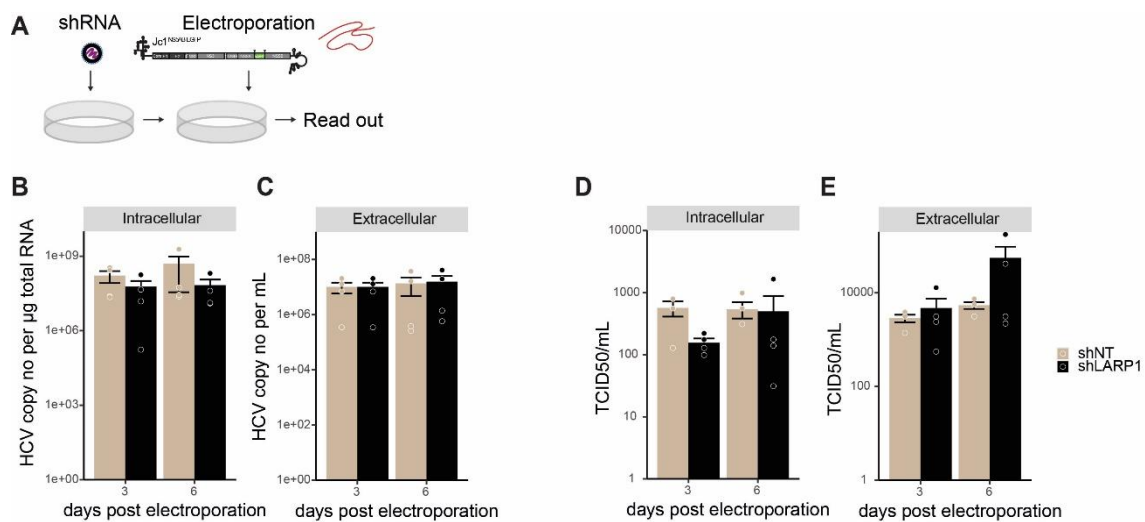


Figure 47: LARP1 knockdown does not affect secreted HCV virions.

(A) Huh7.5 cells were transduced with lentivirus expressing either shLARP1 or shNT and electroporated with $Jc1^{NS5AB-EGFP}$ RNA. (B) Three and 6 dpe, cellular RNA was isolated and HCV RNA copy numbers were determined by qRT-PCR. Shown are the HCV RNA copy numbers per μg of total RNA. (C) Viral RNA was isolated from supernatants and HCV RNA copy numbers were determined by qRT-PCR. Shown are the HCV RNA copy numbers per milliliter supernatant (mL). (D) Equal amounts of electroporated cells as described in (A) were lysed at 3 and 6 dpe and transferred to Huh7.5 RFP-NLS-IPS reporter cells. Three days later the infectivity (TCID₅₀) was determined by limiting dilution titration. (E) Supernatants of electroporated cells were transferred to Huh7.5 RFP-NLS-IPS reporter cells and the TCID₅₀ was analyzed by limiting dilution titration 3 days later. (D–E) Shown is the TCID₅₀/mL. (Mean \pm SEM, $n = 4$).

3.7.6 Cell-to-cell transmission is reduced in LARP1-depleted cells

Studies suggest that HCV spreading to neighboring hepatocytes is not only occurring *via* the classical cell entry pathway, but also *via* direct cell-to-cell transmission (Brimacombe *et al.*, 2011; Catanese *et al.*, 2013a; Timpe *et al.*, 2008). Therefore, cell-to-cell transmission in LARP1-knockdown cells was analyzed by determining the number of infected cells per foci using immunofluorescence analysis. shLARP1 and shNT cells were infected with a Jc1^{p7-GLuc-2A-NS2} reporter construct and stained with a core-specific antibody 3 dpi (Figure 48A). Since the lentiviral shRNA constructs also express mCherry, the mCherry signal was used to discriminate successfully transduced cells. Strikingly, the number of infected cells per foci was significantly diminished in LARP1-knockdown cells compared to the control (Figure 48B), indicating an impaired cell-to-cell transmission of HCV in LARP1-knockdown cells. To further evaluate this effect in a second approach, non-infected cells were mixed with a fully infected population of LARP1-knockdown cells or control cells in a 1:10 ratio (Figure 48C). To distinguish between the populations, uninfected cells were previously transduced with lentiviral particles for EGFP expression. The spreading efficiency was evaluated by analyzing the number of infected cells per EGFP-positive cells 3 days after mixing the populations. In LARP1-depleted cells the number of infected EGFP-positive cells was significantly reduced compared to control cells (Figure 48D), supporting the hypothesis that cell-to-cell spreading in LARP1-knockdown cell is impaired.

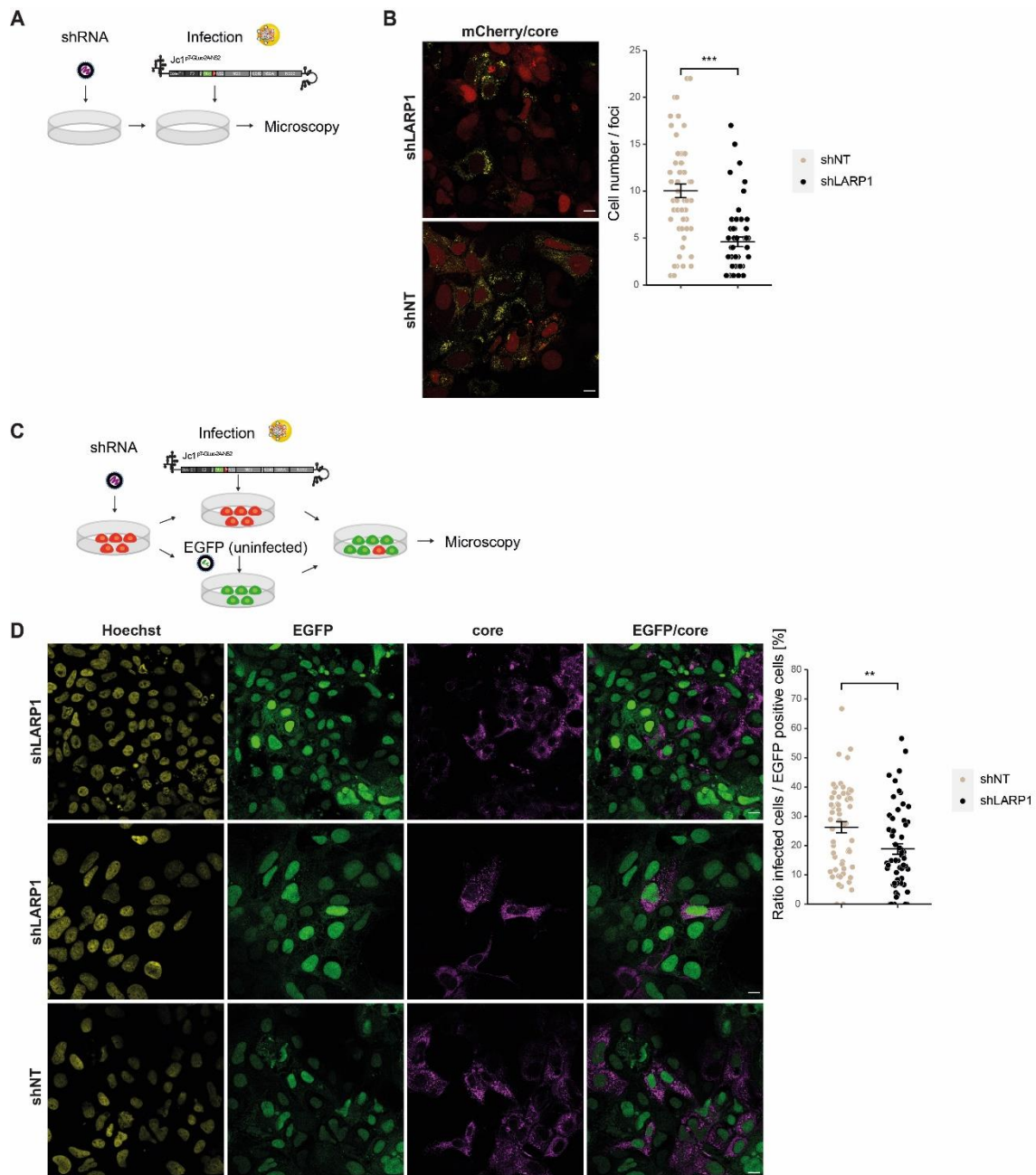


Figure 48: LARP1 knockdown impairs HCV cell-to-cell transmission.

(A) Huh7.5 cells were transduced with lentivirus expressing shLARP1 or shNT, infected with Jc1^{NS5AB-EGFP} (MOI 0.1–0.15) and fixed 3 dpi. (B) For immunofluorescence analysis cells were stained with a core-specific antibody (yellow) and mCherry expression (red) is shown as transduction control. The number of infected cells per foci was counted from 2 experiment in 2 to 3 independent wells (Foci: n = 57 (shNT), n = 53 (shLARP1); Mean ± SEM, ***p ≤ 0.001). (C) Huh7.5 cells were transduced with lentivirus expressing shLARP1 or shNT and either infected with Jc1^{p7-GLuc-2A-NS2} (MOI 0.25) or transduced with a lentivirus expressing EGFP and kept uninfected. Once the infected population was fully infected, cells were mixed in a ratio of 1:10 (infected:uninfected) and fixed 3 days later. (D) For immunofluorescence analysis, cells were stained with a core-specific antibody (magenta) and Hoechst (yellow). The ratio of infected cells per EGFP-positive cells was determined from 3 independent experiments in 2 independent wells (shNT: n = 58, shLARP1: n = 60; Mean ± SEM, **p ≤ 0.01). Scale bars = 10 µm.

4 Discussion

4.1 Strength and limitations of proximity labeling using BioID2 and APEX2

Proximity labeling is a relatively new approach to investigate the interactome of a protein of interest. An advantage is that labeling occurs in living cells, without having to use harsh buffers. This allows labeling of transient interactions. Here, two different methods were used to study the LD proteome in HCV-infected cells: (1) BioID2 and (2) APEX2. Though both methods rely on biotinylation, the labeling time frame as well as the assumed labeling radius differ. Another important factor are the labeled amino acids. Whereas BioID2 predominantly biotinylates lysines (Kim *et al.*, 2016), APEX2 most likely labels tyrosine, but also other electron-rich amino acids such as tryptophan, histidine, and cytosine (Hung *et al.*, 2016). Assumingly, different labeling mechanisms impact the outcome of those screens, due to protein folding and varying distances between proteins. Importantly, BioID2 and APEX2 preserve the membrane integrity (Huang *et al.*, 2020; Hung *et al.*, 2017). Considering that membrane contact sites of LDs play an important role in cellular communication (Herker *et al.*, 2021), this poses as an optimal tool to investigate LD-associated proteins. Interestingly, comparison of the resulting LD proteome identified by the two different methods showed that a large number of proteins were found in both, BioID2 and APEX2 labeling approaches. As expected, some proteins were only found using BioID2, but not APEX2 or *vice versa*.

In this study BioID2 and APEX2 labeling was performed with two different proteins of interest: ANXA3 and PLIN2. PLIN2 is the main LD-decorating protein in hepatocytes and has been used before in combination with proximity labeling (Bersuker *et al.*, 2018). ANXA3 was recently identified as an essential host factor in HCV-infected cells that relocates to LDs during infection (Rösch *et al.*, 2016).

Western blot analyses of streptavidin pull down experiments were used to confirm proper biotinylation and immunofluorescence staining and streptavidin detection of biotin visualized correct localization of the fusion proteins and of biotinylated substrates. Importantly, western blotting of lysates from APEX2-expressing cells confirmed a functional biotinylation after treatment with BP/H₂O₂, however, the bait protein itself was not detected in the streptavidin pull down. Peptide coverage of the bait proteins by MS confirmed the presence of all proteins in the respective screen. Analysis of enriched proteins in ANXA3 or PLIN2 fusion protein expressing cells compared to only BioID2 or APEX2-expressing cells revealed a strong enrichment of ANXA3 or PLIN2, respectively.

This indicates that western blotting might not be sensitive enough to detect of specific biotinylated targets.

For MS, proximity labeling was combined with SILAC to distinguish between two cell populations (e.g. HCV-infected and uninfected cells). Interestingly, a discrepancy was observed between identified proteins that were “light” or “heavy” labeled. It has been reported that arginine-to-proline conversion can lead to major experimental errors in SILAC (Bicho *et al.*, 2010). The arginine can be converted to proline by arginase activity in the cells, resulting in proteins with proline residues that are labeled with ^{13}C or ^{15}N from the introduced arginine (O'Quinn *et al.*, 2002; Ong *et al.*, 2003). Thus, leading to decreased ion intensities of the “heavy” labeled peptides. However, it was proposed that dataset normalization, but mainly label-switch replicates – as performed here – can minimize quantification errors (Park *et al.*, 2012).

4.1.1 Identification of the LD proteome using PLIN2-associated proximity labeling

Investigation of enriched proteins in biotin pull downs from non-infected cells confirmed previously described LD-associated proteins such as the acyl-CoA synthetase long-chain family members (ACSL) 3 and 4 and Ras-related in brain (Rab) proteins in cells expressing PLIN2-BioID2 and PLIN2-APEX2. A recent study suggested Rab18 binds to PLIN2 and forms a complex with PLIN2 and ACSL3 in murine myoblast cells (Deng *et al.*, 2021), validating the here performed analysis as a successful tool to identify the LD interactome.

For western blot analysis, BioID2 or APEX2 fusion protein-expressing cells were compared to cells expressing only BioID2 or APEX2 as respective controls. Surprisingly, the viral proteins NS3 and NS5A were captured by streptavidin pull down after proximity labeling in HCV-replicating cells that expressed PLIN2-BioID2, PLIN2-APEX2, BioID2 or APEX2. It is important to mention that in BioID2 and APEX2 control cells biotinylation occurs throughout the cytoplasm and nucleus. As NS3 and NS5A are located in spatial proximity to LDs during HCV replication (Lee *et al.*, 2019; Romero-Brey *et al.*, 2012), this indicates that proteins that are identified in control cells as well as in cells expressing the bait are not necessarily to exclude as functional interactors, as labeling with only BioID2 or only APEX2 could occur randomly.

As expected, MS data of cells expressing PLIN2-BioID2 or PLIN2-APEX2 revealed elevated levels of PLIN2 in the streptavidin pull down. Interestingly, PLIN3 levels were not altered using PLIN2-APEX2 compared to the control (APEX2) and even reduced using PLIN2-BioID2 when compared to the control (BioID2), suggesting that an

overexpression of PLIN2 replaces PLIN3 to some extent. Compensatory effects between PLIN2 and PLIN3 have been reported before, as an upregulation of PLIN3 in PLIN2 null embryonic cells was reported (Sztalryd *et al.*, 2006).

In comparison to published LD proteomes obtained by proximity labeling, the here presented PLIN2 proximity labeling overlapped only partially. Nevertheless, multiple Rab proteins were identified in agreement with previous studies (Bersuker *et al.*, 2018; Brasaemle *et al.*, 2004; Liu *et al.*, 2004). It has been suggested that LDs serve as depots for Rab GTPases and thus act as central hubs for vesicular trafficking by providing Rab proteins to targeting membranes (Goodman, 2018). Taken together, the here presented LD proteome analysis using PLIN2-associated proximity labeling identified proteins involved in the lipid metabolism of the cell, and thereby may contribute to understanding the role of LDs as central organelles.

4.1.2 Proximity labeling in HCV-infected cells

In order to investigate the LD proteome during HCV infection, identified hits in in close proximity of PLIN2 or ANXA3 in HCV-infected over uninfected cells were analyzed. GO analysis revealed that identified proteins found in close proximity of ANXA3 or PLIN2 in HCV-infected cells are involved in viral processes, RNA metabolism, viral genome replication, or RNA localization. This is in agreement with previously published data proposing that a number of RNA-binding proteins or proteins involved in RNA metabolism are recruited to LDs in HCV-infected cells (Chatel-Chaix *et al.*, 2011; Rösch *et al.*, 2016; Schöbel *et al.*, 2021).

Various proteins that were enriched in HCV-infected cells in all proximity screens have been reported as host factors before. Importantly, ANXA3 was enriched in HCV-infected cells compared to uninfected cells using PLIN2-BioID2 as well as PLIN2-APEX2 proximity labeling.

Recently, it has been proposed that the RNA-binding protein poly(rC)-binding protein 1 (PCBP1) restricts efficient HCV virion assembly and egress, leading to an intracellular accumulation of viral RNA (Cousineau and Sagan, 2021). PCBP1 has also been reported to bind the HCV 5' UTR (Fan *et al.*, 2014; Flynn *et al.*, 2015; Sp Ngberg and Schwartz, 1999). Intriguingly, PCBP1 was enriched in HCV-infected cells in proximity labeling using all four approaches. Further, PLIN3 was enriched in HCV-infected cells using both ANXA3 proximity labeling methods and by using PLIN2-APEX2. The LD-binding protein PLIN3 interacts with NS5A and thereby tethers NS5A-containing RNA replication complexes to adjacent LDs (Ploen *et al.*, 2013b; Vogt *et al.*, 2013). In addition, various DEAD box proteins (DDX) and Rab GTPases were identified. DDX3X is redistributed to LDs in HCV-infected cells and supports viral RNA replication by interacting with core

(Ariumi *et al.*, 2007; Rösch *et al.*, 2016). The interaction of DDX3X with the HCV 3' UTR activates the I κ B kinase- α (IKK- α) and regulates LD formation, the LD-core interaction and increases HCV assembly (Li *et al.*, 2013). Rab18 associates with LDs and interacts with NS5A, and silencing of Rab18 reduces HCV replication, whereas overexpression promotes infectious particle release without affecting RNA replication (Dansako *et al.*, 2014; Salloum *et al.*, 2013). Likely, Rab18 is important for replication complex proximity to LDs. In this study, Rab18 was enriched in HCV-infected cells using ANXA3-APEX2 and PLIN2-BioID2 proximity labeling. Rab5C and Rab7A were identified in HCV-infected cells with all four proximity labeling approaches. Both proteins associate with NS4B-containing replication complexes and depletion leads to reduced *de novo* synthesis of HCV genomes (Manna *et al.*, 2010). Rab5 accounts for a decrease in particle release by impairing HCV-induced autophagy (Su *et al.*, 2011). Furthermore, Rab5 directly binds to NS4B, indicating an important role in replication complex formation (Elgner *et al.*, 2018; Farquhar *et al.*, 2012; Matsuda *et al.*, 2014).

Strikingly, within both ANXA3 screens as well as the PLIN2-BioID2 screen the vesicle-associated membrane protein-associated protein (VAP) A was identified as an enriched protein in HCV-infected cells. VAPs interact with NS5A and NS5B and are important for HCV replication (Gao *et al.*, 2004; Hamamoto *et al.*, 2005). Notably, VAPA is anchored at ER-membranes and interacts with lipid transfer proteins, which contribute to a consistent lipid flow between ER and HCV replication complexes due to membrane contact sites (Vieyres and Pietschmann, 2019). This emphasizes the advantage of proximity labeling to decipher the complex LD interactome during HCV infection, which extends to the association with membranes of other organelles rather than only proteins at the LD surface.

Taken together, the collected data reflect a comprehensive insight into the functional LD-proteome involved in HCV propagation. Hence, proximity labeling of LD-associated proteins is a promising tool to further understand the interplay of host proteins in the HCV viral life cycle.

Surprisingly, no viral proteins were detected by proximity labeling in HCV-infected cells. This was also the case for the previously performed LD proteome analysis of isolated LDs (Rösch *et al.*, 2016) although it is generally accepted that core and NS5A locate to LDs (Boulant *et al.*, 2006; Camus *et al.*, 2013; Miyanari *et al.*, 2007). Due to the close proximity of replication organelles to LDs and the fact that proteins that associate with HCV replication complexes were identified, it would have been expected that even viral proteins that are not directly at the LD surface should be detectable. These results

indicate that the viral proteins are likely below the limit of detection in proximity labeling of LD-associated proteins in HCV infected cells.

In a complementary approach, overexpression of FLAG-tagged viral proteins in PLIN2-BioID2 or PLIN2-APEX2 expressing HEK293T cells allowed proximity labeling of HCV proteins. The preliminary data were not completely consistent, but indicated that core, E1, E2, p7, NS2, NS3, NS4B, and NS5A are biotinylated upon labeling in close proximity to PLIN2-BioID2 or PLIN2-APEX2. In case of NS5B identification is still unknown due to the lack of a functional FLAG-tagged NS5B construct. These data suggest that viral proteins can be detected by proximity labeling with PLIN2-BioID2 or PLIN2-APEX2 using western blot analysis, indicating a spatiotemporal vicinity; however, until now, only in context of single expression of the different viral proteins, which allows higher expression levels of the proteins. In addition, membranes forming the replication complexes during viral infection and ER-membranes wrapping LDs might shield proteins from effective biotinylation.

4.2 Investigation of identified hits in HCV-infected cells

As mentioned above, ANXA3 redistributes to LDs in HCV-infected cells and is important for the incorporation of APOE into viral particles (Rösch *et al.*, 2016). However, ANXA3 does not interact with viral proteins. Thus, it would be of great interest to identify an interaction partner that could possibly bridge the contact to viral proteins. Since LARP1 was significantly enriched in close proximity to ANXA3-BioID2 in HCV-infected cells, it was investigated if LARP1 would directly interact with ANXA3. Interestingly, a direct interaction between LARP1 and ANXA3 was not observed. Additional hits identified by the here performed proximity labeling analysis should therefore be further evaluated.

4.2.1 FABP5 is not involved in the HCV viral life cycle

The fatty acid-binding protein (FABP) 5 is highly expressed in hepatocellular carcinoma (HCC) and recent studies suggested that FABP5 promotes HCC progression and metastasis (McKillop *et al.*, 2019; Ohata *et al.*, 2017; Ohira *et al.*, 2021). FABP5 is involved in the uptake and transport of fatty acids to cellular compartments for storage and membrane synthesis (Furuhashi and Hotamisligil, 2008). Membrane remodeling is crucial for the formation of HCV replication organelles and the lipid metabolism plays a central role during the HCV viral life cycle (Bley *et al.*, 2020). A transcriptome analysis has shown that the lipid metabolism was severely reprogrammed in HCV-derived HCC tissue and revealed an upregulation of FABP5 (Liu *et al.*, 2020). Though the exact role of FABP5 in HCC remains unclear, it is postulated that the lipid transfer to the HCC tumor is decreased and that lipids required for membrane remodeling are newly synthesized. In this study, FABP5 was slightly enriched in close proximity of ANXA3-BioID2 in HCV-

infected cells compared to uninfected cells. This posed the question if FABP5 would be recruited to LDs during HCV infection supporting HCV replication, by contributing to membrane remodeling.

Interestingly, FABP5 was not identified in the experimental set up using infected over uninfected ANXA3-APEX2, PLIN2-BioID2 or PLIN2-APEX2-expressing cells. The previously performed quantitative LD proteome analysis identified FABP5 significantly reduced at LDs in HCV-infected cells compared to non-infected cells (Rösch *et al.*, 2016). Further analysis of FABP5 showed that FABP5 was not recruited to LDs in Huh7.5 cells. Isolated LD fractions from Huh7 cells showed FABP5 presence, which could also be detected in the absence of HCV replication or viral protein expression. Further analysis revealed that FABP5 was not relocated to LDs by single expression of core, but remained in the cytoplasm and did not directly interact with core. Mechanistically, knockdown of FABP5 did not affect HCV RNA replication or viral spreading. These data lead to the conclusion that FABP5 does not act as host factor for HCV. Nevertheless, as others have shown that FABP5 clearly plays a role in HCV-derived HCC (Liu *et al.*, 2020; Ohata *et al.*, 2017) this indicates that it rather takes part in the later steps of carcinogenesis and not by influencing the HCV viral replication.

Regarding the proximity labeling studies, these data emphasize that while using the ANXA3-BioID2 proximity labeling data of infected cells certainly adds to the identification of LD-associated proteins, it does not exclusively include LD proteins. Even though ANXA3 relocates to LD in HCV-infected cells (Rösch *et al.*, 2016), ANXA3 is also located in the cytoplasm. Subsequently, identified proteins could also be located in the cytoplasm, as it was observed for FABP5.

4.2.2 ARL8B is an HCV host factor

The ADP ribosylation factor-like protein 8B (ARL8B) GTPase localizes to lysosomes and is involved in lysosome distribution (Bagshaw *et al.*, 2006). Efficient lysosome positioning is required for autophagosome-lysosome fusion in the perinuclear region (Korolchuk and Rubinsztein, 2011). Overexpression of ARL8B reduces autophagosome-lysosome fusion, while depletion of ARL8B increases fusion (Korolchuk *et al.*, 2011). Various studies have shown that efficient HCV replication is tightly connected to autophagy by increasing LC3-II protein levels and consequently leading to higher numbers of autophagosomes in infected cells (Dreux *et al.*, 2009b; Kim *et al.*, 2017; L. Wang *et al.*, 2017). LC3-II is the lipidated form of the protein and is associated with the autophagosomal membrane, thus acting as an autophagosomal marker. Interestingly, the viral proteins NS4B and NS5A, that are required for DMV formation, also induce

autophagy (Ploen and Hildt, 2015; Quan *et al.*, 2014; L. Wang *et al.*, 2017). It has been suggested that autophagic membranes likely contribute to HCV replication complex formation (Lee *et al.*, 2019; Sir *et al.*, 2012). HCV infection enhances autophagosome stability by inhibiting autophagosome-lysosome fusion in an ARL8B-dependent manner (Jones-Jamtgaard *et al.*, 2019). In line with published results, reduced particle production in ARL8B-knockdown cells, but no effect on viral replication after infection with a Jc1 strain was observed in this thesis. Spreading infection experiments using flow cytometry as well as the *gaussia* luciferase reporter assay showed reduced HCV infection rates in ARL8B-knockdown cells compared to the control. In order to study HCV RNA replication, ARL8B-knockdown cells were electroporated with Jc1 Δ E1/E2^{NS5AB-FLuc} RNA to ensure comparable amounts of viral RNA, since ARL8B-depleted cells show reduced spreading infection. As described by Jones-Jamtgaard *et al.*, no effect on viral RNA replication was detected. In terms of ARL8B expression, the detection rates of endogenous ARL8B in western blot analysis were very weak. An increase of ARL8B protein levels in HCV-infected cells was only detectable in ARL8B-overexpressing cells. Interestingly, ARL8B overexpression also resulted in increased levels of core protein compared to cells that were not overexpressing ARL8B. These data support the hypothesis that ARL8B expression can enhance HCV infection, likely by inhibiting autophagosome-lysosome fusion. This suggests a positive feedback in which HCV increases ARL8B expression to establish higher infection rates, and artificial overexpression of ARL8B can elevate HCV replication as well.

Notably, lysosome trafficking mediated by ARL8B uses microtubule tracks. ARL8B induces kinesin-1 driven motility towards the cell periphery through interacting with its effector SKIP (SifA and kinesin-interacting protein, also known as PLEKHM2) (Rosa-Ferreira and Munro, 2011). A recent study revealed that Septin-9, another GTPase, associates with the cytoskeleton in JFH1-expressing cells and is involved in LD distribution towards the perinuclear region by interacting with phosphatidylinositol 5-phosphate (PI5P) and microtubules, therefore positively regulating HCV replication (Akil *et al.*, 2016). Depletion of Septin-9 reduced the number and size of LDs in the cell and decreased the TAG/DAG ratio, thus regulating HCV replication *via* LD biogenesis. Consequently, studying LD morphology under ARL8B knockdown conditions in HCV-infected cells could possibly reveal another role for ARL8B in HCV replication.

ARL8B was enriched in HCV-infected cells using proximity labeling with PLIN2-BioID2, PLIN2-APEX2, and ANXA3-BioID2. In line, the previously published LD proteome analysis in HCV-infected cells revealed that ARL8B was significantly enriched at LDs in

HCV-infected cells (Rösch *et al.*, 2016). As others have reported a redistribution of ARL8B in HCV-infected cells (Jones-Jamtgaard *et al.*, 2019; Korolchuk and Rubinsztein, 2011), this indicates an HCV-induced redistribution to LDs. However, western blot analysis of isolated LDs did not indicate a redistribution ARL8B to LD fractions. As mentioned before, it was observed that ARL8B overexpression lead to elevated core levels. Yet, single expression of core did not increase ARL8B levels in the PNS fraction and immunofluorescence analysis showed the previously described distribution of ARL8B throughout the cytoplasm, but ARL8B was not specifically recruited to core-containing LDs. An explanation for the identification of ARL8B in close proximity to LDs might be lysosome-LD membrane contact sites, since LDs interact with other cellular organelles (Schulze *et al.*, 2020). As studies have shown, multiple viruses can induce membranous alterations (Caldas *et al.*, 2021; Doerflinger *et al.*, 2017; Egger *et al.*, 2002; Miller *et al.*, 2007). HCV might induce a redistribution of ARL8B-associated lysosomes towards LDs.

Nevertheless, while the MS analysis was performed with fully infected cells, localization and interaction studies were only performed in core-expressing cells. In order to further investigate the role of ARL8B at LDs, it would be reasonable to repeat these experiments under conditions of HCV infection.

Of note, ARL8B was identified as a host factor for Tomato Mosaic Virus (ToMV) (Nishikiori *et al.*, 2011). ToMV is a positive orientated single-stranded RNA plant virus that forms replication complexes similar to HCV. ARL8B is required for synthesis of the negative strand RNA intermediate and was found in a complex with the viral replication proteins as well as a host protein, TOM1, in solubilized membranes from ToMV-infected tobacco cells. If autophagosomal membranes are indeed used for HCV replication complex formation and ARL8B stabilizes autophagosomes, it would be worth investigating if ARL8B is present in HCV replication complexes. In this study, ARL8B was identified in close proximity to LD-associated proteins, however, ARL8B seemingly is not recruited to LDs. Considering the widely agreed hypothesis that HCV replication organelles reside in close proximity to LDs (Romero-Brey *et al.*, 2012), the presence of ARL8B in those replication organelles would explain the LD proximate localization.

4.2.3 SART3 interacts with core and is recruited to LDs in HCV-infected cells

The RNA-binding protein squamous cell carcinoma antigen recognized by T-cells 3 (SART3) (also known as TIP110) is ubiquitously expressed in the nucleus acting as histone chaperone and pre-mRNA splicing factor (Long *et al.*, 2014). SART3 has multiple HAT (half-a-tetratricopeptide repeat) domains, two nuclear localization sequences

(NLS), and two RNA-recognition motifs (RRM) (Whitmill *et al.*, 2016; Q. Zhang *et al.*, 2016). The HAT domains play an important role for 3' pre-mRNA processing and recruitment of ubiquitin-specific protease (USP) as well as spliceosome recycling (Bell *et al.*, 2002; Long *et al.*, 2014). Specifically, SART3 binds and recruits USP15 and USP4 to the nucleus to control deubiquitination. Recently, an RNA interference (RNAi) screen identified USP15 as an HCV host factor (Kusakabe *et al.*, 2019). USP15 is important for HCV RNA translation and efficient particle propagation. Depletion of USP15 reduces the number of LDs in the cell and subsequently the production of infectious particles. Interestingly, supplementation with palmitic acid restores particle production.

SART3 was significantly enriched in close proximity to PLIN2-APEX2 in HCV-infected cells compared to non-infected cells. Additionally, SART3 was identified using PLIN2-BioID2 and ANXA3-BioID2 in the context of infection. Western blot analysis of isolated LDs confirmed SART3 recruitment to LDs in HCV-infected or HCV RNA-replicating cells. However, expression of viral proteins core or NS5A was not sufficient to recruit SART3 to LDs. USP15 was detectable at LDs of HCV-infected cells as well. Due to the interaction with USP15 and relocalization to LDs during HCV infection, SART3 posed as a promising candidate to study its involvement in HCV replication. Surprisingly, knockdown of SART3 did not affect HCV RNA replication, spreading, or virion production. Overexpression increased HCV spreading and virion production, however, the effect is within the standard deviation since single experiment values varied. HCV RNA replication was not affected by SART3 overexpression.

Due to the RNA-binding properties of SART3, it was hypothesized that SART3 interacts with the viral capsid protein core or NS5A. Co-IP studies revealed an interaction between SART3 and core, but not with NS5A. Both viral proteins are recruited to LDs and have RNA-binding properties (Huang *et al.*, 2005; Ivanyi-Nagy *et al.*, 2006; Santolini *et al.*, 1994; Tellinghuisen *et al.*, 2005; Yu *et al.*, 2009). Multiple studies support the hypothesis that core forms an RNP complex with host RNA-binding proteins including the Y-Box protein 1 (YB-1), poly(A)-binding protein (PABP) C1, LARP1, DDX17, and the LINE-1-encoded ORF1 protein (L1ORF1p) that is redistributed to LDs (Ariumi *et al.*, 2011a; Chatel-Chaix *et al.*, 2013; Chatel-Chaix *et al.*, 2011; Schöbel *et al.*, 2021). Specifically, YB-1 is an RNA-binding protein that is recruited to LDs during HCV infection as part of an RNP complex and is involved in the NS3-dependent steps in the later stages of the HCV viral life cycle (Chatel-Chaix *et al.*, 2013). An interaction between the YB-1 and SART3 has been reported (Timani *et al.*, 2013), supporting the theory of a complex-driven recruitment of SART3 to LDs.

Microscopic analysis could not clearly show a SART3 localization at LDs in core-expressing cells. As described before, SART3 strongly localized to the nucleus. In the

presence of core, a SART3-specific signal was detectable in the cytoplasm, however, this signal was weak compared to the nuclear localization and did not show any clear evidence for a SART3 colocalization with LDs.

In conclusion, SART3 does not contribute to HCV propagation, but is at least partially recruited to LDs during HCV replication and interacts with core, proposing that SART3 is part of an RNP complex that localizes to LDs, likely in a core-dependent manner. Thus, HCV infection induces redistribution of SART3 from the nucleus to cytosolic LDs.

4.2.4 NOB1 is a new potential HCV host factor

The NIN1-binding protein 1 (NOB) is an RNA-binding protein mainly expressed in the liver, lung and spleen. NOB1 has a zinc finger motif and an endonuclease activity (Zhang *et al.*, 2005). It is tightly connected to ribosome biogenesis (Lamanna and Karbstein, 2009; Sloan *et al.*, 2019).

NOB1 was significantly enriched in HCV-infected cells with PLIN2-BioID2 proximity labeling compared to non-infected cells. NOB1 was detectable in isolated LD fractions of Huh7 and Huh7.5 cells, even in the absence of HCV replication or viral proteins. Immunofluorescence of core-expressing cells showed that NOB1 co-occurred with core at LDs. Co-IP studies revealed that NOB interacts with core, but not NS5A.

Seemingly, NOB1 is already present at LDs in uninfected cells, but relocates to interact with core. Others have shown that LDs form distinct subpopulations (S. Zhang *et al.*, 2016). These subpopulations differed in size and protein composition. Interestingly, larger LDs contained ER-associated proteins, while smaller LDs did not. In the presence of core – or during infection – the localization of NOB1 to specific LD subpopulations could change due to the interaction with core. Likely, this reorganization of the LD proteome during infection results in a closer positioning of NOB1 to PLIN2 at LDs compared to non-infected cells, leading to the enhanced proximity labeling of NOB1 by PLIN2-BioID2 in HCV-infected cells.

As mentioned above, many RNA-binding proteins are recruited to LDs in the process of HCV infection and form RNP complexes with core (Ariumi *et al.*, 2011a; Chatel-Chaix *et al.*, 2013; Schöbel *et al.*, 2021). Likely, NOB1 is recruited to these complexes. An RNA-dependent interaction between core and NOB1 – potentially including HCV RNA – would add to a more precise understanding of these RNP complexes.

In NOB1-depleted cells, HCV spreading is impaired, without altering the virion production or HCV RNA replication. Remarkably, NOB1 overexpression resulted in the reversed effect on HCV spreading and led to elevated virion production. Possibly, HCV hijacks other factors to compensate the impaired effect on virion production induced by NOB1

depletion. This identifies NOB1 as a host factor positively regulating HCV replication in the later steps of the viral life cycle.

4.3 LARP1 is a host factor for HCV replication

The La-related protein (LARP) 1 was highly enriched in HCV-infected cells using ANXA3-BioID2, ANXA3-APEX2, and PLIN2-APEX2 labeling, compared to uninfected cells. Intriguingly, LARP1 expression poses as a biomarker for HCC (Xie *et al.*, 2013) and has previously been studied in the context of HCV. However, different groups have published contradictory effects on HCV replication (Chatel-Chaix *et al.*, 2013; Plissonnier *et al.*, 2019), which still leaves open the precise role of LARP1 in HCV infection.

4.3.1 HCV core recruits LARP1 to LDs

It has been reported that LARP1 localizes to LDs in HCV-infected cells (Chatel-Chaix *et al.*, 2013; Plissonnier *et al.*, 2019). In order to confirm the previously published data as well as the here presented proximity labeling results, LDs from infected cells were isolated and analyzed by western blotting. In addition, this study revealed that LARP1 is present in LD fractions isolated from cells that were transfected with Jc1ΔE1/E2^{NS5AB-EGFP-BSD} RNA, but less in LD fractions isolated from Con1-SGR-electroporated cells. During viral assembly, LDs act as a central hub. Both, core and NS5A traffic to LDs and play a central role for viral morphogenesis (Appel *et al.*, 2008; Boulant *et al.*, 2008; Camus *et al.*, 2013; Herker *et al.*, 2010; Miyanari *et al.*, 2007; Paul *et al.*, 2014; Shavinskaya *et al.*, 2007; Vogt *et al.*, 2013). LARP1 recruitment in Jc1ΔE1/E2^{NS5AB-EGFP-BSD} replicating cells, but not in Con1-SGR cells indicates a specific core-dependent recruitment. Importantly, core and NS5A are transferred to LDs when expressed individually (Camus *et al.*, 2013). According to the hypothesis of a core-dependent LARP1 recruitment, LARP1 trafficked to LDs of core-expressing cells, but not NS5A-expressing cells. Consistently, immunofluorescence staining of core-expressing cells detected LARP1 surrounding LDs, similar to the core-specific ring-like pattern. Co-IP studies affirmed that LARP1 interacts with core, but not NS5A. Whereas other groups have shown that LARP1 is present at LDs in infected cells (Chatel-Chaix *et al.*, 2013; Plissonnier *et al.*, 2019), these new data suggest a core-dependent recruitment of LARP1 to LDs, even in the absence of full infection. A core-dependent distribution to LDs has been described for other RNA-binding proteins. The relocalization of the DEAD-box helicase DDX3 as well as L1ORF1p to LDs is driven by core (Angus *et al.*, 2010; Schöbel *et al.*, 2021). A previous study showed that trafficking of YB-1 is dependent on core using a replicon system (Chatel-Chaix *et al.*, 2011). In a later study, YB-1 was found to interact with LARP1 and other proteins such as DDX6, the insulin-like growth factor 2 mRNA-binding protein (IGF2BP) 2 and the complement component 1Q subcomponent-binding

protein (C1QBP) (Chatel-Chaix *et al.*, 2013). Interestingly, as shown in this present thesis, the interaction between LARP1 and core was RNA-dependent and was disrupted by treatment with RNase A.

As mentioned above, others have also observed a relocalization of proteins with RNA-binding properties or involvement in RNA metabolism to LDs in HCV-infected cells (Chatel-Chaix *et al.*, 2011; Rösch *et al.*, 2016; Schöbel *et al.*, 2021). It has been suggested that various host RNA-binding proteins are redistributed to LDs as an RNP complex and that HCV induces the formation of stress granules (Ariumi *et al.*, 2011a; Chatel-Chaix *et al.*, 2013; Pene *et al.*, 2015; Schöbel *et al.*, 2021). LARP1 was identified in close proximity to stress granules and interacts with PABPC1 (Suzuki *et al.*, 2016; Youn *et al.*, 2018). This strongly supports the hypothesis that LARP1 is recruited to HCV assembly sites as part of a complex including other RNA-binding proteins as well as core.

4.3.2 LARP1 deficiency impairs recruitment of viral proteins and dsRNA to LDs

Efficient HCV progeny production is dependent on the trafficking of core and NS5A to LDs (Boulant *et al.*, 2007; Miyanari *et al.*, 2007). In LARP1-depleted cells, the recruitment of core and NS5A to LDs was decreased. For western blot analysis of isolated LDs, shLARP1 or shNT cells were infected and infection rates were monitored *via* immunofluorescence. Even though cultures were equally and at least to 90% HCV positive, quantification of the PNS showed that core levels were slightly lower in LARP1-depleted cells. However, this reduction was minor and does not correlate with the decreased core levels at LDs.

Core trafficking to LDs is mainly induced by the activity of cytosolic phospholipase (cPLA) 2 and diacylglycerol O-acyltransferase (DGAT) 1 (Herker *et al.*, 2010; Menzel *et al.*, 2012; Xu *et al.*, 2012). cPLA2 is responsible for the release of arachidonic acid by cleaving off fatty acids of phospholipids. cPLA2 activity is crucial for core transfer to LDs, core envelopment, and for secretion of viral particles (Menzel *et al.*, 2012). In addition, elevated core levels in whole cell lysates were observed in that study. In contrast, shLARP1 cells rather showed reduced core levels in the PNS and no alteration of the amount of secreted particles. It has been proposed that cPLA2 contributes to membranous web formation by altering membrane fluidity (Xu *et al.*, 2012). Therefore, cPLA2 poses as an important player for HCV RNA replication. Though, LARP1 depletion had no effect on viral RNA replication. Consequently, is it unlikely that the impaired core trafficking to LDs in LARP1-knockdown cells is connected to alterations in cPLA2 activity.

DGAT1 catalyzes the final step in the triglyceride synthesis. By inhibiting DGAT1 or expressing an inactive mutant, the redistribution of core and NS5A to LDs is impaired (Camus *et al.*, 2013; Herker *et al.*, 2010). A connection between LARP1 and DGAT1 activity would explain reduced core levels at LDs, however there are no cell-based assays available to assess DGAT1 activity separately from DGAT2 activity.

Immunofluorescence analysis corroborated a diminished colocalization of core and NS5A with LDs. In line with what others have shown before, investigation by immunofluorescence only showed a slightly reduced colocalization and did not reflect the severe decrease observed by western blot analysis of isolated LDs (Lassen *et al.*, 2019). Likely, the resolution of confocal microscopy is limited in distinguishing between signals directly at the surface at LDs and surrounding membranes. It has been suggested that during HCV assembly LDs are wrapped by ER membranes associated with viral replication vesicles (Lee *et al.*, 2019). Further, PLIN2 knockdown induces membrane wrapping of LDs in HCV-infected cells, thus impairing core and NS5A trafficking to LDs (Lassen *et al.*, 2019). To investigate if core and NS5A trafficking to LDs in shLARP1 cells is impaired by membrane alterations surrounding LDs, EM analysis could be performed comparing LARP1-knockdown cells to shNT cells.

For efficient HCV assembly, phosphorylation of C-terminal NS5A residues is important (Tellinghuisen *et al.*, 2008b). Of note, NS5A phosphorylation was not altered in LARP1-knockdown cells. Likely, NS5A is involved in the association of core with viral RNA and therefore capsid formation (Masaki *et al.*, 2008). Since a reduced recruitment of NS5A to LDs was observed, this could consequently lead to impaired RNA amounts at LDs. Targett-Adams *et al.* showed that dsRNA foci in HCV-infected cells are located on the surface of the ER and are surrounded by an ER network associated with NS5A in close proximity to LDs (Targett-Adams *et al.*, 2008). A reduced signal intensity of dsRNA foci (CTCF) was measured, and a decreased colocalization of dsRNA with LDs in LARP1-depleted cells compared to control cells. Decreased levels of core and NS5A could lead to an impaired recruitment of replication complexes to adjacent LDs in LARP1-depleted cells. LARP1 stabilizes mRNA and regulates the translation machinery (Fonseca *et al.*, 2015; Lahr *et al.*, 2017). The LA-module stabilizes mRNA, in dependency on the interaction with PABPC1 (Mattijssen *et al.*, 2021). If LARP1 stabilizes viral RNA, this would explain the reduced fluorescence of dsRNA signal in LARP1-knockdown cells. However, the amount and size of dsRNA foci was not changed. As described in this study, LARP1 is likely part of an RNP complex that also includes PABPC1. It would be possible that loss of LARP1 disrupts the RNP composition, thus destabilizing viral RNA. Arguably, if LARP1 depletion would destabilize HCV RNA, this should reflect on HCV

RNA replication. Yet, RNA replication was not altered in LARP1-knockdown cells using a Jc1 Δ E1/E2^{NS5AB-FLuc} replicon. Interestingly, replication was slightly lower in LARP1 knockdown-cells that were transfected with a JFH1^{FLuc-P2A-NS3-NS5B} subgenomic replicon. The presence of core and subsequent encapsidation could at least slightly help stabilizing the viral RNA, whereas in the absence of core and the LARP1 knockdown leads to destabilization of RNA.

Seemingly, LARP1 supports stability of a forming RNP complex and its recruitment to LDs that act as assembly sites. By depleting LARP1, the composition of those complexes is altered, leading to an impaired trafficking of viral proteins to LDs. Consequently, the relocalization of viral replication hubs to adjacent LDs is diminished without directly inhibiting HCV RNA replication.

4.3.3 LARP1 is required for efficient HCV cell-to-cell transmission

Strikingly, a severe effect on HCV spreading in cells lacking LARP1 was observed by using two different methods: (1) flow cytometry of Jc1^{NS5AB-EGFP} infected cells as well as (2) a *gaussia* luciferase assay of the supernatant of Jc1^{p7-GLuc-2A-NS2} infected cells. This corresponds with previously published data (Chatel-Chaix *et al.*, 2013). In that respective study Huh7.5 LARP1-knockdown cells were infected with a Jc1/JFH(p7-RLuc2A) reporter strain and *renilla* activity was measured 3 days post infection. Values were ~50% lower compared to a non-targeting control. Concomitantly, analysis of spreading infection in this present thesis showed that viral RNA copy numbers were significantly reduced in infected LARP1-knockdown cells.

However, in contrast to data shown here, Chatel-Chaix *et al.* observed a severe decrease of HCV RNA replication by ~90%. They transduced Huh7-Con1-FLuc cells with shLARP1 lentivirus and performed firefly luciferase assays 3-4 days later, whereas in this thesis LARP1-knockdown cells (Huh7.5) were electroporated with either Jc1 Δ E1/E2^{NS5AB-FLuc} replicon RNA or a JFH1^{FLuc-P2A-NS3-NS5B} SGR, thus the bottleneck of replication is the formation of the replication complexes as well as translation efficacy.

HCV virion production in LARP1-knockdown cells was assessed by electroporation with Jc1^{NS5AB-EGFP} RNA to ensure similar rates of HCV positive cells, as HCV infection led to lower levels of HCV positive cells due to the observed effect on viral spreading. Intra- and extracellular HCV copy numbers were not altered and TCID₅₀ values were slightly increased in supernatants of LARP1-knockdown cells at 6 days post electroporation. Again, Chatel-Chaix *et al.* detected a severe increase in supernatant-associated infectivity (Chatel-Chaix *et al.*, 2013), which was measured by RNA levels of naïve Huh7.5 cells treated with supernatant or cell extracts of transfected LARP1-knockdown or control cells. Importantly, the here present data for HCV RNA copy numbers were

evaluated directly from electroporated LARP1-knockdown or non-targeting cells. Thus, the usage of different approaches might explain the divergent observations. Additionally, Chatel-Chaix *et al.* used a JFH1 plasmid, while in this study, a Jc1 strain was used. Since Jc1 replicates to higher titers in the cell culture system compared to JFH1 (Lohmann and Bartenschlager, 2014; Pietschmann *et al.*, 2006), it would be possible that a slight effect due to LARP1 knockdown is diminished in Jc1-replicating cells.

Another study investigating HCV genotypes (gt) 1a (H77), gt2a (JFH1) as well as gt3a (S52 chimeric strain), described a decrease in extracellular infectivity and increase in intracellular infectivity (Plissonnier *et al.*, 2019). This was determined by TCID₅₀ normalized to RNA. Not normalized values of extracellular HCV RNA or TCID₅₀ did not change in LARP1-knockdown cells. Intracellular HCV RNA levels were reduced and TCID₅₀ was increased in LARP1-depleted cells.

Including the previously published studies to the new data presented in this thesis, LARP1 can be confirmed as a host factor for HCV involved in later steps of the life cycle. Though, data from this study suggest that LARP1 has no effect on virion production and release.

Since the data shown in this thesis clearly suggest that LARP1 knockdown impairs efficient HCV spreading without altering the infectivity of secreted virions, this implies an effect on HCV cell-to-cell transmission. Direct transmission to neighboring cells contributes profoundly to HCV spreading, as cell-to-cell transmission is resistant to anti-HCV glycoprotein monoclonal antibodies as well as polyclonal immunoglobulin from infected patients (Brimacombe *et al.*, 2011; Timpe *et al.*, 2008). Similar to cell-free viral transmission, the tight-junction components OCLN and CLDN1 contribute to cell-to-cell transmission (Catanese *et al.*, 2013a; Ciesek *et al.*, 2011), whereas the role of CD81 in HCV spreading remains controversial (Brimacombe *et al.*, 2011; Jones *et al.*, 2010; Witteveldt *et al.*, 2009). Nevertheless, studies have revealed a more outstanding role of SRBI in cell-to-cell transmission (Brimacombe *et al.*, 2011; Catanese *et al.*, 2013a). Additionally, one study described the importance of an intact actin network (Liu and He, 2013).

Analysis by immunofluorescence of Jc1-infected LARP1-knockdown or control cells revealed significantly smaller foci of infected cells. As expected, co-culturing of infected donor cells with uninfected recipient cells showed a significantly lower ratio of infected recipient cells when shLARP1 cells were used as donors compared to shNT donor cells. Therefore, LARP1 is likely involved in cell-to-cell-mediated spreading.

As most host factors involved in cell-to-cell transmission are also important for cell-free transmission, it cannot be excluded that initial entry is impaired in LARP1-knockdown

cells. Nevertheless, the observed changes in core and NS5A trafficking in shLARP1 cells rather indicate an effect on the later steps in the viral life cycle.

Interestingly, purified exosomes from HCV-transfected hepatocytes contain full viral RNA, viral proteins, transfer to naïve cells and establish infection, even with subgenomic replicons (Dreux *et al.*, 2012; Ramakrishnaiah *et al.*, 2013). Exosome-mediated infection is partially resistant to treatment with neutralizing antibodies. Exosomes are formed within multivesicular bodies (MVBs) and are secreted from multiple cell types for cell-to-cell communication by transferring proteins, mRNA, and microRNA (El Andaloussi *et al.*, 2013; Simpson *et al.*, 2009; Valadi *et al.*, 2007). LARP1 could associate with exosomes and thereby contribute to successful transmission. However, the role of exosomes for cell-to-cell transmission is still under debate.

Intriguingly, in HeLa cells, expression of LARP1 affects cytoskeleton organization (Burrows *et al.*, 2010). The study showed that in LARP1 RNAi-treated cells actin diffusely localizes in the cytoplasm, whereas LARP1 overexpression leads to a redistribution of γ -actin towards the cell membrane within lamellipodia. As it has been suggested that LARP1 associates with a RNP complex (Chatel-Chaix *et al.*, 2013), this poses the question if LARP1 initiates a direct transmission of viral RNA complexes to neighboring cells by altering the organization of the cytoskeleton.

4.4 Concluding remarks

The present thesis elucidates the LD proteome in HCV-infected cells using the proximity labeling methods BioID2 and APEX2. As bait proteins the LD-coating protein PLIN2 and the host factor ANXA3 were used. In line with previously published data, the LD proteome was considerably altered during HCV infection and GO analysis revealed a high abundance of RNA-binding proteins.

This study provides extended data on the virus-host interplay at LDs during the later steps of HCV infection, such as assembly and egress. Further, this analysis considers not only direct binding partners, but also new potential host factors in close proximity to HCV replication sites.

The identified proteins FABP5, ARL8B, SART3, NOB1, and LARP1 were selected and studied in more detail in the context of HCV infection. The RNA-binding proteins SART3, NOB1 and LARP1 were identified as new core-interacting partners, likely as part of an RNP complex located at LDs. Further, ARL8B and NOB1 depletion impaired HCV spreading and SART3 overexpression supported HCV spreading and virion production. However, the specific role of ARL8B, SART3 and NOB1 during HCV replication remains to be elucidated.

Focusing on LARP1, a core-dependent recruitment to LDs and RNA-dependent interaction with core was observed even in the absence of HCV infection. Redistribution of dsRNA and the viral proteins core and NS5A to LDs in infected cells was dependent on LARP1. Importantly, depletion of LARP1 significantly impaired HCV spreading *via* cell-to-cell transmission, but not the secretion of infectious virions for cell-free transmission. Thus, these new data expand the functional role of LARP1 as a proviral factor for HCV infection (Figure 49).

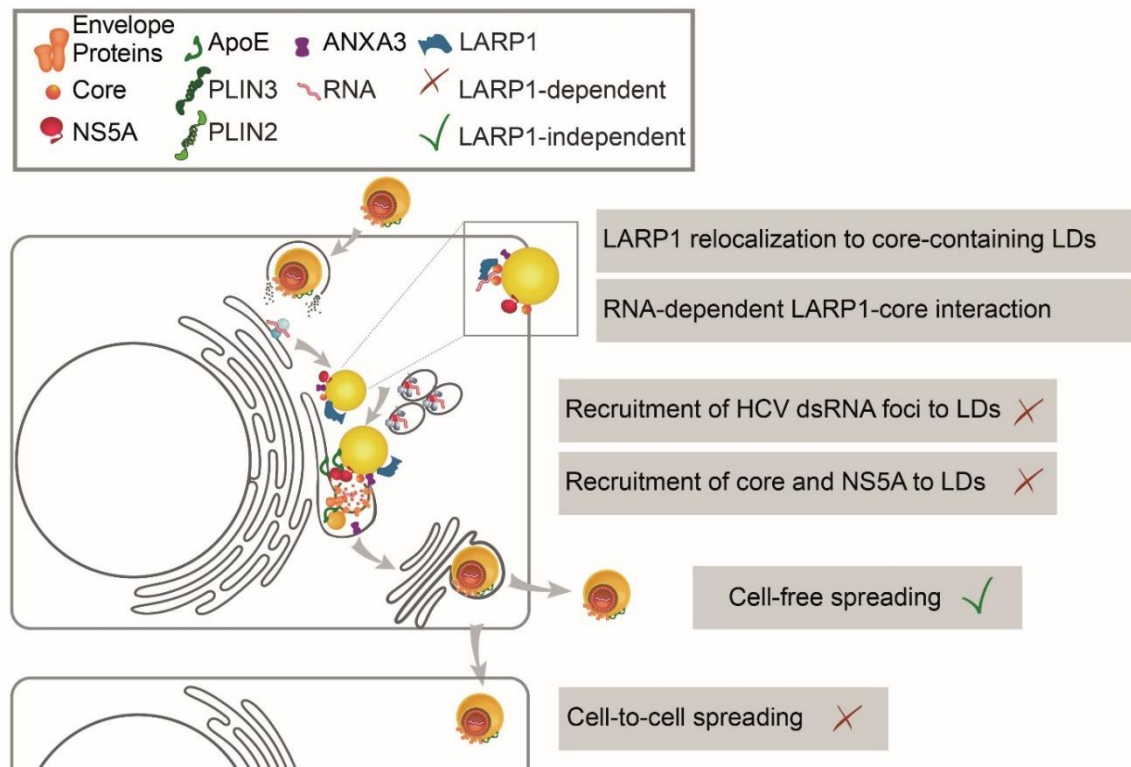


Figure 49: **LARP1 participates in cell-to-cell but not in cell-free spread of HCV.**

LARP1 redistributes to core-containing LDs and interacts with core in an RNA-dependent manner. Depletion of LARP1 impairs the recruitment of dsRNA and the viral proteins core and NS5A to LDs in HCV-infected cells. LARP1 significantly contributes to HCV spreading *via* cell-to-cell transmission.

5 Material

5.1 Bacteria

Table 2: Bacterial strains

Name	Genotype	Company
DH5 α	F- Φ 80/ <i>lacZ</i> Δ M15 Δ (<i>lacZYA-argF</i>) U169 <i>recA1 endA1 hsdR17</i> (rk-, mk+) <i>phoA supE44 thi-1 gyrA96 relA1</i> λ -	Thermo Fisher Scientific, Darmstadt

Table 3: Media for bacterial culture

Name	Components	Quantity
LB medium	Yeast extract	5 g
	Tryptone	10 g
	NaCl	10 g
	NaOH (5M)	200 μ L
	dH ₂ O	Ad 1 L

Prepared LB media was autoclaved and before usage 100 μ g/mL ampicillin were added. For LB agar plates, 12 g/L agar (biological grade) were added prior to autoclaving. Antibiotics were added prior to preparing plates under sterile conditions. Plates were stored at 4 °C.

5.2 Eukaryotic cell lines

The human embryonic kidney cell line HEK293T were obtained from the American Type Culture Collection (ATCC). The cell line supports the replication of plasmids carrying the SV40 origin of replication due to a stable expression of a mutant version of the SV40 large T antigen (DuBridge *et al.*, 1987).

The human hepatoma cell line Huh7 was generated from a hepatocellular carcinoma isolation (Nakabayashi *et al.*, 1982). From Huh7 cells, the sub-cell line Huh7.5 was established (Blight *et al.*, 2002). This cell line originates from Huh7 cells expressing an HCV replicon and successful clearance with IFN α . Deriving from Huh7.5 cells, the sub-cell line Huh7.5.1 was generated, which shows fast HCV infection kinetics (Zhong *et al.*, 2005). All 3 hepatoma cell lines are permissive for HCV infection *in vitro*, supporting viral replication. Huh7.5 and Huh7.5.1 cells are characterized by an even higher permissiveness compared to the parental Huh7 cell lines due to a point mutation in the antiviral pattern recognition receptor *retinoic-acid-inducible gene-1* (RIG-I) (Sumpter *et*

al., 2005). Huh7 cells were kindly provided from Ralf Bartenschlager, Huh7.5 cells were provided by Charles M. Rice and Huh7.5.1 cells were obtained from Apath, LLC.

For TCID₅₀ assays, Huh7.5-RFP-NLS-IPS cells were used. Huh7.5 cells were transduced with lentiviral particles for stable expression of a red fluorescence protein (RFP) fused to a nuclear localization site (NLS) and parts of the mitochondrial antiviral signaling protein (MAVS) (also known as IPS, Cardiff or VISA) to monitor HCV infection (Jones *et al.*, 2010). In uninfected cells, the RFP signal localizes to mitochondria. In HCV-infected cells, MAVS is cleaved by the HCV NS3-NS4A protease, leading to a translocation of RFP to the nucleus. Thus, this reporter system allows to visually distinguish between HCV-infected and uninfected cells.

Table 4: Media, buffers and supplements for cell culture

Name	Components
DMEM	Dulbecco's Modified Eagle Medium (high glucose, no glutamine), 10% (v/v) fetal bovine calf serum (FCS), 1% (v/v) GlutaMAX, 1% (v/v) penicillin/streptomycin Dulbecco's Modified Eagle Medium (high glucose, sodium pyruvate, no glutamine), 10% (v/v) fetal bovine calf serum (FCS), 1% (v/v) Glutamine, 1% (v/v) penicillin/streptomycin
SILAC media (R0K0) light	Dulbecco's Modified Eagle Medium (high glucose, unlabeled arginine and lysine amino acids, 1% (v/v) L-glutamine, sodium pyruvate), 10% (v/v) fetal bovine calf serum (FCS), 1% (v/v) penicillin/streptomycin
SILAC media (R10K8) heavy	Dulbecco's Modified Eagle Medium (high glucose, ¹³ C- and ¹⁵ N-labeled arginine, and ¹³ C- and ¹⁵ N-labeled lysine amino acids, 1% (v/v) L-glutamine, sodium pyruvate), 10% (v/v) fetal bovine calf serum (FCS), 1% (v/v) penicillin/streptomycin
Freezing media	90% (v/v) FCS, 10% (v/v) DMSO
2x HEPES buffered saline (HBS)	275 mM NaCl, 10 mM KCl, 1.4 mM Na ₂ PO ₄ , 42 mM HEPES, 11 mM glucose, adjust pH to 7.05
Chloroquine	25 mM chloroquine diphosphate in ddH ₂ O, sterile filtered
Polybrene	4 mg/ml polybrene in PBS, sterile filtered
Cytomix	10 mM potassium phosphate buffer (pH 7.6), 120 mM KCl, 5 mM MgCl ₂ , 25 mM HEPES, 0.15 mM CaCl ₂ , 2 mM EGTA (pH 7.6) in dH ₂ O; adjust pH 7.6 with 1 N KOH, sterile filtered. Add fresh prior to electroporation: 5 mM glutathione, 2 mM ATP

Trypsin-EDTA	0.05% Trypsin-EDTA
DPBS/PBS	1x Dulbecco's phosphate buffered saline, without CaCl ₂ and MgCl ₂
PEG	40% (w/v) polyethylene glycol (PEG) in PBS

5.3 Solvents and buffers

5.3.1 Lysis buffer

Table 5: Lysis buffers

Name	Components
RIPA buffer	150 mM NaCl, 50 mM Tris/HCl pH 7.4, 1% NP-40, 0.5% sodium deoxycholate, 1 mM EDTA, 0.1% SDS, supplemented with 1x protease inhibitor cocktail (Sigma) and 1 mM phenylmethylsulfonyl fluoride (PMSF)
NP-40 lysis buffer	50 mM Tris, pH 7.4, 150 mM NaCl, 1% Nonidet-P40, supplemented with 1 mM PMSF and 1x protease inhibitor cocktail (Sigma)

5.3.2 SDS PAGE and western blotting

Table 6: SDS PAGE and western blotting buffers and solutions

Name	Components
6x Laemmli	375 mM Tris-HCl (pH 8.6), 25.8% (v/v) glycerol, 12.3% (w/v) SDS, 600 µg/ml bromophenol blue, 6% (v/v) β-mercaptoethanol in dH ₂ O
3x Laemmli	50% (v/v) 6x Laemmli, in dH ₂ O
10x running buffer	250 mM Tris base, 2.5 M glycine, 35 mM SDS in dH ₂ O
10x transfer buffer	250 mM Tris base, 1.92 M glycine in dH ₂ O
1x transfer buffer	10% (v/v) 10x transfer buffer, 20% (v/v) methanol in dH ₂ O
20x TBS-T	200 mM Tris-HCl (pH 7.7), 3 M NaCl, 1% (v/v) Tween-20 in dH ₂ O
Blocking buffer	5% (w/v) nonfat dried milk powder in 1x TBS-T
Ponceau S	0.1% (w/v) ponceau S in 5% acetic acid
Stripping buffer	62.5 mM Tris pH 6.8, 2% SDS, 0.7% (v/v) β-mercaptoethanol
Stacking gel	130 mM Tris (pH 6.8), 17% (v/v) acrylamide, 1% SDS, 1% APS, 0.2% (v/v) TEMED in ddH ₂ O
12% running gel	500 mM Tris (pH 8.8), 40% (v/v) acrylamide, 1% SDS, 1% APS, 0.16% (v/v) TEMED in ddH ₂ O
6% running gel	230 mM Tris (pH 8.8), 26% (v/v) acrylamide, 1% SDS, 1% APS, 0.08% (v/v) TEMED in ddH ₂ O
20% running gel	240 mM Tris (pH 8.8), 66.5% (v/v) acrylamide, 1% SDS, 1% APS, 0.08% (v/v) TEMED in ddH ₂ O

5.3.3 Agarose gel electrophoresis

Table 7: Agarose gel electrophoresis

Name	Components
50x TAE buffer	2 M Tris base, 5.71% acetic acid, 50 mM EDTA (pH 8) in dH ₂ O
Agarose gel	1–2% (w/v) agarose 1 µg/ml ethidium bromide (EtBr) in 1x TAE or GelGreen (1:20000)
10x DNA loading dye	3.7 mM Bromophenol blue, 50 mM Tris (pH 7.6), 84 mM glycerol in dH ₂ O

5.3.4 DNA and protein ladder

Table 8: DNA and protein standards

Name	Application	Company
GeneRuler DNA Ladder Mix	DNA/agarose gel electrophoresis	Thermo Fisher Scientific, Darmstadt
PAGERuler Prestained Protein Ladder	Protein/western blotting	Thermo Fisher Scientific, Darmstadt

5.3.5 LD isolation buffer

Table 9: Buffers used for LD isolation

Name	Components
Sucrose buffer	1.05 M sucrose in isotonic buffer
Hypotonic buffer	50 mM HEPES, 1 mM EDTA, 2 mM MgCl ₂ , pH 7.4, supplemented with 1x protease inhibitor cocktail (Sigma)
Isotonic buffer	50 mM HEPES, 100 mM KCl, 2 mM MgCl ₂ , supplemented with 1 mM PMSF

5.3.6 Buffers for proximity labeling

Table 10: Solutions and buffers for proximity labeling

Name	Stock concentration/components
Biotin	10 mM in DMSO
Biotin-Phenol	500 mM in DMSO
Hydrogen peroxide (H ₂ O ₂)	100 mM in PBS
Sodium azide	1 M in dH ₂ O
Sodium ascorbate	1 M in dH ₂ O

Trolox	500 mM in DMSO
Quencher solution (for APEX2)	10 mM sodium azide, 10 mM sodium ascorbate, 5 mM Trolox in PBS
Lysis buffer for APEX2	10 mM sodium azide, 10 mM sodium ascorbate, 5 mM Trolox in RIPA lysis buffer supplemented with 1x protease inhibitor cocktail (Sigma) and 1 mM PMSF

Biotin, biotin-phenol and sodium azide stock solutions were prepared and stored at -20 °C or -80 °C. The H₂O₂ solution was freshly prepared from a 30% (w/w) solution (Sigma). Sodium ascorbate, Trolox, quencher solution and supplemented lysis buffers were prepared freshly.

5.3.7 Solutions for immunofluorescence staining

Table 11: Solutions used for microscopy

Name	Components
Blocking solution	5% bovine serum albumin (BSA), 1% fish skin gelatin, 50 mM Tris
Mowiol	10% (w/v) Mowiol 4-88, 0.1 M Tris-HCl (pH 8.5), 25% (w/v) glycerol
Triton X-100	0.1% (v/v) Triton-X-100 in PBS
PFA	16% (w/v) paraformaldehyde in PBS

5.3.8 Buffer for annealing of primers

Table 12: Annealing buffer

Component	Concentration
Potassium acetate	200 mM
HEPES pH 7.4	60 mM
Magnesium acetate	4 mM

5.4 Inhibitors

Table 13: Inhibitors

Inhibitor	Stock concentration	Company
Phenylmethylsulfonyl fluoride (PMSF)	100 mM in isopropanol	Sigma-Aldrich Chemie GmbH, Taufkirchen
Protease inhibitor cocktail	100x	Sigma-Aldrich Chemie GmbH, Taufkirchen
RNAseOut	40 U/μL	Thermo Fisher Scientific, Darmstadt

5.5 Enzymes

Table 14: Restriction buffers

Enzyme	Company
EcoRI (10000 U/mL)	New England Biolabs GmbH, Frankfurt am Main
MluI (10000 U/mL)	New England Biolabs GmbH, Frankfurt am Main
NheI (10000 U/mL)	New England Biolabs GmbH, Frankfurt am Main
NotI (10000 U/mL)	New England Biolabs GmbH, Frankfurt am Main
SpeI (10000 U/mL)	New England Biolabs GmbH, Frankfurt am Main
XbaI (10000 U/mL)	New England Biolabs GmbH, Frankfurt am Main
XhoI (10000 U/mL)	New England Biolabs GmbH, Frankfurt am Main

Restriction enzymes were used according to the manufacturer's instructions with supplied buffers.

Table 15: Enzymes used in this study

Enzyme	Company
Alkaline phosphatase, calf intestine (CIP)	New England Biolabs GmbH, Frankfurt am Main
Phusion high-fidelity DNA polymerase	Thermo Fisher Scientific, Darmstadt
RNAse A	Thermo Fisher Scientific, Darmstadt
Superscript III reverse transcriptase	Thermo Fisher Scientific, Darmstadt
Taq DNA polymerase	Thermo Fisher Scientific, Darmstadt
T4 DNA ligase	Thermo Fisher Scientific, Darmstadt
T4 Polynucleotide kinase	New England Biolabs GmbH, Frankfurt am Main
Mung bean nuclease	New England Biolabs GmbH, Frankfurt am Main

5.6 Kits

Table 16: Commercial kits

Kit	Company
DC protein assay	Bio-Rad Laboratories GmbH München
Pierce 660 nm protein assay	Thermo Fisher Scientific, Darmstadt
Pierce Coomassie Plus (Bradford) assay reagent	Thermo Fisher Scientific, Darmstadt
DNA-free DNA removal kit (Ambion)	Thermo Fisher Scientific, Darmstadt
Maxima SYBR green qPCR master mix	Thermo Fisher Scientific, Darmstadt
Luna Universal qPCR Mastermix	New England Biolabs, Frankfurt am Main
Megascript T7 transcription kit	Thermo Fisher Scientific, Darmstadt
Dual-Luciferase reporter assay system	Promega GmbH, Mannheim
Luciferase assay system	Promega GmbH, Mannheim

Nucleobond XtraMaxi kit	Machery-Nagel, Düren
NucleoSpin Gel and PCR clean-up kit	Machery-Nagel, Düren
NucleoSpin Plasmid kit	Machery-Nagel, Düren
NucleoSpin RNA Virus	Machery-Nagel, Düren

5.7 Plasmids

Table 17: Expression plasmids

Number	Name	Description	Source/Reference
HH71	pSicoR-MS1	Lentiviral vector expressing an mCherry. Used as backbone for shRNA constructs	(Wissing <i>et al.</i> , 2011)
HH230	pSicoR-NT	Lentiviral vector carrying non-targeting (NT) shRNA	Anja Schöbel (Rösch <i>et al.</i> , 2016) shNT sequence modified from (Neufeldt <i>et al.</i> , 2013)
HH344	pcDNA3.1 MCS-BioID2-HA	Plasmid expressing BioID2 with a C-terminal HA	Addgene #74224
HH345	pcDNA3 FLAG-APEX2-NES	Plasmid expressing APEX2 with a N-terminal FLAG and C-terminal nuclear export signal (NES)	Addgene #49386
HH362	pSicoR ANXA3-BioID2-HA	Lentiviral vector expressing ANXA3-BioID2-HA fusion protein	This thesis
HH363	pSicoR PLIN2-BioID2-HA	Lentiviral vector expressing PLIN2-BioID2-HA fusion protein	This thesis
HH364	pSicoR ANXA3-FLAG-APEX2	Lentiviral vector expressing ANXA3-FLAG-APEX2 fusion protein	This thesis
HH365	pSicoR PLIN2-FLAG-APEX2	Lentiviral vector expressing PLIN2-FLAG-APEX2 fusion protein	This thesis
HH379	pSicoR ANXA3-BioID2-HA_2A-mCherry	Lentiviral vector expressing ANXA3-BioID2-HA fusion protein and mCherry with a 2A ribosomal skipping site	This thesis
HH380	pSicoR ANXA3-FLAG-APEX2_2A-mCherry	Lentiviral vector expressing ANXA3-FLAG-APEX2 fusion protein and mCherry with a 2A ribosomal skipping site	This thesis

HH381	pSicoR PLIN2-BioID2-HA_2A-mCherry	Lentiviral vector expressing PLIN2-BioID2-HA fusion protein and mCherry with a 2A ribosomal skipping site	This thesis
HH382	pSicoR PLIN2-FLAG-APEX2_2A-mCherry	Lentiviral vector expressing PLIN2-FLAG-APEX2 fusion protein and mCherry with a 2A ribosomal skipping site	This thesis
HH383	pSicoR BioID2-HA_2A-mCherry	Lentiviral vector expressing BioID2-HA and mCherry with a 2A ribosomal skipping site. Used as control vector for BioID2-based proximity labeling	This thesis
HH384	pSicoR FLAG-APEX2_2A-mCherry	Lentiviral vector expressing FLAG-APEX2 and mCherry with a 2A ribosomal skipping site. Used as control vector for APEX2-based proximity labeling	This thesis
HH449	pSicoR shLARP1	Lentiviral vector carrying LARP1 shRNA	Elisa Heidenfels (This study)
HH451	pSicoR shFABP5	Lentiviral vector carrying FABP5 shRNA	Elisa Heidenfels (This study)
HH452	pSicoR shNOB1	Lentiviral vector carrying NOB1 shRNA	Elisa Heidenfels (This study)
HH453	pSicoR shARL8B	Lentiviral vector carrying ARL8B shRNA	Elisa Heidenfels (This study)
HH454	pSicoR T7-core-IRES-EGFP	Lentiviral vector expressing HCV core (gt1b) with an N-terminal T7-tag and an IRES-driven EGFP	Elisa Heidenfels (This study)
HH455	pSicoR shSART3	Lentiviral vector carrying SART3 shRNA	This thesis
HH465	pcDNA3.1+/C-(K)-DYK LARP1	LARP1 expression vector	GenScript
HH467	pcDNA3.1+/C-(K)-DYK FABP5	FABP5 expression vector	GenScript
HH468	pcDNA3.1+/C-(K)-DYK NOB1	NOB1 expression vector	GenScript
HH469	pcDNA3.1+/C-(K)-DYK ARL8B	ARL8B expression vector	GenScript

Material & Methods

HH470	pcDNA3.1+/C-(K)-DYK SART3	SART3 expression vector	GenScript
HH478	pSicoR MCS-IRES-EGFP	Lentiviral vector with a multiple cloning site and an IRES-driven EGFP	Elisa Heidenfels (This study)
HH479	pSicoR T7-LARP1-IRES-EGFP	Lentiviral expressing LARP1 with an N-terminal T7-tag and an IRES-driven EGFP	Elisa Heidenfels (This study)
HH481	pSicoR T7-FABP5-IRES-EGFP	Lentiviral expressing FABP5 with an N-terminal T7-tag and an IRES-driven EGFP	Elisa Heidenfels (This study)
HH482	pSicoR T7-NOB1-IRES-EGFP	Lentiviral expressing NOB1 with an N-terminal T7-tag and an IRES-driven EGFP	Elisa Heidenfels (This study)
HH483	pSicoR T7-ARL8B-IRES-EGFP	Lentiviral expressing ARL8B with an N-terminal T7-tag and an IRES-driven EGFP	Elisa Heidenfels (This study)
HH484	pSicoR T7-SART3-IRES-EGFP	Lentiviral expressing SART3 with an N-terminal T7-tag and an IRES-driven EGFP	Elisa Heidenfels (This study)
HH232	LeGO-iCer2	Expression plasmid	(Weber <i>et al.</i> , 2008)
HH233	LeGO-iCer2 ANXA3-HA	Eukaryotic vector expressing ANXA3 with a C-terminal HA	Kathrin Rösch (Rösch <i>et al.</i> , 2016)
pMO535	pEBB	Expression plasmid. Used as empty vector control	(Tanaka <i>et al.</i> , 1995)
HH176	pEBB ANXA3-HA	Eukaryotic vector expressing ANXA3 with a C-terminal HA	Anja Schöbel (Rösch <i>et al.</i> , 2016)
HH38	pCMV6-XL4 PLIN2	Eukaryotic vector expressing PLIN2	OriGene Technologies
HH361	pSicoR-MS1ΔU6 PLIN2-HA rescue mutant	Lentiviral vector expressing PLIN2 with a C-terminal HA	Susan Lassen (Lassen <i>et al.</i> , 2019)
HH96	pcDNA3.1	Eukaryotic expression vector. Used as empty vector control for transfection	Thermo Fisher Scientific, Darmstadt
HH98	Trip-RFP-NLS-IPS	Reporter plasmid for HCV titration	Charles M. Rice (Jones <i>et al.</i> , 2010)
HH158	pSicoR-MS1ΔU6	Lentiviral expression vector carrying an mCherry and EF1α promoter	Anja Schöbel

HH106	LeGO-iCer2	Lentiviral vector containing cerulean and an IRES	Boris Fehse (Weber <i>et al.</i> , 2008)
HH245	LeGO-iCer FLAG-core	Lentiviral vector expressing 3xFLAG-core (gt2a). Expresses cerulean from an IRES	Kathrin Rösch (Rösch <i>et al.</i> , 2016)
HH309	LeGO-iCer2 NS5A-FLAG	Lentiviral vector expressing NS5A-FLAG (gt2a). Expresses cerulean from an IRES	Kathrin Rösch (Rösch <i>et al.</i> , 2016)
pMO155	pHR EGFP	Lentiviral vector expressing an IRES-driven EGFP	(Herker <i>et al.</i> , 2010)
pMO160	pHR core EGFP	Lentiviral vector expressing HCV core (gt1b) and an IRES-driven EGFP	(Herker <i>et al.</i> , 2010)
HH436	pSicoR-MS1ΔU6 EGFP	Lentiviral vector expressing EGFP	Anja Schöbel (unpublished)
pGL4.75	pGL4.75[hRluc/CMV]	Control plasmid for Dual-Luciferase assay. Expresses the <i>Renilla</i> luciferase	Promega GmbH, Mannheim
pMO86	pCMVΔR8.91	Lentiviral packaging vector	(Naldini <i>et al.</i> , 1996)
pMO87	pMD.G	VSV-G envelope glycoprotein	(Naldini <i>et al.</i> , 1996)
pHR319	pcDNA-TO FLAG-core	Eukaryotic expression vector containing HCV core (gt2a) with an N-terminal 3x FLAG under a CMV promoter in a pcDNA-TO backbone	Holly Ramage (Ramage <i>et al.</i> , 2015)
pHR315	pcDNA-TO FLAG-NS2	Eukaryotic expression vector containing HCV NS2 (gt2a) with an N-terminal 3x FLAG under a CMV promoter in a pcDNA-TO backbone	Holly Ramage (Ramage <i>et al.</i> , 2015)
pHR316	pcDNA-TO FLAG-E1	Eukaryotic expression vector containing HCV E1 (gt2a) with an N-terminal 3x FLAG under a CMV promoter in a pcDNA-TO backbone	Holly Ramage (Ramage <i>et al.</i> , 2015)
pHR317	pcDNA-TO FLAG-NS4A	Eukaryotic expression vector containing HCV NS4A (gt2a) with an N-terminal 3x FLAG under a CMV promoter in a pcDNA-TO backbone	Holly Ramage (Ramage <i>et al.</i> , 2015)
pHR323	pcDNA-TO NS4B-FLAG	Eukaryotic expression vector containing HCV NS4B (gt2a) with a	Holly Ramage (Ramage <i>et al.</i> , 2015)

		C-terminal 3x FLAG under a CMV promoter in a pcDNA-TO backbone	
pHR325	pcDNA-TO p7-FLAG	Eukaryotic expression vector containing HCV p7 (gt2a) with a C-terminal 3x FLAG under a CMV promoter in a pcDNA-TO backbone	Holly Ramage (Ramage <i>et al.</i> , 2015)
pHR329	pcDNA-TO E2-FLAG	Eukaryotic expression vector containing HCV E2 (gt2a) with a C-terminal 3x FLAG under a CMV promoter in a pcDNA-TO backbone	Holly Ramage (Ramage <i>et al.</i> , 2015)
pHR330	pcDNA-TO NS5A-FLAG	Eukaryotic expression vector containing HCV NS5A (gt2a) with a C-terminal 3x FLAG under a CMV promoter in a pcDNA-TO backbone	Holly Ramage (Ramage <i>et al.</i> , 2015)
pHR331	pcDNA-TO NS3-FLAG	Eukaryotic expression vector containing HCV NS3 (gt2a) with a C-terminal 3x FLAG under a CMV promoter in a pcDNA-TO backbone	Holly Ramage (Ramage <i>et al.</i> , 2015)

Table 18: HCV plasmids

Number	Name	Description	Source/Reference
pMO977	pBR322 Jc1 ^{NS5AB} -EGFP	Jc1 reporter encoding an EGFP in a duplicated NS5AB cleavage site	Brian Webster (Webster <i>et al.</i> , 2013)
HH183	pBR322 Jc1 ^{p7-GLuc-2A-NS2}	Jc1 strain expressing a secreted <i>gaussia</i> luciferase followed by a modified p2A ribosomal skipping site between p7 and NS2	Anja Schöbel (Rösch <i>et al.</i> , 2016)
HH337	pBR322 Jc1 Δ E1/E2 ^{NS5AB-FLuc}	Jc1 replicon with partly deleted envelope proteins and a firefly luciferase in a duplicated NS5AB cleavage site	Susan Lassen (Lassen <i>et al.</i> , 2019)
HH366	pBR322 Jc1 Δ E1/E2 ^{NS5AB-EGFP-BSD}	Jc1 replicon with partly deleted envelope proteins and an EGFP and a blasticidin resistance gene in a duplicated NS5AB cleavage site	Brian Webster/ Anja Schöbel
HH443	pBR322 JFH1 ^{FLuc-p2A-NS3-NS5B} subgenomic replicon	HCV JFH1 subgenomic replicon expressing a firefly luciferase followed by a modified p2A	Van Nguyen-Dinh (unpublished)

		ribosomal skipping site and NS3-NS5B	
HH166	pUC Con1 replicon	HCV gt1b subgenomic replicon. Expresses NS3-NS5B and a neomycin resistance gene	James Ou (Choi <i>et al.</i> , 2004)

5.8 Oligonucleotides

Oligonucleotides were purchased from Sigma-Aldrich, Taufkirchen.

Table 19: PCR primers used for cloning of BioID2 and APEX2 constructs

Description	Primer No	Sequence 5'-3'
pSicoR ANXA3 sense	1	CTGTGACCGGCGCCTACGATGGCATCTATCTGGGTT
ANXA3-BioID2-HA antisense	2	CAGGTTCTTGAACATACCACCGTCATCTCC
ANXA3-BioID2-HA sense	3	GATGACGGTGGTATGTTCAAGAACCTGATC
pSicoR BioID2-HA antisense	4	TAGGTCCCTCGACGAATTTTATGCGTAATCCGGTAC
pSicoR PLIN2 sense	5	CTGTGACCGGCGCCTACGATGGCATCCGTTGCAGTT
PLIN2-BioID2-HA antisense	6	GATCAGGTTCTTGAACATACCACCATGAGT
PLIN2-BioID2-HA sense	7	AAAACTCATGGTGGTATGTTCAAGAACCTG
ANXA3-FLAG-APEX2 antisense	8	CATGGTGGCGGCCGCACCACCGTCATCTCC
ANXA3-FLAG-APEX2 sense	9	GGAGATGACGGTGGTGCGGCCGCCACCATG
pSicoR FLAG-APEX2 antisense	10	TAGGTCCCTCGACGAATTCTATTAGTCCAGGGTCAG

PLIN2-FLAG- APEX2 antisense	11	GGTGGCGGCCGCGCACCACCATGAGTTTTATG
PLIN2-FLAG- APEX2 sense	12	AAAACTCATGGTGGTGGCGCCGCCACCATG
NheI pSicoR ANXA3 sense	17	GCCTACGCTAGCATGGCATCTATCTGGGTT
BioID2-HA-2A antisense	18	GACGTCTCCCGCAAGCTTAAGAAGGTCAAATTGTC GTAATCCGGTAC
FLAG-APEX2- 2A antisense	19	GACGTCTCCCGCAAGCTTAAGAAGGTCAAATTGTC CAGGGTCAGGCG
NheI BioID2 sense	20	GCCTACGCTAGCATGTTCAAGAACCTGATC
NheI APEX2 sense	21	GCCTACGCTAGCGCGGCCGCCACCATG
NheI pSicoR PLIN2 sense	22	GCCTACGCTAGCATGGCATCCGTTGCA
PLIN2-BioID2- HA antisense_new	23	GATCAGGTTCTTGAACATACCACCATGAGTTTTATGCTC
2A-mCherry sense		TGCGGGAGACGTGAGTCCAACCCTGGGCCAGTGAGC AAGGGCGAG
EcoRI mCherry as		CTCGACGAATTCTTACTTGTACAG

Table 20: Primers used to clone shRNAs

Description	Sequence 5'-3'
LARP1 fw	TGCGCCAGATTGAATACTACTTTTCAAGAGAAAGTAGTATTCAATCTGG CGCTTTTTTC
LARP1 rev	TCGAGAAAAAAGCGCCAGATTGAATACTACTTTCTCTTGAAAAGTAGTA TTCAATCTGGCGCA
FABP5 fw	TCTTTGGACAGGAGTTAATTAATTCAAGAGATTAATTAACCTGTCCA AAGTTTTTTC
FABP5 rev	TCGAGAAAAAAGTTTGGACAGGAGTTAATTAATCTCTTGAATTAATTAAC TCCTGTCCAAAGA
NOB1 fw	TCCAAGGAAGTGCAATTGCATATTCAAGAGATATGCAATTGCACTTCCT TGGTTTTTTC
NOB1 rev	TCGAGAAAAAAGCAAGGAAGTGCAATTGCATATCTCTTGAATATGCAAT TGCACTTCCTTGGA

ARL8B fw	TGCCTGCTTTATCTAATGTAATTTCAAGAGAATTACATTAGATAAAGCAG GCTTTTTTC
ARL8B rev	TCGAGAAAAAAGCCTGCTTTATCTAATGTAATTCTCTTGAAATTACATTA GATAAAGCAGGCA
SART3 fw	TCGAGAGTTTGAAAGTGCGATTTTCAAGAGAAATCGCACTTTCAAACCTC TCGTTTTTTC
SART3 rev	TCGAGAAAAAACGAGAGTTTGAAAGTGCGATTTCTCTTGAAAATCGCAC TTTCAAACCTCTCGA
pSicoR sequencing primer	TGCAGGGGAAAGAATAGTAGAC (sequence obtained from Tyler Jacks)

Table 21: PCR primers used to clone lentiviral expression plasmids

Description	Sequence 5'-3'
NheI-MCS-IRES fw	GCTAGCTCTAGAACGCGCGGTGACCCTCGAGTACTAGGATC CATTAGGGGATCCGCCCTCTC
EcoRI-eGFP rev	AGGTCCCTCGACGAATTCTTACTTGTACAGCTCGTCCAT
SpeI-T7-LARP1 fw	ACCGGCGCCTACACTAGTGCTATGGCTAGCATGACTGGTGG ACAGCAAATGGGTATGCTTTGGAGGGTG
LARP1-XhoI rev	GTACTCGAGCTTTCCCAAAGTCTGTGT
SpeI-T7-FABP5 fw	ACCGGCGCCTACACTAGTGCTATGGCTAGCATGACTGGTGG ACAGCAAATGGGTATGGCCACAGTTCAG
FABP5-XhoI rev	GTACTCGAGTTCTACTTTTTCATA
SpeI-T7-NOB1 fw	ACCGGCGCCTACACTAGTGCTATGGCTAGCATGACTGGTGG ACAGCAAATGGGTATGGCTCCAGTGGAGCACGTT
NOB1-XhoI rev	GTACTCGAGCCTTTTCTTCACAAA
SpeI-T7-ARL8B fw	ACCGGCGCCTACACTAGTGCTATGGCTAGCATGACTGGTGG ACAGCAAATGGGTATGCTGGCGCTCATCTCCCGC
ARL8B-XhoI rev	GTACTCGAGGCTTCTTCTAGATTT
SpeI-T7-SART3 fw	ACCGGCGCCTACACTAGTGCTATGGCTAGCATGACTGGTGG ACAGCAAATGGGTATGGCGACTGCGGCC
SART3-XhoI rev	GTACTCGAGCTTTCTCAGAAACAG

Table 22: Primers used for qRT-PCR

Description	Sequence 5'-3'	Reference / Harvard Primer Bank ID
JFH1 fw	CGGGAGAGCCATAGTGG	(Herker <i>et al.</i> , 2010)
JFH1 rev	AGTACCACAAGGCCTTTTCG	
18S rRNA fw	GTAACCCGTTGAACCCATT	
18S rRNA rev	CCATCCAATCGGTAGTAGCG	

LARP1 fw	GCCTGGCAACCAGAGATCAAA	61102726c3
LARP1 rev	TCAAACCTTCGGTAGCCAAACT	
FABP5 fw	TGAAGGAGCTAGGAGTGGGAA	323462197c1
FABP5 rev	TGCACCATCTGTAAAGTTGCAG	
NOB1 fw	CAGGACATCGGGAAGAACATTT	7661531c1
NOB1 rev	CCGCACGTATTCCGGTAAGG	
ARL8B fw	CATCGCGTCAGGTCAATTGAG	49472838c1
ARL8B rev	GTTGTCCTCCTATGTCCCAGA	
SART3 fw	TGAGGTTAAGGCGGCTAGGA	119393885c1
SART3 rev	CATGGCGTACTCATCCCCATC	

qRT-PCR primers were selected from the Harvard primer bank.

5.9 Antibodies and dyes

Table 23: Primary antibodies

Antigen/clone	Species	Dilution	Company	Catalogue no
HA	rb	WB 1:1000 IF 1:100	Sigma-Aldrich Chemie, Taufkirchen	H6908-100UL
HA (Y-11)	gt	WB 1:500 IF 1:50	Santa Cruz Biotechnology, Heidelberg	sc-805-G
HCV NS5A (2F6/G11)	ms	WB 1:250 IF 1:20	IBT-GmbH, Reutlingen	HCM-131-5
HCV NS5A	ms	WB 1:250	Merck, Darmstadt	MAB8694
HCV core (C7-50)	ms	WB 1:250 IF 1:20	Santa Cruz Biotechnology, Heidelberg	sc-57800
HCV NS3	ms	WB 1:1000	abcam	ab65407
dsRNA (J2)	ms	IF 1:200	Scicons	
FLAG	rb	WB 1:000 IF 1:100	Sigma-Aldrich Chemie, Taufkirchen	F7425-.2MG
FLAG M2	ms	WB 1:250	Sigma-Aldrich Chemie, Taufkirchen	F1804
PLIN2	ms	WB 1:250	Progen Biotechnik GmbH	610102
PLIN2	gp	WB 1:1000 IF 1:100	Progen Biotechnik GmbH	GP40
Tubulin (B 5-1-2)	ms	WB 1:2000	Sigma-Aldrich Chemie, Taufkirchen	T6074
T7	ms	WB 1:2000 IF 1:100	Merck, Darmstadt	69522-3
T7	rb	WB 1:1000	Merck, Darmstadt	AB3790

		IF 1:100		
LARP1	rb	WB 1:1000 IF 1:50 IP 0.7 µg (3.5 µL)	Novus Biologicals	NBP1-19128
ANXA3	rb	WB 1:1000	Sigma-Aldrich Chemie, Taufkirchen	hpa013431
NOB1	rb	WB 1:1000 IF 1:100	Thermo Fisher Scientific, Darmstadt	PA5-31785
ARL8 A/B	ms	WB 1:250 IF 1:20	Santa Cruz Biotechnology	Sc-398679
SART3	rb	WB 1:1000 IF 1:100	abcam	Ab176822
FABP5	ms	WB 1:250 IF 1:20	Santa Cruz Biotechnology	Sc-365236
USP15	ms	WB 1:250	Santa Cruz Biotechnology	Sc-100629

Table 24: Secondary antibodies

Antibody	Dilution	Company
Peroxidase-AffiniPure goat anti-mouse IgG (H+L)	WB 1:10000	JacksonImmunoResearch Laboratories, Suffolk (UK)
Peroxidase-AffiniPure goat anti-rabbit IgG (H+L)	WB 1:10000	JacksonImmunoResearch Laboratories, Suffolk (UK)
Peroxidase AffiniPure Goat Anti-Guinea Pig IgG (H+L)	WB 1:10000	JacksonImmunoResearch Laboratories, Suffolk (UK)
Peroxidase-AffiniPure donkey anti-goat IgG (H+L)	WB 1:10000	JacksonImmunoResearch Laboratories, Suffolk (UK)
Rabbit TrueBlot: ULTRA: Anti-Rabbit IgG HRP	WB 1:1000	Rockland antibodies and assays via Biomol GmbH, Hamburg
Mouse TrueBlot ULTRA: Anti-Mouse IgG HRP clone eB144	WB 1:1000	Rockland antibodies and assays via Biomol GmbH, Hamburg
Alexa Fluor 555 donkey anti-mouse IgG (H+L)	IF: 1:1000; 1:1500	Thermo Fisher Scientific, Darmstadt
Alexa Fluor 647 Donkey anti-rabbit IgG (H+L)	IF: 1:1000; 1:1500	Thermo Fisher Scientific, Darmstadt
Alexa Fluor 647 Donkey anti-mouse IgG (H+L)	IF: 1:1000; 1:1500	Thermo Fisher Scientific, Darmstadt
Alexa Fluor 488 Donkey anti-rabbit IgG (H+L)	IF: 1:1000; 1:1500	Thermo Fisher Scientific, Darmstadt

Alexa Fluor 488 Donkey anti-mouse IgG (H+L)	IF: 1:1000; 1:1500	Thermo Fisher Scientific, Darmstadt
Alexa Fluor 488 Donkey anti-rabbit IgG (H+L) Streptavidin conjugate	IF: 1:1000	Thermo Fisher Scientific, Darmstadt
Alexa Fluor 405 Donkey anti-rabbit IgG (H+L) Streptavidin conjugate	IF: 1:1000	Thermo Fisher Scientific, Darmstadt
Streptavidin (HRP)	WB 1:20000	Abcam

Table 25: Fluorescent dyes

Dye	Dilution	Company
BODIPY 493/503 (1mg/mL)	1:750	Thermo Fisher Scientific, Darmstadt
BODIPY 665 (1mg/mL)	IF 1:20000	Thermo Fisher Scientific, Darmstadt
Hoechst	IF 1:6000	Sigma-Aldrich GmbH, Taufkirchen

Table 26: Agarose beads

Description	Quantity	Company	Catalogue no
Anti-FLAG M2 affinity gel (ms)	IP: 30 µL/sample	Sigma-Aldrich Chemie GmbH, Taufkirchen	A2220-5ML
HA agarose (HA-7) (ms)	IP: 30 µL/sample	Sigma-Aldrich Chemie GmbH, Taufkirchen	A2095-1ML
Streptavidin agarose resins	IP: 30 µL/sample MS: 35 µL/sample	Thermo Fisher Scientific, Darmstadt	20349
T7-Tag Antibody agarose	IP: 30 µL/sample	Merck, Darmstadt	69026
rProtein G Agarose	IP: 30 µL	Invitrogen	15920-010

5.10 Consumables

Table 27: Consumables

Name	Company
Adhesive PCR seal	Sarstedt AG & Co KG, Nümbrecht
Amersham Hyperfilm ECL	Geyer Th. GmbH & Co.KG, Renningen
Blunt-end cannula (Sterican 20G x 2")	B. Braun Melsungen
Cannula (Sterican 23G x 1 ¼")	B. Braun Melsungen
Amersham Protran Premium Nitrocellulose membrane	Geyer Th. GmbH & Co.KG, Renningen
96 Fast PCR Plate half skirt	Sarstedt AG & Co KG, Nümbrecht
1.5 ml-reaction tubes RNase free	Sarstedt AG & Co KG, Nümbrecht
5 Prime Phase-Lock Tube	5Prime GmbH, Hilden
Biosphere Filter Tips, RNase free	Sarstedt AG & Co KG, Nümbrecht

Cryo-Tubes	Sarstedt AG & Co KG, Nümbrecht
Centrifuge tube, thinwall ultraclear	Beckman Coulter GmbH, Krefeld
15 ml- and 50 ml-tubes (conical)	Greiner GmbH, Frickenhausen
96-Well microtestplate conical bottom	Sarstedt AG & Co KG, Nümbrecht
Cell scraper	VWR International GmbH, Darmstadt
Cell culture dishes	Sarstedt AG & Co KG, Nümbrecht; Greiner GmbH, Frickenhausen
Cell culture flasks	Sarstedt AG & Co KG, Nümbrecht Greiner GmbH, Frickenhausen
Cellstar serological pipettes	Greiner GmbH, Frickenhausen
Combitips advanced (Eppendorf)	VWR International GmbH, Darmstadt
Cover slips	VWR International GmbH, Darmstadt
Microscope slides	Marienfeld GmbH & Co KG Lauda, Königshofen
Electroporation cuvette 2 mm	VWR International GmbH, Darmstadt
Electroporation cuvette 4 mm	VWR International GmbH, Darmstadt
Omnifix Luer-Lock solo syringe	B. Braun, Melsungen
C-Chip disposable Neubauer counting chamber	VWR International GmbH, Darmstadt
Glass slides	VWR International GmbH, Darmstadt
Dounce homogenizer, 2 ml	Thermo Fisher Scientific, Darmstadt
Microtest plate	Sarstedt AG & Co KG, Nümbrecht
Multiply µStrip Pro 8-Strip RNase free	Sarstedt AG & Co KG, Nümbrecht
Mini Protean Gel Any kDa	BioRad Laboratories GmbH München
Nunc-Immuno MicroWell 96 well polystyrene plates (white)	Thermo Fisher Scientific, Darmstadt
PCR tubes	Sarstedt AG & Co KG, Nümbrecht
Pipette tips	VWR International GmbH, Darmstadt or STARLAB International GmbH, Hamburg
SafeSeal 1.5 ml-reaction tube	Sarstedt AG & Co KG, Nümbrecht
SafeSeal 2 ml-reaction tube	Sarstedt AG & Co KG, Nümbrecht
Parafilm	Bemis, Oshkosh, USA
Rotilabo liquid-reservoirs	Roth GmbH + Co. KG, Karlsruhe
Steriflip 0.22 µm	Merck Millipore, Darmstadt
Sterile filter 0.22 µm	Thermo Fisher Scientific, Darmstadt
Sterile filter 0.45 µm	Thermo Fisher Scientific, Darmstadt
Syringe	neoLab GmbH, Heidelberg
Whatman paper	GE Healthcare, München

5.11 Chemicals

Table 28: Chemicals

Chemical	Company
1,4-Dithiothreitol (DTT)	Thermo Fisher Scientific, Darmstadt
100x BSA (bovine serum albumin for restriction enzymes)	New England Biolabs GmbH, Frankfurt am Main
10x Mung bean nuclease buffer	New England Biolabs GmbH, Frankfurt am Main
10x NEBuffer (NEB)	New England Biolabs GmbH, Frankfurt am Main
10x T4-ligase buffer	Thermo Fisher Scientific, Darmstadt
10x Taq buffer - MgCl ₂ + (NH ₄) ₂ SO ₄	Thermo Fisher Scientific, Darmstadt
25 mM MgCl ₂ (PCR)	Thermo Fisher Scientific, Darmstadt
2-Propanol	AppliChem GmbH, Darmstadt

5x Phusion HF buffer	Sigma-Aldrich Chemie GmbH, Taufkirchen
6x DNA loading dye	Thermo Fisher Scientific, Darmstadt
Acetic acid	Thermo Fisher Scientific, Darmstadt
Acrylamide solution (30%) - Mix 37.5	AppliChem GmbH, Darmstadt
Adenosine triphosphate (ATP)	AppliChem GmbH, Darmstadt
Agar bacteriology grade	AppliChem GmbH, Darmstadt
Agarose basic	AppliChem GmbH, Darmstadt
Albumin from bovine serum	AppliChem GmbH, Darmstadt
Ammonium persulfate (APS)	AppliChem GmbH, Darmstadt
Ampicillin sodium salt	AppliChem GmbH, Darmstadt
Biotin	Sigma-Aldrich Chemie GmbH, Taufkirchen
Biotin-Phenol (biotin tyramide)	Biomol GmbH, Hamburg
Blasticidin S	Invivogen, Toulouse, France
Bromophenol blue	AppliChem GmbH, Darmstadt
Calcium chloride (CaCl ₂)	AppliChem GmbH, Darmstadt
Chloroform	AppliChem GmbH, Darmstadt
Chloroquine diphosphate	Sigma-Aldrich Chemie GmbH, Taufkirchen
Coelenterazin	Roth GmbH + Co. KG, Karlsruhe
Dimethyl sulfoxide (DMSO)	AppliChem GmbH, Darmstadt
Dimethyl sulfoxide (DMSO) for PCR	Thermo Fisher Scientific, Darmstadt
dNTP Mix 10 mM	Thermo Fisher Scientific, Darmstadt
Dulbecco's modified eagle medium (high glucose) (Gibco)	Thermo Fisher Scientific, Darmstadt
Dulbecco's modified eagle medium (4.5 g/L glucose, 0.11 g/L sodium pyruvate) (Gibco)	Thermo Fisher Scientific, Darmstadt
Dulbecco's phosphate buffered saline (DPBS)	Sigma-Aldrich Chemie GmbH, Taufkirchen
DMEM SILAC media (R0K0) light (LM014)	DC Biosciences Ltd.
DMEM SILAC media (R10K8) heavy (LM015)	DC Biosciences Ltd.
ECL Lumi-Light western blotting substrate	Hoffmann-la Roche, Basel (Switzerland)
EDTA	AppliChem GmbH, Darmstadt
Ethanol	Geyer Th. GmbH & Co.KG, Renningen
Ethanol absolute (used for RNA isolation)	AppliChem GmbH, Darmstadt
Ethidium bromide (EtBr)	AppliChem GmbH, Darmstadt
Fetal calf serum (FCS)	Biochrom AG, Berlin or Thermo Fisher Scientific, Darmstadt
Fishskin gelatine	AppliChem GmbH, Darmstadt
Fugene6 transfection reagent	Promega GmbH, Mannheim
G418 disulfate solution	AppliChem GmbH, Darmstadt
GelGreen Nucleic Acid Gel Stain	Biotinium
GlutaMAX 100x (Gibco)	Thermo Fisher Scientific, Darmstadt
Glutamine (Gibco)	Thermo Fisher Scientific, Darmstadt
Glutathione	AppliChem GmbH, Darmstadt
Glycerol anhydrous	AppliChem GmbH, Darmstadt
Glycine	AppliChem GmbH, Darmstadt
HEPES	Sigma-Aldrich Chemie GmbH, Taufkirchen
Hydrogen chloride (HCl)	AppliChem GmbH, Darmstadt
Hydrogen peroxide solution 30% (w/w)	Sigma-Aldrich Chemie GmbH, Taufkirchen

Isopropanol (used for RNA isolation)	Sigma-Aldrich Chemie GmbH, Taufkirchen
Magnesium acetate	Sigma-Aldrich Chemie GmbH, Taufkirchen
Magnesium chloride (MgCl ₂)	AppliChem GmbH, Darmstadt
Methanol (MeOH)	AppliChem GmbH, Darmstadt
Mowiol 4-88	AppliChem GmbH, Darmstadt
Nonfat dried milk powder	AppliChem GmbH, Darmstadt
Nonidet P-40	AppliChem GmbH, Darmstadt
Nuclease-free water (Ambion)	Thermo Fisher Scientific, Darmstadt
Oleic acid	Sigma-Aldrich Chemie GmbH, Taufkirchen
OptiMEM (Gibco)	Thermo Fisher Scientific, Darmstadt
Paraformaldehyde (PFA)	AppliChem GmbH, Darmstadt
Penicillin/streptomycin 100x	Sigma-Aldrich Chemie GmbH, Taufkirchen or Life Technologies GmbH, Darmstadt
Phenol-chloroform-isoamyl alcohol (25:24:1 vol/vol/vol)	AppliChem GmbH, Darmstadt
Phenylmethylsulfonyl fluoride (PMSF)	AppliChem GmbH, Darmstadt
Polybrene (hexadimethrine bromide)	Sigma-Aldrich Chemie GmbH, Taufkirchen
Polyethylene glycol (PEG) - 8000	AppliChem GmbH, Darmstadt
Ponceau S	AppliChem GmbH, Darmstadt
Potassium acetate	AppliChem GmbH, Darmstadt
Potassium chloride (KCl)	AppliChem GmbH, Darmstadt
Potassium hydroxide (KOH)	AppliChem GmbH, Darmstadt
Random hexamer primer	QIAGEN, Hilden
Recombinant protein G agarose	Thermo Fisher Scientific, Darmstadt
RNase Away	Roth GmbH + Co. KG, Karlsruhe
Roti-Blue (5x)	Roth GmbH + Co. KG, Karlsruhe
Sodium acetate (C ₂ H ₃ NaO ₂) 3 M pH 5.2	AppliChem GmbH, Darmstadt
Sodium ascorbate	Sigma-Aldrich Chemie GmbH, Taufkirchen
Sodium azide	Sigma-Aldrich Chemie GmbH, Taufkirchen
Sodium deoxycholate	AppliChem GmbH, Darmstadt
Sodium dodecyl sulfate (SDS)	AppliChem GmbH, Darmstadt
Sodium hydroxide	AppliChem GmbH, Darmstadt
Sodium hypochlorite	Merck, Darmstadt
Sucrose	AppliChem GmbH, Darmstadt
SuperSignal West Femto	Thermo Fisher Scientific, Darmstadt
TEMED (Tetramethylethylenediamine)	AppliChem GmbH, Darmstadt
TRI reagent	Sigma-Aldrich Chemie GmbH, Taufkirchen
Tris ultrapure (Tris-base)	AppliChem GmbH, Darmstadt
Triton X-100	AppliChem GmbH, Darmstadt
Trolox	Sigma-Aldrich Chemie GmbH, Taufkirchen
Trypan blue solution 0,4%	Thermo Fisher Scientific, Darmstadt
Trypsin/EDTA (0,05%/0,02% w/v) (Gibco)	Thermo Fisher Scientific, Darmstadt
Tryptone	AppliChem GmbH, Darmstadt
Tween 20	AppliChem GmbH, Darmstadt
Virkon S	Bayer AG, Leverkusen
Yeast extract	AppliChem GmbH, Darmstadt
β-Mercaptoethanol	AppliChem GmbH, Darmstadt

5.12 Devices

Table 29: Devices and Equipment

Name	Company
Eppendorf Research plus pipettes	Eppendorf AG, Hamburg
Gilson PIPETMAN pipettes	Gilson International
Erlenmeyer flask 1000 ml	VWR International GmbH, Darmstadt
Glass flask	VWR International GmbH, Darmstadt
Beaker 50–4000 ml	VWR International GmbH, Darmstadt
Centrifuge bottles	Thermo Fisher Scientific, Darmstadt
Agarose casting stand	Bio-Rad Laboratories GmbH München, VWR International GmbH, Darmstadt,
Agarose gel chamber comb	Bio-Rad Laboratories GmbH München, VWR International GmbH, Darmstadt,
Centrifuge 5424R	Eppendorf AG, Hamburg
Centrifuge 5425	Eppendorf AG, Hamburg
Centrifuge 5810R	Eppendorf AG, Hamburg
Centrifuge 5417R	Eppendorf AG, Hamburg
Mikrofuge 20	Beckman Coulter GmbH, Krefeld
Mikro 200R Centrifuge	Hettich GmbH & Co. KG, Tuttlingen
Heraeus Centrifuge Multifuge 3 SR	Thermo Fisher Scientific, Darmstadt
Centrifuge Sorvall RC5C Plus	Thermo Fisher Scientific, Darmstadt
Haereus Centrifuge Multifuge 4 KR	Thermo Fisher Scientific, Darmstadt
BD LSR Fortessa flow cytometer	BD Bioscience, Heidelberg
GelDoc	Bio-Rad Laboratories GmbH München
Gene Pulser Xcell electroporation system	Bio-Rad Laboratories GmbH München
GeneAmp PCR system 9700	Applied Biosystems, Darmstadt
ProFlex PCR System	Thermo Fisher Scientific, Darmstadt
7500 fast real time PCR system	Applied Biosystems, Darmstadt
StepOne Real-Time PCR System	Applied Biosystems, Darmstadt
HERAfreezer	Thermo Fisher Scientific, Darmstadt
HERAsafe incubator	Thermo Fisher Scientific, Darmstadt
HERAsafe sterile bench	Thermo Fisher Scientific, Darmstadt
Infinite M200 plate reader	Tecan Group Ltd, Männedorf
Epoch plate reader	Biotek Instruments, Inc.
Centro LB 960 luminometer	Berthold Technologies
Leica DMIL microscope	Leica Camera AG, Wetzlar
Leica CSLM TCS sp5 II	Leica Camera AG, Wetzlar
Laser: 405 Diode, Argon, DPSS 561, HeNe 633, UV lamp	
63x/1.4-0.6 Oil CS objective	
Nikon Eclipse Ts2	Nikon, Düsseldorf
Magnetic stirrer heating plate IKA RH basic	IKA-Werke GmbH & CO. KG, Staufen
Innova 43 incubator	New Brunswick Scientific, Hamburg
Micro centrifuge	STARLAB International GmbH, Hamburg
Mini Trans-Blot Module	Bio-Rad Laboratories GmbH München
Mini-PROTEAN Tetra Cell	Bio-Rad Laboratories GmbH München
Multipipette plus	Eppendorf AG, Hamburg
Nanodrop 1000 Spectrophotometer	Peqlab Biotechnologie GmbH, Erlangen
Neubauer Counting Chamber	Cellomics Technology, Halseth (MD)
Nikon C2plus	Nikon, Düsseldorf

Pipette boy	VWR International GmbH, Darmstadt
accu-jet pro	Brand Scientific GmbH
PowerPac HC High-Current Power Supply	Bio-Rad Laboratories GmbH München
Power Supply EV3020	Consort bvba
Analytical balance Extend ED224S	Sartorius AG, Göttingen
Scale PM4600 DeltaRange	Mettler Toledo, Gießen
Thermomixer comfort	Eppendorf AG, Hamburg
UV Illuminator	VWR International GmbH, Darmstadt
Dark Reader Transilluminator	Clare Chemical Research
Vortex-Genie 2	VWR International GmbH, Darmstadt
Water bath WBT-series	LTF Labortechnik, Wasserburg
Wide Mini Sub Cell GT	BioRad Laboratories GmbH München
Optima L-90K ultracentrifuge	Beckman Coulter GmbH, Krefeld
Optima XE-90 ultracentrifuge	Beckman Coulter GmbH, Krefeld
Optima L-100K ultracentrifuge	Beckman Coulter GmbH, Krefeld
Beckmann L7-55 ultracentrifuge	Beckman Coulter GmbH, Krefeld
SW 60 Ti Swinging-Bucket Rotor with buckets	Beckman Coulter GmbH, Krefeld
SW 28 Swinging-Bucket Rotor with buckets	Beckman Coulter GmbH, Krefeld
SW 41 Swinging-Bucket Rotor with buckets	Beckman Coulter GmbH, Krefeld
SW 32 Swinging-Bucket Rotor with buckets	Beckman Coulter GmbH, Krefeld
Plan Apo VC 60x H Oil objective	Nikon, Düsseldorf
Sorvall SLA-3000 Super-Lite rotor	Thermo Fisher Scientific, Darmstadt
Avanti J-26 XP Centrifuge	Beckman Coulter GmbH, Krefeld
JA-10 fixed angle rotor	Beckman Coulter GmbH, Krefeld
Heraeus UT 6200	Thermo Fisher Scientific, Darmstadt
Platform rocker	LTF Labortechnik, Wasserburg
Tube roller SRT1	Stuart Equipment, Staffordshire (UK)
Tube roller SRT6	Stuart Equipment, Staffordshire (UK)
Rotator Mixer Multi-1	STARLAB International GmbH, Hamburg
Graduated cylinder 50–2000 ml	VWR International GmbH, Darmstadt

5.13 Software

Table 30: Software

Name	Company
7500 Software v2.3	AB Applied Biosystems, Darmstadt
StepOne Software v2.1	AB Applied Biosystems, Darmstadt
BD FACSDiva 5.0.3	BD Bioscience, Heidelberg
BD FACSDiva 8.0.1	BD Bioscience, Heidelberg
Chromas 2	Technelysium Pty Ltd.
Gen5	Biotek Instruments, Inc.
Fiji/ ImageJ 1.48t	Wayne Resband, National Institutes of Health (USA)
FlowJo	Treestar Inc., Ashland (USA)
ImageLab	Bio-Rad Laboratories GmbH München
NIS-Elements Ar 4.3	Nikon, Düsseldorf
NIS-Element Viewer 4.2	Nikon, Düsseldorf
LAS X	Leica Camera AG, Wetzlar

R Studio Version 4.0.2
Serial Cloner 2.6.1
Microsoft Office

R Studio Inc., Boston (USA)
Serial Basics
Microsoft

6 Methods

6.1 Molecular biological methods

6.1.1 Cultivation of bacteria

Transformed *E. coli* DH5 α were cultivated in LB media supplemented with 100 μ g/mL ampicillin at 37 °C on a shaking device or on LB agar plates at 37 °C. Successful transformation of clones was validated by selection on agar plates containing 100 μ g/mL ampicillin.

6.1.2 Plasmid isolation

Plasmids were isolated using commercial plasmid isolation kits following the manufacturer's instructions. Cultures were incubated overnight in 3-4 mL and for small-scale isolation DNA was isolated using the NucleoSpin plasmid kit. For large scale isolation, a starter culture was transferred into 500 mL LB and incubated overnight. Plasmid DNA was isolated using the Nucleobond Xtra Maxi Kit and resuspended in TE-buffer. DNA purity and concentration was determined photometrically (NanoDrop).

6.1.3 Glycerol stocks

Glycerol stocks were prepared by mixing 500 μ L bacteria suspension with 500 μ L 80% glycerol and stored at -80 °C.

6.1.4 Cloning

6.1.4.1 Polymerase chain reaction (PCR)

DNA fragments were amplified by PCR under the conditions mentioned below with specific primers. Annealing temperatures were adjusted to the primers' T_m and extension time according to fragment length.

PCR products were verified by agarose gel electrophoresis (1%) and excised for purification using the NucleoSpin Gel & PCR Clean-up Kit following manufacturer's instructions.

Table 31: PCR reaction mix

Component	Volume
5x Phusion HF buffer	10 µL
10 mM dNTPs	1 µL
Primer sense (10µM)	2.5 µL
Primer antisense (10 µM)	2.5 µL
Template	200 ng
Phusion DNA polymerase	0.5 µL
dH ₂ O	Ad 50 µL

Table 32: PCR conditions

Cycle step	Temperature	Time	Repeat
Initial Denaturation	98 °C	2 min	1x
Denaturation	98 °C	10 sec	30x
Annealing	46-65 °C	30 sec	
Extension	72 °C	30-90 sec	
Final Extension	72 °C	10 min	1x
hold	4 °C	∞	

6.1.4.2 Overlap extension PCR

The two PCR products were mixed for hybridization and amplification (overlap). Equimolar amounts of the PCR products were mixed and for amplification and purification of the overlap fragment, outer primers were used. PCR reaction mixture and condition are listed in tables 33 and 34.

Table 33: Overlap PCR reaction mix

Component	Volume
5x Phusion HF buffer	10 µL
10 mM dNTPs	1 µL
PCR Product I (850 ng)	x µL
PCR Product II (850 ng)	x µL
Phusion DNA polymerase	0.5 µL
dH ₂ O	Ad 45 µL

Table 34: Overlap PCR conditions

Cycle step	Temperature	Time	Repeats
Initial Denaturation	98 °C	2 min	1x
Denaturation	98 °C	10 sec	15x
Annealing	60 °C	30 sec	
Extension	72 °C	90-150 sec	

To the overlap PCR mix 2.5 µL of outer sense and antisense primers were added and a purification PCR was performed as described below (Table 35).

Table 35: Purification PCR conditions

Cycle step	Temperature	Time	Repeats
Initial Denaturation	98 °C	2 min	1x
Denaturation	98 °C	10 sec	20x
Annealing	61-70 °C	30 sec	
Extension	72 °C	90-150 sec	
Final Extension	72 °C	10 min	1x
hold	4 °C	∞	

6.1.4.3 Restriction endonuclease digestion

To insert an amplified PCR product into to the preferred vector backbone, restriction endonuclease digestion was performed. The standard conditions are listed in Table 36. To avoid re-ligation of the digested vector, it was dephosphorylated for 30 minutes at 37 °C by adding 1 µL CIP to the vector restriction digestion mixture. Successful digestion was validated by agarose gel electrophoresis (1%). Fragments were excised and purified using the NucleoSpin Gel & PCR Clean-up Kit following manufacturer's instructions.

Table 36: Restriction digest

Component	Insert	Vector
DNA	0.1-0.5 µg	3 µg
NEB buffer	2 µL	2 µL
Restriction enzyme I	0.5 µL	0.5 µL
Restriction enzyme II	0.5 µL	0.5 µL
dH ₂ O	Ad 20 µL	Ad 20 µL

6.1.4.4 Ligation

Ligation of inserts with vector DNA was performed as described below (Table 37). As a negative control a ligation mixture without insert was used. Ligation was performed by

incubating the mixture at 28 °C for 20 seconds followed by 20 seconds at 4 °C for 50 cycles. Alternatively, ligation mixture was incubated at 16 °C overnight.

Table 37: Standard ligation mixture

Component	Volume
Vector	10-50 ng
Insert	3:1 molar ratio over vector
10x T4 Ligase Buffer	1 µL
T4 Ligase	0.5 µL
dH ₂ O	Ad 10 µL

6.1.4.5 Ligation independent cloning

For ligation independent cloning (LIC), DNA fragments are inserted into plasmids with complementary overhangs. The digested vector (without de-phosphorylation (CIP) treatment) and the insert were digested using the T4 DNA polymerase as described below (Table 38). The reaction mixture was incubated for 30 minutes at 22 °C, followed by 20 minutes at 75 °C.

Table 38: LIC reaction mixture

Component	Volume (Vector or insert)
DNA	50 ng
10x NEB 2.1	2 µL
100 mM DTT	1 µL
T4 DNA polymerase (LIC-qualified)	0.4 µL
dH ₂ O	Ad 20 µL

Vector and insert were annealed by mixing 2 µL vector and 4 µL insert and incubation for 30 seconds at 70 °C followed by 5 minutes at room temperature. The DNA was transformed into chemical competent bacteria

6.1.4.6 Bacterial transformation

For transformation, 5 µL ligation mixture or 100 ng plasmid DNA were added to 50 µL competent *E. coli* DH5α and kept on ice for 30 minutes. A heatshock was performed for 30 seconds at 42 °C followed by 2 minutes incubation on ice. 250 µL antibiotic-free LB were added to the bacteria and plated on ampicillin-containing LB agar plates. Colonies were grown at 37 °C. Cloning was validated by culturing few clones in a small-scale culture followed by control restriction digestion of the purified plasmid DNA.

6.1.4.7 Cloning of BioID2 and APEX2 fusion constructs

For the generation of BioID2 and APEX2 expression plasmids, BioID2 and APEX2 plasmids were obtained from Addgene (HH344, 345 listed in Table 17). BioID2 or APEX2 were amplified by PCR as described in (Table 31 and 32) and ANXA3 was amplified by PCR using HH176 (listed in Table 17) as a template. PLIN2 was amplified by PCR using HH38 (Table 17) as a template. ANXA3 or PLIN2 PCR products were fused to BioID2 or APEX2 PCR products by overlap extension PCR as described in 6.1.4.2 (Tables 33–35) and ligated into the lentiviral backbone HH158 (linearized *via* NheI and EcoRI sites as described in Table 36) *via* ligation independent cloning (LIC) described in table 38. Used plasmids, primers and specific conditions are listed in table 39 and table 40 for overlap extension PCR.

Table 39: PCR conditions for BioID2 and APEX2 fusion proteins

PCR	Template	Primers (Table 19)	T _m [°C]	Extension time [sec]
ANXA3 (for BioID2)	HH176	#1 + #2	50	30
BioID2-HA (for ANXA3)	HH344	#3 + #4	46	30
PLIN2 (for BioID2)	HH38	#5 + #6	53	45
BioID2-HA (for PLIN2)	HH344	#7 + #4	46	30
ANXA3 (for APEX2)	HH176	#1 + #8	50	30
FLAG-APEX2 (for ANXA3)	HH345	#9 + #10	58	30
PLIN2 (for APEX2)	HH38	#5 + #11	53	45
FLAG-APEX2 (for PLIN2)	HH345	#12 + #10	57	30

Table 40: Overlap extension PCR conditions for BioID2 and APEX2 fusion proteins

Plasmid	PCR Product I (from Table 39)	PCR Product II (from Table 39)	Primers (Table 19)	T _m [°C]	Extension time [sec]
HH362	ANXA3 (for BioID2)	BioID2-HA (for ANXA3)	#1 + #4	70	150
HH363	PLIN2 (for BioID2)	BioID2-HA (for PLIN2)	#5 + #4	70	150
HH364	ANXA3 (for APEX2)	FLAG-APEX2 (for ANXA3)	#1 + #10	70	150
HH365	PLIN2 (for APEX2)	FLAG-APEX2 (for PLIN2)	#5 + #10	70	150

In order to add an mCherry reporter following a 2A-skipping site, fusion constructs were again amplified and overlapped with an 2A-mCherry PCR product as described before. PCR products were then ligated into the lentiviral backbone HH158 (listed in Table 17)

via the restriction sites NheI and EcoRI. Used plasmids, primers and specific conditions are listed in table 41 and table 42 for overlap extension PCR.

Table 41: PCR conditions for 2A-mCherry fusion to BioID2 and APEX2 fusion proteins

PCR	Template	Primers (Table 19)	Tm [°C]	Extension time [sec]
ANXA3-BioID2	HH362	#17 + #18	61	60
ANXA3-APEX2	HH364	#17 + #19	61	60
2A-mCherry	HH158	2A-mCherry sense + EcoRI mCherry as	61	60
PLIN2 (for PLIN2-BioID2-HA_2A-mCherry)	HH38	#22 + #23	61	60
BioID2 (for PLIN2-BioID2-HA_2A-mCherry)	HH344	#7 + #18	61	60
PLIN2-APEX2	HH365	#22 + #19	61	60
BioID2	HH344	#20 + #18	61	60
APEX2	HH345	#21 + #19	61	60

Table 42: Overlap extension PCR conditions for 2A-mCherry fusion to BioID2 and APEX2 fusion proteins

Plasmid	PCR Product I (from Table 41)	PCR Product II (from Table 41)	Primers (Table 19)	Tm [°C]	Extension time [sec]
HH379	ANXA3-BioID2	2A-mCherry	#17 + EcoRI mCherry as	61	90
HH380	ANXA3-APEX2	2A-mCherry	#17 + EcoRI mCherry as	61	90
PLIN2-BioID2-HA (intermediate plasmid)	PLIN2 (for PLIN2-BioID2-HA_2A-mCherry)	BioID2 (for PLIN2-BioID2-HA_2A-mCherry)	#22 + #18	61	90
HH381	PLIN2-BioID2	2A-mCherry	#22 + EcoRI mCherry as	61	90
HH382	PLIN2-APEX2	2A-mCherry	#22 + EcoRI mCherry as	61	90
HH383	BioID2	2A-mCherry	# 20 + EcoRI mCherry as	61	90
HH384	APEX2	2A-mCherry	# 21 + EcoRI mCherry as	61	90

6.1.4.8 Cloning of lentiviral expression plasmids for overexpression of identified hits

In order to generate pSicoR MCS-IRES-EGFP (HH478, listed in Table 17) as a backbone for the overexpression plasmids of the identified hits, the lentiviral vector pSicoR-MSΔU6 (HH158) was digested using the restriction endonucleases XbaI and NotI as described in table 36. The linearized vector was blunted by incubation with T4 DNA polymerase (3 U/μL) and dNTPs (100 μM) in 1x NEB 2.1 buffer for 15 minutes at 12 °C. EDTA was added to a final concentration of 10 mM and the reaction mixture was incubated at 75 °C for 20 minutes. For purification, the NucleoSpin PCR Clean-up kit was used according to manufacturer's instructions. The blunted vector was re-ligated as described in table 37 using 189 ng DNA.

The resulting vector was transformed into competent *E. coli* DH5α and DNA isolated as described in 6.1.4.6.

In order to insert a multiple cloning site (MCS) followed by an internal ribosome entry site (IRES) and enhanced green fluorescent protein (EGFP), PCR was performed as described in tables 31-32 using primers listed in table 21 (NheI-MCS-IRES fw, EcoRI-eGFP rev) and pMO160 (see Table 17) as a template (Tm: 68 °C, Extension time: 45 sec). The correct PCR product was inserted *via* NheI and EcoRI restriction sites resulting in the lentiviral expression vector HH478.

To clone vectors to overexpress identified proteins, PCR reactions were performed as described in tables 31–32 using primers in table 21 and template plasmids purchased from GenScript listed in table 17. Specific conditions are listed in table 43. PCR products were digested using the restriction endonucleases SpeI and XhoI, and ligated into the NheI and XhoI-digested vector (HH478) as described in table 36 and table 37.

Table 43: Annealing temperatures and extension times for lentiviral expression constructs for overexpression of hits

Protein	Template	Primers (Table 21)	Tm [°C]	Extension time [sec]
LARP1	HH465	SpeI-T7-LARP1 fw + LARP1-XhoI rev	65	90
FABP5	HH467	SpeI-T7-FABP5 fw + FABP5-XhoI rev	65	14
NOB1	HH468	SpeI-T7-NOB1 fw + NOB1-XhoI rev	57	45
ARL8B	HH469	SpeI-T7-ARL8B fw + ARL8B-XhoI rev	57	45
SART3	HH470	SpeI-T7-SART3 fw + SART3-XhoI rev	65	90

6.1.4.9 Phosphorylation and annealing of oligonucleotides

In order to generate shRNA-expressing vectors, specific primers (Table 20) were phosphorylated and annealed. The standard protocol for phosphorylation of primers is listed below (Table 44). The reaction was performed at 37 °C for 45 minutes, followed by 20 minutes at 65 °C to inactivate the kinase PNK.

Table 44: Phosphorylation of primers

Component	Volume
Primer (100 µM)	2 µL
T4 PNK	0.4 µL
T4 Ligation buffer	1 µL
dH ₂ O	6.6 µL

The phosphorylated primers were annealed as described in Table 45. After incubation at 95 °C for 5 minutes, the temperature dropped 1 °C by minute for 88 minutes.

Table 45: Annealing of primers

Component	Volume
Phosphorylated primer sense	5 µL
Phosphorylated primer antisense	5 µL
Annealing buffer	25 µL
dH ₂ O	15 µL

Ligation of annealed primers with vector DNA was performed as described below (Table 46). Ligation was performed by incubating the mixture at 28 °C for 20 seconds followed by 20 seconds at 4 °C for 50 cycles.

Table 46: Ligation mixture for annealed primers

Component	Volume
Vector	2 µL
Annealed primers	1 µL
10x T4 Ligase Buffer	1 µL
T4 Ligase	0.5 µL
dH ₂ O	5.5 µL

6.1.4.10 DNA Sequencing

In order to confirm successful cloning, plasmid DNA was sequenced. DNA was sequenced by GATC Biotech AG, Konstanz.

6.1.5 HCV RNA *in vitro* transcription

In order to generate HCV RNA, HCV plasmids were linearized and used as templates for *in vitro* transcription. 16 µg DNA were digested with MluI as described before (Table 36) for 1 hour or overnight. To remove single strand overhangs, Mung bean nuclease treatment was performed as described in Table 47 for 30 minutes at 30 °C.

Table 47: Mung bean nuclease treatment

Component	Volume
Linearized DNA	19 µL
10x Mung bean buffer	3 µL
Mung bean nuclease	1.3 µL
dH ₂ O	ad 30 µL

Linearization was verified by agarose gel electrophoresis. The linearized plasmid was purified by phenol-chloroform extraction as described below under RNase-free conditions. For *in vitro* transcription of HCV RNA the MEGAscript T7 transcription kit was used following the manufacturer's instructions. RNA integrity was validated by agarose gel electrophoresis. RNA concentration was determined photometrically (NanoDrop) and RNA was stored in 10 µg aliquots at -80 °C.

6.1.6 Phenol-chloroform extraction

For phenol-chloroform extraction, linearized plasmid samples were filled with nuclease-free water to a total volume of 100 µL and transferred into 5 Prime Phase Lock Gel Heavy tubes (2 mL). 100 µL phenol:chloroform:isoamylalcohol was added, inverted and centrifuged at 12000 x *g* at room temperature for 15 minutes. 100 µL chloroform was added and the sample was again mixed by inversion and centrifuged at 12000 x *g* at room temperature for 5 minutes. The aqueous phase was transferred into a RNase-free 1.5 mL tube and 10 µL 3M sodium acetate as well as 250 µL 99% ethanol were added. The DNA was precipitated by centrifugation at 12000 x *g* for 20 minutes, 4 °C. The pellet was washed with 500 µL 75% ethanol and centrifuged at 12000 x *g* for 15 minutes at 4 °C. The supernatant was removed, the pellet was dried for ~5 minutes at room temperature and resolved in 20 µL nuclease-free water.

6.2 Cell culture techniques

6.2.1 Cell culture

Cells were grown in high glucose DMEM supplemented with 10 % FBS and 1 % Glutamine and 1 % Penicillin/Streptomycin at 37 °C, 5% CO₂ and 95% relative humidity.

Cells were passaged every 3–4 days at 80–90% confluency. For splitting, the media was removed, cells washed with PBS and incubated with trypsin/EDTA at 37 °C until detachment. Cells were resuspended in fresh supplemented DMEM and partially transferred into a new cell culture flask. For seeding, cells were counted using a Neubauer counting chamber.

6.2.2 Thawing and freezing of eukaryotic cells

Frozen cells ($\sim 10^6$ cells) were thawed in a water bath at 37 °C and transferred into a T75 cell culture flask in 10 mL DMEM. To remove dead cells, media was changed the following day.

For freezing, $\sim 10^6$ cells were pelleted by centrifugation at 200 x *g* for 5 minutes at room temperature. Cells were then resuspended in freezing media. At a volume of ~ 1 mL cell suspensions were transferred into cryovials and cooled down in a cell freezing container for a stable freezing rate of -1 °C/minute at -80 °C. For long term storage cells were stored in a liquid nitrogen tank.

6.2.3 Electroporation of cells with HCV RNA

For HCV RNA transfection, *in vitro* transcribed RNA was electroporated into Huh7, Huh7.5 or Huh7.5.1 cells. For 10 µg RNA, 4×10^6 cells were transferred into a 50 mL tube, pelleted at 200 x *g* for 5 minutes at room temperature and washed with OptiMEM (200 x *g*, 5 minutes, room temperature). Cells were resuspended in 400 µL cytomix, supplemented with 8 µL 0.1 M ATP and 20 µL 0.1 M glutathione. The cell suspension was added to 10 µg RNA and transferred into a 4 mm cuvette. Electroporation was performed at 260 V and 950 µF in a GenePulser II electroporation device. Cells were directly transferred into 10 mL supplemented DMEM in a T75 cell culture flask. The media was changed after 2–4 hours and cells transfected with a full-length HCV construct were further cultured in a BSL3** or BSL3 laboratory.

6.2.4 Generation of HCV stocks

In order to generate HCV stocks, supernatant of HCV RNA electroporated cells (see 6.2.3) was harvested 3 and 5 days post electroporation (dpe). Naïve Huh7.5 or Huh7.5.1 cells were seeded in a T175 cell culture flask and subjected to the supernatant of electroporated cells. To enhance viral spread, cells were split at least once and cultured for up to 8 days. The supernatant was collected, pooled and centrifuged for 5 minutes at 200 x *g* at room temperature to remove cell debris. Supernatants were filtered through a 0.22 µm filter and 10% polyethylene glycol (PEG) was added (v/v; final concentration). After incubation at 4 °C overnight, virus was precipitated by centrifugation at 1200 x *g* for

1–3 hours at 4 °C. Pellets were resuspended in DMEM and aliquots of ~200–400 µL were stored at -80 °C.

6.2.5 Determination of viral titers (TCID₅₀)

Viral titers were determined with the tissue culture infectious dose TCID₅₀ using Huh 7.5 cells stably expressing the HCV reporter RFP-NLS-IPS (Jones *et al.*, 2010). Briefly, cells were seeded in 96 well plates at a density of 0.8–1x10⁴ per well and one day later infected with viral stocks in a serial dilution of 1:10¹–1:10⁷ or infectious supernatants in a serial dilution of 1:10⁰–1:10⁷. Per dilution 6 wells were infected. Three dpi, cells were fixed in 4% PFA for 1 hour at 4 °C. Positive wells were determined by identification of infected foci and the TCID₅₀ was calculated with the Reed and Muench calculator (Lindenbach, 2009; Rösch *et al.*, 2016).

For analysis of intracellular titers, HCV RNA-electroporated cells were trypsinized and 2x10⁵ cells were resuspended in 2 mL DMEM and lysed by multiple freeze/thaw cycles. Cell debris was removed by centrifugation for 5 min at 100 x g and TCID₅₀ was determined.

6.2.6 HCV infection and viral spreading

For HCV spreading experiments lentivirally transduced cells were infected with HCV reporter strains and analyzed using flow cytometry or *gaussia* luciferase assays at the indicated timepoints as described before (Hofmann *et al.*, 2018; Rösch *et al.*, 2016). For flow cytometry analysis, lentivirally transduced cells were seeded in 6 well plates at a density of 2x10⁵ per well and infected with Jc1^{NS5AB-EGFP} (MOI 0.002) one day post seeding. One day post infection cells were split and harvested at day 2, 4 and 6 dpi for flow cytometry analysis as described in 6.2.8.

6.2.7 Luciferase assays to analyze viral replication

6.2.7.1 HCV viral spreading and virion production

For spreading analysis by secreted *gaussia* luciferase, lentivirally transduced cells were seeded at a density of 5x10⁴ per well in 12 well plates and infected with Jc1^{p7-GLuc-2A-NS2} (MOI 0.5). Three hours post infection, the viral inoculum was removed and cells were supplemented with fresh DMEM. Supernatants were harvested 2, 4 and 6 dpi, centrifuged at 130 x g for 5 minutes at room temperature to remove cell debris. 40 µL of sample were transferred into a 96 well plate, mixed with 40 µL of 2% triton X-100 and inactivated for 1 hour at 4 °C.

To analyze virion production, collected supernatants were diluted 1:10 and 100 µL were transferred to naïve Huh7.5 cells seeded at a density of 1x10⁴ per well in a 96 well plate one day before. Supernatants were collected 2, 4 and 6 days later and lysed with triton

X-100 as described above. To determine *gaussia* luciferase activity, 10 μ L of lysed sample were transferred to a white 96 well plate and 50 μ L coelenterazine (10 μ M diluted in PBS) were injected per well. Luciferase activity was measured using a Centro LB 960 luminometer (Berthold Technologies). Samples were measured in duplicates.

6.2.7.2 HCV RNA replication

To measure HCV RNA replication, lentivirally transduced cells were electroporated with Jc1 Δ E1/E2^{NS5AB-FLuc} or JFH1^{FLuc-P2A-NS3-NS5B} RNA as described in 6.3.2 and Firefly luciferase activity in cell lysates was determined using the Luciferase Assay System (Promega).

For these experiments 2×10^6 Huh7.5 cells were electroporated with 5 μ g *in vitro* transcribed RNA. 2×10^5 electroporated cells per well were seeded in 12 well plates. Cells were harvested 4 hours, 1, 2 and 3 dpe. Briefly, cells were washed in PBS, 150 μ L 1x Passive Lysis Buffer (Promega) were added to each well and samples were stored at -20 °C until further analysis. After thawing, cells were lysed for 30 minutes on ice, equally resuspended and lysates were transferred into a 96 well plate with conical bottom. To remove cell debris, lysates were centrifuged for 5 min at 200 x *g* and transferred into a fresh 96 well plate. Firefly luciferase activity (relative light units, RLU) was measured with a Centro LB 960 luminometer using either the Dual-Luciferase reporter assay or Firefly-Luciferase reporter assay according to the manufacturer's instructions. Protein levels were determined by Coomassie Plus Assay (Thermo Scientific) following the manufacturer's instructions.

6.2.8 Flow cytometry

Cells were washed with PBS, trypsinized, resuspended in DMEM and pelleted by centrifugation at 200 x *g* for 3 minutes, room temperature. Cell pellets were fixed in 2% PFA for 1 h at 4 °C. Fluorescence was measured using a BD LSR Fortessa (BD Bioscience) and analyzed with Flowjo (Treestar).

6.2.9 MTT viability assay

Cell viability was determined by CellTiter96 Aqueous One Solution Reagent (Promega) according to the manufacturer's instructions.

6.2.10 Production of lentiviral pseudoparticles and lentiviral transduction

For the production of lentiviral pseudoparticles as described before (Naldini *et al.*, 1996), 5×10^6 HEK293T cells were seeded in 150 mm cell culture dishes and transfected by calcium phosphate precipitation the following day. Briefly, 20 μ g transfer plasmid, 15 μ g packaging plasmid and 6 μ g envelope plasmid were mixed with sterile water and 50 μ L

CaCl₂ (2.5M) to a final volume of 500 µL. The DNA/CaCl₂ mixture was slowly added to 500 µL 2xHBS under constant air bubbling and incubated for 10 minutes to generate DNA-phosphate complexes. The media of the HEK293T was changed to DMEM supplemented with 25 µM chloroquine. The transfection mix was added to the media dropwise and cells were incubated for 6 hours, before changing the media to fresh DMEM. Three days post transfection, the media containing lentiviral particles was collected, centrifuged at 500 x *g* for 5 minutes at room temperature and filtered through a 0.22 µm sterile filter. The virus was either directly aliquoted or concentrated by ultracentrifugation at 100000 x *g* for 2 hours at 4 °C. Concentrated particles were resuspended in ~1 mL DMEM, aliquoted and stored at -80 °C.

Lentiviral titration was performed Huh7.5 cells. 5x10⁴ cells per well were seeded in a 12 well plate and transduced with lentiviral stocks at different concentrations (2–100 µL or 50–750 µL). Three days post transduction, cells were fixed in PFA and transduction efficiency was determined by flow cytometry (see 6.2.8) or microscopy. Transduction was performed with cell culture media supplemented with 4 µg/mL polybrene.

6.2.11 Transfection of HEK293T cells using calcium phosphate precipitation

Transfection of HEK293T cells was performed by using the calcium phosphate precipitation method as described in 6.2.10. One–2x10⁶ cells were seeded on 100 mm cell culture dishes and transfected the following day. 10–15 µg total transfer plasmid DNA was mixed with 33 µL CaCl₂ (2.5 M) in 300 µL dH₂O and added to 330 µL 2x HBS under constant air bubbling as described in section. Media was changed to fresh DMEM after 5 hours or the following day, and cells were lysed 2–3 days post transfection.

6.2.12 Transfection of Huh7 cells using FuGENE

Huh7 cells were transfected with FuGene transfection reagent for immunofluorescence staining according to manufacturer's instructions using a FuGene:DNA ratio of 3 µL:1 µg. Media was changed to fresh DMEM one day post transfection.

6.2.13 Immunofluorescence and LD staining for confocal microscopy

Cells were grown on coverslips and fixed in 4 % PFA for 1 h, washed in PBS and permeabilized in 0.1 % Triton X-100 for 5 min. After blocking (5 % BSA, 1 % fish gelatin, 50 mM Tris in PBS) for 1 h, cells were incubated with primary antibodies diluted in blocking solution o/n at 4 °C. Cells were washed and incubated with secondary Alexa-Fluor fluorescence-coupled secondary antibodies (Life Technologies) diluted in blocking solution (1:1000-1:1500) for 1 h. LDs were stained with BODIPY 493/503 (1:750 in PBS, Life Technologies) or BODIPY 655/676 (1:20000 in PBS) for 30 min. Coverslips were

embedded in mowiol mounting media (Longin *et al.*, 1993). Confocal microscopy was performed on a Nikon C2+ or a Leica TCS SP5 II confocal laser scanning microscope. Further analysis was performed with Fiji (Schindelin *et al.*, 2012). For colocalization analysis the coloc2 function was used to calculate the Manders' colocalization coefficient and Pearson's correlation coefficient. dsRNA foci were analyzed using the Particle Analyzer function.

6.2.14 LD isolation

Lipid droplet isolations were performed as described before (Miyanari *et al.*, 2007; Röscher *et al.*, 2016). Briefly, cells were scraped in cold PBS, and lysed in hypotonic buffer (50 mM HEPES, 1 mM EDTA, 2 mM MgCl₂, pH 7.4, supplemented with 1x protease inhibitor cocktail (Sigma)) using a Dounce homogenizer for 5 min. Nuclear fractions were removed by centrifugation for 5 min at 500 x g. Post-nuclear fractions were mixed to an equal volume with 1.05 M sucrose in isotonic buffer (50 mM HEPES, 100 mM KCl, 2 mM MgCl₂, supplemented with 1 mM PMSF) in SW60 Ti or SW41 (Beckman) rotor tubes and centrifuged for 2 hours at 100000 x g, 4 °C. The floating fractions were harvested using a bent cannula and centrifuged for 20 min at 20000 x g, 4 °C. Underlying buffer was removed and for infectious LD fractions, Triton X-100 was added to a final concentration of 1%. Protein levels were determined using the DC Protein Assay (Biorad).

6.2.15 Determination of infected foci for cell-to-cell transmission analysis

To determine foci size, Huh7.5 cells were transduced with lentivirus carrying shLARP1 (HH449) or shNT (HH230). Cells were seeded on coverslips at a density of 4–5x10⁴ cells per well in 24 well plates and infected with Jc1^{p7-GLuc-2A-NS2} or Jc1^{NS5AB-EGFP} (MOI 0.1–0.15). Three dpi, cells were fixed in 4% PFA for 1 hour at 4 °C and stained for immunofluorescence using a core-specific antibody as described in 6.2.13.

6.2.16 Co-culturing for cell-to-cell transmission analysis

For cell-to-cell transmission assays, infected and uninfected cells were co-cultured. First, Huh7.5 cells were transduced with lentivirus carrying shLARP1 (HH449) or shNT (HH230). One part of transduced cells was additionally transduced with a lentivirus for EGFP expression (HH436), the other part was infected with Jc1^{p7-GLuc-2A-NS2} (MOI 0.25). Cells were kept in culture and split at least once to enhance viral spreading. Seven dpi, cells were fixed on coverslips with 4% PFA and stained for immunofluorescence using a core-specific antibody to assure at least 90% infection rate. Infected cells were then mixed with uninfected cells in a 1:10 ratio and seeded on coverslips in 24 well plates at a total count of 0.65–1x10⁵ cells/well in 0.5 mL. Three days later, cells were fixed in 4%

PFA for 1 hour at 4 °C and stained for immunofluorescence using a core-specific antibody and Hoechst as described before (see 6.2.13).

6.2.17 SILAC and proximity labeling

For isotope metabolic protein labeling cells were cultured in Dundee Cell Products DMEM media (“light”, R0K0; “heavy”, R10K8), supplemented with 10 % FBS and 1 % Penicillin/Streptomycin. Incorporation efficiency after 8 passages was determined by MS using cell lysates separated by SDS-PAGE. Gels were stained with Roti-Blue dye (Carl Roth) following the manufacturer’s instructions and analyzed by MS.

For proximity labeling analyses, Huh7.5 cells were cultivated in light or heavy media for 4 passages prior to lentiviral transduction with BioID2 or APEX2 fusion constructs. One week after transduction cells were infected with a Jc1^{NS5AB-EGFP} reporter strain (MOI 0.01) and cultured for two more weeks. One day prior to lysis, 3.3 mg/mL oleic acid were added to the media.

For BioID2 labeling, the media was also supplemented with 10 µM Biotin. After 20 hours of incubation cells were washed 5x in PBS and lysed in RIPA buffer. For APEX2 labeling, the cells were treated with media containing 500 µM Biotin-Phenol for 30 min at 37 °C and 1 mM H₂O₂ for 1 min at room temperature. Cells were washed 5x with a quencher solution and lysed in RIPA buffer (supplemented with 10 mM sodium ascorbate, 5 mM trolox, 10 mM sodium azide).

Protein levels were determined with the Pierce 660 nm Protein Assay following manufacturer’s instruction. Prior to pull down, 35 µL streptavidin agarose resin (Thermo Fisher) were washed 3x in RIPA buffer at 425 x g for 2 min, 4 °C for equilibration. Resins were incubated with a total protein amount of 2 mg (1 mg “light” and 1 mg “heavy” labelled sample) for 1.5–2 hours at 4 °C, rotating. Beads were eluted in 3x Laemmli, supplemented with 2 mM Biotin and 20 mM dithiodreithol (DTT) and boiled at 95 °C for 10 min. Samples were separated by SDS-PAGE as mentioned above and analyzed by MS.

6.3 Biochemical methods

6.3.1 Cell lysates

Cell lysates for protein analysis were prepared in RIPA lysis buffer or NP40 lysis buffer if used for co-immunoprecipitation experiments. Lysis buffers were supplemented with protease inhibitors immediately before usage. Cells were washed with PBS and resuspended in lysis buffer by pipetting up and down. For pull down experiments, cells were removed from culture plates using a cell scraper. After incubation on ice for ~10 minutes or 1 hour for infectious samples, lysates were centrifugated for 10 minutes at

12000 x *g*, 4 °C and transferred to a new 1.5 mL tube. Protein concentrations were determined using the DC protein assay or the Pierce 660 nm protein assay for proximity labeling samples. Protein assays were performed as suggested by the manufacturer and samples were stored at -20 °C or -80 °C until further analysis.

6.3.2 SDS-PAGE and western blotting

Protein separation from cell lysates or LD fractions was performed by discontinuous SDS-polyacrylamide electrophoresis (SDS-PAGE). Samples were mixed with 6x Laemmli buffer (Laemmli, 1970), boiled at 95 °C for 5-10 minutes for denaturation and loaded onto a 12% or 6–20% gradient SDS-polyacrylamide gel. A prestained protein ladder was used as molecular marker. Separation was performed at 220 V until the dye front reached the bottom of the gel. Proteins were transferred to a nitrocellulose membrane by tank blotting at 100 V for 1 hour. Membranes were blocked in blocking solution for 30 minutes to 1 hour. In case of biotin detection using streptavidin-HRP, membranes were blocked in 5% bovine serum albumin (BSA) in 1x TBS-T. Otherwise, blocking was performed in 5% skim milk in 1x TBS-T. Incubation with primary antibodies was performed over night at 4 °C or for 1 hour at room temperature on a rotation device. After 3x washing in 1x TBS-T for 10 minutes, membranes were incubated with secondary HRP-coupled antibodies for 1 hour at room temperature and washed as described before. For chemiluminescent detection of protein bands membranes were incubated with ECL Lumi-Light Western Blotting Substrate or SuperSignal West Femto and visualized either by ECL Hyperfilm or Image Lab. Signal intensities were quantified using the quantification function of Image Lab.

6.3.3 Co-immunoprecipitation

For immunoprecipitation (IP), 1–2x10⁶ cells were lysed in NP40 lysis buffer as described in 6.3.1. For IP experiments either transfected HEK293T (see 6.2.11) cells or lentivirally transduced Huh7.5 cells were used. For specific immunoprecipitation, 30 µL antibody-coupled agarose beads were prepared by washing 3 x in NP40 lysis buffer for 2 minutes at 430 x *g*, 4 °C. 0.5–1 mg protein were added to the equilibrated beads and filled to a total volume of 1–1.2 mL with NP40 lysis buffer. Incubation was performed at 4 °C in an overhead rotation device for 2–20 hours. Beads were washed 4x as described before and resuspended in 30 µL 3x Laemmli for western blot analysis as described in 6.3.2. For endogenous IPs, 0.7–1 µg target-specific antibody was mixed with 0.7–1 mg total protein overnight and then subjected to 30 µL prepared protein G agarose beads for 2 hours. Incubation and washing were performed as described above.

For capturing of biotinylated proteins streptavidin-coupled beads were used as described before.

Final washes for co-IPs of LARP1-core (Figure 40), LARP1-core-ANXA3 (Figure S 5) and NOB1-core-PLIN2 (Figure S 6) from HEK293T cell lysates were performed in high salt NP40 lysis buffer (50 mM Tris, pH 7.4, 500 mM NaCl, 1% Nonidet-P40, supplemented with 1 mM PMSF and 1x protease inhibitor cocktail).

For analysis of RNA-dependent interactions, 700 µg protein lysates were pre-cleared with protein G agarose beads in a total volume of 1.2 mL for 30–60 min at 4 °C, rotating. Lysates were incubated with 100 µg/mL RNase A or 100 U/mL RNaseOUT for 45-60 min at 4 °C, rotating. To validate successful RNase A treatment, 75 µL of each sample were transferred into a 1.5 mL tube and resuspended in 250 µL Tri Reagent for RNA isolation as described in 6.3.4. RNA integrity and successful RNase digest were confirmed by agarose gel electrophoresis. Immunoprecipitation of pre-cleared samples was performed as described above.

6.3.4 RNA isolation

Total cellular RNA was isolated from cells or IP samples using 250 µL for IP samples and 1 mL Tri Reagent directly on cells. Per mL Tri Reagent, 200 µL chloroform were added and samples were mixed by inversion for 15 seconds followed by incubation at room temperature for 3 minutes. Samples were centrifuged at 12000 x *g* for 15 minutes at 4 °C and the upper aqueous phase was transferred into a 1.5 mL tube. 500 µL isopropanol were added and samples were incubated for 10 minutes at room temperature followed by centrifugation at 12000 x *g* for 10 minutes at 4 °C. The precipitated RNA was washed with 1 mL 75% ethanol at 7500 x *g* for 5 minutes at 4 °C. The pellet was air-dried for ~5 minutes and resuspended in 10 µL nuclease-free water. RNA was treated with rDNaseI for 30 minutes at 30 °C. Samples were centrifuged for 1 minute at 15000 x *g* at room temperature and transferred into a fresh 1.5 mL tube. RNA concentration was determined photometrically (NanoDrop) and stored at -80 °C.

Viral RNA from supernatants was isolated using the NucleoSpin RNA Virus Kit (Machery Nagel) following the manufacturer's instructions. RNA levels were adjusted to carrier RNA.

6.3.5 cDNA synthesis

Isolated RNA was reversely transcribed into cDNA using Superscript III reverse transcriptase. The reaction mixture is listed in Table 48. RNA, dNTPs random hexamer primers were incubated at 5 °C for 5 minutes. Then, 5x first strand buffer, DTT, RNaseOUT and SuperScript III were added and the reaction mixture was incubated at 25 °C for 5 minutes, 50 °C for 60 minutes and 70 °C for 15 minutes. cDNA was stored at -80 °C.

Table 48: cDNA synthesis

Components	Quantity	Time and temperature
RNA	1 µg	5 min, 65 °C
10 mM dNTPs	1 µL	
Random hexamer primers (0.04 µg/µL)	1 µL	
Nuclease-free H ₂ O	ad 14 µL	
5x first strand buffer	4 µL	5 min, 25 °C
100 mM DTT	1 µL	60 min, 50 °C
RNAseOUT	0.5 µL	15 min, 70 °C
Superscript III	0.5 µL	

6.3.6 Quantitative reverse transcriptase PCR (qRT-PCR)

For qRT-PCR the Maxima SYBR green master mix was used in a 7500 HTFast Real-time PCR cycler or the Luna Universal qPCR Mastermix in a StepOne Plus Real Time qPCR System. The PCR mixtures are listed in tables 49 and 50. A master mix was prepared and mixed with cDNA in 96 well plates. All samples were measured in triplicates. Cyclor conditions are listed in table 51.

Table 49: qRT-PCR mix using SYBR green master mix

Components	Volume
cDNA	1 µL
2x Maxima SYBR green	10 µL
ROX (5 µM)	0.04 µL
qPCR primer mix (10 mM)	0.6 µL
Nuclease-free H ₂ O	ad 20 µL

Table 50: qRT-PCR mix using Luna universal qPCR Mastermix

Components	Volume
cDNA	1 µL
Luna Universal qPCR Mastermix	5 µL
qPCR primer mix (10mM)	0.5 µL
Nuclease-free H ₂ O	ad 10 µL

Table 51: qRT-PCR conditions

Temperature	Time	Repeats
95 °C	10 min	1x
95 °C	15 s	40x
60 °C	1 min	
95 °C	15 s	1x
60 °C	1 min	1x

6.3.6.1 HCV standards for qRT-PCR

To prepare HCV standards, 1 µg *in vitro* transcribed HCV RNA was reversely transcribed to cDNA as described before in 6.3.5 and prepared in a serial dilution of 1:10²-1:10⁸. One µL of each dilution was used for qRT-PCR as described in 6.3.6, correlating to 10000-0.01 pg HCV RNA per reaction.

6.3.7 Mass spectrometry (MS)

MS as described in 6.3.7.1 – 6.3.7.3 was performed by C. Krisp and H. Schlüter at the Core Facility Mass Spectrometric Proteomics of the University Medical Center Hamburg-Eppendorf.

6.3.7.1 Protein digestion in the SDS-PAGE matrix

In-gel digestion was performed following the protocol by Shevchenko *et al.* (Shevchenko *et al.*, 2006). Shrinking and swelling was performed with 100% acetonitrile (ACN) and 100 mM ammonium hydrogen carbonate (NH₄HCO₃). In-gel reduction was achieved with 10 mM dithiothreitol (dissolved in 100 mM NH₄HCO₃). Alkylation was performed with 55 mM iodoacetamide (dissolved in 100 mM NH₄HCO₃). Proteins in the gel pieces were digested by covering them with a trypsin solution (8 ng/µL sequencing-grade trypsin, dissolved in 50 mM NH₄HCO₃) and incubating the mixture at 37 °C overnight. Tryptic peptides were yielded by extraction with 0.1 % formic acid (FA) in 80 % ACN. Samples were lyophilized using a vacuum centrifuge.

6.3.7.2 LC-MS/MS in Data Dependent and Data Independent mode

Samples were resuspended in 0.1% FA and transferred into a full recovery autosampler vial (Waters). Chromatographic separation was achieved on a UPLC system (nanoAcquity, Waters) with a two buffer system (buffer A: 0.1% FA in water, buffer B: 0.1% FA in ACN). Attached to the UPLC was a C18 trap column (Symmetry C18 Trap Column, 100Å, 5 µm, 180 µm x 20 mm, Waters) for online desalting and sample purification followed by an C18 separation column (BEH130 C18 column, 75 µm x 25 cm, 130 Å pore size, 1.7 µm particle size, Waters). Peptides were separated using a 60

min gradient with increasing ACN concentration from 2%–30% ACN. The eluting peptides were analyzed on a quadrupole orbitrap mass spectrometer (QExactive, Thermo Fisher Scientific) in data dependent acquisition (DDA).

For LC-MS/MS analysis on the QExactive, the 15 most intense ions per precursor scan (1×10^6 ions, 70,000 Resolution, 100 ms fill time) were analyzed by MS/MS (HCD at 25 normalized collision energy, 2×10^5 ions, 17,500 Resolution, 50 ms fill time) in a range of 400–1200 m/z. A dynamic precursor exclusion of 20 s was used.

6.3.7.3 Data analysis and processing

Acquired DDA LC-MS/MS data to generate a reference peptide spectra library for SILAC based MS1 area data extraction were searched against the reviewed human protein data base downloaded from Uniprot (November 2017, as well as protein sequences of proteins introduced by transfection) using the Sequest algorithm integrated in the Proteome Discoverer software version 2.0. Mass tolerances for precursors were set to 10 ppm and 0.02 Da for fragments. Carbamidomethylation was set as a fixed modification for cysteine residues and $^{13}\text{C}_6$, $^{15}\text{N}_2$ labeled lysine, $^{13}\text{C}_6$, $^{15}\text{N}_4$ labeled arginine, the oxidation of methionine, pyro-glutamate formation at glutamine residues at the peptide N-terminus as well as acetylation of the protein N-terminus, methionine loss at the protein N-terminus and the Acetylation after methionine loss at the protein N-terminus were allowed as variable modifications. Only peptide with a high confidence (false discovery rate < 1% using a decoy data base approach) were accepted as identified.

Proteome Discoverer search results were imported into Skyline software (MacCoss Lab, University of Washington, Seattle, USA) allowing only high confidence peptides to be imported. Peptide areas for the light and heavy variant of each peptide were extracted and filtered for each sample condition for peptides with an isotope dot product of > 0.85 in either light or heavy or in both variants of a given peptide. Peptide peak areas ratios for light over heavy were calculated and a median ratio per protein was calculated which were then used for relative abundance comparison.

6.3.8 Data analysis and statistical analysis

The detection ratios of light over heavy (L/H) or heavy over light (H/L) were centered by dividing through the median. Analysis was performed using RStudio (RStudio, 2020). For plotting, gdata (Warnes, 2017), lattice (Sarkar, 2020), gplots (Warnes, 2020), ggplots2 (Wickham, 2020) and pheatmap (Kolde, 2019) packages were used. Gene ontology annotation was generated using the online tool MetaScape (Zhou *et al.*, 2019) using the sources: KEGG pathway, GO Biological Processes, GO Molecular Function,

Reactome Gene Set, Canonical Pathways and CORUM with a p-value < 0.01, minimum count 3 and enrichment factor > 1.5.

For statistical analysis R and RStudio was used (RStudio, 2020). Analysis was performed using an unpaired two tailed t-test with unequal variance (Welch t-test). Indicated sample sizes (n) represent independent experiments, if not stated otherwise.

7 References

- Agnello, V., Abel, G., Elfahal, M., Knight, G. B., & Zhang, Q. X. (1999). Hepatitis C virus and other flaviviridae viruses enter cells via low density lipoprotein receptor. *Proc Natl Acad Sci U S A*, 96(22), 12766-12771.
- Ahn, J., Chung, K. S., Kim, D. U., Won, M., Kim, L., Kim, K. S., Nam, M., Choi, S. J., Kim, H. C., Yoon, M., Chae, S. K., & Hoe, K. L. (2004). Systematic identification of hepatocellular proteins interacting with NS5A of the hepatitis C virus. *J Biochem Mol Biol*, 37(6), 741-748.
- Aizaki, H., Morikawa, K., Fukasawa, M., Hara, H., Inoue, Y., Tani, H., Saito, K., Nishijima, M., Hanada, K., Matsuura, Y., Lai, M. M., Miyamura, T., Wakita, T., & Suzuki, T. (2008). Critical role of virion-associated cholesterol and sphingolipid in hepatitis C virus infection. *J Virol*, 82(12), 5715-5724.
- Akil, A., Peng, J., Omrane, M., Gondeau, C., Desterke, C., Marin, M., Tronchere, H., Taveneau, C., Sar, S., Briolotti, P., Benjelloun, S., Benjouad, A., Maurel, P., Thiers, V., Bressanelli, S., Samuel, D., Brechot, C., & Gassama-Diagne, A. (2016). Septin 9 induces lipid droplets growth by a phosphatidylinositol-5-phosphate and microtubule-dependent mechanism hijacked by HCV. *Nat Commun*, 7, 12203.
- Andre, P., Komurian-Pradel, F., Deforges, S., Perret, M., Berland, J. L., Sodoyer, M., Pol, S., Brechot, C., Paranhos-Baccala, G., & Lotteau, V. (2002). Characterization of low- and very-low-density hepatitis C virus RNA-containing particles. *J Virol*, 76(14), 6919-6928.
- Angus, A. G., Dalrymple, D., Boulant, S., McGivern, D. R., Clayton, R. F., Scott, M. J., Adair, R., Graham, S., Owsianka, A. M., Targett-Adams, P., Li, K., Wakita, T., McLauchlan, J., Lemon, S. M., & Patel, A. H. (2010). Requirement of cellular DDX3 for hepatitis C virus replication is unrelated to its interaction with the viral core protein. *J Gen Virol*, 91(Pt 1), 122-132.
- Aoki, K., Adachi, S., Homoto, M., Kusano, H., Koike, K., & Natsume, T. (2013). LARP1 specifically recognizes the 3' terminus of poly(A) mRNA. *FEBS Lett*, 587(14), 2173-2178.
- Appel, N., Pietschmann, T., & Bartenschlager, R. (2005). Mutational analysis of hepatitis C virus nonstructural protein 5A: potential role of differential phosphorylation in RNA replication and identification of a genetically flexible domain. *J Virol*, 79(5), 3187-3194.
- Appel, N., Zayas, M., Miller, S., Krijnse-Locker, J., Schaller, T., Friebe, P., Kallis, S., Engel, U., & Bartenschlager, R. (2008). Essential role of domain III of nonstructural protein 5A for hepatitis C virus infectious particle assembly. *PLoS Pathog*, 4(3), e1000035.
- Ariumi, Y., Kuroki, M., Abe, K., Dansako, H., Ikeda, M., Wakita, T., & Kato, N. (2007). DDX3 DEAD-box RNA helicase is required for hepatitis C virus RNA replication. *J Virol*, 81(24), 13922-13926.
- Ariumi, Y., Kuroki, M., Kushima, Y., Osugi, K., Hijikata, M., Maki, M., Ikeda, M., & Kato, N. (2011a). Hepatitis C virus hijacks P-body and stress granule components around lipid droplets. *J Virol*, 85(14), 6882-6892.
- Ariumi, Y., Kuroki, M., Maki, M., Ikeda, M., Dansako, H., Wakita, T., & Kato, N. (2011b). The ESCRT system is required for hepatitis C virus production. *PLoS One*, 6(1), e14517.
- Arora, S., Lim, W., Bist, P., Perumalsamy, R., Lukman, H. M., Li, F., Welker, L. B., Yan, B., Sethi, G., Tambyah, P. A., Fairhurst, A. M., Alonso, S., & Lim, L. H. (2016). Influenza A virus enhances its propagation through the modulation of Annexin-A1 dependent endosomal trafficking and apoptosis. *Cell Death Differ*, 23(7), 1243-1256.

- Backes, P., Quinkert, D., Reiss, S., Binder, M., Zayas, M., Rescher, U., Gerke, V., Bartenschlager, R., & Lohmann, V. (2010). Role of annexin A2 in the production of infectious hepatitis C virus particles. *J Virol*, 84(11), 5775-5789.
- Bagshaw, R. D., Callahan, J. W., & Mahuran, D. J. (2006). The Arf-family protein, Arl8b, is involved in the spatial distribution of lysosomes. *Biochem Biophys Res Commun*, 344(4), 1186-1191.
- Baktash, Y., Madhav, A., Collier, K. E., & Randall, G. (2018). Single Particle Imaging of Polarized Hepatoma Organoids upon Hepatitis C Virus Infection Reveals an Ordered and Sequential Entry Process. *Cell Host Microbe*, 23(3), 382-394 e385.
- Barretto, N., Sainz, B., Jr., Hussain, S., & Uprichard, S. L. (2014). Determining the involvement and therapeutic implications of host cellular factors in hepatitis C virus cell-to-cell spread. *J Virol*, 88(9), 5050-5061.
- Bartenschlager, R., Penin, F., Lohmann, V., & Andre, P. (2011). Assembly of infectious hepatitis C virus particles. *Trends Microbiol*, 19(2), 95-103.
- Barth, H., Cerino, R., Arcuri, M., Hoffmann, M., Schurmann, P., Adah, M. I., Gissler, B., Zhao, X., Ghisetti, V., Lavezzo, B., Blum, H. E., von Weizsacker, F., Vitelli, A., Scarselli, E., & Baumert, T. F. (2005). Scavenger receptor class B type I and hepatitis C virus infection of primary tupaia hepatocytes. *J Virol*, 79(9), 5774-5785.
- Barth, H., Liang, T. J., & Baumert, T. F. (2006a). Hepatitis C virus entry: molecular biology and clinical implications. *Hepatology*, 44(3), 527-535.
- Barth, H., Schnober, E. K., Zhang, F., Linhardt, R. J., Depla, E., Boson, B., Cosset, F. L., Patel, A. H., Blum, H. E., & Baumert, T. F. (2006b). Viral and cellular determinants of the hepatitis C virus envelope-heparan sulfate interaction. *J Virol*, 80(21), 10579-10590.
- Bartosch, B., Vitelli, A., Granier, C., Goujon, C., Dubuisson, J., Pascale, S., Scarselli, E., Cortese, R., Nicosia, A., & Cosset, F. L. (2003). Cell entry of hepatitis C virus requires a set of co-receptors that include the CD81 tetraspanin and the SR-B1 scavenger receptor. *J Biol Chem*, 278(43), 41624-41630.
- Bayer, K., Banning, C., Bruss, V., Wiltzer-Bach, L., & Schindler, M. (2016). Hepatitis C Virus Is Released via a Noncanonical Secretory Route. *J Virol*, 90(23), 10558-10573.
- Bayfield, M. A., Yang, R., & Maraia, R. J. (2010). Conserved and divergent features of the structure and function of La and La-related proteins (LARPs). *Biochim Biophys Acta*, 1799(5-6), 365-378.
- Bell, M., Schreiner, S., Damianov, A., Reddy, R., & Bindereif, A. (2002). p110, a novel human U6 snRNP protein and U4/U6 snRNP recycling factor. *EMBO J*, 21(11), 2724-2735.
- Bell, M., Wang, H., Chen, H., McLenithan, J. C., Gong, D. W., Yang, R. Z., Yu, D., Fried, S. K., Quon, M. J., Londos, C., & Sztalryd, C. (2008). Consequences of lipid droplet coat protein downregulation in liver cells: abnormal lipid droplet metabolism and induction of insulin resistance. *Diabetes*, 57(8), 2037-2045.
- Benedicto, I., Molina-Jimenez, F., Bartosch, B., Cosset, F. L., Lavillette, D., Prieto, J., Moreno-Otero, R., Valenzuela-Fernandez, A., Aldabe, R., Lopez-Cabrera, M., & Majano, P. L. (2009). The tight junction-associated protein occludin is required for a postbinding step in hepatitis C virus entry and infection. *J Virol*, 83(16), 8012-8020.
- Benga, W. J., Krieger, S. E., Dimitrova, M., Zeisel, M. B., Parnot, M., Lupberger, J., Hildt, E., Luo, G., McLauchlan, J., Baumert, T. F., & Schuster, C. (2010). Apolipoprotein E interacts with hepatitis C virus nonstructural protein 5A and determines assembly of infectious particles. *Hepatology*, 51(1), 43-53.
- Berger, K. L., Kelly, S. M., Jordan, T. X., Tartell, M. A., & Randall, G. (2011). Hepatitis C virus stimulates the phosphatidylinositol 4-kinase III alpha-dependent phosphatidylinositol 4-phosphate production that is essential for its replication. *J Virol*, 85(17), 8870-8883.

- Berri, F., Haffar, G., Le, V. B., Sadewasser, A., Paki, K., Lina, B., Wolff, T., & Riteau, B. (2014). Annexin V incorporated into influenza virus particles inhibits gamma interferon signaling and promotes viral replication. *J Virol*, 88(19), 11215-11228.
- Bersuker, K., Peterson, C. W. H., To, M., Sahl, S. J., Savikhin, V., Grossman, E. A., Nomura, D. K., & Olzmann, J. A. (2018). A Proximity Labeling Strategy Provides Insights into the Composition and Dynamics of Lipid Droplet Proteomes. *Dev Cell*, 44(1), 97-112 e117.
- Bicho, C. C., de Lima Alves, F., Chen, Z. A., Rappsilber, J., & Sawin, K. E. (2010). A genetic engineering solution to the "arginine conversion problem" in stable isotope labeling by amino acids in cell culture (SILAC). *Mol Cell Proteomics*, 9(7), 1567-1577.
- Bidell, M. R., McLaughlin, M., Faragon, J., Morse, C., & Patel, N. (2016). Desirable Characteristics of Hepatitis C Treatment Regimens: A Review of What We Have and What We Need. *Infect Dis Ther*, 5(3), 299-312.
- Blanchard, E., Belouzard, S., Goueslain, L., Wakita, T., Dubuisson, J., Wychowski, C., & Rouille, Y. (2006). Hepatitis C virus entry depends on clathrin-mediated endocytosis. *J Virol*, 80(14), 6964-6972.
- Bley, H., Schobel, A., & Herker, E. (2020). Whole Lotta Lipids-from HCV RNA Replication to the Mature Viral Particle. *Int J Mol Sci*, 21(8).
- Blight, K. J., Kolykhalov, A. A., & Rice, C. M. (2000). Efficient initiation of HCV RNA replication in cell culture. *Science*, 290(5498), 1972-1974.
- Blight, K. J., McKeating, J. A., & Rice, C. M. (2002). Highly permissive cell lines for subgenomic and genomic hepatitis C virus RNA replication. *J Virol*, 76(24), 13001-13014.
- Bosch, M., Sweet, M. J., Parton, R. G., & Pol, A. (2021). Lipid droplets and the host-pathogen dynamic: FATal attraction? *J Cell Biol*, 220(8).
- Boulant, S., Douglas, M. W., Moody, L., Budkowska, A., Targett-Adams, P., & McLauchlan, J. (2008). Hepatitis C virus core protein induces lipid droplet redistribution in a microtubule- and dynein-dependent manner. *Traffic*, 9(8), 1268-1282.
- Boulant, S., Montserret, R., Hope, R. G., Ratnier, M., Targett-Adams, P., Laverne, J. P., Penin, F., & McLauchlan, J. (2006). Structural determinants that target the hepatitis C virus core protein to lipid droplets. *J Biol Chem*, 281(31), 22236-22247.
- Boulant, S., Targett-Adams, P., & McLauchlan, J. (2007). Disrupting the association of hepatitis C virus core protein with lipid droplets correlates with a loss in production of infectious virus. *J Gen Virol*, 88(Pt 8), 2204-2213.
- Boulant, S., Vanbelle, C., Ebel, C., Penin, F., & Laverne, J. P. (2005). Hepatitis C virus core protein is a dimeric alpha-helical protein exhibiting membrane protein features. *J Virol*, 79(17), 11353-11365.
- Bousquet-Antonelli, C., & Deragon, J. M. (2009). A comprehensive analysis of the La-motif protein superfamily. *RNA*, 15(5), 750-764.
- Bradley, D., McCaustland, K., Krawczynski, K., Spelbring, J., Humphrey, C., & Cook, E. H. (1991). Hepatitis C virus: buoyant density of the factor VIII-derived isolate in sucrose. *J Med Virol*, 34(3), 206-208.
- Branon, T. C., Bosch, J. A., Sanchez, A. D., Udeshi, N. D., Svinkina, T., Carr, S. A., Feldman, J. L., Perrimon, N., & Ting, A. Y. (2018). Efficient proximity labeling in living cells and organisms with TurboID. *Nat Biotechnol*, 36(9), 880-887.
- Brasaemle, D. L., Barber, T., Wolins, N. E., Serrero, G., Blanchette-Mackie, E. J., & Londos, C. (1997). Adipose differentiation-related protein is an ubiquitously expressed lipid storage droplet-associated protein. *J Lipid Res*, 38(11), 2249-2263.
- Brasaemle, D. L., Dolios, G., Shapiro, L., & Wang, R. (2004). Proteomic analysis of proteins associated with lipid droplets of basal and lipolytically stimulated 3T3-L1 adipocytes. *J Biol Chem*, 279(45), 46835-46842.

- Brass, V., Berke, J. M., Montserret, R., Blum, H. E., Penin, F., & Moradpour, D. (2008). Structural determinants for membrane association and dynamic organization of the hepatitis C virus NS3-4A complex. *Proc Natl Acad Sci U S A*, 105(38), 14545-14550.
- Brass, V., Bieck, E., Montserret, R., Wolk, B., Hellings, J. A., Blum, H. E., Penin, F., & Moradpour, D. (2002). An amino-terminal amphipathic alpha-helix mediates membrane association of the hepatitis C virus nonstructural protein 5A. *J Biol Chem*, 277(10), 8130-8139.
- Brazzoli, M., Bianchi, A., Filippini, S., Weiner, A., Zhu, Q., Pizza, M., & Crotta, S. (2008). CD81 is a central regulator of cellular events required for hepatitis C virus infection of human hepatocytes. *J Virol*, 82(17), 8316-8329.
- Bressanelli, S., Tomei, L., Roussel, A., Incitti, I., Vitale, R. L., Mathieu, M., De Francesco, R., & Rey, F. A. (1999). Crystal structure of the RNA-dependent RNA polymerase of hepatitis C virus. *Proc Natl Acad Sci U S A*, 96(23), 13034-13039.
- Brimacombe, C. L., Grove, J., Meredith, L. W., Hu, K., Syder, A. J., Flores, M. V., Timpe, J. M., Krieger, S. E., Baumert, T. F., Tellinghuisen, T. L., Wong-Staal, F., Balfe, P., & McKeating, J. A. (2011). Neutralizing antibody-resistant hepatitis C virus cell-to-cell transmission. *J Virol*, 85(1), 596-605.
- Burrows, C., Abd Latip, N., Lam, S. J., Carpenter, L., Sawicka, K., Tzolovsky, G., Gabra, H., Bushell, M., Glover, D. M., Willis, A. E., & Blagden, S. P. (2010). The RNA binding protein Larp1 regulates cell division, apoptosis and cell migration. *Nucleic Acids Res*, 38(16), 5542-5553.
- Caldas, L. A., Carneiro, F. A., Monteiro, F. L., Augusto, I., Higa, L. M., Miranda, K., Tanuri, A., & de Souza, W. (2021). Intracellular host cell membrane remodelling induced by SARS-CoV-2 infection in vitro. *Biol Cell*, 113(6), 281-293.
- Camus, G., Herker, E., Modi, A. A., Haas, J. T., Ramage, H. R., Farese, R. V., Jr., & Ott, M. (2013). Diacylglycerol acyltransferase-1 localizes hepatitis C virus NS5A protein to lipid droplets and enhances NS5A interaction with the viral capsid core. *J Biol Chem*, 288(14), 9915-9923.
- Cao, X., Ding, Q., Lu, J., Tao, W., Huang, B., Zhao, Y., Niu, J., Liu, Y. J., & Zhong, J. (2015). MDA5 plays a critical role in interferon response during hepatitis C virus infection. *J Hepatol*, 62(4), 771-778.
- Carrere-Kremer, S., Montpelier-Pala, C., Cocquerel, L., Wychowski, C., Penin, F., & Dubuisson, J. (2002). Subcellular localization and topology of the p7 polypeptide of hepatitis C virus. *J Virol*, 76(8), 3720-3730.
- Catanese, M. T., Graziani, R., von Hahn, T., Moreau, M., Huby, T., Paonessa, G., Santini, C., Luzzago, A., Rice, C. M., Cortese, R., Vitelli, A., & Nicosia, A. (2007). High-avidity monoclonal antibodies against the human scavenger class B type I receptor efficiently block hepatitis C virus infection in the presence of high-density lipoprotein. *J Virol*, 81(15), 8063-8071.
- Catanese, M. T., Loureiro, J., Jones, C. T., Dorner, M., von Hahn, T., & Rice, C. M. (2013a). Different requirements for scavenger receptor class B type I in hepatitis C virus cell-free versus cell-to-cell transmission. *J Virol*, 87(15), 8282-8293.
- Catanese, M. T., Uryu, K., Kopp, M., Edwards, T. J., Andrus, L., Rice, W. J., Silvestry, M., Kuhn, R. J., & Rice, C. M. (2013b). Ultrastructural analysis of hepatitis C virus particles. *Proc Natl Acad Sci U S A*, 110(23), 9505-9510.
- Chang, K. S., Jiang, J., Cai, Z., & Luo, G. (2007). Human apolipoprotein e is required for infectivity and production of hepatitis C virus in cell culture. *J Virol*, 81(24), 13783-13793.
- Chatel-Chaix, L., Germain, M. A., Motorina, A., Bonneil, E., Thibault, P., Baril, M., & Lamarre, D. (2013). A host YB-1 ribonucleoprotein complex is hijacked by hepatitis C virus for the control of NS3-dependent particle production. *J Virol*, 87(21), 11704-11720.
- Chatel-Chaix, L., Melancon, P., Racine, M. E., Baril, M., & Lamarre, D. (2011). Y-box-binding protein 1 interacts with hepatitis C virus NS3/4A and influences the

- equilibrium between viral RNA replication and infectious particle production. *J Virol*, 85(21), 11022-11037.
- Choi-Rhee, E., Schulman, H., & Cronan, J. E. (2004). Promiscuous protein biotinylation by *Escherichia coli* biotin protein ligase. *Protein Sci*, 13(11), 3043-3050.
- Choi, J., Lee, K. J., Zheng, Y., Yamaga, A. K., Lai, M. M., & Ou, J. H. (2004). Reactive oxygen species suppress hepatitis C virus RNA replication in human hepatoma cells. *Hepatology*, 39(1), 81-89.
- Choo, Q. L., Kuo, G., Weiner, A. J., Overby, L. R., Bradley, D. W., & Houghton, M. (1989). Isolation of a cDNA clone derived from a blood-borne non-A, non-B viral hepatitis genome. *Science*, 244(4902), 359-362.
- Ciesek, S., Westhaus, S., Wicht, M., Wappler, I., Henschen, S., Sarrazin, C., Hamdi, N., Abdelaziz, A. I., Strassburg, C. P., Wedemeyer, H., Manns, M. P., Pietschmann, T., & von Hahn, T. (2011). Impact of intra- and interspecies variation of occludin on its function as coreceptor for authentic hepatitis C virus particles. *J Virol*, 85(15), 7613-7621.
- Cole, N. B., Murphy, D. D., Grider, T., Rueter, S., Brasaemle, D., & Nussbaum, R. L. (2002). Lipid droplet binding and oligomerization properties of the Parkinson's disease protein alpha-synuclein. *J Biol Chem*, 277(8), 6344-6352.
- Colpitts, C. C., Tsai, P. L., & Zeisel, M. B. (2020). Hepatitis C Virus Entry: An Intriguingly Complex and Highly Regulated Process. *Int J Mol Sci*, 21(6).
- Conte, M., Franceschi, C., Sandri, M., & Salvioli, S. (2016). Perilipin 2 and Age-Related Metabolic Diseases: A New Perspective. *Trends Endocrinol Metab*, 27(12), 893-903.
- Corless, L., Crump, C. M., Griffin, S. D., & Harris, M. (2010). Vps4 and the ESCRT-III complex are required for the release of infectious hepatitis C virus particles. *J Gen Virol*, 91(Pt 2), 362-372.
- Counihan, N. A., Rawlinson, S. M., & Lindenbach, B. D. (2011). Trafficking of hepatitis C virus core protein during virus particle assembly. *PLoS Pathog*, 7(10), e1002302.
- Cousineau, S. E., & Sagan, S. M. (2021). Poly(rC)-binding protein 1 limits hepatitis C virus assembly and egress. *bioRxiv*, 2021.2002.2028.433252.
- Cronan, J. E. (2005). Targeted and proximity-dependent promiscuous protein biotinylation by a mutant *Escherichia coli* biotin protein ligase. *J Nutr Biochem*, 16(7), 416-418.
- Da Costa, D., Turek, M., Felmlee, D. J., Girardi, E., Pfeffer, S., Long, G., Bartenschlager, R., Zeisel, M. B., & Baumert, T. F. (2012). Reconstitution of the entire hepatitis C virus life cycle in nonhepatic cells. *J Virol*, 86(21), 11919-11925.
- Dansako, H., Hiramoto, H., Ikeda, M., Wakita, T., & Kato, N. (2014). Rab18 is required for viral assembly of hepatitis C virus through trafficking of the core protein to lipid droplets. *Virology*, 462-463, 166-174.
- Dao Thi, V. L., Granier, C., Zeisel, M. B., Guerin, M., Mancip, J., Granio, O., Penin, F., Lavillette, D., Bartenschlager, R., Baumert, T. F., Cosset, F. L., & Dreux, M. (2012). Characterization of hepatitis C virus particle subpopulations reveals multiple usage of the scavenger receptor BI for entry steps. *J Biol Chem*, 287(37), 31242-31257.
- Deleersnyder, V., Pillez, A., Wychowski, C., Blight, K., Xu, J., Hahn, Y. S., Rice, C. M., & Dubuisson, J. (1997). Formation of native hepatitis C virus glycoprotein complexes. *J Virol*, 71(1), 697-704.
- Deng, Y., Zhou, C., Mirza, A. H., Bamigbade, A. T., Zhang, S., Xu, S., & Liu, P. (2021). Rab18 binds PLIN2 and ACSL3 to mediate lipid droplet dynamics. *Biochim Biophys Acta Mol Cell Biol Lipids*, 1866(7), 158923.
- Ding, Q., von Schaewen, M., Hrebikova, G., Heller, B., Sandmann, L., Plaas, M., & Ploss, A. (2017). Mice Expressing Minimally Humanized CD81 and Occludin Genes Support Hepatitis C Virus Uptake In Vivo. *J Virol*, 91(4).
- Doerflinger, S. Y., Cortese, M., Romero-Brey, I., Menne, Z., Tubiana, T., Schenk, C., White, P. A., Bartenschlager, R., Bressanelli, S., Hansman, G. S., & Lohmann,

- V. (2017). Membrane alterations induced by nonstructural proteins of human norovirus. *PLoS Pathog*, 13(10), e1006705.
- Dorner, M., Rice, C. M., & Ploss, A. (2013). Study of hepatitis C virus entry in genetically humanized mice. *Methods*, 59(2), 249-257.
- Dreux, M., Dao Thi, V. L., Fresquet, J., Guerin, M., Julia, Z., Verney, G., Durantel, D., Zoulim, F., Lavillette, D., Cosset, F. L., & Bartosch, B. (2009a). Receptor complementation and mutagenesis reveal SR-BI as an essential HCV entry factor and functionally imply its intra- and extra-cellular domains. *PLoS Pathog*, 5(2), e1000310.
- Dreux, M., Garaigorta, U., Boyd, B., Decembre, E., Chung, J., Whitten-Bauer, C., Wieland, S., & Chisari, F. V. (2012). Short-range exosomal transfer of viral RNA from infected cells to plasmacytoid dendritic cells triggers innate immunity. *Cell Host Microbe*, 12(4), 558-570.
- Dreux, M., Gastaminza, P., Wieland, S. F., & Chisari, F. V. (2009b). The autophagy machinery is required to initiate hepatitis C virus replication. *Proc Natl Acad Sci U S A*, 106(33), 14046-14051.
- DuBridge, R. B., Tang, P., Hsia, H. C., Leong, P. M., Miller, J. H., & Calos, M. P. (1987). Analysis of mutation in human cells by using an Epstein-Barr virus shuttle system. *Mol Cell Biol*, 7(1), 379-387.
- Dubuisson, J., Penin, F., & Moradpour, D. (2002). Interaction of hepatitis C virus proteins with host cell membranes and lipids. *Trends Cell Biol*, 12(11), 517-523.
- Egger, D., Wolk, B., Gosert, R., Bianchi, L., Blum, H. E., Moradpour, D., & Bienz, K. (2002). Expression of hepatitis C virus proteins induces distinct membrane alterations including a candidate viral replication complex. *J Virol*, 76(12), 5974-5984.
- El Andaloussi, S., Lakhal, S., Mager, I., & Wood, M. J. (2013). Exosomes for targeted siRNA delivery across biological barriers. *Adv Drug Deliv Rev*, 65(3), 391-397.
- Elgner, F., Hildt, E., & Bender, D. (2018). Relevance of Rab Proteins for the Life Cycle of Hepatitis C Virus. *Front Cell Dev Biol*, 6, 166.
- Failla, C., Tomei, L., & De Francesco, R. (1994). Both NS3 and NS4A are required for proteolytic processing of hepatitis C virus nonstructural proteins. *J Virol*, 68(6), 3753-3760.
- Fan, B., Lu, K. Y., Raymond Sutandy, F. X., Chen, Y. W., Konan, K., Zhu, H., Kao, C. C., & Chen, C. S. (2014). A human proteome microarray identifies that the heterogeneous nuclear ribonucleoprotein K (hnRNP K) recognizes the 5' terminal sequence of the hepatitis C virus RNA. *Mol Cell Proteomics*, 13(1), 84-92.
- Fan, Z., Yang, Q. R., Twu, J. S., & Sherker, A. H. (1999). Specific in vitro association between the hepatitis C viral genome and core protein. *J Med Virol*, 59(2), 131-134.
- Farquhar, M. J., Hu, K., Harris, H. J., Davis, C., Brimacombe, C. L., Fletcher, S. J., Baumert, T. F., Rappoport, J. Z., Balfe, P., & McKeating, J. A. (2012). Hepatitis C virus induces CD81 and claudin-1 endocytosis. *J Virol*, 86(8), 4305-4316.
- Flynn, R. A., Martin, L., Spitale, R. C., Do, B. T., Sagan, S. M., Zarnegar, B., Qu, K., Khavari, P. A., Quake, S. R., Sarnow, P., & Chang, H. Y. (2015). Dissecting noncoding and pathogen RNA-protein interactomes. *RNA*, 21(1), 135-143.
- Fonseca, B. D., Zakaria, C., Jia, J. J., Graber, T. E., Svitkin, Y., Tahmasebi, S., Healy, D., Hoang, H. D., Jensen, J. M., Diao, I. T., Lussier, A., Dajadian, C., Padmanabhan, N., Wang, W., Matta-Camacho, E., Hearnden, J., Smith, E. M., Tsukumo, Y., Yanagiya, A., Morita, M., Petroulakis, E., Gonzalez, J. L., Hernandez, G., Alain, T., & Damgaard, C. K. (2015). La-related Protein 1 (LARP1) Represses Terminal Oligopyrimidine (TOP) mRNA Translation Downstream of mTOR Complex 1 (mTORC1). *J Biol Chem*, 290(26), 15996-16020.
- Fujimoto, Y., Itabe, H., Sakai, J., Makita, M., Noda, J., Mori, M., Higashi, Y., Kojima, S., & Takano, T. (2004). Identification of major proteins in the lipid droplet-enriched

- fraction isolated from the human hepatocyte cell line HuH7. *Biochim Biophys Acta*, 1644(1), 47-59.
- Furuhashi, M., & Hotamisligil, G. S. (2008). Fatty acid-binding proteins: role in metabolic diseases and potential as drug targets. *Nat Rev Drug Discov*, 7(6), 489-503.
- Gao, L., Aizaki, H., He, J. W., & Lai, M. M. (2004). Interactions between viral nonstructural proteins and host protein hVAP-33 mediate the formation of hepatitis C virus RNA replication complex on lipid raft. *J Virol*, 78(7), 3480-3488.
- Gastaminza, P., Cheng, G., Wieland, S., Zhong, J., Liao, W., & Chisari, F. V. (2008). Cellular determinants of hepatitis C virus assembly, maturation, degradation, and secretion. *J Virol*, 82(5), 2120-2129.
- Gastaminza, P., Dryden, K. A., Boyd, B., Wood, M. R., Law, M., Yeager, M., & Chisari, F. V. (2010). Ultrastructural and biophysical characterization of hepatitis C virus particles produced in cell culture. *J Virol*, 84(21), 10999-11009.
- Gastaminza, P., Kapadia, S. B., & Chisari, F. V. (2006). Differential biophysical properties of infectious intracellular and secreted hepatitis C virus particles. *J Virol*, 80(22), 11074-11081.
- Gawlik, K., & Gallay, P. A. (2014). HCV core protein and virus assembly: what we know without structures. *Immunol Res*, 60(1), 1-10.
- Gentilella, A., Moron-Duran, F. D., Fuentes, P., Zweig-Rocha, G., Riano-Canalias, F., Pelletier, J., Ruiz, M., Turon, G., Castano, J., Tauler, A., Bueno, C., Menendez, P., Kozma, S. C., & Thomas, G. (2017). Autogenous Control of 5'TOP mRNA Stability by 40S Ribosomes. *Mol Cell*, 67(1), 55-70 e54.
- Gondar, V., Molina-Jimenez, F., Hishiki, T., Garcia-Buey, L., Koutsoudakis, G., Shimotohno, K., Benedicto, I., & Majano, P. L. (2015). Apolipoprotein E, but Not Apolipoprotein B, Is Essential for Efficient Cell-to-Cell Transmission of Hepatitis C Virus. *J Virol*, 89(19), 9962-9973.
- Goodman, J. M. (2018). Understanding the Lipid Droplet Proteome and Protein Targeting. *Dev Cell*, 44(1), 1-2.
- Gosert, R., Egger, D., Lohmann, V., Bartenschlager, R., Blum, H. E., Bienz, K., & Moradpour, D. (2003). Identification of the hepatitis C virus RNA replication complex in Huh-7 cells harboring subgenomic replicons. *J Virol*, 77(9), 5487-5492.
- Grakoui, A., McCourt, D. W., Wychowski, C., Feinstone, S. M., & Rice, C. M. (1993). A second hepatitis C virus-encoded proteinase. *Proc Natl Acad Sci U S A*, 90(22), 10583-10587.
- Greenberg, A. S., Coleman, R. A., Kraemer, F. B., McManaman, J. L., Obin, M. S., Puri, V., Yan, Q. W., Miyoshi, H., & Mashek, D. G. (2011). The role of lipid droplets in metabolic disease in rodents and humans. *J Clin Invest*, 121(6), 2102-2110.
- Griffin, S. D., Beales, L. P., Clarke, D. S., Worsfold, O., Evans, S. D., Jaeger, J., Harris, M. P., & Rowlands, D. J. (2003). The p7 protein of hepatitis C virus forms an ion channel that is blocked by the antiviral drug, Amantadine. *FEBS Lett*, 535(1-3), 34-38.
- Hamamoto, I., Nishimura, Y., Okamoto, T., Aizaki, H., Liu, M., Mori, Y., Abe, T., Suzuki, T., Lai, M. M., Miyamura, T., Moriishi, K., & Matsuura, Y. (2005). Human VAP-B is involved in hepatitis C virus replication through interaction with NS5A and NS5B. *J Virol*, 79(21), 13473-13482.
- Harris, H. J., Davis, C., Mullins, J. G., Hu, K., Goodall, M., Farquhar, M. J., Mee, C. J., McCaffrey, K., Young, S., Drummer, H., Balfe, P., & McKeating, J. A. (2010). Claudin association with CD81 defines hepatitis C virus entry. *J Biol Chem*, 285(27), 21092-21102.
- Harris, H. J., Farquhar, M. J., Mee, C. J., Davis, C., Reynolds, G. M., Jennings, A., Hu, K., Yuan, F., Deng, H., Hubscher, S. G., Han, J. H., Balfe, P., & McKeating, J. A. (2008). CD81 and claudin 1 coreceptor association: role in hepatitis C virus entry. *J Virol*, 82(10), 5007-5020.

- Herker, E., Harris, C., Hernandez, C., Carpentier, A., Kaehlcke, K., Rosenberg, A. R., Farese, R. V., Jr., & Ott, M. (2010). Efficient hepatitis C virus particle formation requires diacylglycerol acyltransferase-1. *Nat Med*, 16(11), 1295-1298.
- Herker, E., & Ott, M. (2012). Emerging role of lipid droplets in host/pathogen interactions. *J Biol Chem*, 287(4), 2280-2287.
- Herker, E., Vieyres, G., Beller, M., Krahmer, N., & Bohnert, M. (2021). Lipid Droplet Contact Sites in Health and Disease. *Trends Cell Biol*, 31(5), 345-358.
- Hijikata, M., Mizushima, H., Tanji, Y., Komoda, Y., Hirowatari, Y., Akagi, T., Kato, N., Kimura, K., & Shimotohno, K. (1993). Proteolytic processing and membrane association of putative nonstructural proteins of hepatitis C virus. *Proc Natl Acad Sci U S A*, 90(22), 10773-10777.
- Hiramoto, H., Dansako, H., Takeda, M., Satoh, S., Wakita, T., Ikeda, M., & Kato, N. (2015). Annexin A1 negatively regulates viral RNA replication of hepatitis C virus. *Acta Med Okayama*, 69(2), 71-78.
- Hishiki, T., Shimizu, Y., Tobita, R., Sugiyama, K., Ogawa, K., Funami, K., Ohsaki, Y., Fujimoto, T., Takaku, H., Wakita, T., Baumert, T. F., Miyanari, Y., & Shimotohno, K. (2010). Infectivity of hepatitis C virus is influenced by association with apolipoprotein E isoforms. *J Virol*, 84(22), 12048-12057.
- Hofmann, S., Krajewski, M., Scherer, C., Scholz, V., Mordhorst, V., Truschow, P., Schobel, A., Reimer, R., Schwudke, D., & Herker, E. (2018). Complex lipid metabolic remodeling is required for efficient hepatitis C virus replication. *Biochim Biophys Acta Mol Cell Biol Lipids*, 1863(9), 1041-1056.
- Hong, S., Freeberg, M. A., Han, T., Kamath, A., Yao, Y., Fukuda, T., Suzuki, T., Kim, J. K., & Inoki, K. (2017). LARP1 functions as a molecular switch for mTORC1-mediated translation of an essential class of mRNAs. *Elife*, 6.
- Hopkins, T. G., Mura, M., Al-Ashtal, H. A., Lahr, R. M., Abd-Latip, N., Sweeney, K., Lu, H., Weir, J., El-Bahrawy, M., Steel, J. H., Ghaem-Maghami, S., Aboagye, E. O., Berman, A. J., & Blagden, S. P. (2016). The RNA-binding protein LARP1 is a post-transcriptional regulator of survival and tumorigenesis in ovarian cancer. *Nucleic Acids Res*, 44(3), 1227-1246.
- Huang, A., Tang, Y., Shi, X., Jia, M., Zhu, J., Yan, X., Chen, H., & Gu, Y. (2020). Proximity labeling proteomics reveals critical regulators for inner nuclear membrane protein degradation in plants. *Nature Communications*, 11(1), 3284.
- Huang, H., Sun, F., Owen, D. M., Li, W., Chen, Y., Gale, M., Jr., & Ye, J. (2007). Hepatitis C virus production by human hepatocytes dependent on assembly and secretion of very low-density lipoproteins. *Proc Natl Acad Sci U S A*, 104(14), 5848-5853.
- Huang, L., Hwang, J., Sharma, S. D., Hargittai, M. R., Chen, Y., Arnold, J. J., Raney, K. D., & Cameron, C. E. (2005). Hepatitis C virus nonstructural protein 5A (NS5A) is an RNA-binding protein. *J Biol Chem*, 280(43), 36417-36428.
- Hueging, K., Doepke, M., Vieyres, G., Bankwitz, D., Frentzen, A., Doerrbecker, J., Gumz, F., Haid, S., Wolk, B., Kaderali, L., & Pietschmann, T. (2014). Apolipoprotein E codetermines tissue tropism of hepatitis C virus and is crucial for viral cell-to-cell transmission by contributing to a postenvelopment step of assembly. *J Virol*, 88(3), 1433-1446.
- Hung, V., Lam, S. S., Udeshi, N. D., Svinkina, T., Guzman, G., Mootha, V. K., Carr, S. A., & Ting, A. Y. (2017). Proteomic mapping of cytosol-facing outer mitochondrial and ER membranes in living human cells by proximity biotinylation. *Elife*, 6.
- Hung, V., Udeshi, N. D., Lam, S. S., Loh, K. H., Cox, K. J., Pedram, K., Carr, S. A., & Ting, A. Y. (2016). Spatially resolved proteomic mapping in living cells with the engineered peroxidase APEX2. *Nat Protoc*, 11(3), 456-475.
- Hung, V., Zou, P., Rhee, H. W., Udeshi, N. D., Cracan, V., Svinkina, T., Carr, S. A., Mootha, V. K., & Ting, A. Y. (2014). Proteomic mapping of the human mitochondrial intermembrane space in live cells via ratiometric APEX tagging. *Mol Cell*, 55(2), 332-341.

- Ipsen, D. H., Lykkesfeldt, J., & Tveden-Nyborg, P. (2018). Molecular mechanisms of hepatic lipid accumulation in non-alcoholic fatty liver disease. *Cell Mol Life Sci*, 75(18), 3313-3327.
- Ivanyi-Nagy, R., Kanevsky, I., Gabus, C., Lavergne, J. P., Ficheux, D., Penin, F., Fosse, P., & Darlix, J. L. (2006). Analysis of hepatitis C virus RNA dimerization and core-RNA interactions. *Nucleic Acids Res*, 34(9), 2618-2633.
- Ivashkina, N., Wolk, B., Lohmann, V., Bartenschlager, R., Blum, H. E., Penin, F., & Moradpour, D. (2002). The hepatitis C virus RNA-dependent RNA polymerase membrane insertion sequence is a transmembrane segment. *J Virol*, 76(24), 13088-13093.
- Jiang, J., Cun, W., Wu, X., Shi, Q., Tang, H., & Luo, G. (2012). Hepatitis C virus attachment mediated by apolipoprotein E binding to cell surface heparan sulfate. *J Virol*, 86(13), 7256-7267.
- Jiang, J., & Luo, G. (2009). Apolipoprotein E but not B is required for the formation of infectious hepatitis C virus particles. *J Virol*, 83(24), 12680-12691.
- Jirasko, V., Montserret, R., Lee, J. Y., Gouttenoire, J., Moradpour, D., Penin, F., & Bartenschlager, R. (2010). Structural and functional studies of nonstructural protein 2 of the hepatitis C virus reveal its key role as organizer of virion assembly. *PLoS Pathog*, 6(12), e1001233.
- Jones-Jamtegaard, K. N., Wozniak, A. L., Koga, H., Ralston, R., & Weinman, S. A. (2019). Hepatitis C virus infection increases autophagosome stability by suppressing lysosomal fusion through an Arl8b-dependent mechanism. *J Biol Chem*, 294(39), 14257-14266.
- Jones, C. T., Catanese, M. T., Law, L. M., Khetani, S. R., Syder, A. J., Ploss, A., Oh, T. S., Schoggins, J. W., MacDonald, M. R., Bhatia, S. N., & Rice, C. M. (2010). Real-time imaging of hepatitis C virus infection using a fluorescent cell-based reporter system. *Nat Biotechnol*, 28(2), 167-171.
- Jones, C. T., Murray, C. L., Eastman, D. K., Tassello, J., & Rice, C. M. (2007). Hepatitis C virus p7 and NS2 proteins are essential for production of infectious virus. *J Virol*, 81(16), 8374-8383.
- Jopling, C. L., Schutz, S., & Sarnow, P. (2008). Position-dependent function for a tandem microRNA miR-122-binding site located in the hepatitis C virus RNA genome. *Cell Host Microbe*, 4(1), 77-85.
- Jopling, C. L., Yi, M., Lancaster, A. M., Lemon, S. M., & Sarnow, P. (2005). Modulation of hepatitis C virus RNA abundance by a liver-specific MicroRNA. *Science*, 309(5740), 1577-1581.
- Kachko, A., Costafreda, M. I., Zubkova, I., Jacques, J., Takeda, K., Wells, F., Kaplan, G., & Major, M. E. (2018). Determinants in the Ig Variable Domain of Human HAVCR1 (TIM-1) Are Required To Enhance Hepatitis C Virus Entry. *J Virol*, 92(6).
- Kalemera, M., Mincheva, D., Grove, J., & Illingworth, C. J. R. (2019). Building a mechanistic mathematical model of hepatitis C virus entry. *PLoS Comput Biol*, 15(3), e1006905.
- Kaushik, S., & Cuervo, A. M. (2015). Degradation of lipid droplet-associated proteins by chaperone-mediated autophagy facilitates lipolysis. *Nat Cell Biol*, 17(6), 759-770.
- Khaliq, S., Jahan, S., & Pervaiz, A. (2011). Sequence variability of HCV Core region: important predictors of HCV induced pathogenesis and viral production. *Infect Genet Evol*, 11(3), 543-556.
- Khan, I., Katikaneni, D. S., Han, Q., Sanchez-Felipe, L., Hanada, K., Ambrose, R. L., Mackenzie, J. M., & Konan, K. V. (2014). Modulation of hepatitis C virus genome replication by glycosphingolipids and four-phosphate adaptor protein 2. *J Virol*, 88(21), 12276-12295.
- Kim, D. I., Jensen, S. C., Noble, K. A., Kc, B., Roux, K. H., Motamedchaboki, K., & Roux, K. J. (2016). An improved smaller biotin ligase for BioID proximity labeling. *Mol Biol Cell*, 27(8), 1188-1196.

- Kim, J. Y., Wang, L., Lee, J., & Ou, J. J. (2017). Hepatitis C Virus Induces the Localization of Lipid Rafts to Autophagosomes for Its RNA Replication. *J Virol*, 91(20).
- Klein, K. C., Dellos, S. R., & Lingappa, J. R. (2005). Identification of residues in the hepatitis C virus core protein that are critical for capsid assembly in a cell-free system. *J Virol*, 79(11), 6814-6826.
- Kohli, A., Osinusi, A., Sims, Z., Nelson, A., Meissner, E. G., Barrett, L. L., Bon, D., Marti, M. M., Silk, R., Kotb, C., Gross, C., Jolley, T. A., Sidharthan, S., Petersen, T., Townsend, K., Egerson, D., Kapoor, R., Spurlin, E., Sneller, M., Proschan, M., Herrmann, E., Kwan, R., Teferi, G., Talwani, R., Diaz, G., Kleiner, D. E., Wood, B. J., Chavez, J., Abbott, S., Symonds, W. T., Subramanian, G. M., Pang, P. S., McHutchison, J., Polis, M. A., Fauci, A. S., Masur, H., & Kottlil, S. (2015). Virological response after 6 week triple-drug regimens for hepatitis C: a proof-of-concept phase 2A cohort study. *Lancet*, 385(9973), 1107-1113.
- Kolde, R. (2019). *pheatmap: Pretty Heatmaps*. In
- Korolchuk, V. I., & Rubinshtein, D. C. (2011). Regulation of autophagy by lysosomal positioning. *Autophagy*, 7(8), 927-928.
- Korolchuk, V. I., Saiki, S., Lichtenberg, M., Siddiqi, F. H., Roberts, E. A., Imarisio, S., Jahreiss, L., Sarkar, S., Futter, M., Menzies, F. M., O'Kane, C. J., Deretic, V., & Rubinshtein, D. C. (2011). Lysosomal positioning coordinates cellular nutrient responses. *Nat Cell Biol*, 13(4), 453-460.
- Koutsoudakis, G., Kaul, A., Steinmann, E., Kallis, S., Lohmann, V., Pietschmann, T., & Bartenschlager, R. (2006). Characterization of the early steps of hepatitis C virus infection by using luciferase reporter viruses. *J Virol*, 80(11), 5308-5320.
- Kunkel, M., & Watowich, S. J. (2002). Conformational changes accompanying self-assembly of the hepatitis C virus core protein. *Virology*, 294(2), 239-245.
- Kusakabe, S., Suzuki, T., Sugiyama, Y., Haga, S., Horike, K., Tokunaga, M., Hirano, J., Zhang, H., Chen, D. V., Ishiga, H., Komoda, Y., Ono, C., Fukuhara, T., Yamamoto, M., Ikawa, M., Satoh, T., Akira, S., Tanaka, T., Moriishi, K., Fukai, M., Taketomi, A., Yoshio, S., Kanto, T., Suzuki, T., Okamoto, T., & Matsuura, Y. (2019). USP15 Participates in Hepatitis C Virus Propagation through Regulation of Viral RNA Translation and Lipid Droplet Formation. *J Virol*, 93(6).
- Laemmli, U. K. (1970). Cleavage of structural proteins during the assembly of the head of bacteriophage T4. *Nature*, 227(5259), 680-685.
- Lahr, R. M., Fonseca, B. D., Ciotti, G. E., Al-Ashtal, H. A., Jia, J. J., Niklaus, M. R., Blagden, S. P., Alain, T., & Berman, A. J. (2017). La-related protein 1 (LARP1) binds the mRNA cap, blocking eIF4F assembly on TOP mRNAs. *Elife*, 6.
- Lam, S. S., Martell, J. D., Kamer, K. J., Deerinck, T. J., Ellisman, M. H., Mootha, V. K., & Ting, A. Y. (2015). Directed evolution of APEX2 for electron microscopy and proximity labeling. *Nat Methods*, 12(1), 51-54.
- Lamanna, A. C., & Karbstein, K. (2009). Nob1 binds the single-stranded cleavage site D at the 3'-end of 18S rRNA with its PIN domain. *Proc Natl Acad Sci U S A*, 106(34), 14259-14264.
- Lassen, S., Gruttner, C., Nguyen-Dinh, V., & Herker, E. (2019). Perilipin-2 is critical for efficient lipoprotein and hepatitis C virus particle production. *J Cell Sci*, 132(1).
- Lavie, M., & Dubuisson, J. (2017). Interplay between hepatitis C virus and lipid metabolism during virus entry and assembly. *Biochimie*, 141, 62-69.
- Lee, J. Y., Acosta, E. G., Stoeck, I. K., Long, G., Hiet, M. S., Mueller, B., Fackler, O. T., Kallis, S., & Bartenschlager, R. (2014). Apolipoprotein E likely contributes to a maturation step of infectious hepatitis C virus particles and interacts with viral envelope glycoproteins. *J Virol*, 88(21), 12422-12437.
- Lee, J. Y., Cortese, M., Haselmann, U., Tabata, K., Romero-Brey, I., Funaya, C., Schieber, N. L., Qiang, Y., Bartenschlager, M., Kallis, S., Ritter, C., Rohr, K., Schwab, Y., Ruggieri, A., & Bartenschlager, R. (2019). Spatiotemporal Coupling of the Hepatitis C Virus Replication Cycle by Creating a Lipid Droplet- Proximal Membranous Replication Compartment. *Cell Rep*, 27(12), 3602-3617 e3605.

- Lemay, K. L., Treadaway, J., Angulo, I., & Tellinghuisen, T. L. (2013). A hepatitis C virus NS5A phosphorylation site that regulates RNA replication. *J Virol*, 87(2), 1255-1260.
- Lesburg, C. A., Cable, M. B., Ferrari, E., Hong, Z., Mannarino, A. F., & Weber, P. C. (1999). Crystal structure of the RNA-dependent RNA polymerase from hepatitis C virus reveals a fully encircled active site. *Nat Struct Biol*, 6(10), 937-943.
- Li, K., Foy, E., Ferreon, J. C., Nakamura, M., Ferreon, A. C., Ikeda, M., Ray, S. C., Gale, M., Jr., & Lemon, S. M. (2005). Immune evasion by hepatitis C virus NS3/4A protease-mediated cleavage of the Toll-like receptor 3 adaptor protein TRIF. *Proc Natl Acad Sci U S A*, 102(8), 2992-2997.
- Li, Q., Pene, V., Krishnamurthy, S., Cha, H., & Liang, T. J. (2013). Hepatitis C virus infection activates an innate pathway involving IKK-alpha in lipogenesis and viral assembly. *Nat Med*, 19(6), 722-729.
- Li, X. D., Sun, L., Seth, R. B., Pineda, G., & Chen, Z. J. (2005). Hepatitis C virus protease NS3/4A cleaves mitochondrial antiviral signaling protein off the mitochondria to evade innate immunity. *Proc Natl Acad Sci U S A*, 102(49), 17717-17722.
- Libby, A. E., Bales, E., Orlicky, D. J., & McManaman, J. L. (2016). Perilipin-2 Deletion Impairs Hepatic Lipid Accumulation by Interfering with Sterol Regulatory Element-binding Protein (SREBP) Activation and Altering the Hepatic Lipidome. *J Biol Chem*, 291(46), 24231-24246.
- Lindenbach, B. D. (2009). Measuring HCV infectivity produced in cell culture and in vivo. *Methods Mol Biol*, 510, 329-336.
- Lindenbach, B. D. (2013). Virion assembly and release. *Curr Top Microbiol Immunol*, 369, 199-218.
- Lindenbach, B. D., Evans, M. J., Syder, A. J., Wolk, B., Tellinghuisen, T. L., Liu, C. C., Maruyama, T., Hynes, R. O., Burton, D. R., McKeating, J. A., & Rice, C. M. (2005). Complete replication of hepatitis C virus in cell culture. *Science*, 309(5734), 623-626.
- Lindenbach, B. D., Meuleman, P., Ploss, A., Vanwolleghem, T., Syder, A. J., McKeating, J. A., Lanford, R. E., Feinstone, S. M., Major, M. E., Leroux-Roels, G., & Rice, C. M. (2006). Cell culture-grown hepatitis C virus is infectious in vivo and can be recultured in vitro. *Proc Natl Acad Sci U S A*, 103(10), 3805-3809.
- Lindenbach, B. D., & Rice, C. M. (2013). The ins and outs of hepatitis C virus entry and assembly. *Nat Rev Microbiol*, 11(10), 688-700.
- Listenberger, L. L., Ostermeyer-Fay, A. G., Goldberg, E. B., Brown, W. J., & Brown, D. A. (2007). Adipocyte differentiation-related protein reduces the lipid droplet association of adipose triglyceride lipase and slows triacylglycerol turnover. *J Lipid Res*, 48(12), 2751-2761.
- Liu, F., Liu, W., Zhou, S., Yang, C., Tian, M., Jia, G., Wang, H., Zhu, B., Feng, M., Lu, Y., Qiao, T., Wang, X., Cao, W., Wang, X., Shi, Y., & Wu, D. (2020). Identification of FABP5 as an immunometabolic marker in human hepatocellular carcinoma. *J Immunother Cancer*, 8(2).
- Liu, P., Ying, Y., Zhao, Y., Mundy, D. I., Zhu, M., & Anderson, R. G. (2004). Chinese hamster ovary K2 cell lipid droplets appear to be metabolic organelles involved in membrane traffic. *J Biol Chem*, 279(5), 3787-3792.
- Liu, S., Kuo, W., Yang, W., Liu, W., Gibson, G. A., Dorko, K., Watkins, S. C., Strom, S. C., & Wang, T. (2010). The second extracellular loop dictates Occludin-mediated HCV entry. *Virology*, 407(1), 160-170.
- Liu, Z., & He, J. J. (2013). Cell-cell contact-mediated hepatitis C virus (HCV) transfer, productive infection, and replication and their requirement for HCV receptors. *J Virol*, 87(15), 8545-8558.
- Lohmann, V., & Bartenschlager, R. (2014). On the history of hepatitis C virus cell culture systems. *J Med Chem*, 57(5), 1627-1642.
- Long, L., Thelen, J. P., Furgason, M., Haj-Yahya, M., Brik, A., Cheng, D., Peng, J., & Yao, T. (2014). The U4/U6 recycling factor SART3 has histone chaperone activity

- and associates with USP15 to regulate H2B deubiquitination. *J Biol Chem*, 289(13), 8916-8930.
- Longatti, A., Boyd, B., & Chisari, F. V. (2015). Virion-independent transfer of replication-competent hepatitis C virus RNA between permissive cells. *J Virol*, 89(5), 2956-2961.
- Longin, A., Souchier, C., Ffrench, M., & Bryon, P. A. (1993). Comparison of anti-fading agents used in fluorescence microscopy: image analysis and laser confocal microscopy study. *J Histochem Cytochem*, 41(12), 1833-1840.
- Lupberger, J., Zeisel, M. B., Xiao, F., Thumann, C., Fofana, I., Zona, L., Davis, C., Mee, C. J., Turek, M., Gorke, S., Royer, C., Fischer, B., Zahid, M. N., Lavillette, D., Fresquet, J., Cosset, F. L., Rothenberg, S. M., Pietschmann, T., Patel, A. H., Pessaux, P., Doffoel, M., Raffelsberger, W., Poch, O., McKeating, J. A., Brino, L., & Baumert, T. F. (2011). EGFR and EphA2 are host factors for hepatitis C virus entry and possible targets for antiviral therapy. *Nat Med*, 17(5), 589-595.
- Lussignol, M., Kopp, M., Molloy, K., Vizcay-Barrena, G., Fleck, R. A., Dorner, M., Bell, K. L., Chait, B. T., Rice, C. M., & Catanese, M. T. (2016). Proteomics of HCV virions reveals an essential role for the nucleoporin Nup98 in virus morphogenesis. *Proc Natl Acad Sci U S A*, 113(9), 2484-2489.
- Maillard, P., Huby, T., Andreo, U., Moreau, M., Chapman, J., & Budkowska, A. (2006). The interaction of natural hepatitis C virus with human scavenger receptor SR-BI/Cla1 is mediated by ApoB-containing lipoproteins. *FASEB J*, 20(6), 735-737.
- Mak, K. M., Ren, C., Ponomarenko, A., Cao, Q., & Lieber, C. S. (2008). Adipose differentiation-related protein is a reliable lipid droplet marker in alcoholic fatty liver of rats. *Alcohol Clin Exp Res*, 32(4), 683-689.
- Mann, M. (2006). Functional and quantitative proteomics using SILAC. *Nat Rev Mol Cell Biol*, 7(12), 952-958.
- Manna, D., Aligo, J., Xu, C., Park, W. S., Koc, H., Heo, W. D., & Konan, K. V. (2010). Endocytic Rab proteins are required for hepatitis C virus replication complex formation. *Virology*, 398(1), 21-37.
- Manns, M. P., Wedemeyer, H., & Cornberg, M. (2006). Treating viral hepatitis C: efficacy, side effects, and complications. *Gut*, 55(9), 1350-1359.
- Martell, J. D., Deerinck, T. J., Sancak, Y., Poulos, T. L., Mootha, V. K., Sosinsky, G. E., Ellisman, M. H., & Ting, A. Y. (2012). Engineered ascorbate peroxidase as a genetically encoded reporter for electron microscopy. *Nat Biotechnol*, 30(11), 1143-1148.
- Martin, D. N., & Uprichard, S. L. (2013). Identification of transferrin receptor 1 as a hepatitis C virus entry factor. *Proc Natl Acad Sci U S A*, 110(26), 10777-10782.
- Martinez-Vicente, M., Tallozy, Z., Wong, E., Tang, G., Koga, H., Kaushik, S., de Vries, R., Arias, E., Harris, S., Sulzer, D., & Cuervo, A. M. (2010). Cargo recognition failure is responsible for inefficient autophagy in Huntington's disease. *Nat Neurosci*, 13(5), 567-576.
- Masaki, T., Suzuki, R., Murakami, K., Aizaki, H., Ishii, K., Murayama, A., Date, T., Matsuura, Y., Miyamura, T., Wakita, T., & Suzuki, T. (2008). Interaction of hepatitis C virus nonstructural protein 5A with core protein is critical for the production of infectious virus particles. *J Virol*, 82(16), 7964-7976.
- Matsuda, M., Suzuki, R., Kataoka, C., Watashi, K., Aizaki, H., Kato, N., Matsuura, Y., Suzuki, T., & Wakita, T. (2014). Alternative endocytosis pathway for productive entry of hepatitis C virus. *J Gen Virol*, 95(Pt 12), 2658-2667.
- Matsumoto, M., Hwang, S. B., Jeng, K. S., Zhu, N., & Lai, M. M. (1996). Homotypic interaction and multimerization of hepatitis C virus core protein. *Virology*, 218(1), 43-51.
- Mattijssen, S., Kozlov, G., Gaidamakov, S., Ranjan, A., Fonseca, B. D., Gehring, K., & Maraia, R. J. (2021). The isolated La-module of LARP1 mediates 3' poly(A) protection and mRNA stabilization, dependent on its intrinsic PAM2 binding to PABPC1. *RNA Biol*, 18(2), 275-289.

- McKillop, I. H., Girardi, C. A., & Thompson, K. J. (2019). Role of fatty acid binding proteins (FABPs) in cancer development and progression. *Cell Signal*, 62, 109336.
- McLauchlan, J., Lemberg, M. K., Hope, G., & Martoglio, B. (2002). Intramembrane proteolysis promotes trafficking of hepatitis C virus core protein to lipid droplets. *EMBO J*, 21(15), 3980-3988.
- Medvedev, R., Hildt, E., & Ploen, D. (2017). Look who's talking-the crosstalk between oxidative stress and autophagy supports exosomal-dependent release of HCV particles. *Cell Biol Toxicol*, 33(3), 211-231.
- Meertens, L., Bertaux, C., & Dragic, T. (2006). Hepatitis C virus entry requires a critical postinternalization step and delivery to early endosomes via clathrin-coated vesicles. *J Virol*, 80(23), 11571-11578.
- Menzel, N., Fischl, W., Hueging, K., Bankwitz, D., Frentzen, A., Haid, S., Gentzsch, J., Kaderali, L., Bartenschlager, R., & Pietschmann, T. (2012). MAP-kinase regulated cytosolic phospholipase A2 activity is essential for production of infectious hepatitis C virus particles. *PLoS Pathog*, 8(7), e1002829.
- Merz, A., Long, G., Hiet, M. S., Brugger, B., Chlanda, P., Andre, P., Wieland, F., Krijnse-Locker, J., & Bartenschlager, R. (2011). Biochemical and morphological properties of hepatitis C virus particles and determination of their lipidome. *J Biol Chem*, 286(4), 3018-3032.
- Messina, J. P., Humphreys, I., Flaxman, A., Brown, A., Cooke, G. S., Pybus, O. G., & Barnes, E. (2015). Global distribution and prevalence of hepatitis C virus genotypes. *Hepatology*, 61(1), 77-87.
- Meylan, E., Curran, J., Hofmann, K., Moradpour, D., Binder, M., Bartenschlager, R., & Tschopp, J. (2005). Cardif is an adaptor protein in the RIG-I antiviral pathway and is targeted by hepatitis C virus. *Nature*, 437(7062), 1167-1172.
- Miao, Z., Xie, Z., Miao, J., Ran, J., Feng, Y., & Xia, X. (2017). Regulated Entry of Hepatitis C Virus into Hepatocytes. *Viruses*, 9(5).
- Micallef, J. M., Kaldor, J. M., & Dore, G. J. (2006). Spontaneous viral clearance following acute hepatitis C infection: a systematic review of longitudinal studies. *J Viral Hepat*, 13(1), 34-41.
- Miller, S., Kastner, S., Krijnse-Locker, J., Buhler, S., & Bartenschlager, R. (2007). The non-structural protein 4A of dengue virus is an integral membrane protein inducing membrane alterations in a 2K-regulated manner. *J Biol Chem*, 282(12), 8873-8882.
- Min, S., Lim, Y. S., Shin, D., Park, C., Park, J. B., Kim, S., Windisch, M. P., & Hwang, S. B. (2017). Abl Tyrosine Kinase Regulates Hepatitis C Virus Entry. *Front Microbiol*, 8, 1129.
- Miyanari, Y., Atsuzawa, K., Usuda, N., Watashi, K., Hishiki, T., Zayas, M., Bartenschlager, R., Wakita, T., Hijikata, M., & Shimotohno, K. (2007). The lipid droplet is an important organelle for hepatitis C virus production. *Nat Cell Biol*, 9(9), 1089-1097.
- Molina, S., Castet, V., Fournier-Wirth, C., Pichard-Garcia, L., Avner, R., Harats, D., Roitelman, J., Barbaras, R., Graber, P., Ghera, P., Smolarsky, M., Funaro, A., Malavasi, F., Larrey, D., Coste, J., Fabre, J. M., Sa-Cunha, A., & Maurel, P. (2007). The low-density lipoprotein receptor plays a role in the infection of primary human hepatocytes by hepatitis C virus. *J Hepatol*, 46(3), 411-419.
- Monazahian, M., Bohme, I., Bonk, S., Koch, A., Scholz, C., Grethe, S., & Thomssen, R. (1999). Low density lipoprotein receptor as a candidate receptor for hepatitis C virus. *J Med Virol*, 57(3), 223-229.
- Moradpour, D., Penin, F., & Rice, C. M. (2007). Replication of hepatitis C virus. *Nat Rev Microbiol*, 5(6), 453-463.
- Morikawa, K., Zhao, Z., Date, T., Miyamoto, M., Murayama, A., Akazawa, D., Tanabe, J., Sone, S., & Wakita, T. (2007). The roles of CD81 and glycosaminoglycans in the adsorption and uptake of infectious HCV particles. *J Med Virol*, 79(6), 714-723.

- Moriya, K., Fujie, H., Shintani, Y., Yotsuyanagi, H., Tsutsumi, T., Ishibashi, K., Matsuura, Y., Kimura, S., Miyamura, T., & Koike, K. (1998). The core protein of hepatitis C virus induces hepatocellular carcinoma in transgenic mice. *Nat Med*, 4(9), 1065-1067.
- Moriya, K., Yotsuyanagi, H., Shintani, Y., Fujie, H., Ishibashi, K., Matsuura, Y., Miyamura, T., & Koike, K. (1997). Hepatitis C virus core protein induces hepatic steatosis in transgenic mice. *J Gen Virol*, 78 (Pt 7), 1527-1531.
- Murphy, D. G., Willems, B., Deschenes, M., Hilzenrat, N., Mousseau, R., & Sabbah, S. (2007). Use of sequence analysis of the NS5B region for routine genotyping of hepatitis C virus with reference to C/E1 and 5' untranslated region sequences. *J Clin Microbiol*, 45(4), 1102-1112.
- Nakabayashi, H., Taketa, K., Miyano, K., Yamane, T., & Sato, J. (1982). Growth of human hepatoma cells lines with differentiated functions in chemically defined medium. *Cancer Res*, 42(9), 3858-3863.
- Nakai, K., Okamoto, T., Kimura-Someya, T., Ishii, K., Lim, C. K., Tani, H., Matsuo, E., Abe, T., Mori, Y., Suzuki, T., Miyamura, T., Nunberg, J. H., Moriishi, K., & Matsuura, Y. (2006). Oligomerization of hepatitis C virus core protein is crucial for interaction with the cytoplasmic domain of E1 envelope protein. *J Virol*, 80(22), 11265-11273.
- Naldini, L., Blomer, U., Gallay, P., Ory, D., Mulligan, R., Gage, F. H., Verma, I. M., & Trono, D. (1996). In vivo gene delivery and stable transduction of nondividing cells by a lentiviral vector. *Science*, 272(5259), 263-267.
- Neufeldt, C. J., Cortese, M., Acosta, E. G., & Bartenschlager, R. (2018). Rewiring cellular networks by members of the Flaviviridae family. *Nat Rev Microbiol*, 16(3), 125-142.
- Neufeldt, C. J., Joyce, M. A., Levin, A., Steenberg, R. H., Pang, D., Shields, J., Tyrrell, D. L., & Wozniak, R. W. (2013). Hepatitis C virus-induced cytoplasmic organelles use the nuclear transport machinery to establish an environment conducive to virus replication. *PLoS Pathog*, 9(10), e1003744.
- Nielsen, S. U., Bassendine, M. F., Burt, A. D., Martin, C., Pumeekochchai, W., & Toms, G. L. (2006). Association between hepatitis C virus and very-low-density lipoprotein (VLDL)/LDL analyzed in iodixanol density gradients. *J Virol*, 80(5), 2418-2428.
- Nielsen, S. U., Bassendine, M. F., Martin, C., Lowther, D., Purcell, P. J., King, B. J., Neely, D., & Toms, G. L. (2008). Characterization of hepatitis C RNA-containing particles from human liver by density and size. *J Gen Virol*, 89(Pt 10), 2507-2517.
- Nishikiori, M., Mori, M., Dohi, K., Okamura, H., Katoh, E., Naito, S., Meshi, T., & Ishikawa, M. (2011). A host small GTP-binding protein ARL8 plays crucial roles in tobamovirus RNA replication. *PLoS Pathog*, 7(12), e1002409.
- Nolandt, O., Kern, V., Muller, H., Pfaff, E., Theilmann, L., Welker, R., & Krausslich, H. G. (1997). Analysis of hepatitis C virus core protein interaction domains. *J Gen Virol*, 78 (Pt 6), 1331-1340.
- O'Quinn, P. R., Knabe, D. A., & Wu, G. (2002). Arginine catabolism in lactating porcine mammary tissue. *J Anim Sci*, 80(2), 467-474.
- Ohata, T., Yokoo, H., Kamiyama, T., Fukai, M., Aiyama, T., Hatanaka, Y., Hatanaka, K., Wakayama, K., Orimo, T., Kakisaka, T., Kobayashi, N., Matsuno, Y., & Taketomi, A. (2017). Fatty acid-binding protein 5 function in hepatocellular carcinoma through induction of epithelial-mesenchymal transition. *Cancer Med*, 6(5), 1049-1061.
- Ohira, M., Yokoo, H., Ogawa, K., Fukai, M., Kamiyama, T., Sakamoto, N., & Taketomi, A. (2021). Serum fatty acid-binding protein 5 is a significant factor in hepatocellular carcinoma progression independent of tissue expression level. *Carcinogenesis*, 42(6), 794-803.
- Olofsson, S. O., Stillemark-Billton, P., & Asp, L. (2000). Intracellular assembly of VLDL: two major steps in separate cell compartments. *Trends Cardiovasc Med*, 10(8), 338-345.

- Olzmann, J. A., & Carvalho, P. (2019). Dynamics and functions of lipid droplets. *Nat Rev Mol Cell Biol*, 20(3), 137-155.
- Ong, S. E., Kratchmarova, I., & Mann, M. (2003). Properties of ¹³C-substituted arginine in stable isotope labeling by amino acids in cell culture (SILAC). *J Proteome Res*, 2(2), 173-181.
- Op De Beeck, A., Montserret, R., Duvet, S., Cocquerel, L., Cacan, R., Barberot, B., Le Maire, M., Penin, F., & Dubuisson, J. (2000). The transmembrane domains of hepatitis C virus envelope glycoproteins E1 and E2 play a major role in heterodimerization. *J Biol Chem*, 275(40), 31428-31437.
- Park, S. S., Wu, W. W., Zhou, Y., Shen, R. F., Martin, B., & Maudsley, S. (2012). Effective correction of experimental errors in quantitative proteomics using stable isotope labeling by amino acids in cell culture (SILAC). *J Proteomics*, 75(12), 3720-3732.
- Paul, D., Madan, V., & Bartenschlager, R. (2014). Hepatitis C virus RNA replication and assembly: living on the fat of the land. *Cell Host Microbe*, 16(5), 569-579.
- Pavlovic, D., Neville, D. C., Argaud, O., Blumberg, B., Dwek, R. A., Fischer, W. B., & Zitzmann, N. (2003). The hepatitis C virus p7 protein forms an ion channel that is inhibited by long-alkyl-chain iminosugar derivatives. *Proc Natl Acad Sci U S A*, 100(10), 6104-6108.
- Pei, K., Gui, T., Kan, D., Feng, H., Jin, Y., Yang, Y., Zhang, Q., Du, Z., Gai, Z., Wu, J., & Li, Y. (2020). An Overview of Lipid Metabolism and Nonalcoholic Fatty Liver Disease. *Biomed Res Int*, 2020, 4020249.
- Pene, V., Li, Q., Sodroski, C., Hsu, C. S., & Liang, T. J. (2015). Dynamic Interaction of Stress Granules, DDX3X, and IKK-alpha Mediates Multiple Functions in Hepatitis C Virus Infection. *J Virol*, 89(10), 5462-5477.
- Penin, F., Brass, V., Appel, N., Ramboarina, S., Montserret, R., Ficheux, D., Blum, H. E., Bartenschlager, R., & Moradpour, D. (2004). Structure and function of the membrane anchor domain of hepatitis C virus nonstructural protein 5A. *J Biol Chem*, 279(39), 40835-40843.
- Perlemuter, G., Sabile, A., Letteron, P., Vona, G., Topilco, A., Chretien, Y., Koike, K., Pessayre, D., Chapman, J., Barba, G., & Brechot, C. (2002). Hepatitis C virus core protein inhibits microsomal triglyceride transfer protein activity and very low density lipoprotein secretion: a model of viral-related steatosis. *FASEB J*, 16(2), 185-194.
- Philippe, L., van den Elzen, A. M. G., Watson, M. J., & Thoreen, C. C. (2020). Global analysis of LARP1 translation targets reveals tunable and dynamic features of 5' TOP motifs. *Proc Natl Acad Sci U S A*, 117(10), 5319-5328.
- Philippe, L., Vasseur, J. J., Debart, F., & Thoreen, C. C. (2018). La-related protein 1 (LARP1) repression of TOP mRNA translation is mediated through its cap-binding domain and controlled by an adjacent regulatory region. *Nucleic Acids Res*, 46(3), 1457-1469.
- Pietschmann, T., Kaul, A., Koutsoudakis, G., Shavinskaya, A., Kallis, S., Steinmann, E., Abid, K., Negro, F., Dreux, M., Cosset, F. L., & Bartenschlager, R. (2006). Construction and characterization of infectious intragenotypic and intergenotypic hepatitis C virus chimeras. *Proc Natl Acad Sci U S A*, 103(19), 7408-7413.
- Pileri, P., Uematsu, Y., Campagnoli, S., Galli, G., Falugi, F., Petracca, R., Weiner, A. J., Houghton, M., Rosa, D., Grandi, G., & Abrignani, S. (1998). Binding of hepatitis C virus to CD81. *Science*, 282(5390), 938-941.
- Plissonnier, M. L., Cottarel, J., Piver, E., Kullolli, M., Centonze, F. G., Pitteri, S., Farhan, H., Meunier, J. C., Zoulim, F., & Parent, R. (2019). LARP1 binding to hepatitis C virus particles is correlated with intracellular retention of viral infectivity. *Virus Res*, 271, 197679.
- Plissonnier, M. L., Lahlali, T., Michelet, M., Lebosse, F., Cottarel, J., Beer, M., Neveu, G., Durantel, D., Bartosch, B., Accardi, R., Clement, S., Paradisi, A., Devouassoux-Shisheboran, M., Einav, S., Mehlen, P., Zoulim, F., & Parent, R. (2016). Epidermal Growth Factor Receptor-Dependent Mutual Amplification between Netrin-1 and the Hepatitis C Virus. *PLoS Biol*, 14(3), e1002421.

- Ploen, D., Hafirassou, M. L., Himmelsbach, K., Sauter, D., Biniossek, M. L., Weiss, T. S., Baumert, T. F., Schuster, C., & Hildt, E. (2013a). TIP47 plays a crucial role in the life cycle of hepatitis C virus. *J Hepatol*, 58(6), 1081-1088.
- Ploen, D., Hafirassou, M. L., Himmelsbach, K., Schille, S. A., Biniossek, M. L., Baumert, T. F., Schuster, C., & Hildt, E. (2013b). TIP47 is associated with the hepatitis C virus and its interaction with Rab9 is required for release of viral particles. *Eur J Cell Biol*, 92(12), 374-382.
- Ploen, D., & Hildt, E. (2015). Hepatitis C virus comes for dinner: How the hepatitis C virus interferes with autophagy. *World J Gastroenterol*, 21(28), 8492-8507.
- Ploss, A., Evans, M. J., Gaysinskaya, V. A., Panis, M., You, H., de Jong, Y. P., & Rice, C. M. (2009). Human occludin is a hepatitis C virus entry factor required for infection of mouse cells. *Nature*, 457(7231), 882-886.
- Popescu, C. I., Callens, N., Trinel, D., Roingeard, P., Moradpour, D., Descamps, V., Duverlie, G., Penin, F., Heliot, L., Rouille, Y., & Dubuisson, J. (2011). NS2 protein of hepatitis C virus interacts with structural and non-structural proteins towards virus assembly. *PLoS Pathog*, 7(2), e1001278.
- Popescu, C. I., Riva, L., Vlaicu, O., Farhat, R., Rouille, Y., & Dubuisson, J. (2014). Hepatitis C virus life cycle and lipid metabolism. *Biology (Basel)*, 3(4), 892-921.
- Qian, X. J., Zhu, Y. Z., Zhao, P., & Qi, Z. T. (2016). Entry inhibitors: New advances in HCV treatment. *Emerg Microbes Infect*, 5, e3.
- Quan, M., Liu, S., Li, G., Wang, Q., Zhang, J., Zhang, M., Li, M., Gao, P., Feng, S., & Cheng, J. (2014). A functional role for NS5A^{TP} in the induction of HCV NS5A-mediated autophagy. *J Viral Hepat*, 21(6), 405-415.
- Ramage, H. R., Kumar, G. R., Verschuere, E., Johnson, J. R., Von Dollen, J., Johnson, T., Newton, B., Shah, P., Horner, J., Krogan, N. J., & Ott, M. (2015). A combined proteomics/genomics approach links hepatitis C virus infection with nonsense-mediated mRNA decay. *Mol Cell*, 57(2), 329-340.
- Ramakrishnaiah, V., Thumann, C., Fofana, I., Habersetzer, F., Pan, Q., de Ruiter, P. E., Willemsen, R., Demmers, J. A., Stalin Raj, V., Jenster, G., Kwekkeboom, J., Tilanus, H. W., Haagmans, B. L., Baumert, T. F., & van der Laan, L. J. (2013). Exosome-mediated transmission of hepatitis C virus between human hepatoma Huh7.5 cells. *Proc Natl Acad Sci U S A*, 110(32), 13109-13113.
- Reiss, S., Rebhan, I., Backes, P., Romero-Brey, I., Erfle, H., Matula, P., Kaderali, L., Poenisch, M., Blankenburg, H., Hiet, M. S., Longerich, T., Diehl, S., Ramirez, F., Balla, T., Rohr, K., Kaul, A., Buhler, S., Pepperkok, R., Lengauer, T., Albrecht, M., Eils, R., Schirmacher, P., Lohmann, V., & Bartenschlager, R. (2011). Recruitment and activation of a lipid kinase by hepatitis C virus NS5A is essential for integrity of the membranous replication compartment. *Cell Host Microbe*, 9(1), 32-45.
- Rhee, H. W., Zou, P., Udeshi, N. D., Martell, J. D., Mootha, V. K., Carr, S. A., & Ting, A. Y. (2013). Proteomic mapping of mitochondria in living cells via spatially restricted enzymatic tagging. *Science*, 339(6125), 1328-1331.
- Roingeard, P., & Melo, R. C. (2017). Lipid droplet hijacking by intracellular pathogens. *Cell Microbiol*, 19(1).
- Romero-Brey, I., Merz, A., Chiramel, A., Lee, J. Y., Chlanda, P., Haselman, U., Santarella-Mellwig, R., Habermann, A., Hoppe, S., Kallis, S., Walther, P., Antony, C., Krijnse-Locker, J., & Bartenschlager, R. (2012). Three-dimensional architecture and biogenesis of membrane structures associated with hepatitis C virus replication. *PLoS Pathog*, 8(12), e1003056.
- Rosa-Ferreira, C., & Munro, S. (2011). Arl8 and SKIP act together to link lysosomes to kinesin-1. *Dev Cell*, 21(6), 1171-1178.
- Rösch, K., Kwiatkowski, M., Hofmann, S., Schobel, A., Gruttner, C., Wurlitzer, M., Schluter, H., & Herker, E. (2016). Quantitative Lipid Droplet Proteome Analysis Identifies Annexin A3 as a Cofactor for HCV Particle Production. *Cell Rep*, 16(12), 3219-3231.

- Rose, M., Allen Myers, J., Ryan, N., Prince, A., Talbot, M., & Espinosa, C. M. (2019). 293. Hepatitis C is now a Millennial Disease in Response to the Opioid Crisis: A Demographic Shift in Hepatitis C Infection. *Open Forum Infectious Diseases*, 6(Supplement_2), S159-S159.
- Roux, K. J., Kim, D. I., Raida, M., & Burke, B. (2012). A promiscuous biotin ligase fusion protein identifies proximal and interacting proteins in mammalian cells. *J Cell Biol*, 196(6), 801-810.
- RStudio, T. (2020). *RStudio: Integrated Development for R*. RStudio. In PBC, Boston, MA. <http://www.rstudio.com/>
- Sainz, B., Jr., Barretto, N., Martin, D. N., Hiraga, N., Imamura, M., Hussain, S., Marsh, K. A., Yu, X., Chayama, K., Alrefai, W. A., & Uprichard, S. L. (2012). Identification of the Niemann-Pick C1-like 1 cholesterol absorption receptor as a new hepatitis C virus entry factor. *Nat Med*, 18(2), 281-285.
- Salloum, S., Wang, H., Ferguson, C., Parton, R. G., & Tai, A. W. (2013). Rab18 binds to hepatitis C virus NS5A and promotes interaction between sites of viral replication and lipid droplets. *PLoS Pathog*, 9(8), e1003513.
- Santolini, E., Migliaccio, G., & La Monica, N. (1994). Biosynthesis and biochemical properties of the hepatitis C virus core protein. *J Virol*, 68(6), 3631-3641.
- Sarkar, D. (2020). *lattice: Trellis Graphics for R*. In
- Saxena, V., Lai, C. K., Chao, T. C., Jeng, K. S., & Lai, M. M. (2012). Annexin A2 is involved in the formation of hepatitis C virus replication complex on the lipid raft. *J Virol*, 86(8), 4139-4150.
- Scarselli, E., Ansuini, H., Cerino, R., Roccasecca, R. M., Acali, S., Filocamo, G., Traboni, C., Nicosia, A., Cortese, R., & Vitelli, A. (2002). The human scavenger receptor class B type I is a novel candidate receptor for the hepatitis C virus. *EMBO J*, 21(19), 5017-5025.
- Scheel, T. K., & Rice, C. M. (2013). Understanding the hepatitis C virus life cycle paves the way for highly effective therapies. *Nat Med*, 19(7), 837-849.
- Schindelin, J., Arganda-Carreras, I., Frise, E., Kaynig, V., Longair, M., Pietzsch, T., Preibisch, S., Rueden, C., Saalfeld, S., Schmid, B., Tinevez, J. Y., White, D. J., Hartenstein, V., Eliceiri, K., Tomancak, P., & Cardona, A. (2012). Fiji: an open-source platform for biological-image analysis. *Nat Methods*, 9(7), 676-682.
- Schmidt-Mende, J., Bieck, E., Hugle, T., Penin, F., Rice, C. M., Blum, H. E., & Moradpour, D. (2001). Determinants for membrane association of the hepatitis C virus RNA-dependent RNA polymerase. *J Biol Chem*, 276(47), 44052-44063.
- Schmidt, N., Lareau, C. A., Keshishian, H., Ganskih, S., Schneider, C., Hennig, T., Melanson, R., Werner, S., Wei, Y., Zimmer, M., Ade, J., Kirschner, L., Zielinski, S., Dolken, L., Lander, E. S., Caliskan, N., Fischer, U., Vogel, J., Carr, S. A., Bodem, J., & Munschauer, M. (2021). The SARS-CoV-2 RNA-protein interactome in infected human cells. *Nat Microbiol*, 6(3), 339-353.
- Schöbel, A., Nguyen-Dinh, V., Schumann, G. G., & Herker, E. (2021). Hepatitis C virus infection restricts human LINE-1 retrotransposition in hepatoma cells. *PLoS Pathog*, 17(4), e1009496.
- Schulze, R. J., Krueger, E. W., Weller, S. G., Johnson, K. M., Casey, C. A., Schott, M. B., & McNiven, M. A. (2020). Direct lysosome-based autophagy of lipid droplets in hepatocytes. *Proc Natl Acad Sci U S A*, 117(51), 32443-32452.
- Sedano, C. D., & Sarnow, P. (2014). Hepatitis C virus subverts liver-specific miR-122 to protect the viral genome from exoribonuclease Xrn2. *Cell Host Microbe*, 16(2), 257-264.
- Shavinskaya, A., Boulant, S., Penin, F., McLauchlan, J., & Bartenschlager, R. (2007). The lipid droplet binding domain of hepatitis C virus core protein is a major determinant for efficient virus assembly. *J Biol Chem*, 282(51), 37158-37169.
- Shevchenko, A., Tomas, H., Havlis, J., Olsen, J. V., & Mann, M. (2006). In-gel digestion for mass spectrometric characterization of proteins and proteomes. *Nat Protoc*, 1(6), 2856-2860.

- Shimizu, Y., Hishiki, T., Sugiyama, K., Ogawa, K., Funami, K., Kato, A., Ohsaki, Y., Fujimoto, T., Takaku, H., & Shimotohno, K. (2010). Lipoprotein lipase and hepatic triglyceride lipase reduce the infectivity of hepatitis C virus (HCV) through their catalytic activities on HCV-associated lipoproteins. *Virology*, 407(1), 152-159.
- Shimoike, T., Mimori, S., Tani, H., Matsuura, Y., & Miyamura, T. (1999). Interaction of hepatitis C virus core protein with viral sense RNA and suppression of its translation. *J Virol*, 73(12), 9718-9725.
- Simmonds, P., Becher, P., Bukh, J., Gould, E. A., Meyers, G., Monath, T., Muerhoff, S., Pletnev, A., Rico-Hesse, R., Smith, D. B., Stapleton, J. T., & Ictv Report, C. (2017). ICTV Virus Taxonomy Profile: Flaviviridae. *J Gen Virol*, 98(1), 2-3.
- Simpson, R. J., Lim, J. W., Moritz, R. L., & Mathivanan, S. (2009). Exosomes: proteomic insights and diagnostic potential. *Expert Rev Proteomics*, 6(3), 267-283.
- Sir, D., Kuo, C. F., Tian, Y., Liu, H. M., Huang, E. J., Jung, J. U., Machida, K., & Ou, J. H. (2012). Replication of hepatitis C virus RNA on autophagosomal membranes. *J Biol Chem*, 287(22), 18036-18043.
- Sloan, K. E., Knox, A. A., Wells, G. R., Schneider, C., & Watkins, N. J. (2019). Interactions and activities of factors involved in the late stages of human 18S rRNA maturation. *RNA Biol*, 16(2), 196-210.
- Smith, D. B., Bukh, J., Kuiken, C., Muerhoff, A. S., Rice, C. M., Stapleton, J. T., & Simmonds, P. (2014). Expanded classification of hepatitis C virus into 7 genotypes and 67 subtypes: updated criteria and genotype assignment web resource. *Hepatology*, 59(1), 318-327.
- Sourisseau, M., Michta, M. L., Zony, C., Israelow, B., Hopcraft, S. E., Narbus, C. M., Parra Martin, A., & Evans, M. J. (2013). Temporal analysis of hepatitis C virus cell entry with occludin directed blocking antibodies. *PLoS Pathog*, 9(3), e1003244.
- Sp Ngberg, K., & Schwartz, S. (1999). Poly(C)-binding protein interacts with the hepatitis C virus 5' untranslated region. *J Gen Virol*, 80 (Pt 6), 1371-1376.
- Steinmann, E., Penin, F., Kallis, S., Patel, A. H., Bartenschlager, R., & Pietschmann, T. (2007). Hepatitis C virus p7 protein is crucial for assembly and release of infectious virions. *PLoS Pathog*, 3(7), e103.
- Stoeck, I. K., Lee, J. Y., Tabata, K., Romero-Brey, I., Paul, D., Schult, P., Lohmann, V., Kaderali, L., & Bartenschlager, R. (2018). Hepatitis C Virus Replication Depends on Endosomal Cholesterol Homeostasis. *J Virol*, 92(1).
- Su, W. C., Chao, T. C., Huang, Y. L., Weng, S. C., Jeng, K. S., & Lai, M. M. (2011). Rab5 and class III phosphoinositide 3-kinase Vps34 are involved in hepatitis C virus NS4B-induced autophagy. *J Virol*, 85(20), 10561-10571.
- Sumpter, R., Jr., Loo, Y. M., Foy, E., Li, K., Yoneyama, M., Fujita, T., Lemon, S. M., & Gale, M., Jr. (2005). Regulating intracellular antiviral defense and permissiveness to hepatitis C virus RNA replication through a cellular RNA helicase, RIG-I. *J Virol*, 79(5), 2689-2699.
- Suzuki, Y., Chin, W. X., Han, Q., Ichiyama, K., Lee, C. H., Eyo, Z. W., Ebina, H., Takahashi, H., Takahashi, C., Tan, B. H., Hishiki, T., Ohba, K., Matsuyama, T., Koyanagi, Y., Tan, Y. J., Sawasaki, T., Chu, J. J., Vasudevan, S. G., Sano, K., & Yamamoto, N. (2016). Characterization of RyDEN (C19orf66) as an Interferon-Stimulated Cellular Inhibitor against Dengue Virus Replication. *PLoS Pathog*, 12(1), e1005357.
- Sztalryd, C., Bell, M., Lu, X., Mertz, P., Hickenbottom, S., Chang, B. H., Chan, L., Kimmel, A. R., & Londos, C. (2006). Functional compensation for adipose differentiation-related protein (ADFP) by Tip47 in an ADFP null embryonic cell line. *J Biol Chem*, 281(45), 34341-34348.
- Sztalryd, C., & Brasaemle, D. L. (2017). The perilipin family of lipid droplet proteins: Gatekeepers of intracellular lipolysis. *Biochim Biophys Acta Mol Cell Biol Lipids*, 1862(10 Pt B), 1221-1232.

- Takahashi, Y., Shinoda, A., Kamada, H., Shimizu, M., Inoue, J., & Sato, R. (2016). Perilipin2 plays a positive role in adipocytes during lipolysis by escaping proteasomal degradation. *Sci Rep*, 6, 20975.
- Tallorin, L., Villareal, V. A., Hsia, C. Y., Rodgers, M. A., Burri, D. J., Pfeil, M. P., Llopis, P. M., Lindenbach, B. D., & Yang, P. L. (2020). Hepatitis C virus NS3-4A protease regulates the lipid environment for RNA replication by cleaving host enzyme 24-dehydrocholesterol reductase. *J Biol Chem*, 295(35), 12426-12436.
- Tanaka, M., Gupta, R., & Mayer, B. J. (1995). Differential inhibition of signaling pathways by dominant-negative SH2/SH3 adapter proteins. *Mol Cell Biol*, 15(12), 6829-6837.
- Tanaka, N., Moriya, K., Kiyosawa, K., Koike, K., & Aoyama, T. (2008). Hepatitis C virus core protein induces spontaneous and persistent activation of peroxisome proliferator-activated receptor alpha in transgenic mice: implications for HCV-associated hepatocarcinogenesis. *Int J Cancer*, 122(1), 124-131.
- Tanaka, T., Kuroda, K., Ikeda, M., Wakita, T., Kato, N., & Makishima, M. (2013). Hepatitis C virus NS4B targets lipid droplets through hydrophobic residues in the amphipathic helices. *J Lipid Res*, 54(4), 881-892.
- Targett-Adams, P., Boulant, S., & McLauchlan, J. (2008). Visualization of double-stranded RNA in cells supporting hepatitis C virus RNA replication. *J Virol*, 82(5), 2182-2195.
- Tcherkezian, J., Cargnello, M., Romeo, Y., Huttlin, E. L., Lavoie, G., Gygi, S. P., & Roux, P. P. (2014). Proteomic analysis of cap-dependent translation identifies LARP1 as a key regulator of 5'TOP mRNA translation. *Genes Dev*, 28(4), 357-371.
- Tellinghuisen, T. L., Foss, K. L., & Treadaway, J. (2008a). Regulation of hepatitis C virion production via phosphorylation of the NS5A protein. *PLoS Pathog*, 4(3), e1000032.
- Tellinghuisen, T. L., Foss, K. L., Treadaway, J. C., & Rice, C. M. (2008b). Identification of residues required for RNA replication in domains II and III of the hepatitis C virus NS5A protein. *J Virol*, 82(3), 1073-1083.
- Tellinghuisen, T. L., Marcotrigiano, J., & Rice, C. M. (2005). Structure of the zinc-binding domain of an essential component of the hepatitis C virus replicase. *Nature*, 435(7040), 374-379.
- Thiam, A. R., Farese, R. V., Jr., & Walther, T. C. (2013). The biophysics and cell biology of lipid droplets. *Nat Rev Mol Cell Biol*, 14(12), 775-786.
- Thursz, M., & Fontanet, A. (2014). HCV transmission in industrialized countries and resource-constrained areas. *Nat Rev Gastroenterol Hepatol*, 11(1), 28-35.
- Timani, K. A., Liu, Y., & He, J. J. (2013). Tip110 interacts with YB-1 and regulates each other's function. *BMC Mol Biol*, 14, 14.
- Timpe, J. M., Stamataki, Z., Jennings, A., Hu, K., Farquhar, M. J., Harris, H. J., Schwarz, A., Desombere, I., Roels, G. L., Balfe, P., & McKeating, J. A. (2008). Hepatitis C virus cell-cell transmission in hepatoma cells in the presence of neutralizing antibodies. *Hepatology*, 47(1), 17-24.
- Tingting, P., Caiyun, F., Zhigang, Y., Pengyuan, Y., & Zhenghong, Y. (2006). Subproteomic analysis of the cellular proteins associated with the 3' untranslated region of the hepatitis C virus genome in human liver cells. *Biochem Biophys Res Commun*, 347(3), 683-691.
- Tsai, T. Y., Wang, W. T., Li, H. K., Chen, W. J., Tsai, Y. H., Chao, C. H., & Wu Lee, Y. H. (2017). RNA helicase DDX3 maintains lipid homeostasis through upregulation of the microsomal triglyceride transfer protein by interacting with HNF4 and SHP. *Sci Rep*, 7, 41452.
- Tscherne, D. M., Jones, C. T., Evans, M. J., Lindenbach, B. D., McKeating, J. A., & Rice, C. M. (2006). Time- and temperature-dependent activation of hepatitis C virus for low-pH-triggered entry. *J Virol*, 80(4), 1734-1741.
- Valadi, H., Ekstrom, K., Bossios, A., Sjostrand, M., Lee, J. J., & Lotvall, J. O. (2007). Exosome-mediated transfer of mRNAs and microRNAs is a novel mechanism of genetic exchange between cells. *Nat Cell Biol*, 9(6), 654-659.

- Vieyres, G., & Pietschmann, T. (2019). HCV Pit Stop at the Lipid Droplet: Refuel Lipids and Put on a Lipoprotein Coat before Exit. *Cells*, 8(3).
- Vieyres, G., Reichert, I., Carpentier, A., Vondran, F. W. R., & Pietschmann, T. (2020). The ATGL lipase cooperates with ABHD5 to mobilize lipids for hepatitis C virus assembly. *PLoS Pathog*, 16(6), e1008554.
- Vieyres, G., Thomas, X., Descamps, V., Duverlie, G., Patel, A. H., & Dubuisson, J. (2010). Characterization of the envelope glycoproteins associated with infectious hepatitis C virus. *J Virol*, 84(19), 10159-10168.
- Vogt, D. A., Camus, G., Herker, E., Webster, B. R., Tsou, C. L., Greene, W. C., Yen, T. S., & Ott, M. (2013). Lipid droplet-binding protein TIP47 regulates hepatitis C Virus RNA replication through interaction with the viral NS5A protein. *PLoS Pathog*, 9(4), e1003302.
- Voisset, C., & Dubuisson, J. (2004). Functional hepatitis C virus envelope glycoproteins. *Biol Cell*, 96(6), 413-420.
- Wang, H., Perry, J. W., Luring, A. S., Neddermann, P., De Francesco, R., & Tai, A. W. (2014). Oxysterol-binding protein is a phosphatidylinositol 4-kinase effector required for HCV replication membrane integrity and cholesterol trafficking. *Gastroenterology*, 146(5), 1373-1385 e1371-1311.
- Wang, H., & Tai, A. W. (2017). Continuous de novo generation of spatially segregated hepatitis C virus replication organelles revealed by pulse-chase imaging. *J Hepatol*, 66(1), 55-66.
- Wang, J., Qiao, L., Hou, Z., & Luo, G. (2017). TIM-1 Promotes Hepatitis C Virus Cell Attachment and Infection. *J Virol*, 91(2).
- Wang, L., Kim, J. Y., Liu, H. M., Lai, M. M. C., & Ou, J. J. (2017). HCV-induced autophagosomes are generated via homotypic fusion of phagophores that mediate HCV RNA replication. *PLoS Pathog*, 13(9), e1006609.
- Warnes, G. R. (2017). *gdata: Various R Programming Tools for Data Manipulation*. In Warnes, G. R. (2020). *gplots: Various R Programming Tools for Plotting Data*. In
- Weber, K., Bartsch, U., Stocking, C., & Fehse, B. (2008). A multicolor panel of novel lentiviral "gene ontology" (LeGO) vectors for functional gene analysis. *Mol Ther*, 16(4), 698-706.
- Webster, B., Ott, M., & Greene, W. C. (2013). Evasion of superinfection exclusion and elimination of primary viral RNA by an adapted strain of hepatitis C virus. *J Virol*, 87(24), 13354-13369.
- Webster, D. P., Klennerman, P., & Dusheiko, G. M. (2015). Hepatitis C. *Lancet*, 385(9973), 1124-1135.
- Weinlich, S., Huttelmaier, S., Schierhorn, A., Behrens, S. E., Ostareck-Lederer, A., & Ostareck, D. H. (2009). IGF2BP1 enhances HCV IRES-mediated translation initiation via the 3'UTR. *RNA*, 15(8), 1528-1542.
- Weller, R., Hueging, K., Brown, R. J. P., Todt, D., Joecks, S., Vondran, F. W. R., & Pietschmann, T. (2017). Hepatitis C Virus Strain-Dependent Usage of Apolipoprotein E Modulates Assembly Efficiency and Specific Infectivity of Secreted Virions. *J Virol*, 91(18).
- Welsch, C., Albrecht, M., Maydt, J., Herrmann, E., Welker, M. W., Sarrazin, C., Scheidig, A., Lengauer, T., & Zeuzem, S. (2007). Structural and functional comparison of the non-structural protein 4B in flaviviridae. *J Mol Graph Model*, 26(2), 546-557.
- Whitmill, A., Timani, K. A., Liu, Y., & He, J. J. (2016). Tip110: Physical properties, primary structure, and biological functions. *Life Sci*, 149, 79-95.
- Wickham, H. (2020). *ggplot2: Create Elegant Data Visualisations Using the Grammar of Graphics*. In
- Wissing, S., Montano, M., Garcia-Perez, J. L., Moran, J. V., & Greene, W. C. (2011). Endogenous APOBEC3B restricts LINE-1 retrotransposition in transformed cells and human embryonic stem cells. *J Biol Chem*, 286(42), 36427-36437.
- Witteveldt, J., Evans, M. J., Bitzegeio, J., Koutsoudakis, G., Owsianka, A. M., Angus, A. G., Keck, Z. Y., Fount, S. K., Pietschmann, T., Rice, C. M., & Patel, A. H. (2009).

- CD81 is dispensable for hepatitis C virus cell-to-cell transmission in hepatoma cells. *J Gen Virol*, 90(Pt 1), 48-58.
- Wolk, B., Buchele, B., Moradpour, D., & Rice, C. M. (2008). A dynamic view of hepatitis C virus replication complexes. *J Virol*, 82(21), 10519-10531.
- Wolk, B., Sansonno, D., Krausslich, H. G., Dammacco, F., Rice, C. M., Blum, H. E., & Moradpour, D. (2000). Subcellular localization, stability, and trans-cleavage competence of the hepatitis C virus NS3-NS4A complex expressed in tetracycline-regulated cell lines. *J Virol*, 74(5), 2293-2304.
- World Health Organization, W. H. O. (2021). *Hepatitis C*. <https://www.who.int/news-room/fact-sheets/detail/hepatitis-c>
- Wozniak, A. L., Griffin, S., Rowlands, D., Harris, M., Yi, M., Lemon, S. M., & Weinman, S. A. (2010). Intracellular proton conductance of the hepatitis C virus p7 protein and its contribution to infectious virus production. *PLoS Pathog*, 6(9), e1001087.
- Wunschmann, S., Medh, J. D., Klinzmann, D., Schmidt, W. N., & Stapleton, J. T. (2000). Characterization of hepatitis C virus (HCV) and HCV E2 interactions with CD81 and the low-density lipoprotein receptor. *J Virol*, 74(21), 10055-10062.
- Xiao, F., Fofana, I., Heydmann, L., Barth, H., Soulier, E., Habersetzer, F., Doffoel, M., Bukh, J., Patel, A. H., Zeisel, M. B., & Baumert, T. F. (2014). Hepatitis C virus cell-cell transmission and resistance to direct-acting antiviral agents. *PLoS Pathog*, 10(5), e1004128.
- Xie, C., Huang, L., Xie, S., Xie, D., Zhang, G., Wang, P., Peng, L., & Gao, Z. (2013). LARP1 predict the prognosis for early-stage and AFP-normal hepatocellular carcinoma. *J Transl Med*, 11, 272.
- Xu, G., Sztalryd, C., Lu, X., Tansey, J. T., Gan, J., Dorward, H., Kimmel, A. R., & Londos, C. (2005). Post-translational regulation of adipose differentiation-related protein by the ubiquitin/proteasome pathway. *J Biol Chem*, 280(52), 42841-42847.
- Xu, S., Pei, R., Guo, M., Han, Q., Lai, J., Wang, Y., Wu, C., Zhou, Y., Lu, M., & Chen, X. (2012). Cytosolic phospholipase A2 gamma is involved in hepatitis C virus replication and assembly. *J Virol*, 86(23), 13025-13037.
- Yamamoto, M., Aizaki, H., Fukasawa, M., Teraoka, T., Miyamura, T., Wakita, T., & Suzuki, T. (2011). Structural requirements of virion-associated cholesterol for infectivity, buoyant density and apolipoprotein association of hepatitis C virus. *J Gen Virol*, 92(Pt 9), 2082-2087.
- You, S., Stump, D. D., Branch, A. D., & Rice, C. M. (2004). A cis-acting replication element in the sequence encoding the NS5B RNA-dependent RNA polymerase is required for hepatitis C virus RNA replication. *J Virol*, 78(3), 1352-1366.
- Youn, J. Y., Dunham, W. H., Hong, S. J., Knight, J. D. R., Bashkurov, M., Chen, G. I., Bagci, H., Rathod, B., MacLeod, G., Eng, S. W. M., Angers, S., Morris, Q., Fabian, M., Cote, J. F., & Gingras, A. C. (2018). High-Density Proximity Mapping Reveals the Subcellular Organization of mRNA-Associated Granules and Bodies. *Mol Cell*, 69(3), 517-532 e511.
- Yu, G. Y., Lee, K. J., Gao, L., & Lai, M. M. (2006). Palmitoylation and polymerization of hepatitis C virus NS4B protein. *J Virol*, 80(12), 6013-6023.
- Yu, K. L., Jang, S. I., & You, J. C. (2009). Identification of in vivo interaction between Hepatitis C Virus core protein and 5' and 3' UTR RNA. *Virus Res*, 145(2), 285-292.
- Yu, T., Yang, Q., Tian, F., Chang, H., Hu, Z., Yu, B., Han, L., Xing, Y., Jiu, Y., He, Y., & Zhong, J. (2021). Glycometabolism regulates hepatitis C virus release. *PLoS Pathog*, 17(7), e1009746.
- Zhang, Q., Harding, R., Hou, F., Dong, A., Walker, J. R., Bteich, J., & Tong, Y. (2016). Structural Basis of the Recruitment of Ubiquitin-specific Protease USP15 by Spliceosome Recycling Factor SART3. *J Biol Chem*, 291(33), 17283-17292.
- Zhang, S., Wang, Y., Cui, L., Deng, Y., Xu, S., Yu, J., Cichello, S., Serrero, G., Ying, Y., & Liu, P. (2016). Morphologically and Functionally Distinct Lipid Droplet Subpopulations. *Sci Rep*, 6, 29539.
- Zhang, X. (2016). Direct anti-HCV agents. *Acta Pharm Sin B*, 6(1), 26-31.

- Zhang, Y., Ni, J., Zhou, G., Yuan, J., Ren, W., Shan, Y., Tang, W., Yu, L., & Zhao, S. (2005). Cloning, expression and characterization of the human NOB1 gene. *Mol Biol Rep*, 32(3), 185-189.
- Zhao, F., Zhao, T., Deng, L., Lv, D., Zhang, X., Pan, X., Xu, J., & Long, G. (2017). Visualizing the Essential Role of Complete Virion Assembly Machinery in Efficient Hepatitis C Virus Cell-to-Cell Transmission by a Viral Infection-Activated Split-Intein-Mediated Reporter System. *J Virol*, 91(2).
- Zhong, J., Gastaminza, P., Cheng, G., Kapadia, S., Kato, T., Burton, D. R., Wieland, S. F., Uprichard, S. L., Wakita, T., & Chisari, F. V. (2005). Robust hepatitis C virus infection in vitro. *Proc Natl Acad Sci U S A*, 102(26), 9294-9299.
- Zhou, Y., Zhou, B., Pache, L., Chang, M., Khodabakhshi, A. H., Tanaseichuk, O., Benner, C., & Chanda, S. K. (2019). Metascope provides a biologist-oriented resource for the analysis of systems-level datasets. *Nat Commun*, 10(1), 1523.
- Zibbell, J. E., Asher, A. K., Patel, R. C., Kupronis, B., Iqbal, K., Ward, J. W., & Holtzman, D. (2018). Increases in Acute Hepatitis C Virus Infection Related to a Growing Opioid Epidemic and Associated Injection Drug Use, United States, 2004 to 2014. *Am J Public Health*, 108(2), 175-181.

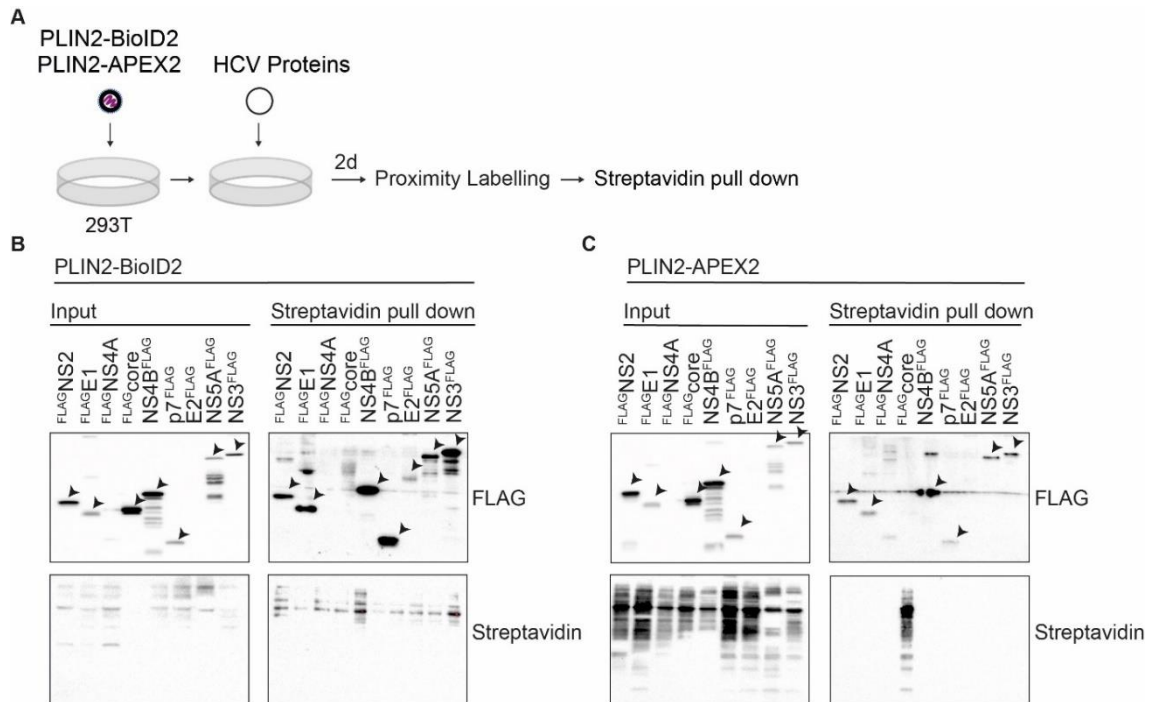


Figure S 3: Transiently expressed HCV proteins are detected in close proximity of PLIN2 expressing HEK293T cells.

(A) HEK293T cells were transduced with lentivirus for stable PLIN2-BioID2 or PLIN2-APEX2 expression followed by transfection with the indicated FLAG-tagged HCV protein expression plasmids 2 days post transduction. One day later cells were supplemented with oleic acid and after one more day, cells were proximity labeled and biotinylated proteins pulled down by streptavidin-coupled agarose beads followed by western blot analysis. (B) Western blot analysis of streptavidin pull down of PLIN2-BioID2-expressing cells. (C) Western blot analysis of streptavidin pull down of PLIN2-APEX2-expressing cells. To detect biotinylated proteins streptavidin-HRP was used and a FLAG specific antibody to detect FLAG-tagged HCV proteins (n = 2).

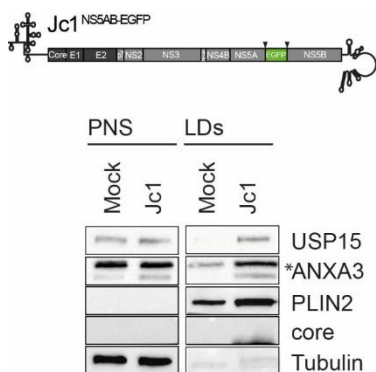


Figure S 4: Recruitment of USP15 to LDs.

(A) Huh7.5 cells were infected with Jc1^{NS5AB-EGFP} (MOI 0.2) and LDs were isolated 7 dpi and analyzed by western blotting. The membrane was probed using specific antibodies against the indicated proteins. Tubulin served as loading control for the post-nuclear supernatant (PNS) and PLIN2 was used as control for equally loaded LDs (n = 1).

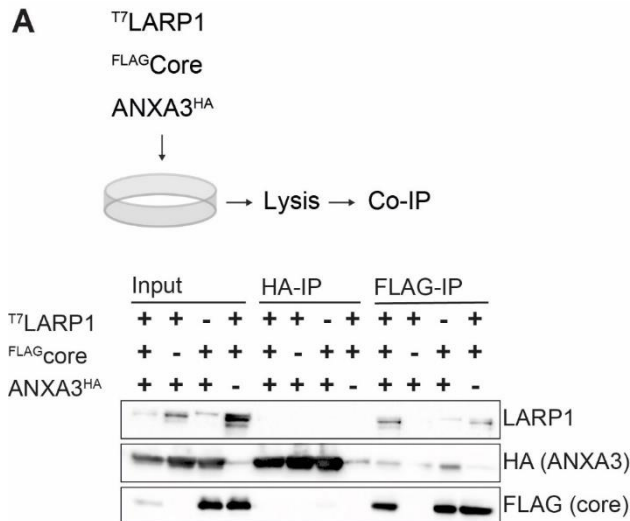


Figure S 5: LARP1 does not interact with ANXA3, but interacts with core independently of ANXA3^{HA} expression.

(A) HEK293T cells were transiently co-transfected with ANXA3^{HA}, T⁷LARP1 and FLAG^{core} expression plasmids. Two days later cells were lysed and co-immunoprecipitations using HA and FLAG-specific beads were performed. HA, FLAG or LARP1-specific antibodies were used for detection in the western blot analysis (n = 2).

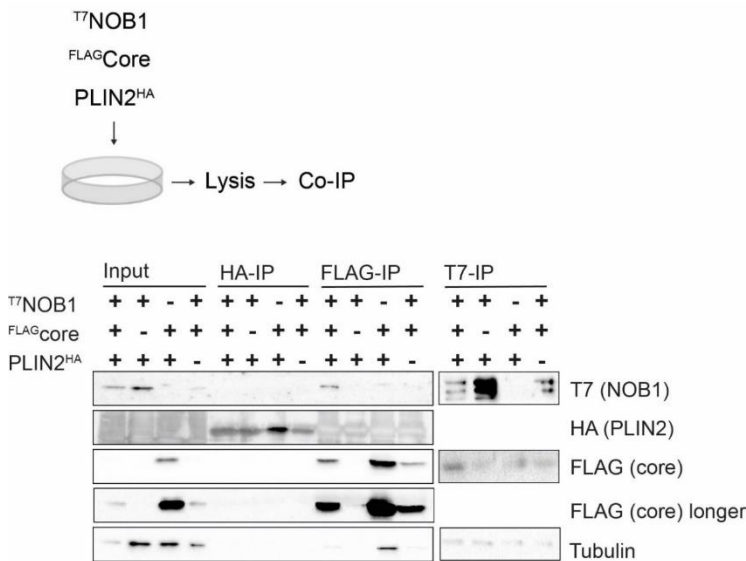


Figure S 6: T⁷NOB1 interacts with core independently of PLIN2^{HA} expression.

HEK293T cells were transiently co-transfected with PLIN2^{HA}, T⁷NOB1 and FLAG^{core} expression plasmids and supplemented with oleic acid the following day. Two days post transfection cells were lysed and co-immunoprecipitations using HA, FLAG and T7-specific beads were performed. HA, FLAG or T7-specific antibodies were used for detection in the western blot analysis (n = 2).

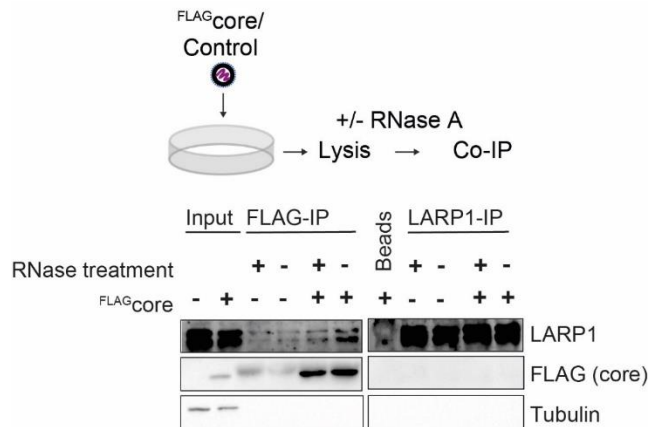


Figure S 7: LARP1 interacts with core in an RNA-dependent manner.

Huh7.5 cells were transduced with lentivirus for FLAG^{core} expression or a control. Lysates were pre-treated with RNase A or RNaseOut and subjected to FLAG-specific immunoprecipitation or immunoprecipitation using a LARP1-specific antibody. Samples were analyzed by western blotting using FLAG and LARP1-specific antibodies. Tubulin served as loading control. (n = 2).

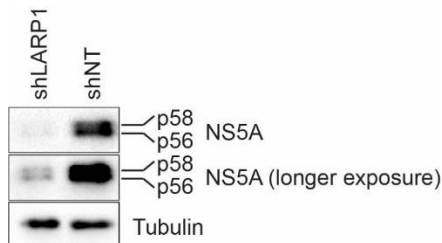


Figure S 8: NS5A phosphorylation is not altered in LARP1-knockdown cells.

Huh7.5 were transduced with lentivirus carrying shLARP1 or shNT. Three days after transduction cells were infected with Jc1^{p7-GLuc-2A-NS2} (MOI 0.5), and cells were lysed 6dpi. Samples were analysed by western blotting using an NS5A-specific antibody. Tubulin served as a loading control. (n = 1).

8.2 List of figures

FIGURE 1: WORLDWIDE PREVALENCE OF HCV.	12
FIGURE 2: MODEL OF THE HCV PARTICLE.	14
FIGURE 3: THE HCV REPLICATION CYCLE.	14
FIGURE 4: MODEL OF HCV ENTRY.	16
FIGURE 5: HCV GENOME ORGANIZATION AND VIRAL PROTEIN MEMBRANE TOPOLOGY.	18
FIGURE 6: MODEL OF HCV ASSEMBLY AND MATURATION.	23
FIGURE 7: SCHEMATIC MODEL OF LDs.	25
FIGURE 8: ANXA3-DEPENDENT STEPS OF THE HCV REPLICATION CYCLE.	27
FIGURE 9: MODEL OF BioID2-MEDIATED LABELING.	28
FIGURE 10: MODEL OF APEX2-MEDIATED LABELING.	29
FIGURE 11: PROXIMITY LABELING WITH ANXA3-BioID2.	34
FIGURE 12: PROXIMITY LABELING WITH PLIN2-BioID2.	35
FIGURE 13: PROXIMITY LABELING WITH ANXA3-APEX2.	37
FIGURE 14: PROXIMITY LABELING WITH PLIN2-APEX2.	39
FIGURE 15: PEPTIDE COVERAGE OF BioID2 AND APEX2 FUSION PROTEINS.	40
FIGURE 16: QUANTITATIVE ANALYSIS OF ANXA3-BioID2 PROXIMITY LABELED CELLS.	41
FIGURE 17: QUANTITATIVE ANALYSIS OF ANXA3-APEX2 PROXIMITY LABELED CELLS.	42
FIGURE 18: QUANTITATIVE ANALYSIS OF PLIN2-BioID2 PROXIMITY LABELED CELLS.	42
FIGURE 19: QUANTITATIVE ANALYSIS OF PLIN2-APEX2 PROXIMITY LABELED CELLS.	43
FIGURE 20: COMPARISON OF LD PROTEOMES.	43
FIGURE 21: MASS SPECTROMETRY OF SILAC LABELED CELLS.	44
FIGURE 22: QUANTITATIVE ANALYSIS OF HCV-INFECTED ANXA3-BioID2 PROXIMITY LABELED CELLS.	44
FIGURE 23: QUANTITATIVE ANALYSIS OF HCV-INFECTED ANXA3-APEX2 PROXIMITY LABELED CELLS.	45
FIGURE 24: QUANTITATIVE ANALYSIS OF HCV-INFECTED PLIN2-BioID2 PROXIMITY LABELED CELLS.	46
FIGURE 25: QUANTITATIVE ANALYSIS OF HCV-INFECTED PLIN2-APEX2 PROXIMITY LABELED CELLS.	47
FIGURE 26: COMPARISON OF LD PROTEOMES OF HCV-INFECTED CELLS.	47
FIGURE 27: COMPARISON OF LD PROTEOMES OF HCV-INFECTED CELLS.	48
FIGURE 28: GENE ONTOLOGY.	48
FIGURE 29: SELECTED HCV PROTEINS ARE DETECTED BY PLIN2 PROXIMITY LABELING DURING HCV REPLICATION.	50
FIGURE 30: TRANSIENTLY EXPRESSED HCV PROTEINS ARE DETECTED IN CLOSE PROXIMITY TO PLIN2 IN HEK293T CELLS.	51
FIGURE 31: TRANSIENTLY EXPRESSED HCV PROTEINS ARE DETECTED IN CLOSE PROXIMITY OF PLIN2 EXPRESSING HEK293T CELLS.	52
FIGURE 32: LD-LOCALIZATION AND INTERACTION WITH VIRAL PROTEINS OF IDENTIFIED HITS.	56
FIGURE 33: FABP5 IS NOT INVOLVED IN THE HCV LIFE CYCLE.	59
FIGURE 34: ARL8B IS REQUIRED FOR HCV SPREADING.	62
FIGURE 35: SART3 INTERACTS WITH CORE.	65
FIGURE 36: SART3 OVEREXPRESSION SUPPORTS HCV VIRION PRODUCTION.	67

FIGURE 37: NOB1 LOCALIZES TO CORE-CONTAINING LDs AND INTERACTS WITH CORE.	69
FIGURE 38: HCV VIRAL SPREADING AND VIRION PRODUCTION IS DELAYED IN NOB1 -KNOCKDOWN CELLS.	71
FIGURE 39: LARP1 LOCALIZES TO CORE-CONTAINING LDs	73
FIGURE 40: LARP1 INTERACTS WITH CORE IN AN RNA -DEPENDENT MANNER.	74
FIGURE 41: VALIDATION OF LARP1 -KNOCKDOWN CELLS.	75
FIGURE 42: LARP1 KNOCKDOWN REDUCES CORE AND NS5A LOCALIZATION TO LDs	75
FIGURE 43: LARP1 KNOCKDOWN IMPAIRS CORE AND NS5A RECRUITMENT TO LDs	77
FIGURE 44: LARP1 KNOCKDOWN REDUCES HCV dsRNA FOCI AND COLOCALIZATION WITH LDs	79
FIGURE 45: HCV VIRAL SPREADING IS DELAYED IN LARP1 -KNOCKDOWN CELLS.	81
FIGURE 46: LARP1 KNOCKDOWN OR OVEREXPRESSION DOES NOT AFFECT HCV RNA REPLICATION.	83
FIGURE 47: LARP1 KNOCKDOWN DOES NOT AFFECT SECRETED HCV VIRIONS.	83
FIGURE 48: LARP1 KNOCKDOWN IMPAIRS HCV CELL-TO-CELL TRANSMISSION.	85
FIGURE 49: LARP1 PARTICIPATES IN CELL-TO-CELL BUT NOT IN CELL-FREE SPREAD OF HCV	102
FIGURE S 1: QUANTITATIVE ANALYSIS OF Bioid2 PROXIMITY LABELED HCV -INFECTED HUH7.5 CELLS.	168
FIGURE S 2: QUANTITATIVE ANALYSIS OF APEX2 PROXIMITY LABELED HCV -INFECTED HUH7.5 CELLS.	168
FIGURE S 3: TRANSIENTLY EXPRESSED HCV PROTEINS ARE DETECTED IN CLOSE PROXIMITY OF PLIN2 EXPRESSING HEK293T CELLS.	169
FIGURE S 4: RECRUITMENT OF USP15 TO LDs	169
FIGURE S 5: LARP1 DOES NOT INTERACT WITH ANXA3 , BUT INTERACTS WITH CORE INDEPENDENTLY OF ANXA3^{HA} EXPRESSION.	170
FIGURE S 6: ¹⁷NOB1 INTERACTS WITH CORE INDEPENDENTLY OF PLIN2^{HA} EXPRESSION.	170
FIGURE S 7: LARP1 INTERACTS WITH CORE IN AN RNA -DEPENDENT MANNER.	171
FIGURE S 8: NS5A PHOSPHORYLATION IS NOT ALTERED IN LARP1 -KNOCKDOWN CELLS.	171









8.3 List of tables



















TABLE 1: INVESTIGATED HITS IDENTIFIED AS LD-PROXIMATE PROTEINS IN HCV -INFECTED CELLS.	53
TABLE 2: BACTERIAL STRAINS.	103
TABLE 3: MEDIA FOR BACTERIAL CULTURE.	103
TABLE 4: MEDIA, BUFFERS AND SUPPLEMENTS FOR CELL CULTURE.	104
TABLE 5: LYSIS BUFFERS.	105
TABLE 6: SDS PAGE AND WESTERN BLOTTING BUFFERS AND SOLUTIONS.	105
TABLE 7: AGAROSE GEL ELECTROPHORESIS.	106
TABLE 8: DNA AND PROTEIN STANDARDS.	106
TABLE 9: BUFFERS USED FOR LD ISOLATION.	106
TABLE 10: SOLUTIONS AND BUFFERS FOR PROXIMITY LABELING.	106
TABLE 11: SOLUTIONS USED FOR MICROSCOPY.	107
TABLE 12: ANNEALING BUFFER.	107

TABLE 13: INHIBITORS.....	107
TABLE 14: RESTRICTION BUFFERS	108
TABLE 15: ENZYMES USED IN THIS STUDY	108
TABLE 16: COMMERCIAL KITS	108
TABLE 17: EXPRESSION PLASMIDS.....	109
TABLE 18: HCV PLASMIDS	113
TABLE 19: PCR PRIMERS USED FOR CLONING OF BIOID2 AND APEX2 CONSTRUCTS.....	114
TABLE 20: PRIMERS USED TO CLONE SHRNAs.....	115
TABLE 21: PCR PRIMERS USED TO CLONE LENTIVIRAL EXPRESSION PLASMIDS.....	116
TABLE 22: PRIMERS USED FOR QRT-PCR.....	116
TABLE 23: PRIMARY ANTIBODIES	117
TABLE 24: SECONDARY ANTIBODIES	118
TABLE 25: FLUORESCENT DYES.....	119
TABLE 26: AGAROSE BEADS.....	119
TABLE 27: CONSUMABLES	119
TABLE 28: CHEMICALS	120
TABLE 29: DEVICES AND EQUIPMENT	123
TABLE 30: SOFTWARE	124
TABLE 31: PCR REACTION MIX.....	126
TABLE 32: PCR CONDITIONS	126
TABLE 33: OVERLAP PCR REACTION MIX	126
TABLE 34: OVERLAP PCR CONDITIONS	127
TABLE 35: PURIFICATION PCR CONDITIONS.....	127
TABLE 36: RESTRICTION DIGEST	127
TABLE 37: STANDARD LIGATION MIXTURE	128
TABLE 38: LIC REACTION MIXTURE	128
TABLE 39: PCR CONDITIONS FOR BIOID2 AND APEX2 FUSION PROTEINS	129
TABLE 40: OVERLAP EXTENSION PCR CONDITIONS FOR BIOID2 AND APEX2 FUSION PROTEINS	129
TABLE 41: PCR CONDITIONS FOR 2A-MCHERRY FUSION TO BIOID2 AND APEX2 FUSION PROTEINS.....	130
TABLE 42: OVERLAP EXTENSION PCR CONDITIONS FOR 2A-MCHERRY FUSION TO BIOID2 AND APEX2 FUSION PROTEINS .	130
TABLE 43: ANNEALING TEMPERATURES AND EXTENSION TIMES FOR LENTIVIRAL EXPRESSION CONSTRUCTS FOR OVEREXPRESSION OF HITS	131
TABLE 44: PHOSPHORYLATION OF PRIMERS	132
TABLE 45: ANNEALING OF PRIMERS	132
TABLE 46: LIGATION MIXTURE FOR ANNEALED PRIMERS	132
TABLE 47: MUNG BEAN NUCLEASE TREATMENT.....	133
TABLE 48: cDNA SYNTHESIS	142
TABLE 49: QRT-PCR MIX USING SYBR GREEN MASTER MIX	142
TABLE 50: QRT-PCR MIX USING LUNA UNIVERSAL QPCR MASTERMIX	142












TABLE 51: QRT-PCR CONDITIONS.....	143
-----------------------------------	-----











8.4 Toxicity of chemicals





Chemical	GHS hazard pictogram	GHS hazard statements	GHS precautionary statements
1,4-Dithiothreitol (DTT)		H302, H315, H319	P302+P350, P305+P351+P338
2-Mercaptoethanol		H301+H331, H310, H315, H317, H318, H373, H410	P273, P280, P302+P352, P304+P341, P305+P351+P338
2-Propanol		H225, H319, H336	P210, P233, P305+P351+P338
Acetic acid		H226, H314	P280, P308+P310, P301+P330+P331, P303+P361+P353, P305+P351+P338, P313
Acetonitrile		H225, H302, H312, H319, H32	P210, P280, P305+P351+P338
Acrylamide solution (30%) - Mix 37.5		H301, H312+H332, H315-H317, H319-H340, H350-H361f, H372	P201, P280, P302+P352, P305+P351+P338
Ammonium hydrogen carbonate		H302	P264, P270, P301+P312, P330, P501
Ammonium persulfate (APS)		H272, H302, H315, H317, H319, H334, H335	P220, P261, P280, P305+P351+P338, P342+P311

Ampicillin		H317, H334	P261, P342+P311 P280,
Blasticidin S		H300, H301	P264, P270, P301+P310, P330, P405, P501
Calcium chloride (CaCl₂)		H319	P264, P280, P305+P351+P338, P337+P313
Chloroform	 	H302, H315, H319, H331, H351, H361d, H372	P260, P301+P312, P280, P305+P351+P338, P405-P50
Chloroquine diphosphate		H302	
DNase I Buffer (10x)		H316	P332 + P313
DNase Inactivation Reagent	 	H315, H335, H318	P280, P305 + P351 + P338
EDTA	 	H319, H332, H373	P260, P261, P271, P304+P340, P305+P351+P338, P312
ELU buffer (NucleoBond Xtra Kit)	 	H226, H319	P210, P233, P280, P05+P351+P338, P337+P313, P403+P235
EQU, WASH buffer (NucleoBond Xtra Kit)		H226	P210, P233, P403+P235
Ethanol	 	H226, H319	P210, P233, P280, P305+P351+P338
Ethidium bromide (EtBr)	 	H302, H330, H341	P281, P302+P352, P304+P340, P305+P351+P338, P309, P310

Formic acid		H314	P260, P264, P280, P301+P330+P331, P303+P61+P53, P304+P340, P305+P351+P338, P310, P321, P363, P405, P501
Guanidine hydrochloride 36–50% (A3 buffer NucleoSpin Plasmid, RAW NucleoSpin RNA Virus)		H302, H315, H319	P264, P280sh, P301+P312, P330
Guanidine thiocyanate 45–60% (RAV1 NucleoSpin RNA Virus)		H302, H412	P273, P301+P312, P330
Hoechst		H302, H315, H319	P280, P305+P351+P338, P313
Hydrochloric acid (HCl)		H290, H335, H314	P280, P301+P330+P331, P305+P351+P338, P308+P310
Hydrogen peroxide solution (30%)		H318, H412	P305, P351, P338
LYS buffer (NucleoBond Xtra)		H315, H319	P234, P280, P302+P352, P05+P351+P338, P332+P313, P337+P313, P390, P406
Methanol (MeOH)		H225, H301+H311+H331, H370	P210, P233, P280, P302+P352, P309, P310, P501
Nonidet-P40		H302, H318, H411	P280, P301+P312, P305+P351+P338
Paraformaldehyde (PFA)		H228, H302, H315, H317, H319, H335, H351	P210, P241, P280, P305+P351+P338, P405, P501

Passive Lysis Buffer 5x		H360	P201, P202, P280, P308+P313, P405, P501
Phenol-Chloroform-Isoamyl alcohol (25:24:1 vol/vol/vol)		H301+H311+H331, H314, H351, H361d, H372, H411	P280b, P301+P330+P331, P305+P351+P338, P309+P311
Phenylmethylsulfonyl fluoride (PMSF)		H301, H314	P280, P305+P351+P338, P310
Pierce Coomassie Plus (Bradford) Assay Reagent (contains phosphoric acid and methanol)		H314, H318, H371	P303 + P361 + P353, P305 + P351 + P338, P304 + P340, P310, P280, P260
Polybrene (Hexadimethrinbromid)		H302	
Potassium hydroxide (KOH)		H290, H302, H314	P280, P301+P330+P331, P305+P351+P338
Renilla Luciferase Assay Substrate		H225	
Renilla Luciferase Assay Lysis Buffer 5x		H351, H360, H412	P201, P202, P280 P273, P308+P313, P405
RNAse A, lyophilized (NucleoBond Xtra)		H317, H334	P261, P280, P302+P352, P304+P340, P333+P313, P342+P311, P363
RNAse Away		H315, H319	
Roti-Blue 5x solution (phosphoric acid <10%)		H290	P234, P309, P406

Sodium azide		H300, H310, H400, H410	P260, P280, P301+P310, P501
Sodium deoxycholate		H302	P264, P270, P301+P312, P501
Sodium dodecyl sulfate (SDS)		H228, H302+H332, H315, H318, H335, H412	P210, P280, P302+P352, P304+P341, P305+P351+P338
Sodium hydroxide		H290, H314	P280, P301+P330+P331, P305+P351+P338
Sodium hypochlorite		H314, H400, EUH031	P280, P301+P330+P331, P305+P351+P338, P308+P310
Stop & Glo Substrate		H225	P243, P280, P241, P303+P361+P353, P370+P378, P403+P235
TEMED (Tetramethylethylenedi amine)		H225, H302+H332, H314	P210, P233, P280, P301+P330+P331, P305+P351+P338
TRI Reagent / Trizol		H301+ H311+ H331, H314, H341, H373, H411	P201, P261, P280, P301+P310+P330, P303+P361+P353, P305+P351+P338
Tris ultrapure (Tris- base)		H315, H319	P302+P352, P305+P351+P338
Triton X-100		H302, H318, H411	P273, P280, P305+P351+P338, P310

Trolox (6-Hydroxy-2,5,7,8-tetramethylchromane-2-carboxylic acid)		H315, H335	H319,	P261, P305+351, P338
Trypan blue solution 0.4%		H350		P201, P308+P313
Tween-20		H315, H335	H319,	P216, P280, P305+P351+P338, P321, P405, P501
Virkon S (potassium peroxymonosulfate sulfate (25-50%), potassium persulfate (<1%), dipentene (<1%))		H318, H412	H315,	P264, P273, P280, P302+P352, P305+P351+P388, P310, P332+P313, P362+P364, P501

GHS pictogram guide



Harmful

Identifies chemicals with the following hazards: skin sensitizer, irritant, acute toxicity (harmful), narcotic effects, respiratory tract infection, hazardous ozone layer



Toxic

Identifies acutely toxic substances (fatal or toxic in case of oral, dermal or inhalative exposure)



Health Hazard

Identifies chemicals with the following hazards: carcinogen, mutagen, reproductive toxicity, respiratory sensitizer, target organ toxicity, aspiration toxicity.



Environmental Hazard

Identifies chemicals with acute or chronic toxicity for aquatic environments



Corrosive

Identifies chemicals with the following hazards: eye damage, skin corrosion, corrosive to metals



Explosive

Identifies unstable explosives, self-reactive substances and mixtures, organic peroxides



Flammable

Identifies flammable agents, pyrophorics, self-reactive and self-heating substances and mixtures, substances emitting flammable gases in context with water, organic peroxides



Oxidizing

Identifies oxidizing agents

GHS hazard statements

Code	Hazard Statement
H200	Unstable explosive.
H201	Explosive; mass explosion hazard.
H202	Explosive; severe projection hazard.
H203	Explosive; fire, blast or projection hazard.
H204	Fire or projection hazard.
H205	May mass explode in fire
H220	Extremely flammable gas.
H221	Flammable gas.
H222	Extremely flammable aerosol.
H223	Flammable aerosol.
H224	Extremely flammable liquid and vapour.
H225	Highly flammable liquid and vapour.
H226	Flammable liquid and vapour.
H227	Combustible liquid.
H228	Flammable solid.
H240	Heating may cause explosion.
H241	Heating may cause fire or explosion.
H242	Heating may cause a fire.
H250	Catches fire spontaneously if exposed to air.
H251	Self-heating; may catch fire.
H252	Self-heating in large quantities; may catch fire.
H260	In contact with water releases flammable gases which may ignite spontaneously
H261	In contact with water releases flammable gas.
H270	May cause or intensify fire; oxidizer.
H271	May cause fire or explosion; strong oxidizer.
H272	May intensify fire; oxidizer.
H280	Contains gas under pressure; may explode if heated.
H281	Contains refrigerated gas; may cause cryogenic burns or injury.
H290	May be corrosive to metals.
H300	Fatal if swallowed.
H301	Toxic if swallowed.
H302	Harmful if swallowed.
H303	May be harmful if swallowed.
H304	May be fatal if swallowed and enters airways.
H305.	May be harmful if swallowed and enters airways

H310	Fatal in contact with skin.
H311	Toxic in contact with skin.
H312	Harmful in contact with skin.
H313	May be harmful in contact with skin.
H314	Causes severe skin burns and eye damage.
H315	Causes skin irritation.
H316	Causes mild skin irritation.
H317	May cause an allergic skin reaction.
H318	Causes serious eye damage.
H319	Causes serious eye irritation.
H320	Causes eye irritation.
H330	Fatal if inhaled.
H331	Toxic if inhaled.
H333	May be harmful if inhaled.
H334	H334 May cause allergy or asthma symptoms or breathing difficulties if inhaled.
H335	May cause respiratory irritation.
H336	May cause drowsiness or dizziness.
H340	May cause genetic defects.
H341	Suspected of causing genetic defects.
H350	May cause cancer.
H351	Suspected of causing cancer.
H360	May damage fertility or the unborn child.
H360F	May damage fertility
H360D	May damage the unborn child
H360FD	May damage fertility; May damage the unborn child
H360Fd	May damage fertility; Suspected of damaging the unborn child
H360Df	May damage the unborn child; Suspected of damaging fertility
H361	Suspected of damaging fertility or the unborn child.
H361f	Suspected of damaging fertility
H361d	Suspected of damaging the unborn child
H361fd	Suspected of damaging fertility; Suspected of damaging the unborn child
H362	May cause harm to breast-fed children.
H370	Causes damage to organs.
H371	May cause damage to organs.
H372	Causes damage to organs through prolonged or repeated exposure.
H373	May cause damage to organs through prolonged or repeated exposure.
H400	Very toxic to aquatic life.
H401	Toxic to aquatic life.
H402	Harmful to aquatic life.

H410	Very toxic to aquatic life with long lasting effects.
H411	Toxic to aquatic life with long lasting effects.
H412	Harmful to aquatic life with long lasting effects.
H413	May cause long lasting harmful effects to aquatic life.
H420	Harms public health and the environment by destroying ozone in the upper atmosphere

Combined H-Codes

H300+H310	Fatal if swallowed or in contact with skin
H300+H330	Fatal if swallowed or if inhaled
H310+H330	Fatal in contact with skin or if inhaled
H300+H310+H330	Fatal if swallowed, in contact with skin or if inhaled
H301+H311	Toxic if swallowed or in contact with skin
H301+H331	Toxic if swallowed or if inhaled
H311+H331	Toxic in contact with skin or if inhaled.
H301+H311+H331	Toxic if swallowed, in contact with skin or if inhaled
H302+H312	Harmful if swallowed or in contact with skin
H302+H332	Harmful if swallowed or if inhaled
H312+H332	Harmful in contact with skin or if inhaled
H302+H312+H332	Harmful if swallowed, in contact with skin or if inhaled
H303+H313	May be harmful if swallowed or in contact with skin
H303+H333	May be harmful if swallowed or if inhaled
H313+H333	May be harmful in contact with skin or if inhaled
H303+H313+H333	May be harmful if swallowed, in contact with skin or if inhaled
H315+H320	Cause skin and eye irritation

GHS precautionary statements

Code	Precautionary statement
P101	If medical advice is needed, have product container or label at hand.
P102	Keep out of reach of children.
P103	Read label before use
P201	Obtain special instructions before use.
P202	Do not handle until all safety precautions have been read and understood.
P210	Keep away from heat, hot surface, sparks, open flames and other ignition sources. - No smoking.
P211	Do not spray on an open flame or other ignition source.
P212	Avoid heating under confinement or reduction of the desensitized agent.
P220	Keep away from clothing and other combustible materials.

P221	Take any precaution to avoid mixing with combustibles/...
P222	Do not allow contact with air.
P223	Do not allow contact with water.
P230	Keep wetted with ...
P231	Handle under inert gas.
P232	Protect from moisture.
P233	Keep container tightly closed.
P234	Keep only in original container.
P235	Keep cool.
P240	Ground/bond container and receiving equipment.
P241	Use explosion-proof [electrical/ventilating/lighting/...] equipment.
P242	Use only non-sparking tools.
P243	Take precautionary measures against static discharge.
P244	Keep valves and fittings free from oil and grease.
P250	Do not subject to grinding/shock/friction/...
P251	Do not pierce or burn, even after use.
P260	Do not breathe dust/fume/gas/mist/vapors/spray.
P261	Avoid breathing dust/fume/gas/mist/vapors/spray.
P262	Do not get in eyes, on skin, or on clothing.
P263	Avoid contact during pregnancy/while nursing.
P264	Wash ... thoroughly after handling.
P270	Do not eat, drink or smoke when using this product.
P271	Use only outdoors or in a well-ventilated area.
P272	Contaminated work clothing should not be allowed out of the workplace.
P273	Avoid release to the environment.
P280	Wear protective gloves/protective clothing/eye protection/face protection.
P281	Use personal protective equipment as required.
P282	Wear cold insulating gloves/face shield/eye protection.
P283	Wear fire resistant or flame retardant clothing.
P284	[In case of inadequate ventilation] Wear respiratory protection.
P285	In case of inadequate ventilation wear respiratory protection.
P231+P232	Handle under inert gas/... Protect from moisture.
P235+P410	Keep cool. Protect from sunlight.
P301	IF SWALLOWED:
P302	IF ON SKIN:
P303	IF ON SKIN (or hair):
P304	IF INHALED:
P305	IF IN EYES:
P306	IF ON CLOTHING:

P307	IF exposed:
P308	IF exposed or concerned:
P309	IF exposed or if you feel unwell
P310	Immediately call a POISON CENTER or doctor/physician.
P311	Call a POISON CENTER or doctor/...
P312	Call a POISON CENTER or doctor/... if you feel unwell.
P313	Get medical advice/attention.
P314	Get medical advice/attention if you feel unwell.
P315	Get immediate medical advice/attention.
P320	Specific treatment is urgent (see ... on this label).
P321	Specific treatment (see ... on this label).
P322	Specific measures (see ...on this label).
P330	Rinse mouth.
P331	Do NOT induce vomiting.
P332	IF SKIN irritation occurs:
P333	If skin irritation or rash occurs:
P334	Immerse in cool water [or wrap in wet bandages].
P335	Brush off loose particles from skin.
P336	Thaw frosted parts with lukewarm water. Do not rub affected area.
P337	If eye irritation persists:
P338	Remove contact lenses, if present and easy to do. Continue rinsing.
P340	Remove victim to fresh air and keep at rest in a position comfortable for breathing.
P341	If breathing is difficult, remove victim to fresh air and keep at rest in a position comfortable for breathing.
P342	If experiencing respiratory symptoms:
P350	Gently wash with plenty of soap and water.
P351	Rinse cautiously with water for several minutes.
P352	Wash with plenty of water/...
P353	Rinse skin with water [or shower].
P360	Rinse immediately contaminated clothing and skin with plenty of water before removing clothes.
P361	Take off immediately all contaminated clothing.
P362	Take off contaminated clothing.
P363	Wash contaminated clothing before reuse.
P364	And wash it before reuse.[Added in 2015 version]
P370	In case of fire:
P371	In case of major fire and large quantities:
P372	Explosion risk.
P373	DO NOT fight fire when fire reaches explosives.
P374	Fight fire with normal precautions from a reasonable distance.

P376	Stop leak if safe to do so.
P377	Leaking gas fire: Do not extinguish, unless leak can be stopped safely.
P378	Use ... to extinguish.
P380	Evacuate area.
P381	In case of leakage, eliminate all ignition sources.
P390	Absorb spillage to prevent material damage.
P391	Collect spillage.
P301+P310	IF SWALLOWED: Immediately call a POISON CENTER/doctor/...
P301+P312	IF SWALLOWED: call a POISON CENTER/doctor/... IF you feel unwell.
P301+P330+P331	IF SWALLOWED: Rinse mouth. Do NOT induce vomiting.
P302+P334	IF ON SKIN: Immerse in cool water [or wrap in wet bandages].
P302+P335+P334	Brush off loose particles from skin. Immerse in cool water [or wrap in wet bandages].
P302+P350	IF ON SKIN: Gently wash with plenty of soap and water.
P302+P352	IF ON SKIN: wash with plenty of water.
P303+P361+P353	IF ON SKIN (or hair): Take off Immediately all contaminated clothing. Rinse SKIN with water [or shower].
P304+P312	IF INHALED: Call a POISON CENTER/doctor/... if you feel unwell.
P304+P340	IF INHALED: Remove person to fresh air and keep comfortable for breathing.
P304+P341	IF INHALED: If breathing is difficult, remove victim to fresh air and keep at rest in a position comfortable for breathing.
P305+P351+P338	IF IN EYES: Rinse cautiously with water for several minutes. Remove contact lenses if present and easy to do - continue rinsing.
P306+P360	IF ON CLOTHING: Rinse Immediately contaminated CLOTHING and SKIN with plenty of water before removing clothes.
P307+P311	IF exposed: call a POISON CENTER or doctor/physician.
P308+P311	IF exposed or concerned: Call a POISON CENTER/doctor/...
P308+P313	IF exposed or concerned: Get medical advice/attention.
P309+P311	IF exposed or if you feel unwell: call a POISON CENTER or doctor/physician.
P332+P313	IF SKIN irritation occurs: Get medical advice/attention.
P333+P313	IF SKIN irritation or rash occurs: Get medical advice/attention.
P335+P334	Brush off loose particles from skin. Immerse in cool water/wrap in wet bandages.
P337+P313	IF eye irritation persists: Get medical advice/attention.
P342+P311	IF experiencing respiratory symptoms: Call a POISON CENTER/doctor/...
P361+P364	Take off immediately all contaminated clothing and wash it before reuse.
P362+P364	Take off contaminated clothing and wash it before reuse.
P370+P376	in case of fire: Stop leak if safe to do so.
P370+P378	In case of fire: Use ... to extinguish.
P370+P380	In case of fire: Evacuate area.
P370+P380+P375	In case of fire: Evacuate area. Fight fire remotely due to the risk of explosion.

P371+P380+P375	In case of major fire and large quantities: Evacuate area. Fight fire remotely due to the risk of explosion.
P401	Store in accordance with ...
P402	Store in a dry place.
P403	Store in a well-ventilated place.
P404	Store in a closed container.
P405	Store locked up.
P406	Store in corrosive resistant/... container with a resistant inner liner.
P407	Maintain air gap between stacks or pallets.
P410	Protect from sunlight.
P411	Store at temperatures not exceeding ... °C/...°F.
P412	Do not expose to temperatures exceeding 50 °C/ 122 °F.
P413	Store bulk masses greater than ... kg/...lbs at temperatures not exceeding ... °C/...°F.
P420	Store separately.
P422	Store contents under ...
P402+P404	Store in a dry place. Store in a closed container.
P403+P233	Store in a well-ventilated place. Keep container tightly closed.
P403+P235	Store in a well-ventilated place. Keep cool.
P410+P403	Protect from sunlight. Store in a well-ventilated place.
P410+P412	Protect from sunlight. Do not expose to temperatures exceeding 50 °C/122°F.
P411+P235	Store at temperatures not exceeding ... °C/...°F. Keep cool.
P501	Dispose of contents/container to ...
P502	Refer to manufacturer or supplier for information on recovery or recycling

8.5 Acknowledgement

Zuerst möchte ich mich bei Prof. Dr. Eva Herker herzlich bedanken für die Betreuung meiner Doktorarbeit, sowie die vielen Anregungen und Ratschläge. Vielen Dank für die offene Arbeitsatmosphäre, die vielen Erfahrungen und die zahlreichen Möglichkeiten zur Präsentation der Forschungsergebnisse.

Außerdem möchte ich mich bei PD Dr. Markus Perbandt für die Zweitbetreuung und Prof. Dr. Wolfram Brune für die Übernahme des Gutachtens dieser Arbeit bedanken. Weiterer Dank gilt Prof. Dr. Kay Grünewald und Prof. Dr. Sebastian Wicha für die Begutachtung der Disputation.

Bei Dr. Christoph Krisp und Prof. Dr. Hartmut Schlüter möchte ich mich für die erfolgreiche Zusammenarbeit bedanken, die dieses Projekt ermöglicht hat.

Vielen Dank an alle ehemaligen und aktuellen Mitglieder der AG Herker, sowohl in Hamburg als auch in Marburg für viel Spaß bei der Arbeit im wissenschaftlichen und nichtwissenschaftlichen Kontext, die Unterstützung und kollegiale Zusammenarbeit! Ein ganz besonderer Dank gilt Dr. Anja Schöbel, nicht nur für deinen Support bei der Arbeit, sondern auch die Freundschaft in allen Situationen.

Danke an meine Familie und Freunde für eure Unterstützung!

8.6 Eidesstattliche Versicherung

Hiermit versichere ich an Eides statt, die vorgelegte Dissertation selbst verfasst und keine anderen als die angegebenen Hilfsmittel benutzt zu haben. Die eingereichte schriftliche Fassung entspricht der auf dem elektronischen Speichermedium. Ich versichere, dass diese Dissertation nicht in einem früheren Promotionsverfahren eingereicht wurde.

Datum, Unterschrift

